



Novel N-bridged diiron phthalocyanine complexes : synthesis, characterization and application in oxidation

Umit Isci

► To cite this version:

Umit Isci. Novel N-bridged diiron phthalocyanine complexes : synthesis, characterization and application in oxidation. Other. Université Claude Bernard - Lyon I; Gebze Institute of Technology (Kocaeli, Turquie), 2010. English. NNT : 2010LYO10016 . tel-00881309

HAL Id: tel-00881309

<https://theses.hal.science/tel-00881309>

Submitted on 8 Nov 2013

HAL is a multi-disciplinary open access archive for the deposit and dissemination of scientific research documents, whether they are published or not. The documents may come from teaching and research institutions in France or abroad, or from public or private research centers.

L'archive ouverte pluridisciplinaire **HAL**, est destinée au dépôt et à la diffusion de documents scientifiques de niveau recherche, publiés ou non, émanant des établissements d'enseignement et de recherche français ou étrangers, des laboratoires publics ou privés.

Année 2010

THESE de DOCTORAT

Université Claude Bernard Lyon

Gebze Institute of Technology

Présentée par

Umit ISCI

**Novel N-bridged diiron phthalocyanine complexes :
Synthesis, characterization and application in oxidation.**

Soutenance prévue le 18 janvier 2010

| | | |
|------|-------------|---------------------------------------|
| Jury | Président | D. LUNEAU |
| | Rapporteurs | D. SEMERIL U. AVCIATA |
| | Examineurs | A. G. GUREK A. SOROKIN V. AHSEN |

TABLE OF CONTENTS

| | |
|-----------------------------------------------------------|-----------|
| 1. INTRODUCTION | 1 |
| 2. BIBLIOGRAPHIC DATA | 4 |
| 2.1. Phthalocyanines | 5 |
| 2.1.1. Generalities | 5 |
| 2.1.2. Methods for Preparation of Phthalocyanines | 9 |
| 2.1.2.1. Metal-free Phthalocyanines | 10 |
| 2.1.2.2. Metallated phthalocyanines | 12 |
| 2.2. Single atom bridged diiron phthalocyanines | 18 |
| 2.2.1. Dimeric μ -oxo iron phthalocyanines | 18 |
| 2.2.2. Dimeric μ -carbido iron phthalocyanines | 20 |
| 2.2.3. N-bridged diiron phthalocyanines | 21 |
| 2.2.4. Supported Iron Phthalocyanines | 34 |
| 2.3. Use of phthalocyanines as oxidation catalysts | 39 |
| 2.3.1 Introduction to bio-inspired heme-like catalysts | 39 |
| 2.3.2. Oxidation of cyclohexene | 43 |
| 2.3.3. Oxidation of toluene and p-xylene | 53 |
| 2.3.3.1. Iron Porphyrins | 54 |
| 2.3.3.2. Iron Phthalocyanines | 56 |
| 2.3.4. Oxidation of alcohols | 58 |

| | |
|------------------------------------------------------------------------------------------------------------------------|------------|
| 2.3.4.1. Iron Porphyrins | 58 |
| 2.3.4.2. Iron Phthalocyanines | 61 |
| 2.3.5. General conclusion | 63 |
| 3. RESULTS AND DISCUSSION | 65 |
| 3.1 Syntheses and characterizations | 66 |
| 3.1.1. Phthalonitriles | 66 |
| 3.1.1.1 Monosulfonylphthalonitriles | 66 |
| 3.1.1.2. Disulfonyl phthalonitrile | 71 |
| 3.1.2. Monomeric iron phthalocyanines | 73 |
| 3.1.2.1 Reaction's conditions | 73 |
| 3.1.2.2. Characterizations | 74 |
| 3.1.3. Dimeric N-bridge diiron phthalocyanines | 77 |
| 3.1.3.1. Reaction's conditions | 77 |
| 3.1.3.2. Characterizations | 78 |
| 3.1.3.3. Conclusions | 103 |
| 3.2 Oxidation tests | 105 |
| 3.2.1. Oxidation of cyclohexene by monomeric sulfonyl substituted Fe(II) phthalocyanines | 105 |
| 3.2.2. Oxidation of toluene and p-xylene by t-butylsulfonyl and hexylsulfonyl substituted μ -nitrido diiron dimers | 111 |
| 3.2.2.1 Oxidation of toluene and p-xylene in homogenous system | 112 |
| 3.2.2.2 Oxidation of toluene and p-xylene by silica supported phthalocyanines | 118 |

| | |
|------------------------------------------------------------------------------------------------------------------------------|------------|
| 3.2.3. Oxidation of alcohols by methyl, ethyl, cyclohexyl and adamantyl sulfonyl substituted μ -nitrido diiron dimers | 122 |
| 4. EXPERIMENTAL PART | 130 |
| 4.1. Synthesis of phthalonitriles | 131 |
| 4.2. Synthesis of monomeric iron phthalocyanines | 147 |
| 4.3. Synthesis of μ -nitrido diiron phthalocyanines | 155 |
| 5. GENERAL CONCLUSION | 162 |
| REFERENCES | 165 |
| List and number of the molecules described in the manuscript | 176 |
| PUBLICATIONS RELATED TO THESE WORKS | 182 |

ACKNOWLEDGEMENTS

I would like first of all to thank my two supervisors, Prof. Dr. Vefa Ahsen and Dr. Alexander Sorokin, who supervised me alternatively at the Gebze Institute of Technology in Turkey and at the Institut de recherches sur la Catalyse et l'Environnement in France, for their leadership during these studies and the preparation of this manuscript, and the French Embassy in Ankara for having provided the PhD co-tutelle fellowship.

My thanks go to Mr. Prakash for the XPS measurements, Dr. Pavel Afanasiev for the assistance in EPR measurements and Mr. Jean-Marc M. Millet for the Mössbauer measurements.

I would also like to thank the members of the Chemistry Department at Gebze Institute of Technology, Dr. Evgeny Kudrik for discussions about chemistry and football as well during my time in Lyon, and Dr. Fabienne Dumoulin for the fruitful discussions.

Finally, I thank my family, for their limitless support. Special thanks go to Durmuş Efe and İrem who are my moral sources.

ABBREVIATIONS

| | |
|-------|------------------------------------------|
| DMAE | <i>N,N</i> -dimethylaminoethanol |
| DBU | 1,8-diazabicyclo[5.4.0] undec-7-ene |
| DMF | Dimethylformamide |
| DBN | 1,5-diazabicyclo[4.3.0]non-5-ene |
| EPR | Electron Paramagnetic Resonance |
| P | Porphyrin |
| Pc | Phthalocyanine |
| IR | Infrared |
| GC | Gas chromatography |
| GC-MS | Gas chromatography-mass spectrometry |
| CPBA | Chloroperoxybenzoic acid |
| DMSO | Dimethylsulfoxide |
| LUMO | Lowest unoccupied molecular orbital |
| HOMO | Highest occupied molecular orbital |
| XPS | X-ray photoelectron spectroscopy |
| MPc | Metallophthalocyanine |
| NMR | Nuclear magnetic resonance |
| TBHP | Tert-butylhydroperoxide |
| XANES | X-ray absorption near-edge structure |
| EXAFS | Extended X-ray absorption fine structure |
| TON | Turnover Numbers |

1. Introduction

The current industrial and environmental preoccupations meet on their common need for more efficient and cheaper catalysts. These high-tech catalysts are required for a more efficient degradation of pollutants, which is one of their two main uses, or for high-scale synthetic purposes. Oxidation of different types of molecules such as alkyl aromatics, alkenes and alcohols are of particular importance as it lead to small molecules used as starting products for more complex syntheses in fine chemicals production (pharmaceutics, cosmetics, polymerization monomers...). As the transformed functions can lead to different products, the selectivity of the catalyst is essential to the overall catalytic system's efficiency.

For these synthetic purposes, bioinspired heme-like catalysts were developed as their natural models are active oxidant catalysts, highly selective and performing. Porphyrin's structure common to these enzymes was therefore used by synthetic chemists aiming at developing new catalytic structures. Phthalocyanines, tetraazabenzoporphyrins analogs of porphyrins, after having been used as simple dyes and pigments, rise interests since a few decades as their multi functional structure (large delocalized aromatic system, metallation, flexibility on a substitution pattern point of view) as well as their exceptional stability in time and extreme conditions (temperature, pH, etc...). They are known to possess better catalytic properties than the prophyrins, especially thanks to their superior stability in oxidation conditions.

All these reasons lead to wide investigation of the oxidation catalytic properties of iron phthalocyanines. Novel edifices were developed, based on the ability of iron to form dimeric structures via single atom bridge. Previous works evidenced that substituted O-bridge diiron phthalocyanines complexes are better oxidation catalysts than corresponding monomers, and following investigations regarding methane's oxidation extended to other types of single atom bridge proved that the most efficient dimers are substituted N-bridged.

Unsubstituted N-bridged dimers were indeed thought during a long time to be inactive, but it was proved that suitable substitution pattern confers them excellent catalytic properties.

The promising results exhibited by the first t-Butyl substituted N-bridged catalyzing methane's oxidation proved that such complexes are worth to be studied more in details.

We therefore prepared a series of N-bridged diiron phthalocyanines, substituted by electron withdrawing alkylsulfonyl moieties. Substituents of different sizes have been chosen in order to compare the effect of their nature with the already known electron-donating t-Butyl substituted $(\text{FePc}^t\text{Bu}_4)_2\text{N}$.

These complexes have been tested towards the oxidation of two families of compounds of considerable industrial importance: alkyl aromatics and alcohols. The monomeric monoiron phthalocyanines have been tested as well for the oxidation of cyclohexene.

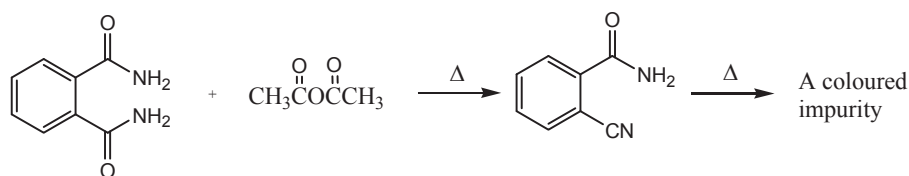
These PhD works have been achieved within a co-directed co-tutelle framework, and therefore included the complete chain from the synthesis of the phthalocyanines until their evaluation as oxidation catalysts. This double thematic directs the organization of this manuscript, with a bibliographic part summarizing firstly the main phthalocyanines synthetic features, then presenting the more important data regarding the use of synthetic heme like oxidation catalysts. We will then develop our results on a synthetic point of view and then detail the results regarding their catalytic properties.

2. Bibliographic Data

2.1. Phthalocyanines

2.1.1. Generalities

The first recorded observation of a phthalocyanine occurred in 1907 (Braun and Tscherniac, 1907). During the synthesis of o-cyanobenzamide from phthalamide and acetic anhydride, Braun and Tcherniac observed the production of a colored impurity of unknown structure and origin [1] (Scheme 2.1). However, this colored by-product was not studied any further.



Scheme 2.1. The first synthesis of a phthalocyanine as reported by Braun and Tcherniac

Similarly, in 1927, de Diesbach and von der Weid (Fribourg University) described an exceptionally stable blue material prepared during the reaction of 1,2-dibromobenzene with copper cyanide in boiling pyridine [2]. Hindsight allows us to interpret these byproducts as being metal-free (H_2Pc) and copper(II) phthalocyanine (CuPc), respectively. In 1928, chemists from the *Scottish Dyes Ltd.* found a dark-blue compound during the synthesis of phthalimide from phthalic anhydride and ammonia. This compound was extremely stable with respect to acids and alkalis, and it was suggested that it has the structure of FePc based on the results of a detailed study of its properties and structure [3–5]. Imperial Chemical Industries (ICI) were eager to understand the structure of this novel substance and a sample was sent to J. F. Thorpe at Imperial College, London. He, in turn, gave it to a newly appointed lecturer, the remarkable R. P. Linstead (1902–1966), ‘as it appeared that the substance might prove to be of academic interest. Thus, a collaboration between Linstead and ICI was initiated that culminated in the publication of a series of six papers in the *Journal of the Chemical Society*, papers that described the structure of phthalocyanine and the synthesis of some of its metal derivatives [6–11]. Linstead conceived the name *phthalocyanine* as a combination of the

prefix *phthalo*, originally from *naphtha* (rock oil), to emphasize the association with its various phthalic acid derived precursors, and *cyanine* (blue). The correct structure of phthalocyanine was elucidated using a combination of elemental analysis, ebullioscopic molecular mass determination and oxidative degradation (which produces phthalimide). Subsequently, work carried out by Robertson was the first example of a single crystal X-ray study being used to confirm a structure postulated from conventional chemical analysis [12–15]. The potential of phthalocyanines as pigments was immediately obvious to workers at ICI, which began trading copper(II) phthalocyanine under the name Monastral Blue in 1935 [5]. I.G. Farbenindustrie and Du Pont also commenced production. Industrial manufacture of phthalocyanine was based on the methodology developed by Wyler at the ICI research center at Blackley, Manchester. The Wyler method involves heating inexpensive phthalic anhydride in a melt of urea, metal salt, and suitable catalyst (e.g., ammonium molybdate) and this is still the method of choice for industrial-scale manufacture of phthalocyanine colorants [5]. Water-soluble dyes based on sulfonated phthalocyanines and, subsequently, reactive dyes for permanent textile coloration were developed in the 1950s and 1960s. Today, many thousands of tons of phthalocyanines are produced worldwide, per annum, to help satisfy the demand for colorants and optoelectronic materials.

Phthalocyanines (formally known as tetrabenzo [5,10,15,20]-tetraazaporphyrins) are more stable analogs of the porphyrins and are more commonly used in industry. Phthalocyanine (Pc) molecules have a conjugated system of 18 π electrons and possess a very high thermal and chemical stability. The structure of the phthalocyanine ring resembles the naturally occurring porphyrins with the only basic difference being the aza groups instead of methine corner links (Figure 2.1).

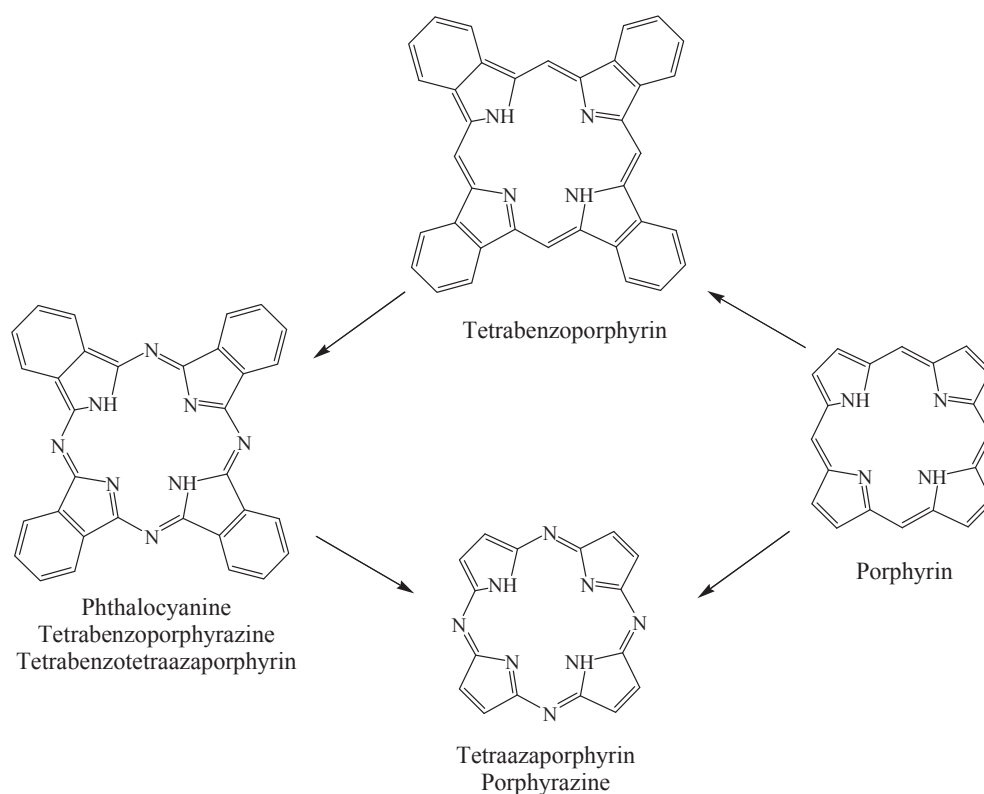


Figure 2.1. Relationship of the phthalocyanine with the porphyrin macrocycle

Phthalocyanine offers up to sixteen sites for substitution and the established numbering system for the basic ring system is given in Figure 2.2, where peripheral refers to the 2, 3 positions and non-peripheral refers to the 1, 4 positions.

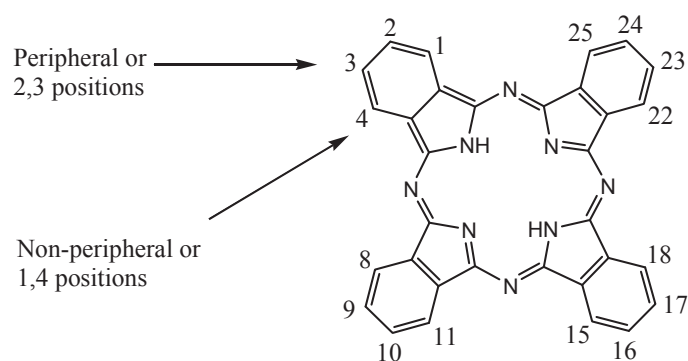


Figure 2.2. Numbering system of the phthalocyanine ring.

Depending on the position of the substituents in the precursor, different structural isomers are formed during the preparation of phthalocyanines. Asymmetric precursors, like 3-, 4-, 3,4-, 3,5- substituted phthalonitriles, form a mixture of structural isomers during the tetracyclomerization. As an example, four isomers of 2,(3)-tetrasubstituted phthalocyanine are shown in Figure 2.3: (C_{4h}) 2,9,16,23-, (D_{2h}) 2,10,16,24-, (C_{2v}) 2,9,17,24- and (C_s) 2,9,16,24- tetra substituted complexes.

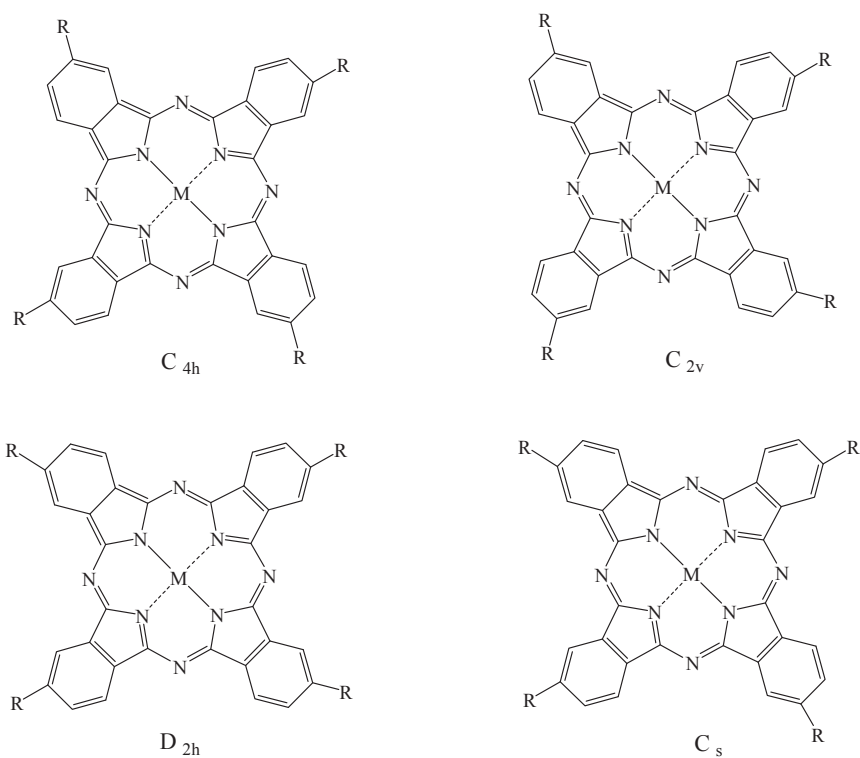


Figure 2.3. Constitutional isomers from 2,(3)-tetrasubstituted phthalocyanines

Symmetrically disubstituted precursors, due to their location, form either the 2,3,9,10,16,17,23,24 or 1,4,8,11,15,18,22,25 octasubstituted phthalocyanines (Figure 2.4)

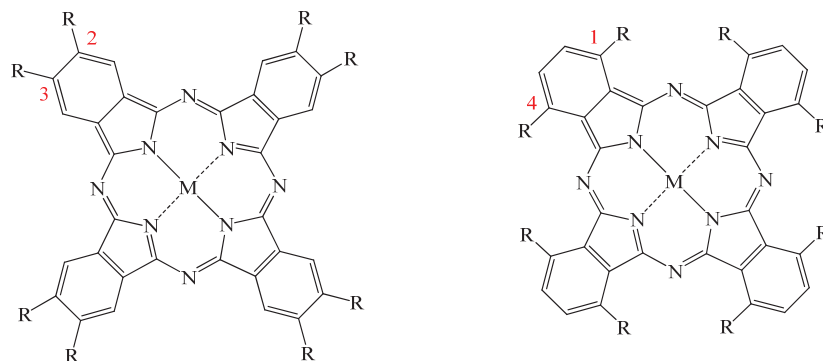


Figure 2.4. 1,4- and 2,3-octasubstituted phthalocyanines.

2.1.2. Methods for the Preparation of Phthalocyanines

It should be noted that the basic reactions used to prepare phthalocyanine derivatives today are fundamentally those developed in the 1930s by Linstead, Wyler, and their co-workers, although with some practical modifications. The various 1,2-disubstituted benzene precursors to metal phthalocyanines are shown in Figure 2.5 [16].

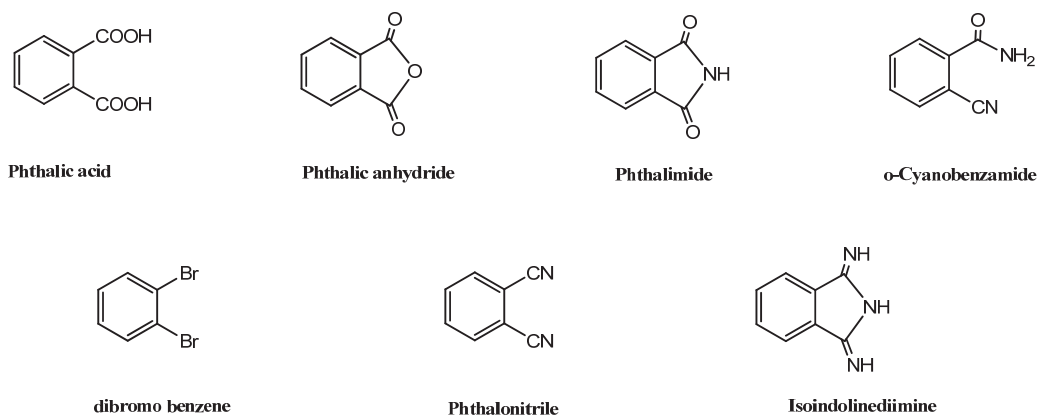


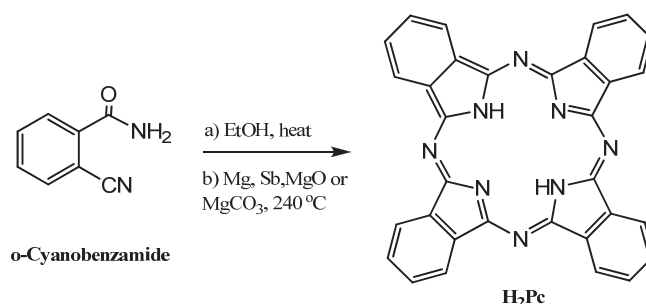
Figure 2.5. Precursors for the Synthesis of Phthalocyanines.

For each of these precursors, the reactants and conditions favor a cyclotetramerization of the precursor to form the phthalocyanine macrocycle. These methods are not discrete as one type of precursor is often an intermediate in the cyclotetramerization reaction of another. For example it is known that phthalonitrile is the intermediate in the copper(I) cyanide induced cyclotetramerization of 1,2-dibromobenzene as, under less forcing conditions, this is a commonly used method of preparing substituted phthalonitriles (the Rosenmund von Braun reaction). Similarly, isoindolinediimine is prepared from the reaction of phthalonitrile with ammonia and it is clearly an intermediate in the cyclotetramerization of phthalonitrile induced by ammonia under more forcing conditions.

2.1.2.1. Metal-free Phthalocyanines

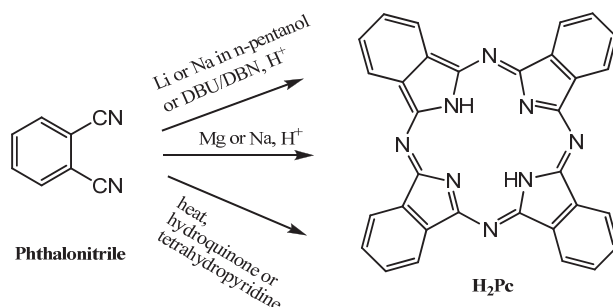
Metal-free phthalocyanines can be obtained directly by the cyclotetramerization of four precursor units, or, in order to benefit from a template effect assistance, from the demetallation of lithium, sodium or magnesium phthalocyanines in acidic conditions.

Most syntheses of metal-free phthalocyanine use either phthalonitrile or isoindolinediimine (diiminoisoindoline) as the starting material. It is also possible to prepare metal-free phthalocyanine from 2-cyanobenzamide by heating in ethanol under reflux (Scheme 2.2.a) to yield the blue product in low yield [1]. Higher yields (40%) were obtained when catalysts like metallic magnesium or magnesium salts were added and the reaction mixture was heated to over 230 °C (Scheme 2.2.b).



Scheme 2.2. Synthesis of metal-free phthalocyanine from o-cyanobenzamide

When phthalonitrile is used as starting material, a very easy synthesis is afforded upon treatment with sodium or lithium in n-pentanol (Scheme 2.3) or other alcohols, at 135-140 °C to give the disodium or dilithium phthalocyanine which could be demetallated with concentrated H₂SO₄ or glacial acetic acid [17,18].



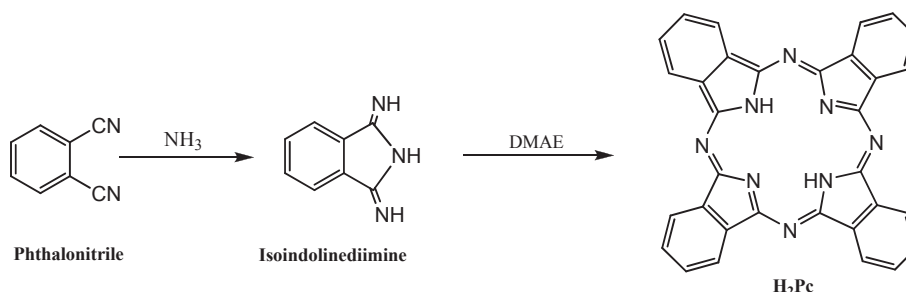
Scheme 2.3. Synthesis of metal-free phthalocyanine from phthalonitrile

Phthalonitrile can also be fused with magnesium or sodium metal (Scheme 2.3) above 200 °C to give the magnesium and sodium phthalocyanines which can be demetallated with concentrated H₂SO₄.

Using reducing agents like hydroquinone, tetrahydropyridine or 4,4'-dihydroxybiphenyl as co-reactants and fusing at 180 °C in a sealed tube yielded the phthalocyanine in 43% yield (Scheme 2.3) [19,20].

Phthalonitrile can easily be converted into 1,3-diiminosoindoline by bubbling gaseous ammonia into a methanol solution of the phthalonitrile at room temperature. When the

1,3-diiminosoindoline was heated in 2-*N,N*-dimethylaminoethanol the substituted metal-free phthalocyanine can be obtained in 85% yield (Scheme 2.4).



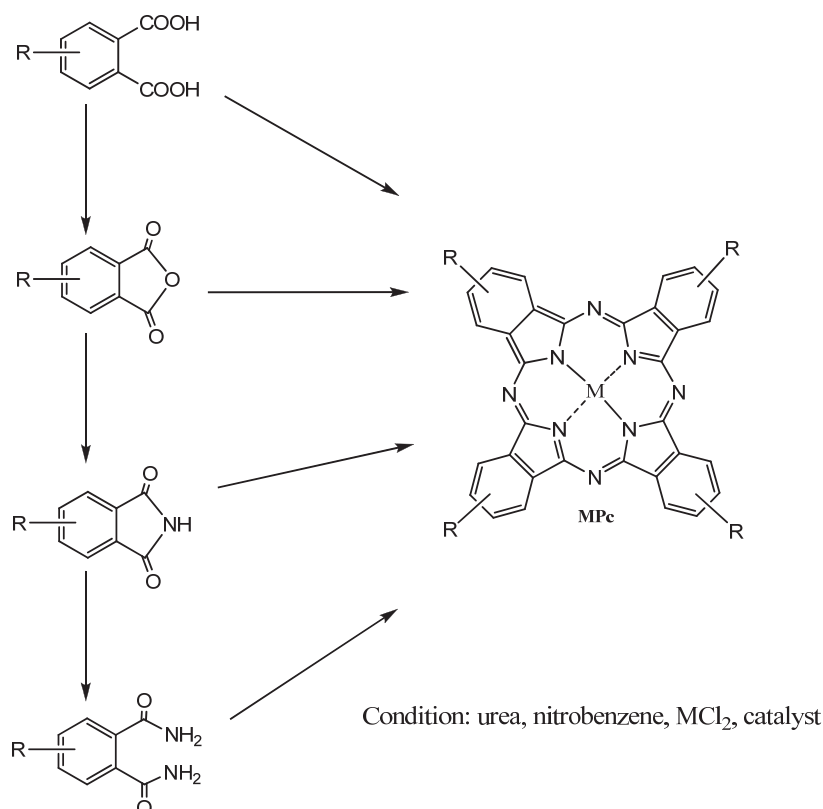
Scheme 2.4. Synthesis of metal-free phthalocyanine from diiminoisoindoline

2.1.2.2. Metallated phthalocyanines

This part will present the different methods available for the preparation of metallated phthalocyanines. As the topic of this thesis is the synthesis of iron phthalocyanines, these methods will be illustrated by examples in which the metal is iron. The precursors presented Figure 2.5 can all be used for the preparation of metal phthalocyanines.

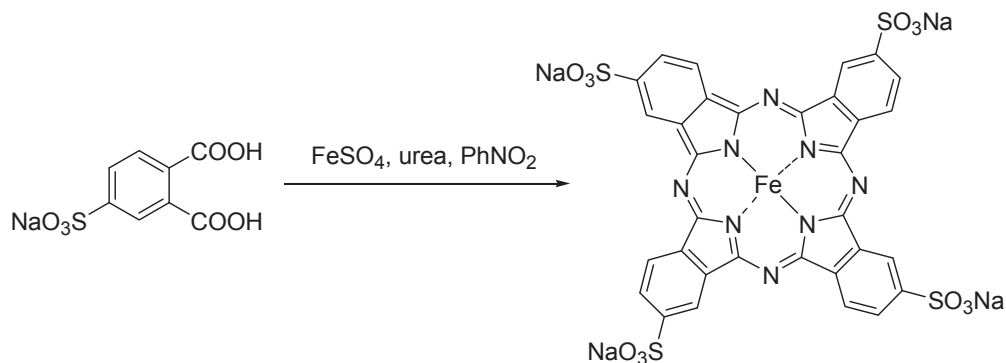
Phthalic acid, phthalic anhydride, phthalimide or phthalamide

Unsubstituted or conveniently substituted phthalic acid, phthalic anhydride, phthalimide or phthalamide together with urea are often used instead of phthalonitrile, and catalysts such as ammonium molybdate may be employed [21-23] to yield metallated substituted phthalocyanines (Wyler method) (Scheme 2.5). Indeed most commercial processes are based on these compounds, especially phthalic anhydrides as starting materials rather than the more expensive phthalonitriles.



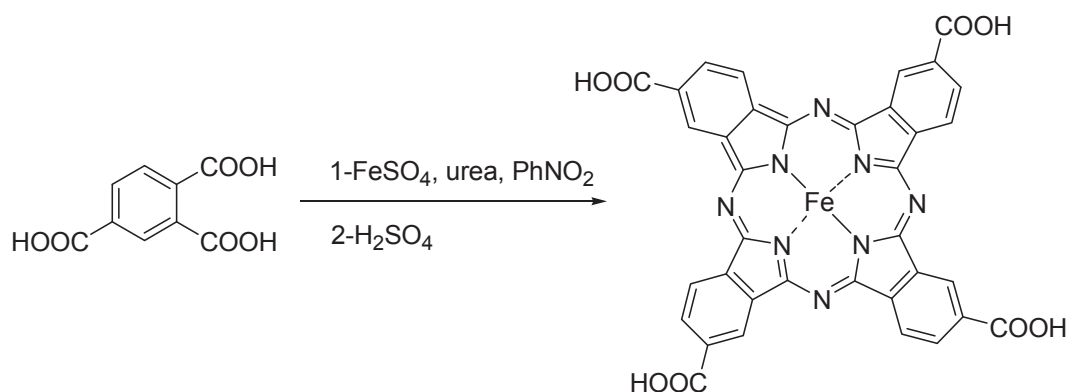
Scheme 2.5. Synthesis of metallated phthalocyanines using substituted phthalic acid, phthalic anhydride, phthalimide or phthalamide as starting materials.

Weber and Bush [24] synthesized the widely employed iron tetrasulfophthalocyanine (FePcS) by refluxing at high temperature (about 180°C) a mixture of the monosodium salt of the 4-sulfophthalic acid, urea and iron salt in nitrobenzene in the presence of ammonium molybdate as catalyst (Scheme 2.6). A mixture of sulfonated FePc complexes (FePcS_{mix}) can be obtained by direct sulfonation of unsubstituted FePc with oleum.

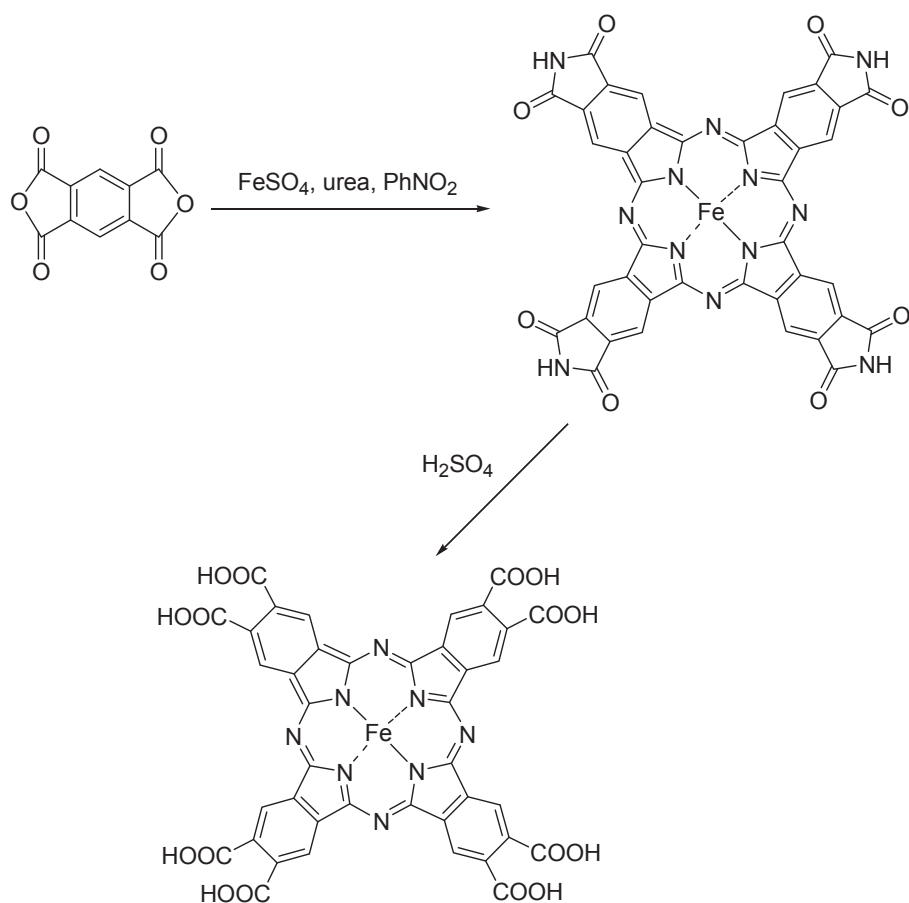


Scheme 2.6. Synthesis of iron tetrasulfophthalocyanine (FePcS).

Iron tetracarboxy- or octacarboxyphthalocyanine (FeTCPc) or (FeOCPc) complexes can be prepared using trimellitic acid or benzene-1,2,4,5-tetracarboxylic dianhydride in the presence of urea. Iron tetraamidophthalocyanine is obtained as the intermediate and is easily converted by acid hydrolysis to iron tetracarboxyphthalocyanine (FeTCPc) (Scheme 2.7) or iron octacarboxyphthalocyanine (FeOCPc) complexes (Scheme 2.8) by reacting with aqueous sulphuric acid.

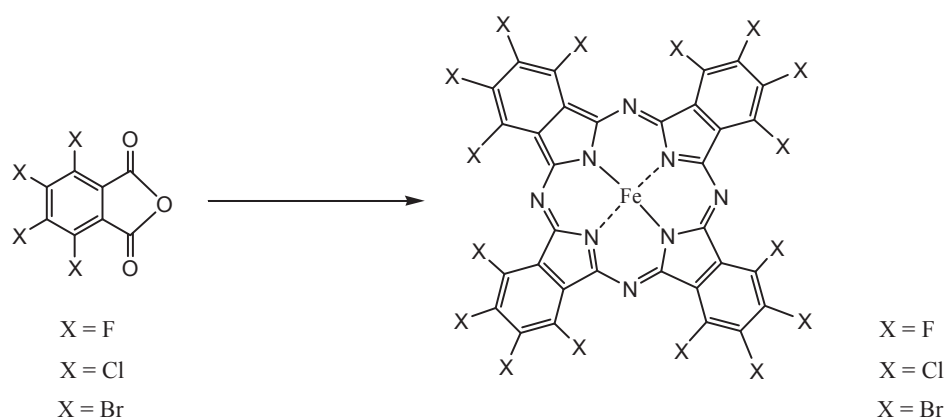


Scheme 2.7. Preparation of iron tetracarboxyphthalocyanine (FeTCPc).



Scheme 2.8. Preparation of octa carboxy (FeOCPC) iron phthalocyanine.

When perhalosubstituted phthalic anhydrides were treated under conditions similar to phthalic acid, the hexadecachlorophthalocyanine, hexadecabromophthalocyanine were obtained in up to 80% yield (Scheme 2.9) [25,26].

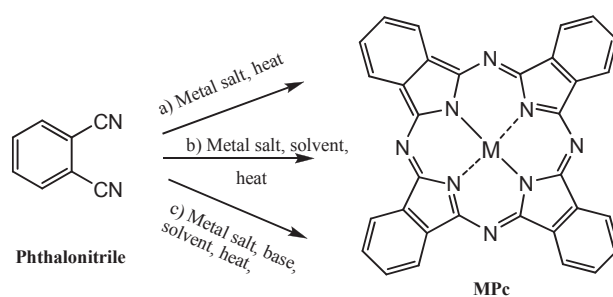


Scheme 2.9. Preparation of iron hexadecahalophthalocyanines.

Phthalimide is clearly an intermediate in the synthesis of metal phthalocyanines from phthalic anhydride and the patent literature is rich in methods that include it as a starting material for phthalocyanine manufacture [27–29].

Phthalonitriles

Heating phthalonitrile with a metal or a metal salt without solvent is a direct and convenient method. It is clear that most reactions are carried out at more than 200 °C. In addition to unsubstituted metal phthalocyanines, substituted derivatives have been prepared using this method (Scheme 2.10.a).



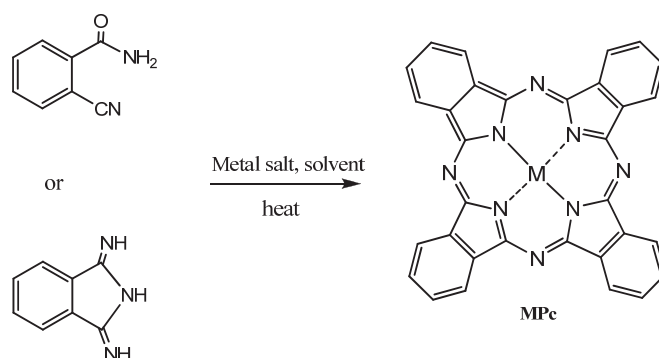
Scheme 2.10. Preparation of Metal Phthalocyanine from Phthalonitrile

Metal phthalocyanines can be prepared from phthalonitrile with suitable metal salts in solution. High boiling solvents such as DMF, DMAE, quinoline and 1-chloronaphthalene are useful to prepare metal phthalocyanines (Scheme 2.10.b).

Using DBU or DBN as a base with metal salt and a solvent such as pentanol provides efficient method to prepare metal phthalocyanine from phthalonitrile (Scheme 2.10.c).

Diiminoisoindoline or o-cyanobenzamide

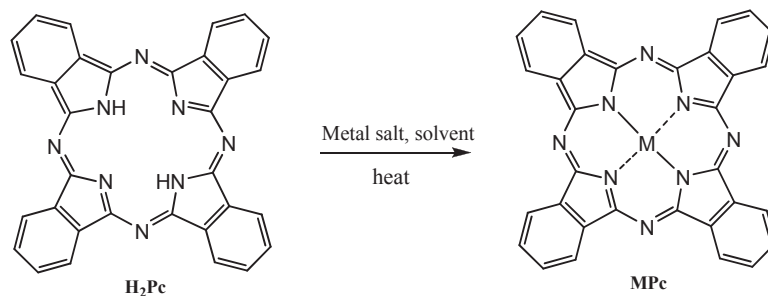
Reactions between diiminoisoindoline or o-cyanobenzamide and a finely divided metal, metal hydride or metal chloride may also be employed to yield the particular metallated phthalocyanine (Scheme 2.11).



Scheme 2.11. Preparation of Metal Phthalocyanine from Diiminoisoindoline or o-cyanobenzamide.

Metallation of free-phthalocyanines

Metal-free phthalocyanines are also metallated by refluxing with the appropriate metal or metal salt in solvents like quinoline or DMF (Scheme 2.12).



Scheme 2.12. Preparation of Metal Phthalocyanine from Metal-free Phthalocyanine

Substituted iron phthalocyanines are prepared as unsubstituted ones, according to these described methods. Complexes FePcR containing different numbers of substituents R, where R is a halogen atom or alkyl, aryl, nitro, alkoxy, aryloxy, alkylthio, arylthio, arylsulfonyl, polyfluoroalkoxy, polyfluorosulfamoyloxy, carboxy, sulfo, etc. groups, are described in the literature [30-42].

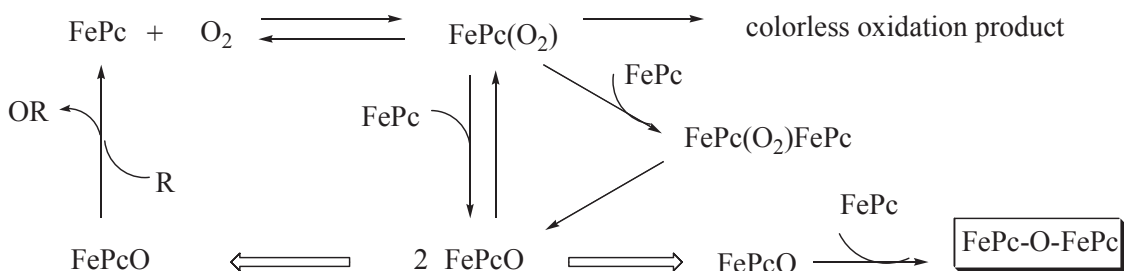
2.2. Single atom bridged diiron phthalocyanines

The nature of iron permits the presence of axial substituents. This property is used to prepare various single atom bridged diiron phthalocyanines. These diiron phthalocyanines can be represented by the formula PcFe-X-FePc , X being O (μ -oxo species), C (μ -carbido species) or N (μ -nitrido species).

2.2.1. Dimeric μ -oxo iron phthalocyanines

In 1965, a first μ -peroxo dimeric complex was reported. It was prepared by adding oxygen to iron (II) tetrasulfophthalocyanine (FePcS) in aqueous solution [43]. Dale reported that unsubstituted iron(II) phthalocyanine in dimethyl sulfoxide (Me_2SO) were unstable in air [44]. Jones and Twigg observed later that solutions of FePc were unstable

in air or in the presence of pure oxygen [45], this was then attributed to the formation [FePc-O-FePc] (Scheme 2.13).



Scheme 2.13. Mechanism of the formation of [FePc-O-FePc]

Ercolani et al. [46] investigated the interaction of FePc with dioxygen and identified the conditions for the interaction between the two species in concentrated H_2SO_4 . It was shown two different crystalline forms of μ -oxo iron phthalocyanine dimer (μ -oxo (1) and μ -oxo (2)) can be prepared depending on experimental conditions (Figure 2.6) [47]. The first μ -oxo (1) dimer was proposed to possess a bent structure while μ -oxo (2) species has linear Fe-O-Fe fragment.

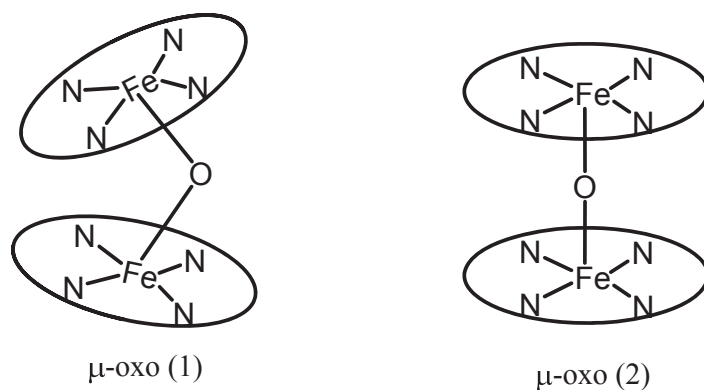


Figure 2.6. Schematic representation of μ -oxo(1) and μ -oxo (2).

Several tetra- and octasubstituted μ -oxo diiron phthalocyanines represented in Figure 2.7 have been studied by mass spectrometry, UV-vis, Mössbauer, NMR and EPR techniques [48]. Mössbauer and magnetic susceptibility data indicate the presence of

antiferromagnetically interacting couples of high-spin (5/2, 5/2) Fe(III) for both isomers [49-51]. The isomer shift and quadrupole splitting values for the μ -oxo (1) are 0.36 and 0.44 mm s⁻¹, and for the μ -oxo(2) are 0.26 and 1.26 mm s⁻¹, respectively. The antiferromagnetic constants J, obtained from measurements in the range 300-4 K, are respectively -120 and -195 cm⁻¹ for μ -oxo(1) and μ -oxo(2) isomers. Voltammetry studies in pyridine, where species were in the [(pyridine) FePc]₂O form, showed two oxidation couples at 0.47 (removal of an electron from Fe) and 0.87 V, and two reductions at - 0.59 and -0.95 V [52].

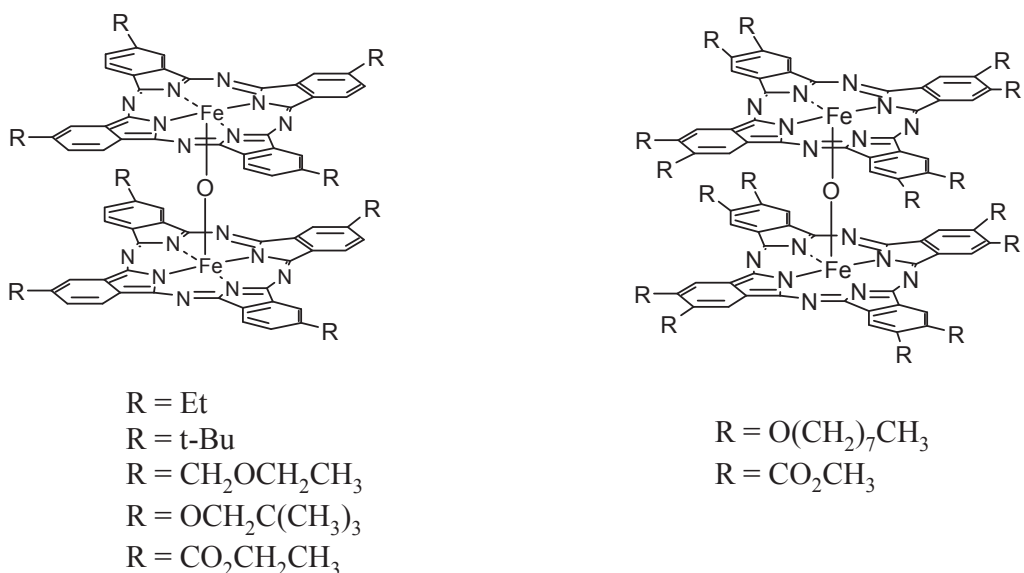


Figure 2.7. Substituted μ -oxo diiron phthalocyanines

2.2.2. Dimeric μ -carbido iron phthalocyanines

The first μ -carbido complex, μ -carbido bis(tetraphenylporphyrinatoiron), [(TPP)Fe=C=Fe(TPP)], was reported by Mansuy et al in 1981[53]. (FePc)₂C was obtained by reacting FePc with Cl₄ in chloronaphthalene at 140-150°C for 30 min in the presence of reducing reagents such as sodium dithionite or iron powder [55,56]. This μ -carbido dimer was also characterized structurally [54]. FePc=C=FePc showed an

antisymmetric Fe-C-Fe stretching vibration at 990 cm^{-1} , a Q band peak at 620 nm in pyridine, and isomer shift and quadruple splitting values of -0.16 and 2.69 mm s^{-1} at 77 K. The negative value of the isomer shift in Mössbauer spectrum indicates that iron is in +4 oxidation state.

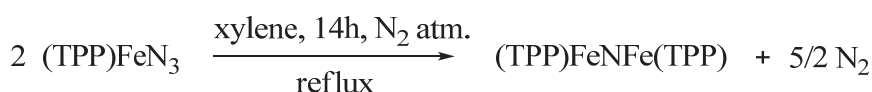
Comparison of the IR data of μ -carbido and μ -oxo diiron complexes is given in Table 2.1. IR spectrum with specific absorption at 940 (for [(TPP)Fe-C-Fe(TPP)]) and 990 (for [FePc-C-FePc]) cm^{-1} to be assigned as ν (Fe-C-Fe), μ -oxo diiron complexes show characteristic Fe-O-Fe peak at 885 (for [(TPP)Fe-O-Fe(TPP)]) and 852 (for [FePc-O-FePc]) cm^{-1} .

Table 2.1. Comparison of the IR data of μ -carbido and μ -oxo diiron complexes.

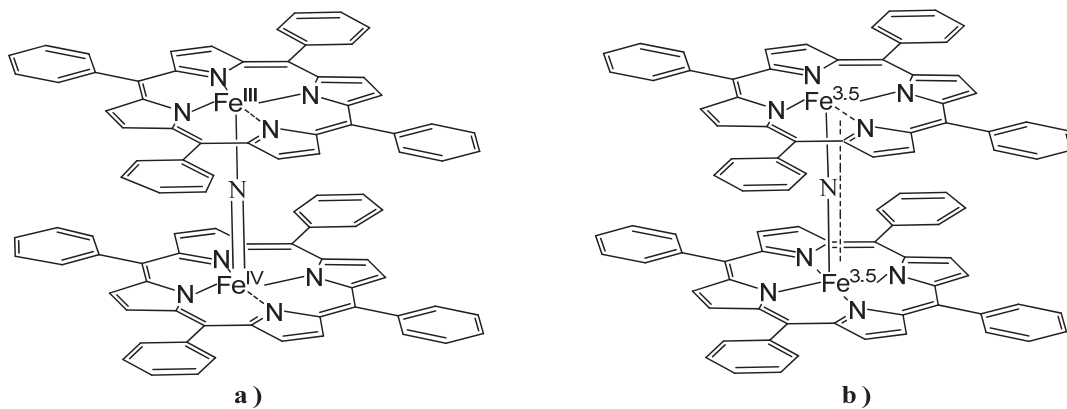
| Compound | ν (Fe-C-Fe) (cm^{-1}) | ν (Fe-O-Fe) (cm^{-1}) |
|---------------------|--------------------------------------|--------------------------------------|
| [(TPP)Fe-C-Fe(TPP)] | 940 | - |
| [FePc-C-FePc] | 990 | - |
| [(TPP)Fe-O-Fe(TPP)] | - | 885 |
| [FePc-O-FePc] | - | 852, 824 |

2.2.3. N-bridged diiron phthalocyanines

The first μ -nitrido species with tetrapyrrolic macrocycles belonging to the class of formula (L)M-N-M(L), (TPP)Fe-N-Fe(TPP) (TPP = tetraphenylporphyrinato anion) was described in 1976. It was extensively investigated and the conclusion was drawn for the presence of both iron centres in the oxidation state +3.5 (Scheme 2.14) [57]. The μ -nitrido bis(tetraphenylporphyrinatoiron) [(TPP)Fe-N-Fe(TPP)] was prepared by thermal or photochemical decomposition of the monomeric azide [(TPP)FeN₃].



(TPP)FeNFe(TPP):



Scheme 2.14. The first μ -nitrido diiron porphyrin complex, a) formally Fe(III)NFe(IV) localized structure and b) Fe(3.5)NFe(3.5) delocalized structure.

[(TPP)Fe-N-Fe(TPP)] is characterized by the presence of Fe-N-Fe band at 910 cm^{-1} in the IR spectrum (Figure 2.8) and by a single doublet in its Mössbauer spectrum exhibit of the presence of only one type Fe center. Although the complex is a formally mixed valence Fe^{III}-Fe^{IV} species, but it is generally accepted that, owing to the electron delocalization, two Fe centers have both an intermediate oxidation state +3.5.

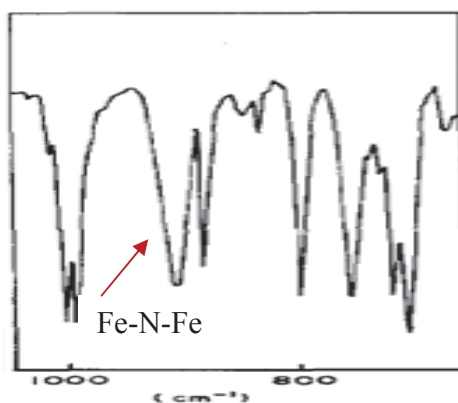
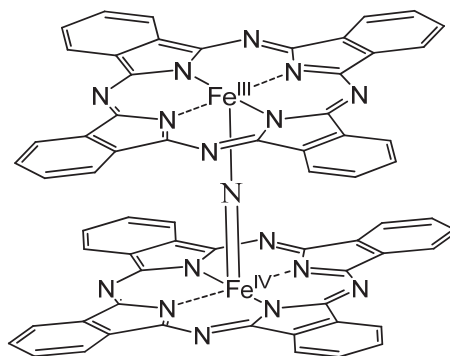


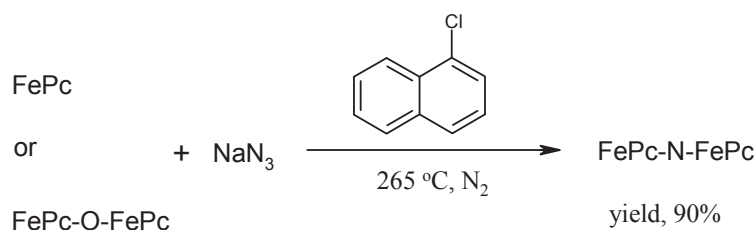
Figure 2.8. IR spectra of [(TPP)Fe-N-Fe(TPP)].

The analogous phthalocyanine counterpart was also prepared and intensively studied. It was shown that the Fe centers also share the same oxidation state (+3.5), $\text{PcFe}^{3.5}\text{-N-Fe}^{3.5}\text{Pc}$ (Scheme 2.15) [58].



Scheme 2.15. The first μ -nitrido diiron phthalocyanine.

This unsubstituted μ -nitrido diiron phthalocyanine was prepared by the reaction of iron phthalocyanine (FePc) with NaN_3 in 1-chloronaphthalene (Scheme 2.16), apparently through the intermediacy of an unstable metal azide specie.



Scheme 2.16. Preparation of FePc-N-FePc complex

No single-crystal X-ray work is available for $[\text{FePc-N-FePc}]$. However, the complex is isomorphous with its μ -oxo analogs $[\text{FePc-O-FePc}]$ (μ -oxo (2)) and $[\text{MnPc-O-MnPc}]$. Available data support the presence of a linear Fe-N-Fe triatomic system in a formally mixed valence Fe(III)-Fe(IV) complex. The IR spectrum of μ -nitrido diiron phthalocyanine shows characteristic Fe-N-Fe vibration at 915 cm^{-1} . Its Mössbauer

spectrum shows single doublet ($\delta = 0.06 \text{ cm}^{-1}$), supporting the presence of two equivalent Fe centers (Figure 2.9 and Figure 2.10). Therefore, both Fe centers have the intermediate oxidation state +3.5 in the proposed formulation $[\text{FePc}^{3.5}\text{-N-FePc}^{3.5}]$ similarly with TPP dimer.

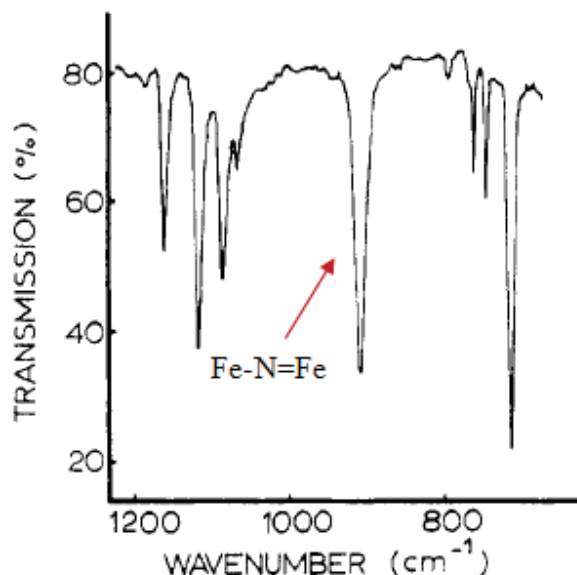


Figure 2.9. IR spectrum of unsubstituted $[\text{FePc-N-FePc}]$.

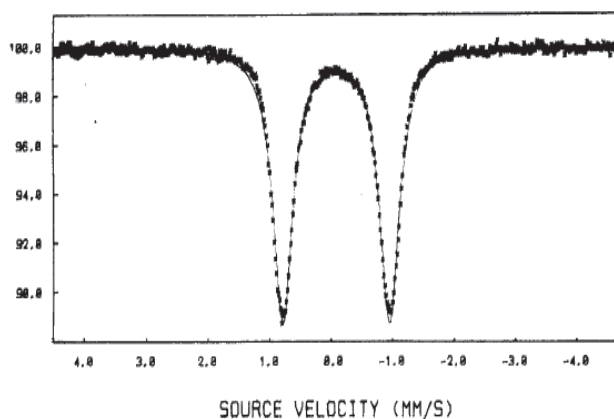


Figure 2.10. Mössbauer spectra of $[\text{FePc-N-FePc}]$.

The EPR spectrum (Figure 2.11) obtained at 77 K on a solid sample of $[\text{FePc}]_2\text{N}$ shows a typically axially symmetry spectrum ($g = 2.03$, $g = 2.13$), consistent with a low-spin complex having an A_1 ground state. These parameters are similar to those observed for $[\text{Fe}(\text{TPP})]_2\text{N}$ [59].

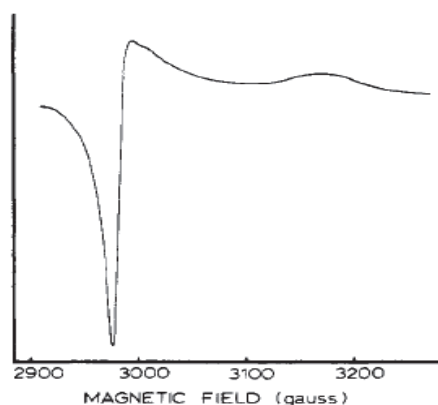


Figure 2.11. EPR spectrum of solid unsubstituted [FePc-N-FePc].

There are a number of interesting aspects associated with the synthesis and characterization of μ -nitrido complexes of general formulas (Pc)M–N–M(Pc), (Pc)M–N–M(P) and (Pc)M–N–M'(P) with M and M' = transition metal ions:

- (a) Reaction mechanisms of formation of formally mixed valence $M^{III}\text{--}N\text{--}M^{IV}$ or $M^{III}\text{--}N\text{--}M^{IV}$ species,
- (b) Extensive electronic charge redistribution and magnetic coupling occurring for the two metal ions operated by the bridging N atom along the linearly arranged M–N–M moiety,
- (c) Oxidation state for the Fe atoms >3 and easy access to stable materials containing iron in a high-valent state, e.g. Fe (IV),
- (d) ‘Metal-centred’ or ‘ligand-centred’ monoelectronic oxidation occurring as a function of the specific nature of the species under investigation,
- (e) Chemical and electrochemical redox behaviour.

μ -nitrido diiron phthalocyanine or porphyrin complexes can be oxidized by $H_5PV_2Mo_{10}O_{40}$ or by ferrocenium hexafluorophosphate. Single doublet in its Mössbauer spectrum with negative isomer shift value (-0.10 mm s^{-1}) indicates two equivalent Fe (IV) sites. Therefore, the oxidized complex can be formulated as $[FePc^{IV}\text{--}N\text{--}FePc^{IV}]^+$. The Mössbauer spectra of $[FePc^{IV}\text{--}N\text{--}FePc^{IV}](PF_6)$, and $[(py)FePc^{IV}\text{--}N\text{--}FePc^{IV}(py)](PF_6)$ are presented in Figure 2.12.

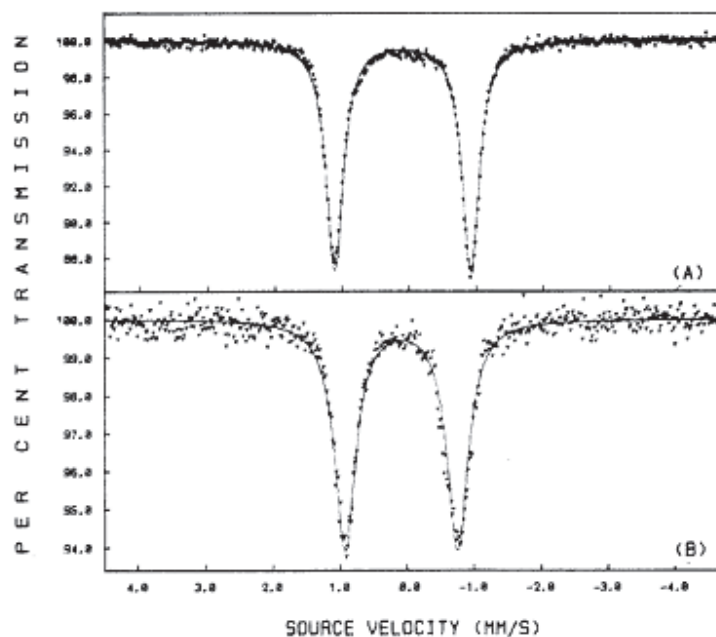


Figure 2.12. Mössbauer spectra of $[\text{FePc}^{\text{IV}}\text{-N-FePc}^{\text{IV}}](\text{PF}_6)$ (A), and $[(\text{py})\text{FePc}^{\text{IV}}\text{-N-FePc}^{\text{IV}}(\text{py})](\text{PF}_6)$ (B).

In the Mössbauer spectra of the oxidized $[\text{FePc}^{\text{IV}}\text{-N-FePc}^{\text{IV}}](\text{PF}_6)$ and $[(\text{py})\text{FePc}^{\text{IV}}\text{-N-FePc}^{\text{IV}}(\text{py})](\text{PF}_6)$, only one quadrupole doublet is observed with a isomer shift of -0.09 and -0.10 mm/s and a quadrupole splitting in the 2.06 and 1.76 mm/s. The isomer shift values are definitely lower, as expected, than those found in the series of $(\mu\text{-oxo})\text{Fe(III)}$ complexes and for the precursor, $[\text{FePc}^{+3.5}\text{-N-FePc}^{+3.5}]$, and fall in the range expected for Fe(IV) as is the case of $[\text{FePc}^{\text{IV}}\text{-N-FePc}^{\text{IV}}](\text{PF}_6)$. Thus, conversion of $[\text{FePc}^{\text{IV}}\text{-N-FePc}^{\text{IV}}](\text{PF}_6)$ into its corresponding six-coordinate N-base adducts leaves the positive charge entirely located on the two Fe ions of these bimetallic systems.

Oxidation of $[\text{FePc}^{3.5}\text{-N-FePc}^{3.5}]$ with bromine, trifluoroacetic acid, or concentrated nitric acid leads to $[(\text{Br})\text{FePc-N-FePc}(\text{Br})]\text{Br}$, $[(\text{CF}_3\text{CO}_2)\text{FePc-N-FePc}(\text{CF}_3\text{CO}_2)](\text{CF}_3\text{CO}_2)$, $[(\text{NO}_3)\text{FePc-N-FePc}(\text{NO}_3)](\text{NO}_3)$ complexes, which contain Fe(IV) as indicated by Mössbauer data [60]. The structure of $[(\text{Br})\text{FePc-N-FePc}(\text{Br})]$ obtained by electrochemical oxidation of $[\text{FePc-N-FePc}]$ in DMF/LiBr containing hexacoordinated Fe centers and linear Br-Fe-N-Fe-Br fragment was reported (Figure 2.13) [60].

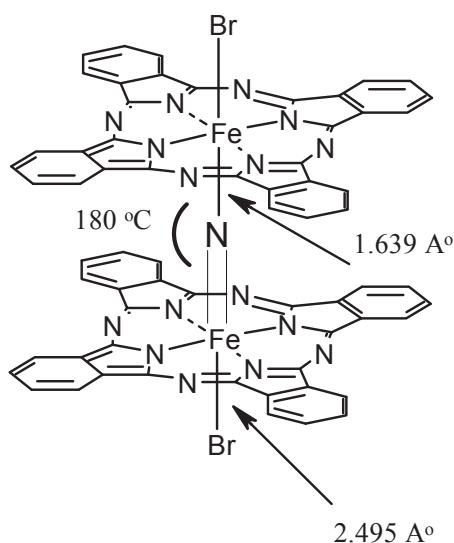


Figure 2.13. Structure of $[(\text{Br})\text{FePc-N-FePc}(\text{Br})]$.

Although a number of N-bridged binuclear complexes on phthalocyanine and porphyrin as well as mixed ligand systems [61] have been described (Figure 2.14), they often contain unsubstituted macrocyclic ligands. Because of that, these μ -nitrido binuclear complexes exhibit only limited solubility in common organic solvents.

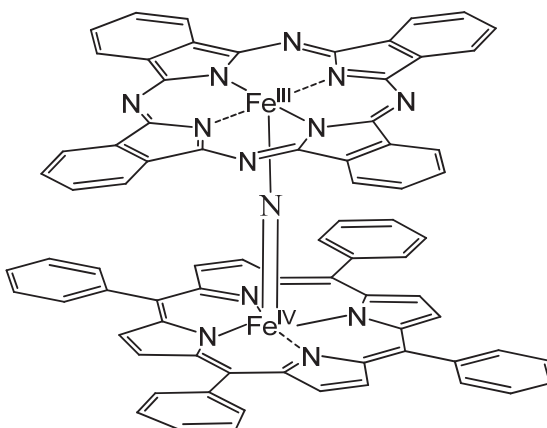


Figure 2.14. The mixed ligand system of μ -nitrido diiron complex.

The mixed ligand complex $[(\text{TPP})\text{Fe-N-FePc}]$ is stable under air and at high temperatures ($>300\text{ }^{\circ}\text{C}$) under inert atmosphere. IR spectrum of $[(\text{TPP})\text{Fe-N-FePc}]$ shows characteristic Fe-N-Fe vibration at 930 cm^{-1} .

Table 2.2. The characteristic Fe-N-Fe vibration values of μ -nitrido complexes.

| Compound | IR [ν (Fe-N-Fe) (cm^{-1})] |
|---------------------|----------------------------------------------------------------------|
| [(TPP)Fe-N-Fe(TPP)] | 910 |
| [FePc-N-FePc] | 915 |
| [(TPP)Fe-N-FePc] | 930 |

Table 2.2 shows that the absorption of [(TPP)Fe-N-FePc] is located at higher frequency than those observed for [(TPP)Fe-N-Fe(TPP)] (910 cm^{-1}) and for [FePc-N-FePc] (915 cm^{-1}).

Table 2.3. Mössbauer data of μ -nitrido species

| Complex | $\delta / \text{mm s}^{-1}$ | $\Delta E_Q / \text{mm s}^{-1}$ | $\Gamma / \text{mm s}^{-1}$ | Iron state | T /K |
|---------------------|-----------------------------|---------------------------------|-----------------------------|-------------------|-------------|
| [(TPP)Fe-N-Fe(TPP)] | 0.148 | 1.07 | 0.44 | Fe (+3.5) | 77 |
| [FePc-N-FePc] | 0.06 | 1.76 | 0.19 | Fe (+3.5) | 77 |
| [(TPP)Fe-N-FePc] | 0.13 | 1.45 | 0.32 | Fe (+3.5) | 77 |
| [(TPP)Mn-N-FePc] | 0.19 | 1.21 | 0.13 | Fe (+3) | 78 |
| [(TPP)Fe-N-RuPc] | 0.03 | 0.90 | 0.22 | Fe (+4) | 78 |

The Mössbauer spectrum of [(TPP)Fe-N-FePc] shows a doublet with an isomer shift $\delta = 0.13 \text{ mm s}^{-1}$ and a quadrupolar splitting $\Delta E_Q = 1.45$. These values are between values of [(TPP)Fe-N-Fe(TPP)] ($\delta = 0.148 \text{ mm s}^{-1}$, $\Delta E_Q = 1.07 \text{ mm s}^{-1}$) and values of [FePc-N-FePc] ($\delta = 0.06 \text{ mm s}^{-1}$, $\Delta E_Q = 1.76 \text{ mm s}^{-1}$) (Table 2.3).

Heterobimetallic μ -nitrido species with identical or different ligands have recently been described, containing the phthalocyanine macrocycle (Figure 2.15) [62].

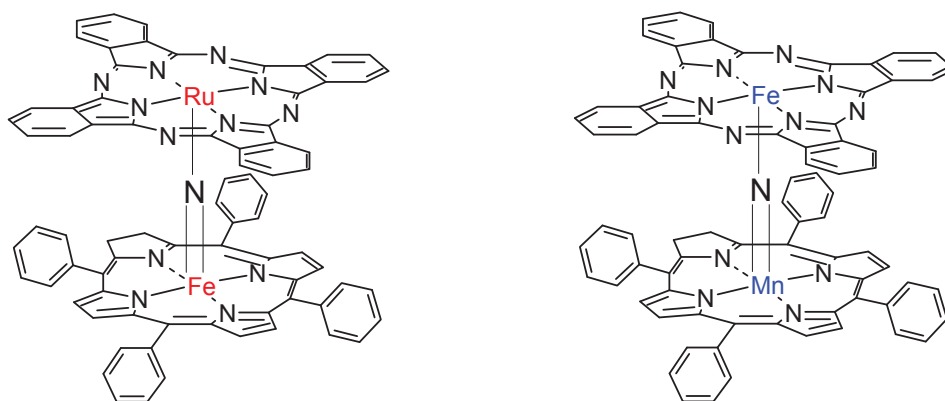
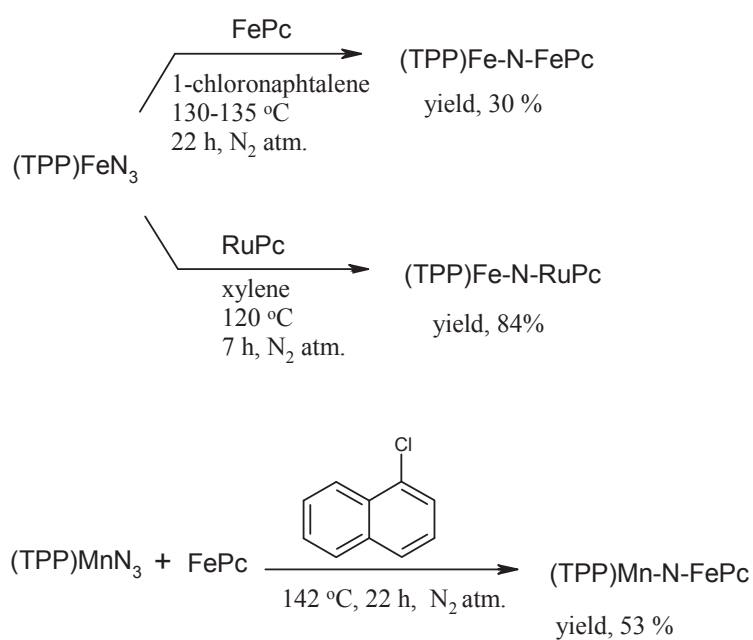


Figure 2.15. Heterobimetallic μ -nitrido complexes

These species were prepared via the corresponding azido complexes according to Scheme 2.17.



Scheme 2.17. Preparation of mixed ligands and mixed metal μ -nitrido species.

Reaction of $[(\text{TPP})\text{FeN}_3]$ with RuPc gave the first example of a μ -nitrido dinuclear heterometallic and heteroleptic complex, $[(\text{TPP})\text{Fe-N-RuPc}]$ [61]. The Mössbauer data

for [(TPP)Fe-N-RuPc] ($\delta = 0.03 \text{ mm s}^{-1}$, $\Delta E_Q = 0.90 \text{ mm s}^{-1}$) evidenced the formulation [(TPP)Fe^{IV}-N-Ru^{III}Pc] (Figure 2.16).

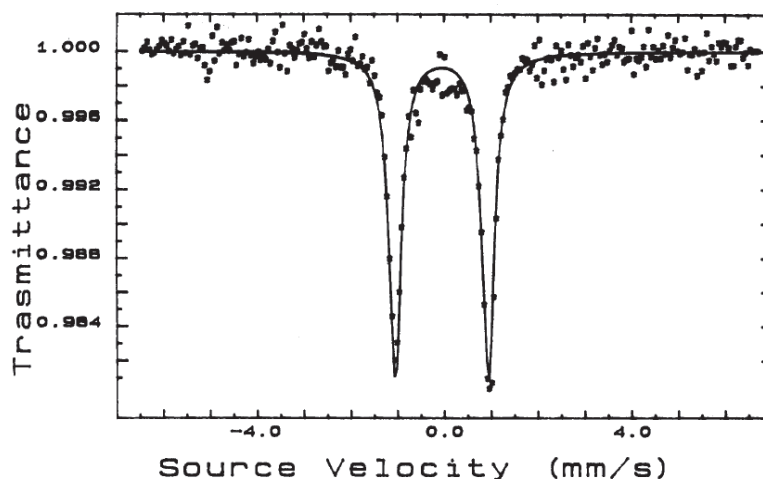


Figure 2.16. Mössbauer spectrum of [(TPP)Fe-N-RuPc].

The [(TPP)Mn-N-FePc] complex was prepared by reaction of corresponding [(TPP)MnN₃] with FePc in 1-chloronaphthalene. Their molecular and electronic structures were characterized by EPR, IR, Raman, UV-Vis, Mössbauer spectroscopies, and X-ray study. Mössbauer spectrum shows a doublet with isomer shift $\delta = 0.19 \text{ mm s}^{-1}$ and quadrupolar splitting $\Delta E_Q = 1.21 \text{ mm s}^{-1}$ (Table 2.3).

All these μ -nitrido diiron phthalocyanines, bearing either same ligands or different ligands and metals were unsubstituted complexes. These unsubstituted dimers are insoluble in common organic solvents that makes their purification and use difficult. This kind of complexes were generally believed to be catalytically inactive, thus they have never been used as oxidation catalysts. Nevertheless, Sorokin and co-workers have recently discovered remarkable catalytic properties of diiron μ -nitrido tetra-*t*-butylphthalocyanine (FePc^{*t*}Bu₄)₂N), in particular in the oxidation of methane and benzene at unprecedentedly mild conditions (Figure 2.17) [63].

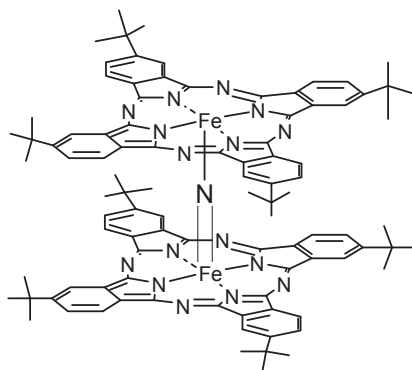


Figure 2.17. Organosoluble (FePc^tBu₄)₂N.

IR spectra of (PcFe^tBu₄)₂N exhibits strong absorption at 938 cm⁻¹ due to Fe-N-Fe anti-symmetric stretching mode (Figure 2.18). These values are close to this observed for unsubstituted (PcFe)₂N at 915 cm⁻¹.

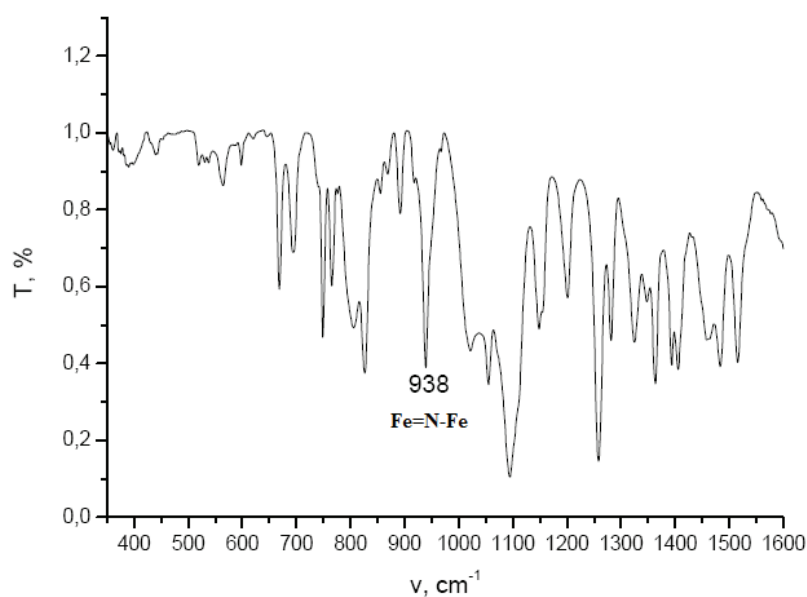


Figure 2.18. IR spectrum of (FePc^tBu₄)₂N.

(FePc^tBu₄)₂N interacts with biologically and ecologically relevant H₂O₂. The addition of H₂O₂ to a solution of (FePc^tBu₄)₂N changed UV-Vis and EPR spectra (Figure 2.19 and Figure 2.20). The intensity of Q band at 636 nm ($\pi - \pi^*$ phthalocyanine transition) was increased and weak band at 710 nm disappeared. These changes indicate a metal-centered

reaction with H_2O_2 without significant transformation of phthalocyanine macrocycle and monomerization. Monomeric phthalocyanine forms exhibit Q band in 665 – 680 nm region. The rate of the spectral changes correlates with H_2O_2 concentration (A). These observations indicate the interaction of H_2O_2 with diiron N-bridged phthalocyanine.

$(\text{FePc}^t\text{Bu}_4)_2\text{N}$ exhibited a signal at $g = 1.99$ indicative of one unpaired electron and of a low spin Fe(III) state, after addition of H_2O_2 at 25 °C, a strong signal at $g = 4.25$ and a feature at $g = 8.16$ along with an enlarged signal at $g = 2.07$ and a small signal at $g = 1.99$ of the $(\text{FePc}^t\text{Bu}_4)_2\text{N}$ left were detected (Figure 2.20).

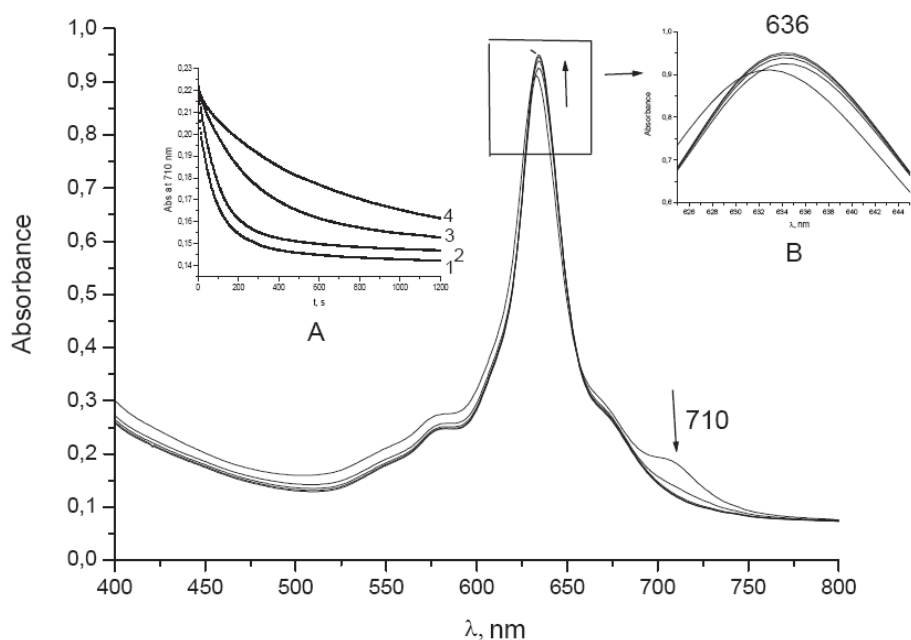


Figure 2.19. UV-Vis spectral changes during the reaction of $(\text{FePc}^t\text{Bu}_4)_2\text{N}$ with 1000 equivs of H_2O_2 . (A) : kinetic curves of interaction of $[(\text{FePc}^t\text{Bu}_4)_2\text{N}$ with H_2O_2 ; $[\text{H}_2\text{O}_2] = 3.4 \times 10^{-3}$ M (curve 1), 2.26×10^{-3} (curve 2), 5.65×10^{-4} (curve 3), 2.82×10^{-4} (curve 4).

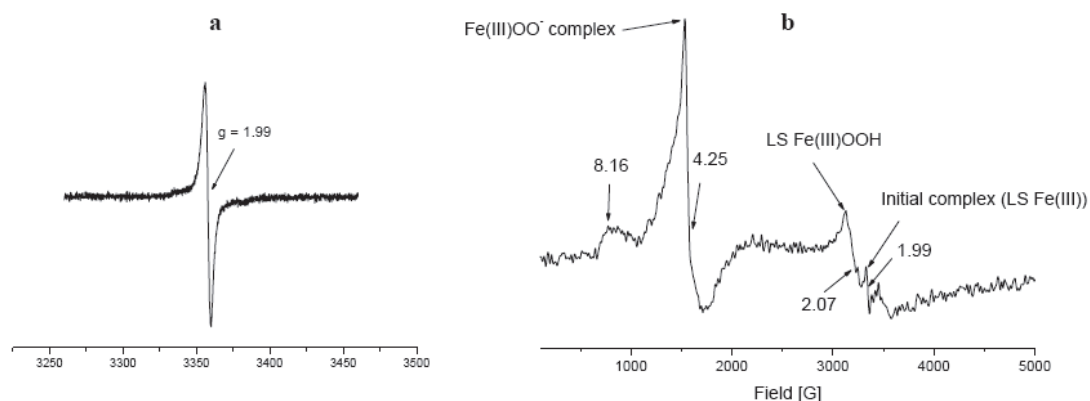
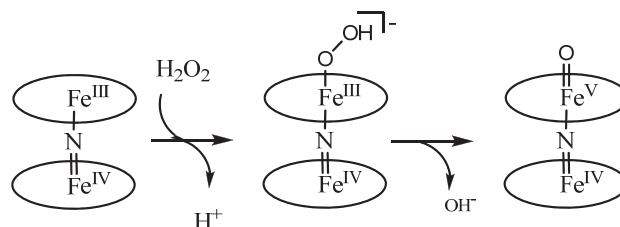


Figure 2.20. EPR spectra of (FePc^tBu₄)₂N in acetone after addition of 5 equivs of H₂O₂

(FePc^tBu₄)₂N coordinates H₂O₂ to form hydroperoxo complex Fe^{IV}NFe^{III}OOH which is probably in equilibrium with the deprotonated form Fe^{IV}NFe^{III}OO⁻. (FePc^tBu₄)₂N oxo complex could be formed from Fe^{IV}NFe^{III}OOH via heterolytic cleavage of the O–O bond (Scheme 2.18).



Scheme 2.18. Proposed mechanism of the formation of high valent diiron oxo species in (FePc^tBu₄)₂N–H₂O₂ system

XPS spectrum of (FePc^tBu₄)₂N was given in Figure 2.21. The 1s N XPS spectrum along with strong signal at 398.7 eV from nitrogen atoms of phthalocyanine cycle exhibits a small signal at 402.4 eV which can be assigned to strongly bonded bridging nitrogen.

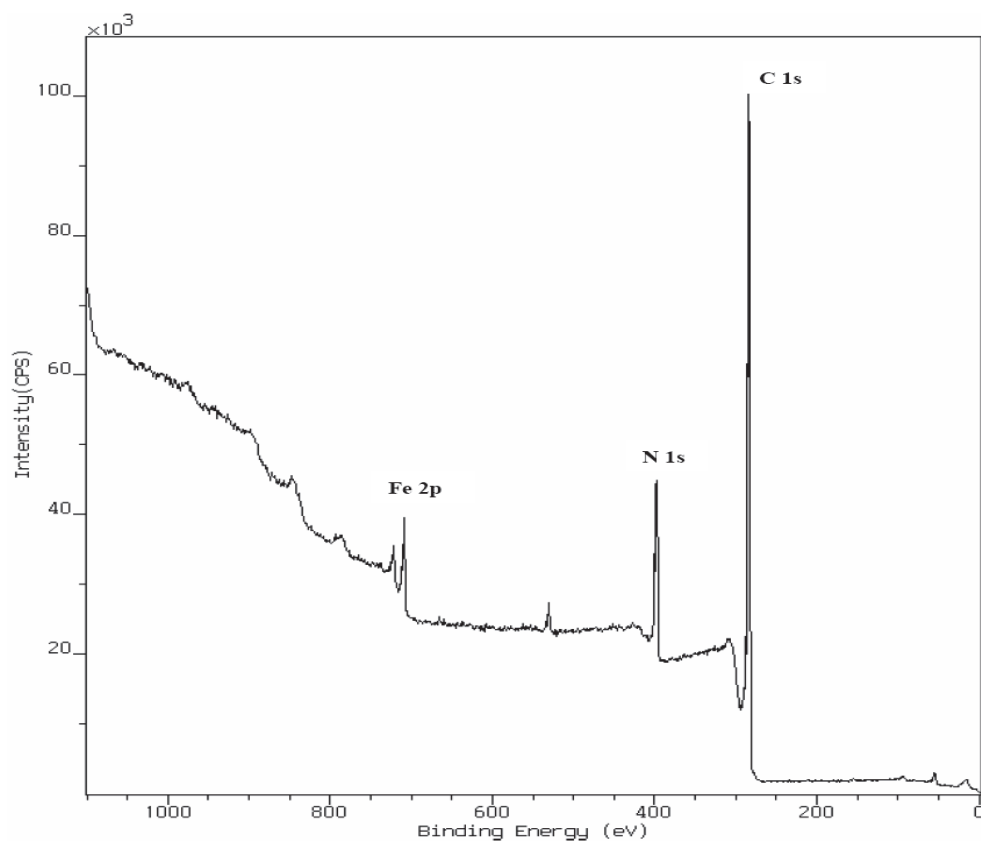
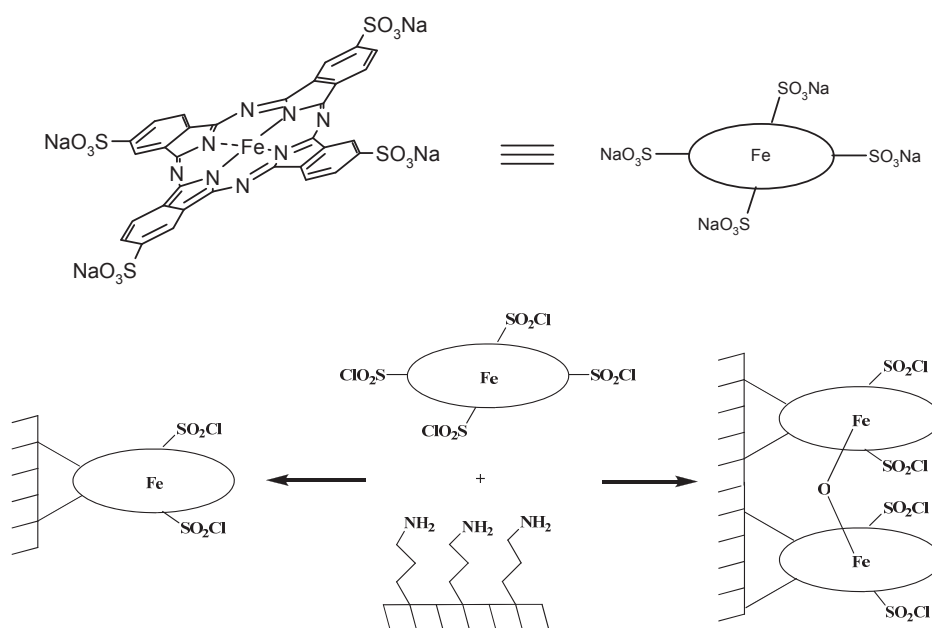


Figure 2.21. XPS spectrum of $(\text{FePc}^t\text{Bu}_4)_2\text{N}$

2.2.4. Supported Iron Phthalocyanines

Solubility of phthalocyanines in the common organic solvents is important for their use as homogeneous catalysts and for mechanistic studies. From practical point of view, it is desirable to separate and to re-use the catalysts after reaction. Heterogeneous catalysts generally offer the advantage of simple separation and recovery. Phthalocyanine complexes can be supported onto different supports to obtain heterogeneous catalysts. Metallophthalocyanines have been fixed onto zeolites [64] and polydimethylsiloxane membranes [65,66], activated carbon black [67], MCM-41-type molecular sieves [68]

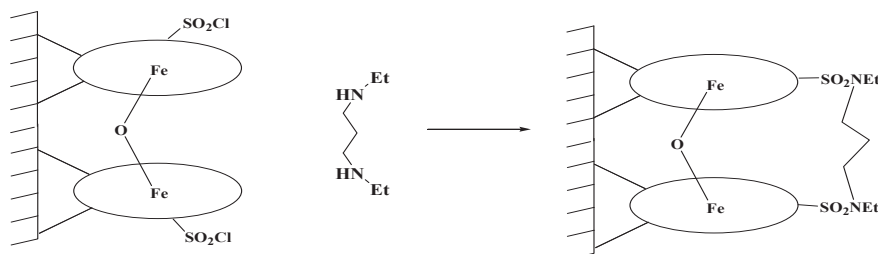
and by sol-gel processing [69]. The fixation of iron phthalocyanines onto suitable supports could provide selective and stable catalysts with facile recovery and recycling. Supported phthalocyanine catalysts were prepared by fixation of monomeric and dimeric forms of FePcS onto amino-modified silica and were used for the selective oxidation of aromatic compounds. Firstly, FePcS was reacted with SO_2Cl to be converted into the corresponding $\text{FePc}(\text{SO}_2\text{Cl})_4$, $\text{FePc}(\text{SO}_2\text{Cl})_4$ was fixed to amino modified mesoporous MCM-41 (Schema 2.19) [70].



Scheme 2.19. Schematic representation of the monomeric and dimeric FePcS catalysts supported on silica.

These supported iron phthalocyanines were tested towards the oxidation of 2,3,6-trimethylphenol to trimethyl-1,4-benzoquinone (precursor of vitamin E) and naphthalene, 2-methylnaphthalene and 2,3-dimethylnaphthalene to corresponding quinones. Noteworthy, dimeric supported catalysts were more active and selective in these aromatic oxidations. However, μ -oxo-dimer structure is unstable during oxidation reactions undergoing transformation to monomer supported species which are less active and selective [71a,71b].

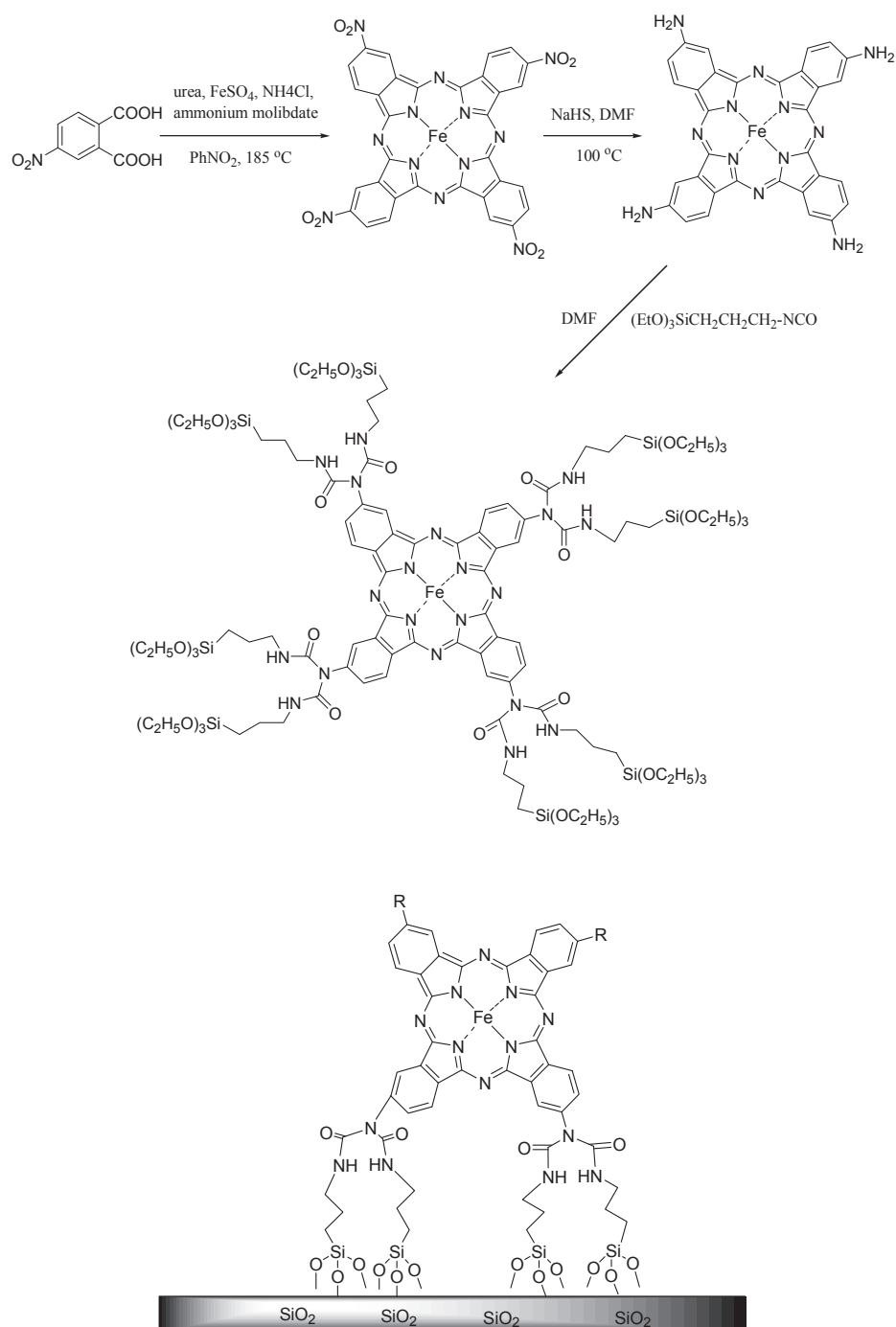
The supported dimer structure can be reinforced by a covalent linking between two phthalocyanines, established by the two amino functions of *N,N'*-diethyl-1,3-propanediamine reacting with phthalocyanines' sulfonyl chloride groups (Schema 2.20) [71b].



Scheme 2.20. Stabilisation of a dimer structure by covalent linking of two adjacent phthalocyanine molecules with *N,N'*-diethyl-1,3-propanediamine.

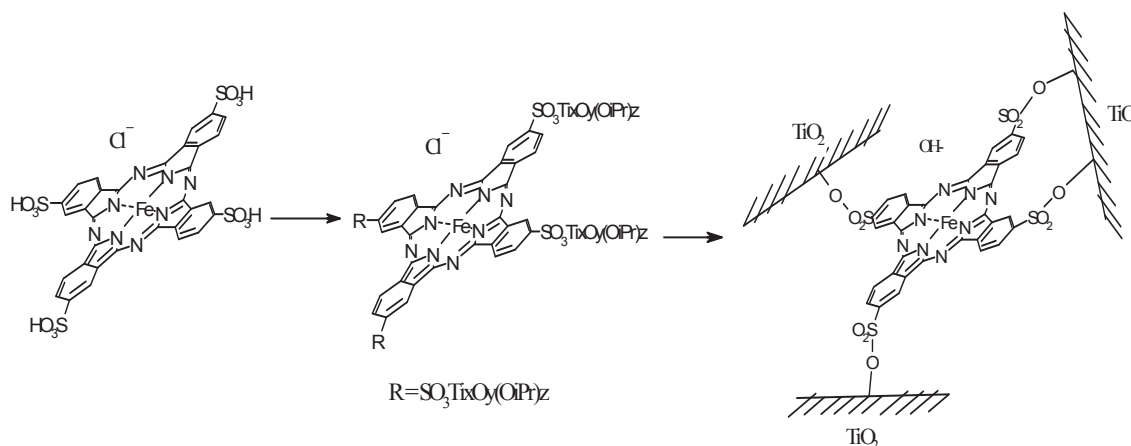
N,N'-diethyl-1,3-propanediamine linked dimeric phthalocyanine complexes proved to be more active and selective in the oxidation of these organic compounds.

Sorokin and coworkers prepared supported iron phthalocyanine bearing eight triethoxysilyl units (Scheme 2.21) and tested the use of this supported catalyst in catalytic epoxidation of olefins and oxidation of phenols [71a + ref. 55 from 71a].



Scheme 2.21. Preparation of FePc-SiO₂

Recently, the direct covalent bonding of functionalized phthalocyanine on nanoparticulate TiO_2 material has been reported (Scheme 2.22) [72]. The good catalytic activity of this TiO_2 supported catalyst was demonstrated in the aerobic oxidation of β -isophorone to ketoisophorone, important intermediate for the preparation of flavors and fragrances fine chemicals.



Scheme 2.22. Preparation of FePcS- TiO_2 .

Generally, the catalytic properties of immobilized μ -oxo dimeric iron phthalocyanines were better than those of the mononuclear species, confirming the interest of the immobilization of these complexes to enhance the catalysis efficiency.

2.3. Use of iron complexes as oxidation catalysts

2.3.1 Introduction to bio-inspired heme-like catalysts

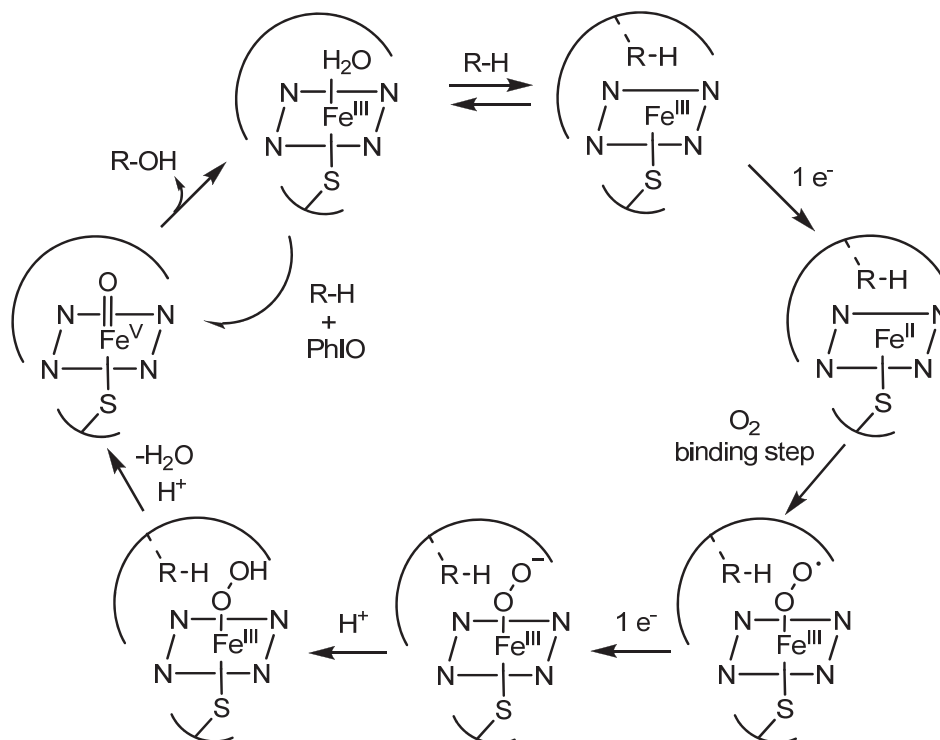
In the area of oxidation catalyzed by transition metal complexes [73,74], synthetic metalloporphyrins occupy a particular place: they are analogues of the prosthetic group of heme-containing enzymes which selectively catalyze various oxidation reactions with the same transition metal (iron) and the same macrocyclic ligand (protoporphyrin IX). Biological oxidations by heme enzyme can be classified as follows: oxygenations of organic substrates catalyzed by cytochrome P-450 [75], oxidations by peroxidases [76], oxidative halogenations by chloroperoxidases and hydrogen peroxide dismutation by catalase [77]. The particular feature of cytochrome P-450 is the axial coordination of cystein ligand to iron porphyrin. There are no close contacts with aminoacids in the distal site [75,78]. In turn, histidine is the proximal ligand in peroxidases while distal amino acids, close to the prosthetic group, are present to favor the heterolytic cleavage of the O-O bond of hydrogen peroxide by a push-pull mechanism [76,78].

The catalytic cycle of cytochrome P450_{cam} is triggered as the camphor molecule enters into the active site and displaces the axial water molecule. Consequently, the displacement of the iron from the plane of the porphyrin ring increases from 0.30 Å in the resting state of the enzyme to 0.44 Å in the pentacoordinated complex (Schema 2.23). This makes the heme a better electron sink and triggers an electron transfer from the reductase protein; this electron-transfer event then initiates the cycle.

After the substrate binding step, an electron transfer from the reductase causes the reduction of the iron(III) center to the ferrous state. The reduced form of cytochrome P450 is an extremely efficient reducing agent as expected for an iron(II) porphyrin complex. One electron from the iron(II) center and one from the triplet oxygen pair create an iron(III)-oxygen bond. This oxygen-iron complex is relatively stable. The intermediate oxygen-iron has to be regarded as an superoxide ion coordinated to an iron(III) center with an unpaired electron on the terminal oxygen atom. The second reduction step is the rate-determining step in many cytochrome P450s. This relatively slow step generates a

negatively charged iron(III)-peroxo complex which is quickly protonated at this stage to generate the iron(III)- hydroperoxo complex. The second proton is necessary to produce an iron(V)-oxo species.

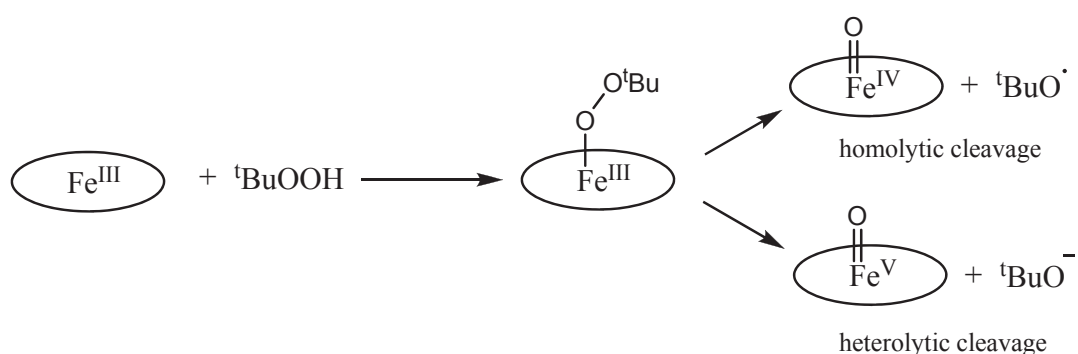
At the end of the cycle, camphor is converted to 5-exo-hydroxycamphor that forms a complex with the heme.



Scheme 2.23. Schematic representation of the different intermediates generated during the catalytic cycle of cytochrome P450 [79].

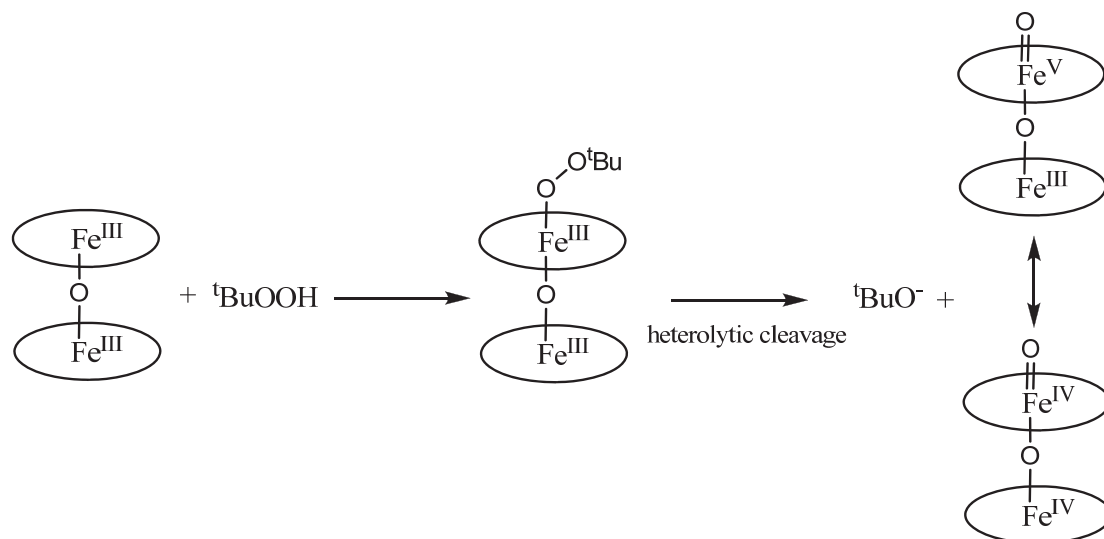
Synthetic iron porphyrin complexes have been investigated as bioinspired models for the catalytic action of the enzyme Cytochrome P-450 in oxidation reactions. Iron porphyrins can catalyze a wide variety of oxidation reactions including epoxidation, hydroxylation, dealkylation, dehydrogenation, and oxidation of amines, sulfides, alcohols and aldehydes, [82] even for unreactive substrates such as unactivated hydrocarbons. Metallophthalocyanine (MPc) complexes have been used as alternative catalysts, because they have a similar structure to porphyrins, are cheaper and more stable to degradation [84–89]. The higher oxidation states of the central transition metal ions are more readily

accessible in the porphyrin series than in the phthalocyanine series [80]. In other words, phthalocyanine ligand tends to stabilize the lower oxidation states of metal compared to porphyrin one. This implies that high oxidation states metallophthalocyanines should be stronger oxidizing agents than their porphyrin analogues in the same oxidation state. In porphyrin series the kind of the cleavage of O–O bond (homolytic vs heterolytic, Scheme 2.24) is determined by the structures of porphyrin ligand and peroxide and the presence of axial ligand, which favors a heterolytic O–O bond cleavage [81].



Scheme 2.24. Proposed mechanism of the formation of active species from monomeric form of FePc and TBHP.

In the case of dimeric FePc complex with a peroxide oxidant, the hypothesis of a heterolytic cleavage of O–O bond with parallel formation of tBuO^{-} (Scheme 2.25) rather than a radical is much more favorable than in the case of monomeric FePc. This is due to the possibility of the delocalization of the charge on two iron atoms of the dimer.



Scheme 2.25. Proposed mechanism of the formation of active species from dimeric form of FePcS and TBHP.

The first oxidation system with synthetic iron porphyrin as a catalyst was developed by Groves and co-workers in 1979 [83]. This oxidation system, which consists of terminal oxidant iodosylbenzene (PhIO) and catalyst $[\text{Fe}^{\text{III}}(\text{por})\text{Cl}]$, can effect both epoxidation of styrenes and cyclohexene, and hydroxylation of cyclohexane and adamantane. However, porphyrins degrade in oxidative media under reaction conditions.

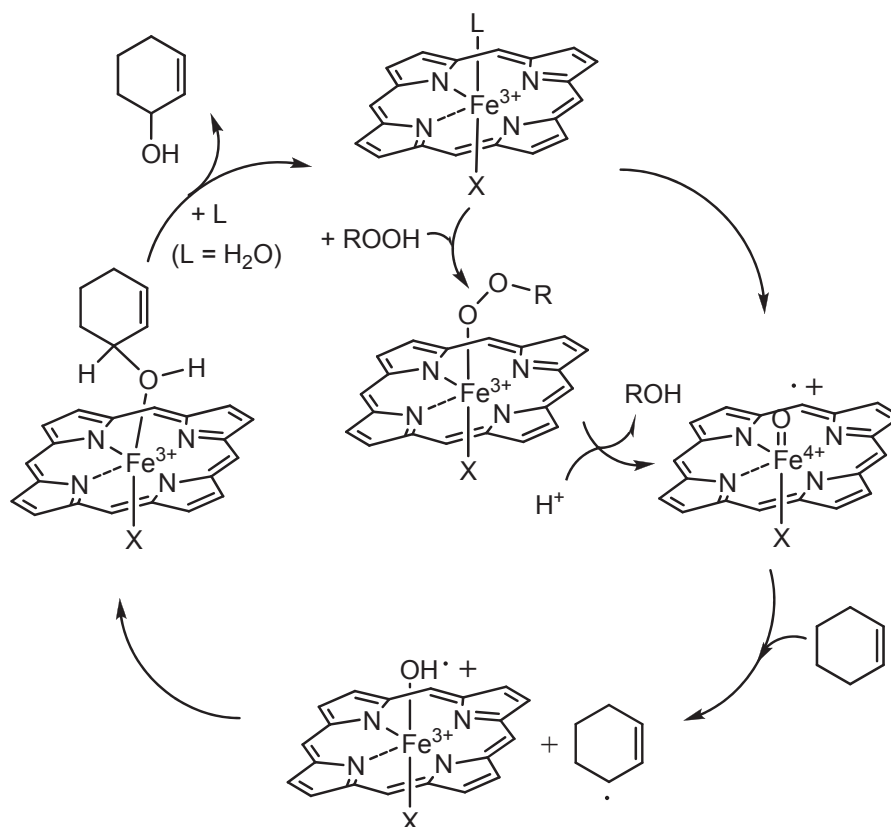
This part of the thesis is limited to the study of iron catalysts in oxidation of cyclohexene, toluene/p-xylene, and alcohols.

The field of oxidation catalyzed by iron complexes is extremely large and can not be reviewed here in full details. We decided to restrict this part to sections related to the analyses performed with the molecules we prepared during the course of this PhD work. Iron complexes can be divided in non-heme and bioinspired heme-like complexes, their use as oxidation catalysts will be detailed hereafter. Reaction conditions, selectivities and terminal oxidants will be given for each reaction.

2.3.2. Oxidation of cyclohexene

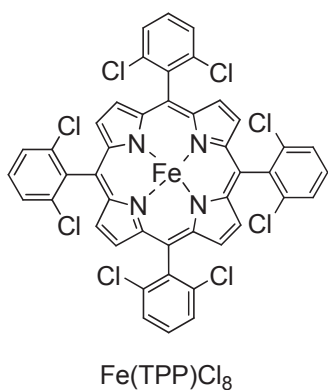
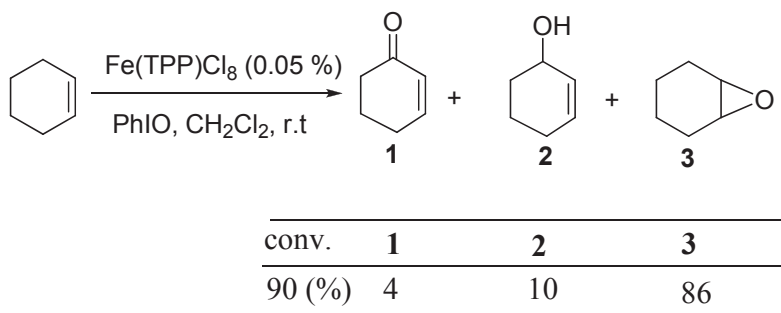
The catalytic oxidation of hydrocarbons (alkanes, aromatics, alkylaromatics, olefins) is an important topic from synthetic, industrial, and biological points of view [90,91]. For example, allylic alcohols are important building blocks in organic chemistry, which can be further functionalized, for example, by Sharpless epoxidation, asymmetric dihydroxylation, rearrangements or cross-metathesis to give access to a broad variety of synthetic intermediates for natural products and fine chemicals. The iron-catalysed oxidation of cyclohexene is discussed in this part. Reaction conditions, selectivities, terminal oxidants are given.

Iron porphyrin complexes have intensively been investigated because they can serve as chemical models for cytochrome P450 monooxygenase [92]. Allylic hydroxylation by heme iron complexes follows the rebound mechanism depicted in Scheme 2.26. Starting from iron(III) porphyrin complex, the high-valent iron(IV)-oxo porphyrin π -cation radical is formed with various oxidants such as single oxygen atom donors (i.e. iodosobenzene) or hydroperoxides (i.e. alkyl hydroperoxides, H_2O_2 , peracids). Iron(IV)-oxo porphyrin π -cation radical species induces hydrogen abstraction from the alkene substrate, resulting in the formation of porphyrin Fe(IV)(OH) complex and allylic radical. Porphyrin complexes, however, are prone to oxidative decomposition and therefore synthetic applications are often hampered by rapid catalyst deactivation. This problem can be overcome by attaching electron-withdrawing groups to the periphery of the porphyrin system. Another problem is the poor chemoselectivity. In many cases, addition to the C=C double bond and formation of the epoxide are much faster than the corresponding hydrogen abstraction, which leads to the allylic alcohols.



Scheme 2.26. Proposed mechanism shown for the hydroxylation of cyclohexene [92].

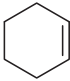
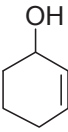
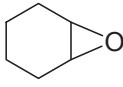
This is illustrated by a study by Appleton et al. [93], who also observed that the chemoselectivity depended on the ring size of the alkene (Scheme 2.27). Cyclohexene oxide was obtained as a major product by Fe(TPP)Cl₈ catalyst.



Scheme 2.27. Oxidation of cyclohexene by Fe(TPP)Cl₈.

Groves and coworkers described oxygen transfer reactions from iodosylbenzene to olefin such as cyclohexene catalyzed by synthetic iron porphyrin [94]. Iodosylbenzene used as oxidant and react with iron porphyrin in the presence of cyclohexene to produce epoxide in good yield (67 %) (Table 2.4).

Table 2.4. Epoxidation Catalyzed by Iron Porphyrin [73].

| Alkene | Catalyst | Products yield (%) | |
|-----------------------------------------------------------------------------------|----------|-----------------------------------------------------------------------------------------|-------------------------------------------------------------------------------------------|
|  | FeTPPCl |  15 |  67 |

Nam and coworkers reported a catalytic oxygenation of cyclohexene by various iron porphyrins (for structures see Figure 2.22) and performed detailed mechanistic studies on cyclohexene epoxidation and a hydroxylation with oxoiron(IV) porphyrin π -cation radicals under various reaction conditions [95]. Cyclohexene oxygenation with oxoiron(IV) porphyrin π -cation radicals bearing electron-rich and electron-deficient porphyrin ligands at different reaction temperatures was tested. Oxoiron(IV) porphyrin π -cation radicals bearing electron-rich porphyrin ligands (**6** and **7**) afforded cyclohexene oxide as a major product at high temperatures. As the reaction temperature became lower, the yields of cyclohexene oxide decreased but the yields of cyclohexen-3-ol increased. At a very low temperature ($-100\text{ }^{\circ}\text{C}$), cyclohexen-3-ol was produced. The selectivity toward C=C and C–H oxidation by **6** and **7** depends on the reaction temperature: C=C epoxidation is preferred at high temperatures and allylic C–H hydroxylation at low temperatures.

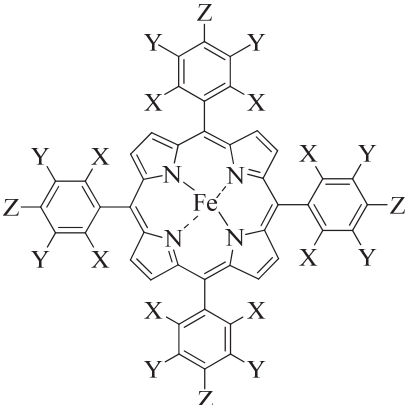
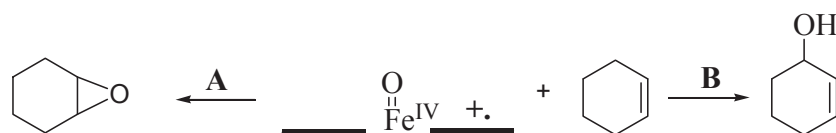
|  | Iron Porphyrins | <u>X</u> | <u>Y</u> | <u>Z</u> |
|-------------------------------------------------------------------------------------|---------------------------------------|-----------------|----------|-----------------|
| | [Fe(TPFPP)] ⁺ (3) | F | F | F |
| | [Fe(TDFPP)] ⁺ (4) | F | H | H |
| | [Fe(TDCPP)] ⁺ (5) | Cl | H | H |
| | [Fe(TMP)] ⁺ (6) | CH ₃ | H | CH ₃ |
| | [Fe(TDMPP)] ⁺ (7) | CH ₃ | H | H |

Figure 2.22. Structures of the iron porphyrin complexes used in oxidation [74].

When cyclohexene oxygenation was tested with oxoiron(IV) porphyrin π -cation radicals bearing electron-deficient porphyrin ligands (**3**, **4**, and **5**), the temperature effect on the regioselectivity of C=C epoxidation versus allylic C–H hydroxylation disappeared and cyclohexene oxide was obtained as a major product (Scheme 2.28).



(a) Reaction temperature



(b) Electronic nature of iron porphyrins



Scheme 2.28. Change of regioselectivity toward C=C epoxidation versus C–H hydroxylation depending on reaction conditions [95].

Bandyopadhyay and coworkers used $F_{20}TPPFe(III)Cl$ (Figure 2.23(a)) as the catalyst and TBHP as the terminal oxidant to oxidize cyclohexene [96]. The oxidation reactions of cyclohexene (200 mM) with TBHP (2 mM) in presence of $F_{20}TPPFe(III)Cl$ (50 μM) were studied in CH_3CN-H_2O (9.09%) at 25 °C under argon and under dioxygen. Oxidation reaction was completed in only 10 min when the reaction was kept under argon and 2-cyclohexen-1-ol was the main product.

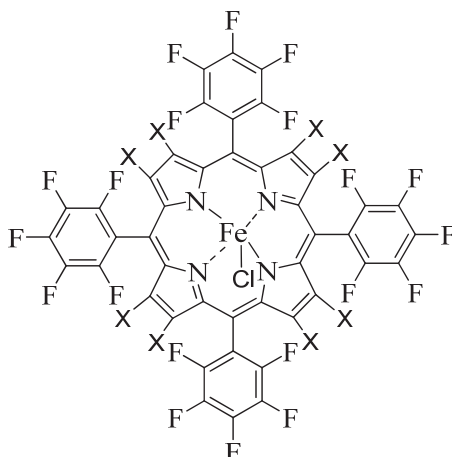
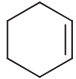
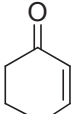
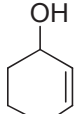
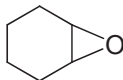


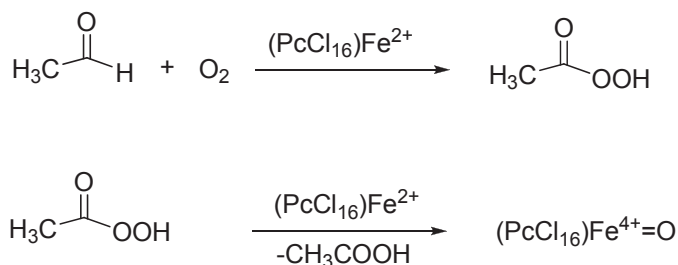
Figure 2.23. Iron porphyrin catalysts $\text{Fe}(\text{TFPP})\text{Cl}$ [$\text{X}=\text{H}$] (a) and $\text{Fe}(\text{TFPPBr}_8)\text{Cl}$ [$\text{X}=\text{Br}$] (b) [96,97].

Tumas and coworkers showed the oxidation of cyclohexene using molecular oxygen and catalyzed by halogenated iron porphyrins (Figure 2.23 (a and b)) in supercritical carbon dioxide [97]. They found that selectivity for epoxidation of cyclohexene is higher in scCO_2 than in organic solvents.

In comparison with metal porphyrins, the corresponding metal phthalocyanines are much more stable against oxidative decomposition. Murahashi et al. reported that chlorinated $\text{Fe}(\text{II})$ phthalocyanine is particularly well suited for aerobic allylic oxidation employing acetic aldehyde as a cofactor (Table 2.5) [98]. Under these conditions, cyclohexene is converted to a mixture of **1** and **2** in 70% overall yield and the epoxide **3** as byproduct (30%). Acetic aldehyde is proposed to form peracetic acid in the presence of Fe catalyst. Although the authors postulate a transfer an oxygen atom to the Fe phthalocyanine complex leading to an iron(IV) species as reactive intermediate, a classical free-radical mechanism involving Ac^\cdot , AcO^\cdot and AcOO^\cdot radicals seems to be operating in this system.

Table 2.5. Oxidation of cyclohexene using chlorinated iron phthalocyanines [98].

| Alkene | Yield (%) | Products (Selectivity, %) | TON |
|-----------------------------------------------------------------------------------|-----------|-------------------------------------------------------------------------------------------------------------------------------------------------------------------------------------------------------------------------------------------------------------------------------------------------------------------------------------------------------------------------------------------------------------------------------------------------------------------------------------------------------------------------------------------------------------------------------------------------------------------------------------------------------------|-----|
|  | 76 | <div style="display: flex; justify-content: space-around; align-items: center;"> <div style="text-align: center;">  1 </div> <div style="text-align: center;">  2 </div> <div style="text-align: center;"> (70) </div> </div> <div style="text-align: center; margin-top: 10px;">  3 </div> <div style="text-align: center; margin-top: 5px;"> (30) </div> | 320 |



The oxidation of cyclohexene catalysed by Fe(II) tetra-*tert*-butylphthalocyanine was reported by Kasuga [99]. The main product after oxidation was cyclohexene oxide and small amount of 2-cyclohexene-1-one.

Weber et al. utilized binuclear μ -oxo iron(III) *t*-butylphthalocyanine (Figure 2.24) as catalyst in the oxidation of cyclohexene. The main products were 2-cyclohexen-1-one (39%) and 2-cyclohexen-1-ol (48%), while cyclohexene oxide was obtained in only 12% yield [100].

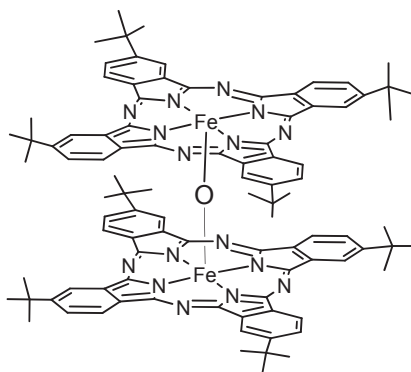


Figure 2.24. Molecular structure of μ -oxo iron(III) phthalocyanines catalysts [100].

Nyokong and coworkers showed oxidation of cyclohexene using iron hexadecachlorophthalocyanine (FePcCl_{16} , Figure 2.25) and the catalytic activity of iron polychloro phthalocyanine is compared to that of unsubstituted FePc [101]. The FePcCl_{16} catalyst is selective to the formation of 2-cyclohexene-1-one (Table 2.6). While unsubstituted PcFe showed the higher selectivity towards 2-cyclohexen-1-ol perchlorinated FePcCl_{16} was more selective for 2-cyclohexene-1-one formation (Table 2.6) [101].

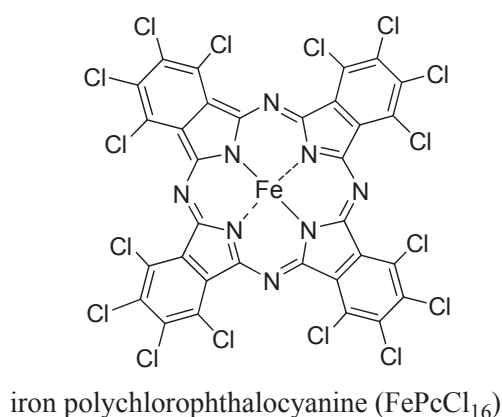


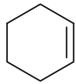
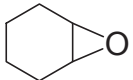
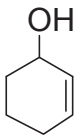
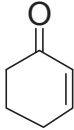
Figure 2.25. Molecular structure of Fe(II) perchlorinated phthalocyanine (FePcCl_{16}) [101].

Table 2.6. Oxidation of cyclohexene by $\text{Cl}_{16}\text{FePc}$. Selectivity values for FePc are given in parentheses [101].

| Product | Yield (%) | Selectivity (%) | TON |
|---------------------|-----------|-----------------|------|
| Cyclohexene oxide | 3.5 | 7.8 (3.8) | 39.8 |
| 2-cyclohexene-1-ol | 9.1 | 20.0 (71.2) | 209 |
| 2-cyclohexene-1-one | 32.7 | 72.2 (25.0) | 494 |

Sorokin and coworkers prepared supported iron phthalocyanines (see part 2.2.4) to test them in cyclohexene oxidation [71]. Oxidation products were obtained using a catalyst: substrate: isobutyraldehyde ratio of 1:265:530. Cyclohexene was oxidized into epoxides with quite good selectivities: the yield of cyclohexene oxide was 78 % (Table 2.7).

Table 2.7. Oxidation of olefins by molecular oxygen catalyzed by FePc@SiO₂-supported catalyst in acetonitrile.

| Alkene | Conversion (%) | Time (h) | Products (Yield, %) |
|-----------------------------------------------------------------------------------|----------------|----------|--------------------------------------------------------------------------------------------------------------------------------------------------------------------------------------------------------------------------------------------------------------------------------|
|  | 91 | 9 |  (78)  (1)  (7) |

Recently, Sorokin et al. reported the activity of FePcS–SiO₂ for the allylic oxidation of cyclohexene with TBHP [102].

The main product of the allylic oxidation of cyclohexene with TBHP over FePcS–SiO₂ was the allylic ketone, 2-cyclohexen-1-one (Table 2.8).

Table 2.8. Product yield in the allylic oxidation of cyclohexene with TBHP over FePcS–SiO₂ [102].

| Entry | Catalyst (mmol) | Solvent | TBHP (mmol) | Temperature (°C) | Yield ^a (%) | | |
|-----------------|-----------------|----------------------------------------------------------|-------------|------------------|------------------------|----|---|
| | | | | | 1 | 2 | 3 |
| 1 | 0.25 | CH ₃ CN | 1.3 | 40 | 25 | 6 | 2 |
| 2 | 0.5 | CH ₃ CN | 1.3 | 40 | 30 ^c | 4 | 1 |
| 3 | 1.0 | CH ₃ CN | 1.3 | 40 | 43 | 7 | 2 |
| 4 | 0.5 | CH ₃ CN | 1.3 | 25 | 25 | 4 | 2 |
| 5 | 0.5 | CH ₃ CN | 1.3 | 60 | 28 | 3 | 0 |
| 6 | 0.5 | CH ₃ CN | 1.3 | 70 | 25 | 5 | 1 |
| 7 | 2.0 | CH ₃ CN/CH ₂ Cl ₂ (1:1) | 2.6 | 40 | 40 | 4 | 1 |
| 8 | 2.0 | CH ₃ CN | 2.6 | 60 | 35 | 2 | 1 |
| 9 | 0.5 | CH ₃ CN | 2.6 | 60 | 28 | 6 | 2 |
| 10 ^b | 2.0 | Ethanol | 2.6 | 60 | 15 | 6 | 2 |
| 11 | 0.5 | Toluene | 1.3 | 40 | 14 | 5 | 4 |
| 12 | 0.5 | Ethyl acetate | 1.3 | 40 | 18 | 3 | 1 |
| 13 | 0.5 | Acetone | 1.3 | 40 | 2 | 11 | 2 |
| 14 | 0.5 | 14 | 1.3 | 40 | 22 | 4 | 1 |

In conclusion, an intensive research in the field of iron-catalyzed allylic oxidations has been performed. It should be noted that in many cases a direct comparison of different catalysts is difficult, because the yields of isolated pure products and detailed experimental procedures are not described in details. This has to be considered as a major drawback concerning synthetic applications. Many studies on oxidation of cyclohexene involved iron porphyrins. These studies can be classified in three different categories: (i) isolation of high-valent iron porphyrin intermediates, (ii) catalytic studies, or (iii) kinetic studies. Some discussions on the product analyses and kinetic studies implicate a high-valent iron-oxo porphyrin radical cation, (Por⁺)Fe^{IV}=O, as oxidizing species which reacts with cyclohexene by different possible reaction pathways: (i) a direct oxygen atom

transfer, (ii) a free radical addition followed by a fast ring closure, (iii) an electrophilic addition and fast ring closure, (iv) a reversible metallaoxetane formation, and (v) an electron transfer followed by a collapse to a radical or to a carbocation. However, a careful analysis of the product distribution indicates a classical free radical mechanism in many cases.

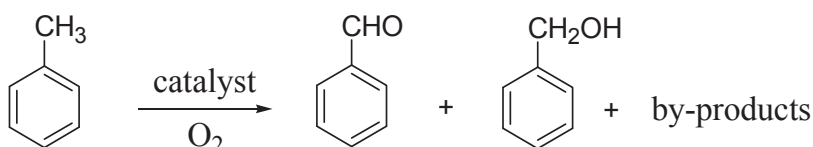
2.3.3. Oxidation of toluene and *p*-xylene

Oxidation of alkyl aromatics is a very important process in industrial chemistry[103]. The production of terephthalic acid by oxidation of *p*-xylene is probably the most sound example of industrial benzylic oxidation: its worldwide annual production is about 44 million t/y. The industrial process is based on the radical oxidation in the presence of Co and Mn ions in acetic acid at harsh conditions (about 200°C, 1.5 MPa) [104]. Stoichiometric oxidation by permanganate or Cr^{VI} oxidants are also used to perform benzylic oxidations. These stoichiometric oxidants are not only relatively expensive, but they also generate copious amounts of waste. From both an economic and environmental point of view, the effective catalytic oxidation processes that use clean, inexpensive oxidants for converting alkyl benzenes to carbonyl compounds on an industrial scale is the most gratifying route. Several catalytic approaches have been described in quest of cleaner and more general processes. Along with dioxygen[105], TBHP is widely used as the oxidant in combination with Cr[106], Co[107], Mn[108], Fe[109] and Rh[110]. based catalysts. Vanadium-based polyoxometalates have been shown to be useful catalysts for benzylic oxidation [111]. Alkyl aromatic compounds can be oxidized either at benzylic positions or in the aromatic nuclear. Consequently, the selectivity issue is very important. Catalytic systems capable of selectively oxidizing either only benzylic or only aromatic sites are highly desirable. However, this task is difficult to achieve. For example, toluene was oxidized by iron (II) complexes bearing hexa-, penta- or tetra-azadentate ligands-H₂O₂ system to mixture of isomeric cresols, benzyl alcohol and benzaldehyde [112]. Benzylic and ring oxidation products were obtained with comparable yields. The addition of reducing

agents shifted oxidation in favour of aromatic ring oxidation to give total TON~7 [112]. Oxidation of toluene performed by metalloporphyrin systems has often resulted in the mixture of products of benzylic and aromatic oxidation [113].

2.3.3.1. Iron Porphyrins

Huang and coworkers used chitosan supported complexes monomeric and dimeric iron tetraphenylporphyrins for oxidation of toluene (Scheme 2.29) [114].



Scheme 2.29. The toluene oxidation catalyzed by the given catalysts with air [114].

The main oxidation products were benzaldehyde and benzyl alcohol along with small amount of benzoic acid. Compared with chitosan-supported μ -oxo dimeric iron tetraphenylporphyrins, the toluene oxidation catalyzed by chitosan-supported monomeric iron tetraphenylporphyrins provided the higher yields of main products, the higher toluene conversion, the better selectivity and the higher catalyst TON, from 1.5 to 4.5 h reaction time, for example, at the reaction time of 4.5 h, they were 5 % vs 2 %, 6 % vs 2 %, 91 % vs 91 % and 6×10^6 vs 1×10^6 . The results indicate that in the toluene oxidation catalyzed by two supported catalysts, chitosan produces better improving effect for the catalytic performance of mono iron tetraphenylporphyrins [114].

μ -oxo bis[(porphyriniron(III))] was prepared by Guo and coworkers for use in toluene oxidation with molecular oxygen (Figure 2.26) [115].

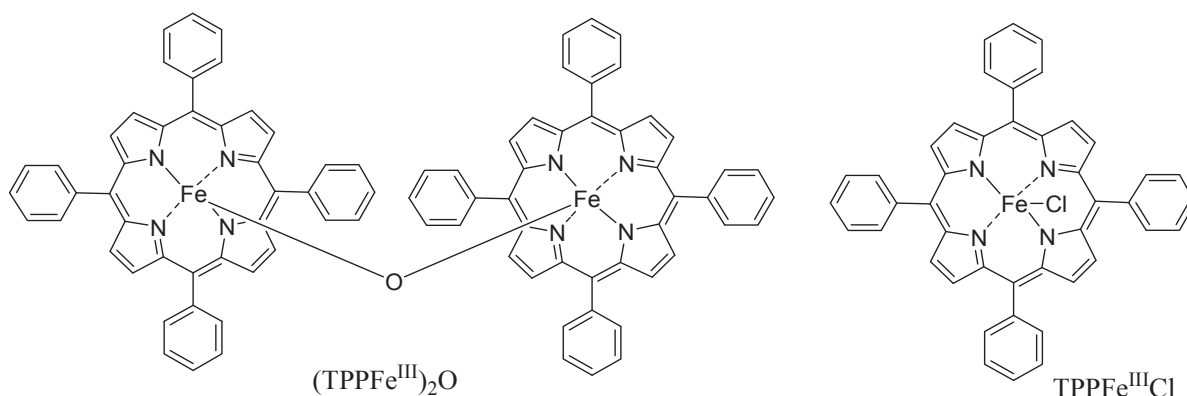
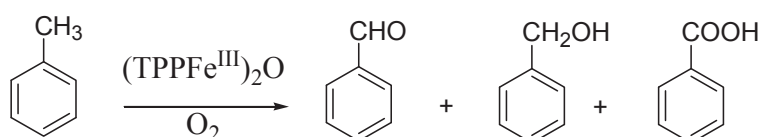


Figure 2.26. Structures of iron tetraphenylporphyrin catalysts [115].

The oxidation of toluene with molecular oxygen catalyzed by $(\text{TPPFe}^{\text{III}})_2\text{O}$ gave benzyl alcohol, benzaldehyde and benzoic acid (Scheme 2.30).



Scheme 2.30. Oxidation of toluene by O_2 to corresponding products [115].

Table 2.9. Comparison of catalytic property of $(\text{TPPFe}^{\text{III}})_2\text{O}$ and $\text{TPPFe}^{\text{III}}\text{Cl}$ [115].

| Catalysts | TON | Toluene conversion | Selectivity (-aldehyde + -ol), % | -aldehyde/-ol |
|-----------------------------------------|-------|--------------------|-------------------------------------|---------------|
| $(\text{TPPFe}^{\text{III}})_2\text{O}$ | 21830 | 7 | 59 | 1 |
| $\text{TPPFe}^{\text{III}}\text{Cl}$ | 12593 | 4 | 61 | 1 |

The results showed that μ -oxo dimeric iron porphyrin $(\text{TPPFe}^{\text{III}})_2\text{O}$ more efficient catalyst for toluene oxidation than monomeric iron porphyrin $\text{TPPFe}^{\text{III}}\text{Cl}$ (Table 2.9) [115]. Although the selectivity of benzaldehyde and benzyl alcohol for the two reactions is similar, the TON and toluene conversion for $(\text{TPPFe}^{\text{III}})_2\text{O}$ are two times more than

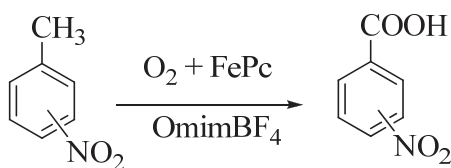
monomeric iron porphyrin $\text{TPPFe}^{\text{III}}\text{Cl}$. This may be due to higher stability of μ -oxo dimeric iron porphyrin $(\text{TPPFe}^{\text{III}})_2\text{O}$ [116].

Castro and coworkers showed selective oxidation of toluene to benzyl alcohol with good yield [117].

The reaction of octaethylporphyrin iron(III) chloride with potassium crown ether (18 crown-6) nitrite in *N*-methylpyrrolidone-1% acetic acid under argon generates the iron(III) nitrite salt (PFeNO_2). The latter is a unique and selective oxygen atom transfer reagent. The reaction of a broad range of substrates (S) proceeds quantitatively to yield the oxidized substrate and the iron(II) porphyrinnitrosyl adduct: $\text{PFeNO}_2 + \text{S} \longrightarrow \text{PFeNO} + \text{SO}$.

2.3.3.2. Iron Phthalocyanines

Zhao and coworkers used iron phthalocyanines to oxidize nitrotoluene in ionic liquid $[\text{omim}][\text{BF}_4]$ (Figure 2.27) [118]. The experimental results showed that both the length of alkyl chains on the 1-alkyl-3-methylimidazolium cations and the anions had some effect on the reaction, and the best results were obtained by using $[\text{omim}][\text{BF}_4]$ as an ionic liquid phase. $[\text{omim}][\text{Tf}_2\text{N}]$, $[\text{omim}][\text{BF}_4]$ and $[\text{dmim}][\text{BF}_4]$ ionic liquids showed good solubility for the phthalocyanines complexes and PNT (Table 2.10).



1: p-nitrotoluene (PNT) 2: o-nitrotoluene (ONT)

3: m-nitrotoluene (MNT) 4: 2,4-dinitrotoluene (DNT)

Figure 2.27. Oxidation of nitrotoluenes to nitrobenzoic acids.

Table 2.10. The oxidation of nitrotoluenes to nitrobenzoic acids by FePc [118].

| Entry | Substrate | Ionic liquid | NaOH | P(O ₂)(MPa) | Isolated yield (%) |
|-------|-----------|---------------------------|------|-------------------------|--------------------|
| 1 | PNT | [omim][BF ₄] | 1.5 | 2.0 | 92.2 |
| 2 | PNT | [omim][BF ₄] | 1.5 | 2.0 | 88.7 |
| 3 | PNT | [omim][BF ₄] | 1.5 | 2.0 | 85.3 |
| 4 | PNT | [omim][BF ₄] | 1 | 2.0 | 70.1 |
| 5 | PNT | [omim][BF ₄] | 1.5 | 2.5 | 93.0 |
| 6 | PNT | [omim][BF ₄] | 1.5 | 1.5 | 83.5 |
| 7 | PNT | [omim][Tf ₂ N] | 1.5 | 2.0 | 12.7 |
| 8 | PNT | [dmim][BF ₄] | 1.5 | 2.0 | 72.4 |
| 9 | PNT | [No ionic liquid] | 1.5 | 2.0 | Trace |
| 10 | PNT | [omim][BF ₄] | 1.5 | 2.0 | 92.0 |
| 11 | ONT | [omim][BF ₄] | 1.5 | 2.0 | 92.8 |
| 12 | MNT | [omim][BF ₄] | 1.5 | 2.0 | Trace |
| 13 | DNT | [omim][BF ₄] | 1.5 | 2.0 | 93.2 |
| 14 | Toluene | [omim][BF ₄] | 1.5 | 2.0 | Trace |

Reaction conditions: 0.2 mol of nitrotoluenes in the solution of 10.0 mL ionic liquid and 5.0 mL water at 90 °C for 12 h.

The oxidation of nitrotoluenes in ionic liquid-water liquid-liquid biphasic catalytic reaction system by iron phthalocyanines were studied and exhibited good yields and selectivities.

2.3.4. Oxidation of alcohols

Oxidation of alcohols to aldehydes and ketones is one of the most important transformations in organic synthesis [119]. In particular; the oxidation of primary alcohols to aldehydes is important since they find wide applications as intermediates in fine chemicals particularly for perfume and pharmaceutical industries [120,121]. Numerous catalytic methods are now known which can be used to oxidize alcohols using either O_2 or H_2O_2 as the oxidant. These oxidants are to be preferred because they are inexpensive and produce water as the sole byproduct. Most of the catalysts reported so far, the use of a solvent in the reaction is required, while it is highly desirable to develop a process without a solvent from the viewpoint of green chemistry. Avoiding the use of solvent is important advantage from environmental and industrial points of view. The world-wide annual production of carbonyl compounds is over 10^7 tonnes and many of these compounds are produced from the oxidation of alcohols. [122].

2.3.4.1. Iron Porphyrins

Nam and coworkers described alcohol oxidation reactions (Figure 2.22) with spectroscopically well characterized oxoiron(IV) porphyrin π -cation radicals, $[(\text{tdcpp})^+Fe^{IV}=O]^+$ (Scheme 2.31) and $[(\text{tmp})^+Fe^{IV}=O]^+$ (Figure 2.28) [123].

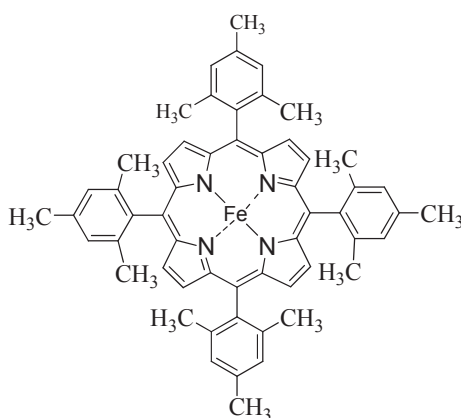
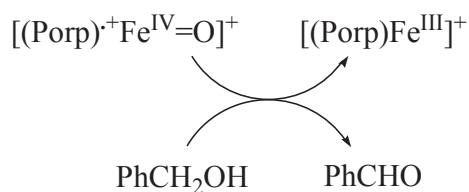


Figure 2.28. Structures of iron porphyrin complexe [123].



Scheme 2.31. Oxidation of benzyl alcohol by high-valent iron oxo complexes porphyrins [123].

Wang and coworkers prepared TEMPO-linked iron porphyrins (Figure 2.29) for selective oxidation of benzyl alcohol to benzaldehyde [104]. The catalytic oxidation system includes catalyst (1 mol %), KBr (10 mol %) and aqueous NaOCl (1.25 equiv, pH 8.6).

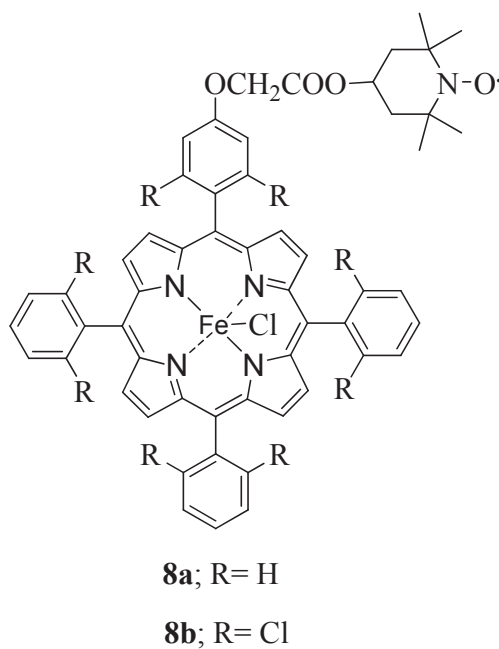
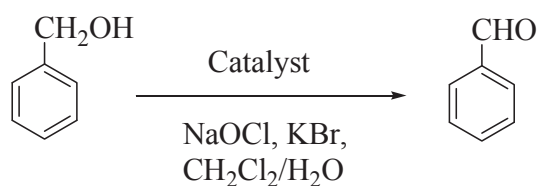


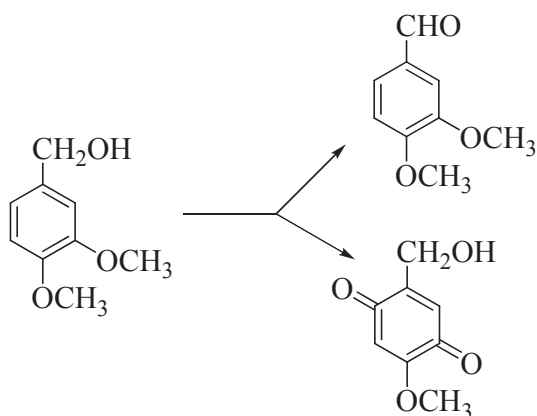
Figure 2.29. Structure of TEMPO-linked iron porphyrins [124].

Benzyl alcohol was oxidized to benzaldehyde by these TEMPO-linked iron porphyrins (Scheme 2.32) in good yields. When **8a** was used as catalyst, benzaldehyde yield was 86%. The yield of benzaldehyde was 92% in the presence of **8b** as catalyst [124].



Scheme 2.32. Oxidation of benzyl alcohol [124].

Meunier and coworkers studied the oxidation of 3,4-dimethoxybenzyl alcohol (veratryl alcohol) in presence of iron porphyrin (Scheme 2.33) [125]. Two categories of catalysts were used: (i) free water-soluble iron derivative of tetrasodium meso-tetrakis(p-sulfonatophenyl) porphyrin (TPPS) and (ii) the same iron porphyrin immobilized onto an ion-exchange resin, Amberlite IRA-900 EGA, by strong physical adsorption.



Scheme 2.33. Oxidation of veratryl alcohol

Studies have been performed on the oxidation of veratryl alcohol by the soluble catalyst, FeTPPS, and the corresponding insoluble one, FeTPPS-Ad (Table 2.11).

Table 2.11. Hydrogen Peroxide and Potassium Monopersulfate Oxidation of Veratryl Alcohol, Catalyzed by FeTPPS, FeTPPS-Ad [125].

| run | catalyst | % of catalyst vs 1 | oxygen donor | ratio of imidazole to catalyst | conversion in 1 min |
|-----|-----------|-----------------------|-------------------------------|-----------------------------------|------------------------|
| 1 | FeTPPS | 0.2 | H ₂ O ₂ | | 5 |
| 2 | FeTPPS | 0.2 | H ₂ O ₂ | 100 | 7 |
| 3 | FeTPPS | 0.2 | KHSO ₅ | | 67 |
| 4 | FeTPPS | 0.2 | KHSO ₅ | 100 | 65 |
| 5 | FeTPPS—Ad | 10 | H ₂ O ₂ | | 6 |
| 6 | FeTPPS—Ad | 10 | KHSO ₅ | | 50 |

The catalytic activity is higher for soluble catalyst FeTPPS, compared to the corresponding resin-immobilized catalyst, FeTPPS-Ad. However, the latter supported catalyst can be recycled, losing only 5% of the initial activity.

2.3.4.2. Iron Phthalocyanines

Zhdankin and coworkers studied the oxidation of alcohols by μ -oxo diiron(III) t-butylphthalocyanine complex (Figure 2.30) using organic iodine (V) compounds as the oxidant species [126].

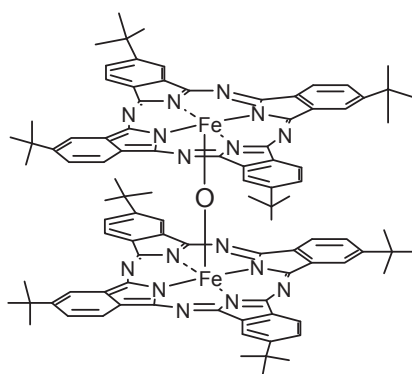


Figure 2.30. Structure of μ -oxo diiron(III) t-butylphthalocyanine complex [126].

The oxidation of alcohols was studied at room temperature in dry dichloromethane with 0.7 mol equiv (1.4 equiv of active oxygene) of the iodine(V) reagent and 0.1 equiv of the appropriate catalyst [126].

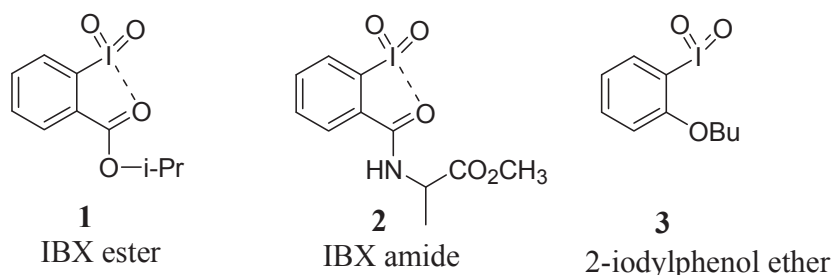


Figure 2.31. Hypervalent iodine (V) oxidants [126].

The oxidation of 4-methoxybenzyl alcohol using oxidant IBX ester **1** at room temperature in the presence of Fe(III) phthalocyanine complex (10 mol %) afforded the aldehyde in a 100% conversion (95% isolated yield after chromatography) after 1 h stirring at room temperature. The conversion was much lower when oxidants **2** (IBX amide) and **3** (2-iodylphenol ether) were employed for the oxidation of benzylic alcohols under similar conditions using the same catalyst Fe(III) phthalocyanine complex [126]. The allylic alcohol oxidation exhibited the same reactivity in the catalytic oxidations while the aliphatic substrates were much less reactive.

Then, Ford and Hampton studied the oxidation of veratryl alcohol in water catalyzed by iron tetrasulfophthalocyanine [127]. The FePcS-catalyzed oxidations of DMBA with hydrogen peroxide and concentrations of 1-3 mol% FePcS based on DMBA, all resulted in the same 31% conversion of DMBA during 15 minutes at 85°C.

2.3.5. General Conclusion

Oxidation processes are carried out in a highly selective manner by mono- or dioxygenases under mild conditions in nature. Monooxygenase is cytochrome P-450, which features an iron porphyrin core and can catalyze a wide variety of oxidation reactions including epoxidation, hydroxylation, dealkylation, dehydrogenation, and oxidation of amines, sulfides, alcohols and aldehydes, even for unreactive substrates such as unactivated hydrocarbons. Metalloporphyrins, with a core structure closely resembling that of the iron porphyrin core of cytochrome P-450, have been extensively studied as catalysts for oxidation reactions. Thus, numerous iron complexes such as iron porphyrins and phthalocyanines were prepared and used in different oxidation reactions. High-valent oxo iron porphyrins have been observed in the reactions of synthetic iron porphyrins with PhIO or m-CPBA (m-chloroperbenzoic acid) and have been reported to be able to oxidize alkenes, alkanes, phosphines, amines and sulfides by oxygen atom transfer and/or insertion reactions. Iron phthalocyanine complexes have been used as alternative catalysts, because they have a similar structure to porphyrins, are cheaper and more stable to degradation.

FePc complexes can be prepared from different precursors such as phthalic acid, phthalic anhydride, phthalamide, phthalonitrile etc... FePcS, which is widely used for oxidation catalysis, is prepared from the corresponding sulfonated phthalic acid. The nature of iron allowing the presence of axial substituents, this property is used to prepare single atom bridged diiron phthalocyanines such as μ -oxo, μ -carbido and μ -nitrido. Sorokin and coworkers showed that μ -oxo diiron sulfophthalocyanine has better catalytic activities than the monomeric iron sulfophthalocyanine. Other μ -oxo diiron phthalocyanines such as μ -oxo diiron t-butylphthalocyanine [126] were then studied more extensively in several oxidation reactions, using different oxidants and reaction conditions. Sorokin et al compared the catalytic activities of μ -oxo, μ -carbido and μ -nitrido diiron t-butyl phthalocyanines towards oxidation of methane: when μ -oxo and μ -carbido diiron t-butyl phthalocyanines were inactive, μ -nitrido diiron t-butyl phthalocyanine proved to be a very efficient catalyst in very mild conditions (water, ambient temperature) [63a]. This

complex was then used in several oxidation reactions (benzene, ethane and propane). The unusual electronic structure of this complex was determined: its formal $\text{Fe}^{\text{III}}\text{--N=Fe}^{\text{IV}}$ structural unit is a $\text{Fe}^{3.5}\text{--N--Fe}^{3.5}$ mixed-valence state with electronically equivalent iron atoms.

In addition to the oxidation of methane, benzene or propane mentioned above, oxidations of other compounds are of importance from environmental and industrial point of view. This is the case of cyclohexene, toluene, xylenes or alcohols, whose oxidation products are used in many applications on a large scale. Currently, these oxidations are often achieved by using of highly polluting heavy-metal derivatives, such as chromates, and there is a strong need for alternative solutions.

3. Results and discussion

3.1 Syntheses and characterizations

3.1.1. Phthalonitriles

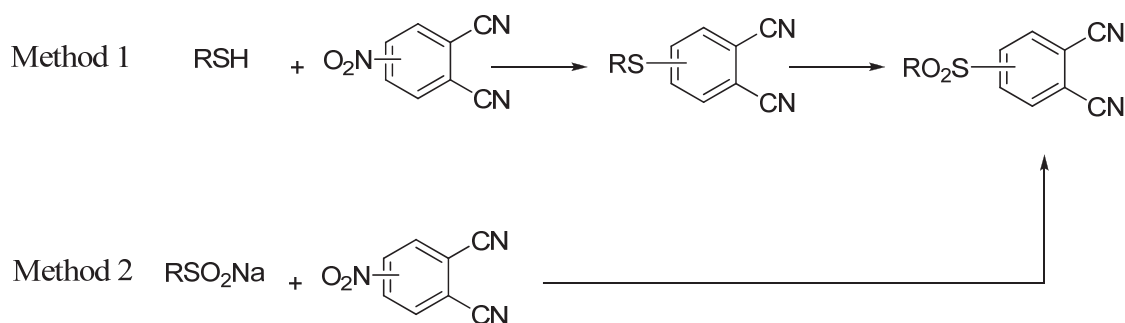
Two types of precursors for the preparation of phthalocyanine complexes have been prepared, namely, mono- and disulfonyl- substituted phthalonitriles.

3.1.1.1. Monosulfonyl phthalonitriles

Monosulfonyl phthalonitriles were prepared in two different methods represented on Scheme 3.1.

Method 1: In two steps from corresponding thiols followed by oxidation,

Method 2: In one step from corresponding alkylsulfinate salts.

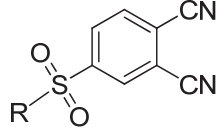


Scheme 3.1. Two methods for the preparation of monosulfonyl phthalonitriles.

Depending on the availability of the starting products, **method 1** or **2** was selected for the preparation of desired monosulfonyl phthalonitrile. 3-nitrophthalonitrile and 4-nitrophthalonitrile are common precursors in both method 1 and 2 to prepare alkylthio

phthalonitriles and alkylsulfonyl phthalonitriles (Table 3.1). These two precursors were synthesized according to literature protocol [128].

Table 3.1. Preparation methods of alkylsulfonyl phthalonitriles.

| |  | |
|-----------|-----------------------------------------------------------------------------------|--------|
| Compound | R | Method |
| 4 | hexyl | 1 |
| 6 | hexyl | 1 |
| 8 | t-butyl | 1 |
| 10 | methyl | 2 |
| 12 | ethyl | 2 |
| 14 | adamantyl | 1 |
| 16 | cyclohexyl | 1 |

In the case of R = hexyl, t-butyl, adamantyl and cyclohexyl, **method 1** was chosen as the starting thiols (hexanethiol, adamantanethiol, cyclohexanethiol, t-Butanethiol) are easy to handle. The syntheses of alkylthio phthalonitriles **3**, **5**, **7**, **13** and **15** were achieved in high yield (around 75%) by base-catalysed nucleophilic substitution of nitro groups in 3 or 4-nitrophthalonitrile using corresponding thiols in classical conditions (K_2CO_3 , DMSO, room temperature).

The resulting alkylthiophthalonitriles were then oxidized by oxidant such as *m*-chloroperbenzoic acid (*m*-CPBA) or hydrogen peroxide (H_2O_2) to lead to the expected alkylsulfonyl. In the case of R = hexyl, adamantyl and cyclohexyl *m*-chloroperbenzoic acid (*m*-CPBA) was used as oxidant to prepare corresponding sulfonylphthalonitrile derivatives **4**, **6**, **14**, **16** in dichloromethane (CH_2Cl_2). t-butylthiophthalonitrile **7** was oxidized with H_2O_2 in acetic acid at reflux temperature.

There is no influence of the nature of R on the nucleophilic substitution's and oxidation's yields (Table 3.2).

Table 3.2. Nucleophilic substitution's and oxidation's yields

| R | Yields (%) | |
|--------------------|---------------------------|-----------|
| | Nucleophilic substitution | Oxidation |
| hexyl (4-position) | 80 | 73 |
| hexyl (3-position) | 85 | 75 |
| t-butyl | 75 | 73 |
| adamantyl | 81 | 73 |
| cyclohexyl | 75 | 73 |
| dihexyl | 82 | 76 |

After oxidation of the alkylthiophthalonitriles to corresponding alkylsulfonyl phthalonitriles, melting points of all nitriles increased. The changes of the melting point are given in Table 3.3.

Table 3.3. The change of the melting point after oxidation

| R | Melting point (°C) | |
|--------------------|----------------------|-------------------------------------|
| | SR Phthalonitrile | SO ₂ R Phthalonitrile |
| hexyl (4-position) | 67 | 104 |
| hexyl (3-position) | 68 | 100 |
| t-butyl | 76 | 180 |
| adamantyl | 144 | 266 |
| cyclohexyl | 93 | 161 |

In addition to the characteristic strong C≡N stretches observed around 2230 cm⁻¹ for both alkylthio and alkylsulfonyl phthalonitriles, the comparison of their IR spectra evidences

the apparition of the O=S=O large vibrations around 1150 and 1320 cm^{-1} after oxidation (Figure 3.1).

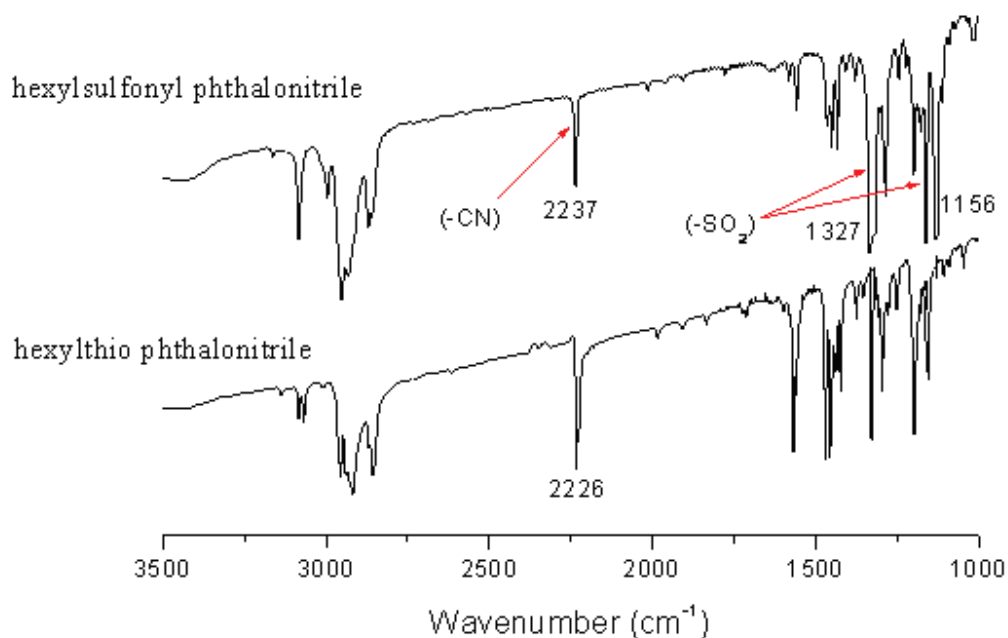


Figure 3.1. Comparison of IR spectra of alkylthio phthalonitrile and alkylsulfonyl phthalonitrile.

^1H NMR spectra of alkylsulfonylphthalonitriles are different from those of alkylthiophthalonitriles. While the aromatic protons of alkylthiophthalonitriles appear at 7.5-7.8 ppm, the aromatic protons of alkylsulfonylphthalonitriles are shifted at 8.0-8.3 ppm reflecting the increase of electron-withdrawing character of substituents upon oxidation to SO_2R (Figure 3.2).

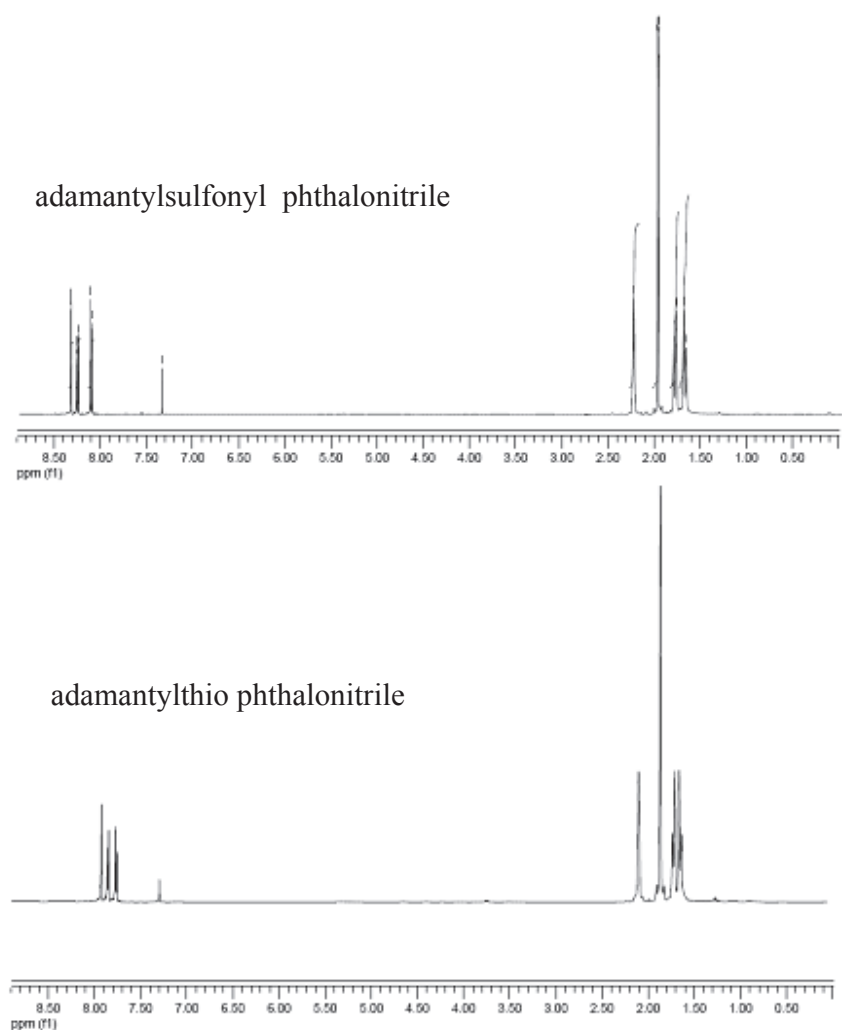
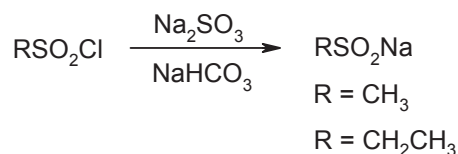


Figure 3.2. ¹H NMR spectra of adamantylthio and adamantylsulfonyl phthalonitriles **13** and **14**.

In the case of R = methyl or ethyl, the use of corresponding thiols was difficult because of their strong smell. To overcome this problem, we used sodium methanesulfinate and sodium ethanesulfinate to obtain alkylsulfonylphthalonitriles **10** and **12** directly thus avoiding an oxidation step (Scheme 3.2) (**Method 2**). Sodium alkylsulfinate salts can easily be prepared from corresponding RSO₂Cl by the treatment with Na₂SO₃ in high yield (92%) [129]. This approach afforded methyl **10** and ethyl **12** sulfonyl phthalonitriles (Table 3.4).



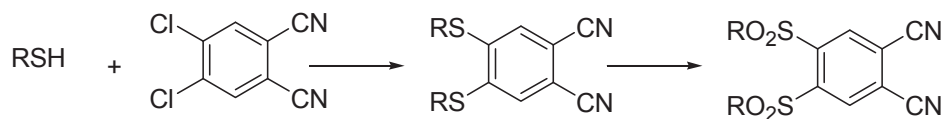
Scheme 3.2. Preparation of sodium alkylsulfinate salts

Table 3.4. Nucleophilic substitution's yields of methyl and ethylsulfonyl phthalonitriles

| R | Yield of nucleophilic substitution (%) |
|--------|----------------------------------------|
| methyl | 60 |
| ethyl | 62 |

3.1.1.2. Disulfonyl phthalonitrile

Phthalonitrile **2** was synthesized in two steps similar to those of method 1, starting from 4,5-dichlorophthalonitrile [130], by nucleophilic substitution with hexylthiol in the presence of K₂CO₃ to give **1**, followed by oxidation with H₂O₂ in acetic acid at refluxing temperature [131] as indicated in Scheme 3.3.



Scheme 3.3. Preparation of disulfonyl phthalonitrile

As for the monosubstituted phthalonitriles, the melting point after oxidation increases. The dialkylthio phthalonitrile's melting point is 70 °C after oxidation, dialkylthio phthalonitrile's melting point is 114 °C.

^1H NMR spectra exhibits changing of aromatic proton after oxidation of dialkylthio phthalonitriles. The aromatic proton of dialkylthiophthalonitrile appear at 7.2 ppm, but aromatic protons of dialkylsulfonylphthalonitriles shifted at 8.6 ppm (Figure 3.3).

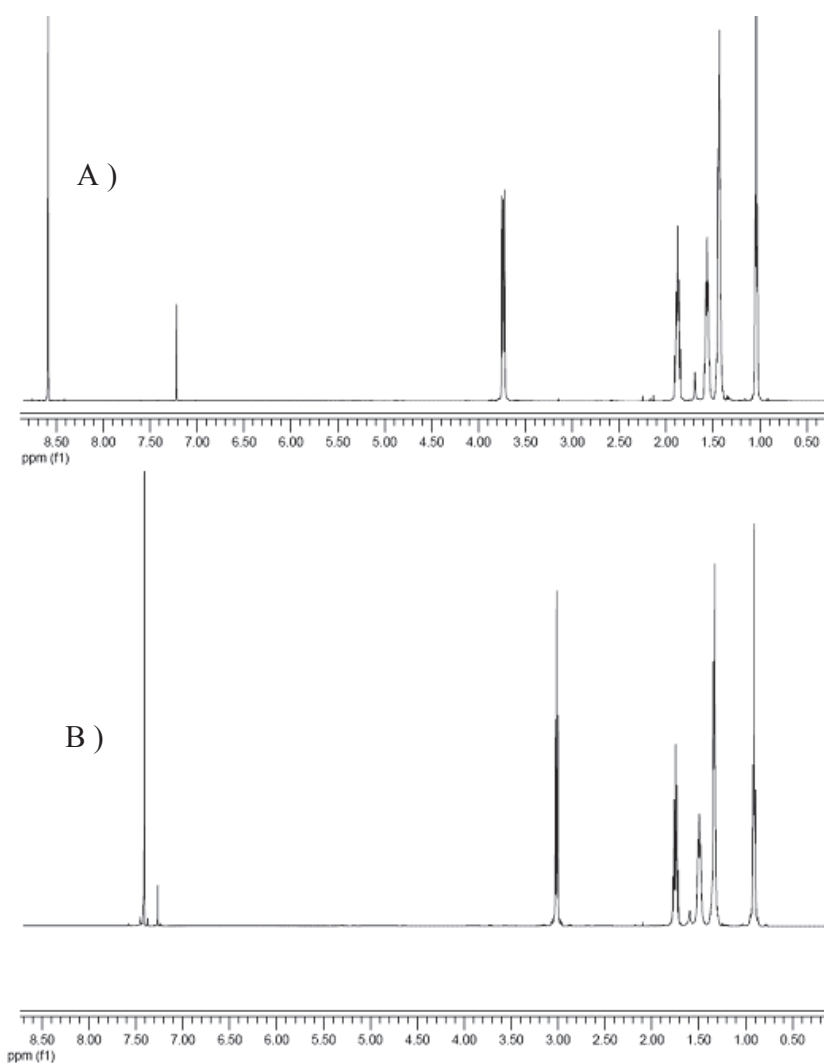
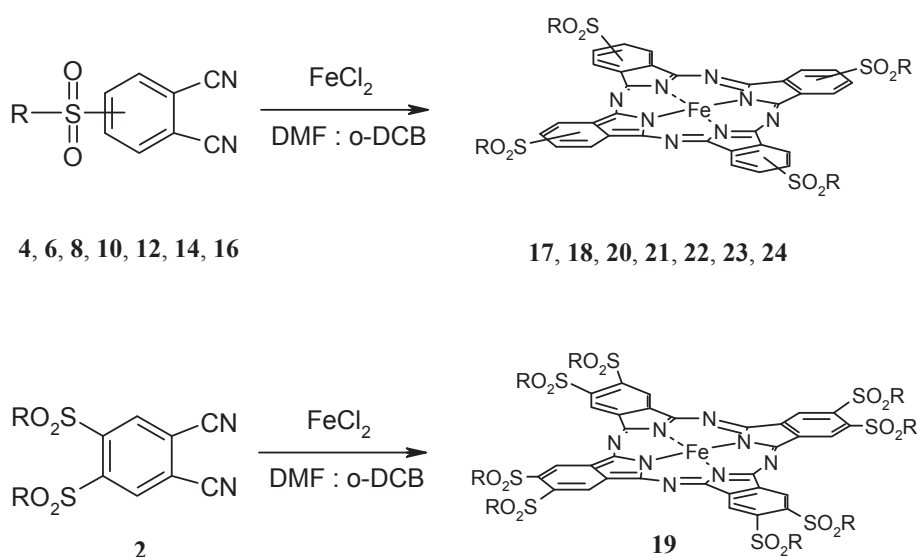


Figure 3.3. ^1H NMR spectra of dihexylsulfonyl(A) and dihexylthio(B) phthalonitriles.

3.1.2 Monomeric iron phthalocyanines

3.1.2.1 Reaction's conditions

The described synthesis of alkylsulfonyl phthalocyanines reports that the best solvent is a *o*-dichlorobenzene-DMF mixture, as other solvents induce the degradation of the starting phthalonitrile [132-135]. Therefore, the monomeric iron sulfonyl phthalocyanines peripheral-tetra hexyl (**17**), nonperipheral-tetra hexyl (**18**), peripheral tetra-*t*-butyl (**20**), peripheral tetra methyl (**21**), peripheral tetra ethyl (**22**), peripheral tetra adamantyl (**23**), peripheral tetra cyclohexyl (**24**) and peripheral octa hexyl (**19**) were obtained by treating the corresponding phthalonitriles (**4**, **6**, **8**, **10**, **12**, **14**, **16** and **2**) in the presence of FeCl₂ in a (3:1) *o*-dichlorobenzene-DMF mixture (Scheme 3.4).



Scheme 3.4. Preparation of monomeric iron phthalocyanines

These monomeric iron phthalocyanine complexes were characterized by classical characterization techniques: FT-IR, UV-vis, EA, ESI-MS and MALDI-MS.

3.1.2.2. Characterizations

Infrared Spectroscopy

Metallated phthalocyanines have very similar infrared spectra, with bands around 3030 cm^{-1} corresponding to the aromatic C-H stretching vibrations, at around 1610 and 1475 cm^{-1} bands to C-C ring skeletal stretching vibrations and at around 720 cm^{-1} bands to C-H out of plane bending vibrations [136]. IR was used to evidence the presence of several characteristic functions (mainly -SO_2 , C-H, C-C). The sharp peak of $\text{C}\equiv\text{N}$ vibrations in the IR spectra of phthalonitriles **2**, **4**, **6**, **8**, **10**, **12**, **14** and **16** (around 2230 cm^{-1}) entirely disappeared after conversion into iron phthalocyanines. The compared IR spectra of cyclohexylsulfonyl phthalonitrile and cyclohexylsulfonyl iron phthalocyanine are given in Figure 3.4.

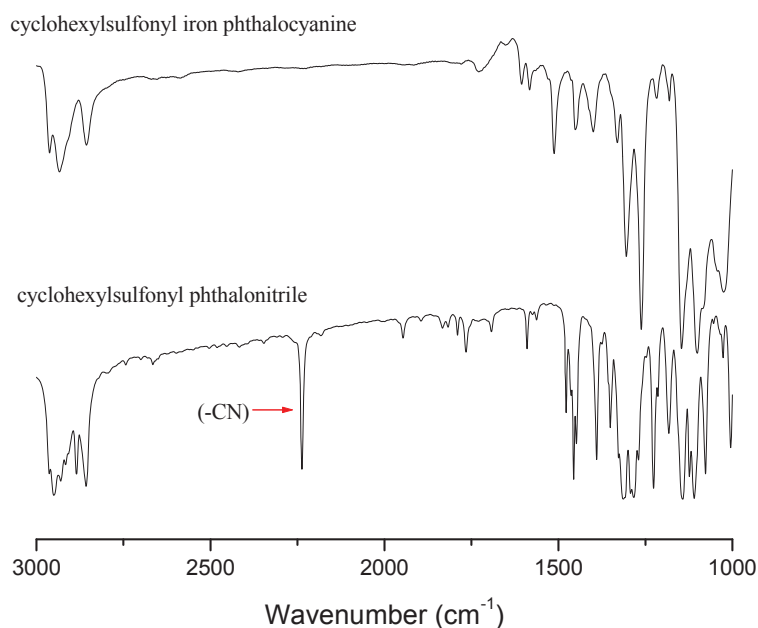


Figure 3.4. The IR spectra of cyclohexylsulfonyl phthalonitrile and cyclohexyl sulfonyl iron phthalocyanines.

UV/Visible Spectroscopy

Metallated phthalocyanines have characteristic UV/Visible spectra with a strong absorption band in the visible region called the Q-band and a weaker absorption in the UV region called the B or the Soret band. UV/Visible data in chloroform for all the monomeric iron phthalocyanines are given in Table 3.5. The UV/Visible spectrum of **19** is given as example in Figure 3.5 and shows a Q band at 670 nm and a B band at 354 nm.

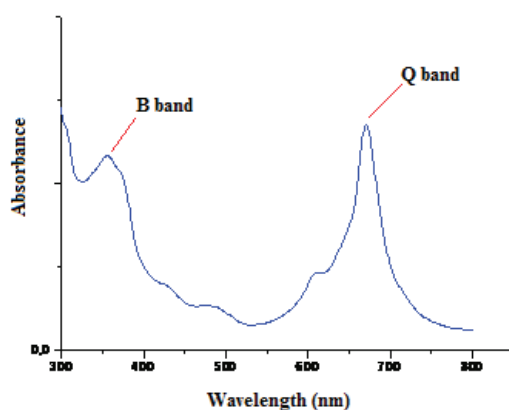


Figure 3.5. UV-vis spectrum of monomeric iron octa-(hexylsulfonyl)phthalocyanine (**19**)

Table 3.5. UV/Visible data of monomeric iron phthalocyanines (* in sulphuric acid).

| Compound | UV-vis (CHCl ₃), λ_{max} (log ϵ) | |
|------------------------------------|-----------------------------------------------------------------------|-----------|
| | Q band | B band |
| 17 tetra-p-hexyl | 680 (4.7) | 306 (4.6) |
| 18 tetra-np-hexyl | 682 (4.8) | 347 (4.6) |
| 19 octa-p-hexyl | 670 (4.8) | 354 (4.6) |
| 20 tetra-p- ^t Bu | 683 (4.8) | 287 (4.7) |
| 21 tetra-p-methyl | 665 (4.7) | 327 (4.6) |
| 22 tetra-p-ethyl | 670 (5.1) | 336 (4.6) |
| 23 tetra-p-adamantyl | 683 (4.8) | 336 (4.5) |
| 24 tetra-p-cyclohexyl | 681 (4.7) | 326 (4.3) |
| FePc (non substituted)* | 780 | 300 |

When compared to the absorption values of the corresponding alkylthio phthalocyanines described in literature, the alkyl sulfonyl iron phthalocyanines with the long alkyl chain, small alkyl chain and bulky substituent (**17-24**) exhibited blue shifted Q bands. This observation may be due to the effect of the electron-withdrawing ability of the Pc ring substituent; the methylsulfonyl and ethylsulfonyl groups may have more electron-withdrawing ability than adamantylsulfonyl and t-butylsulfonyl groups. In addition, the substituent's size may affect this blue shift. Therefore, small electron-withdrawing substituted phthalocyanines shift more than bulky substituted ones.

Mass Spectroscopy

Mass spectra showed expected molecular peaks for **17**, **18**, **19**, **20**, **21**, **22**, **23** and **24**. The ESI-MS spectrum of **22** is given in example in Figure 3.6.

$[M+H]^+$ peak was observed at $m/z = 1161$ for **17**, $[M+H]^+$ peak was observed at $m/z = 1161$ for **18**, $[M+H]^+$ peak was observed at $m/z = 1753$ for **19**, $[M]^+$ peak was observed at $m/z = 1049$ for **20** $[M]^+$ peak was observed at $m/z = 880$ for **21**, and $[M+H]^+$ peak was observed at $m/z = 1361$ for **23**, $[M]^+$ peak was observed at $m/z = 1152$ for **24**.

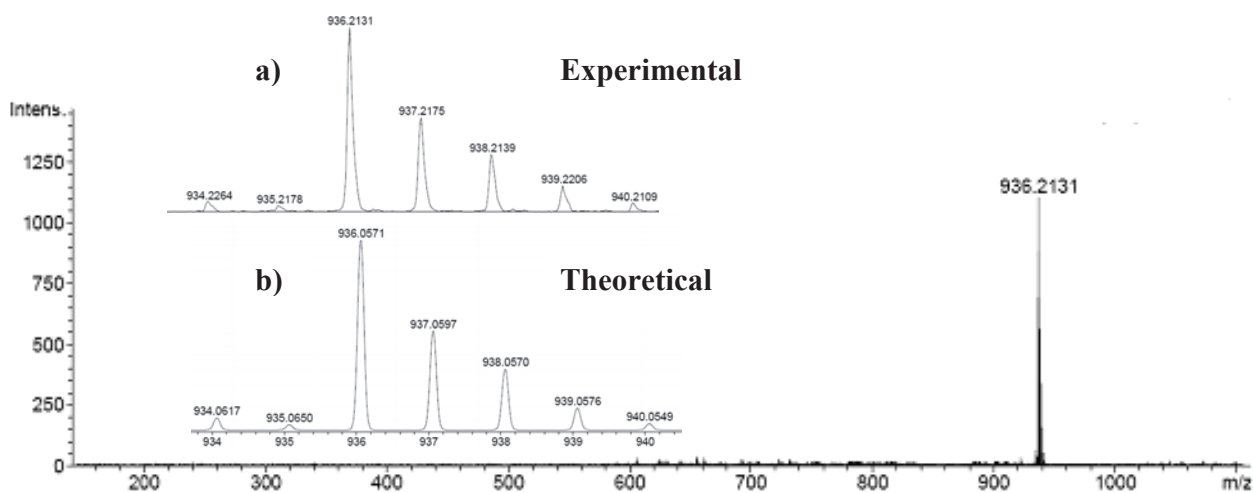
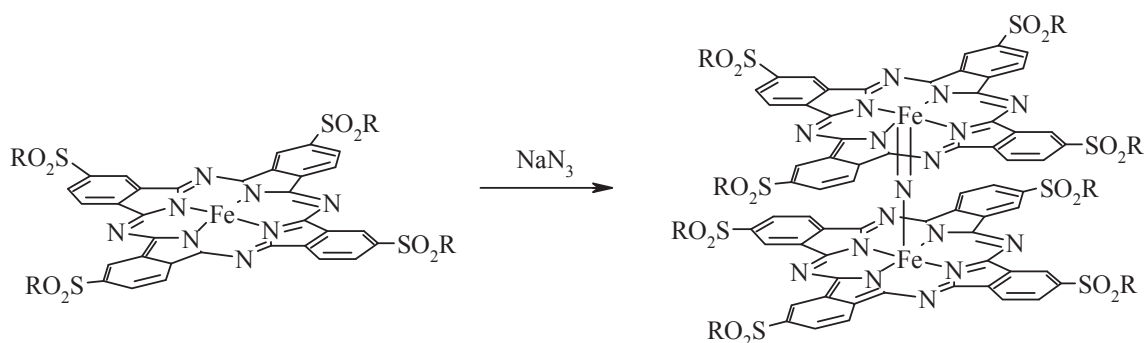


Figure 3.6. Molecular peak cluster of **22** in ESI-MS spectrum (a) and simulated molecular peak cluster for **22**, $C_{40}H_{32}FeN_8O_8S_4$ (b).

3.1.3. Dimeric N bridged diiron phthalocyanines

3.1.3.1. Reaction's conditions

μ -Nitrido diiron phthalocyanines are usually prepared by the treatment of monomeric iron complex with NaN_3 at high temperature in chloronaphthalene (Scheme 3.5) [61,62,137]. In our case, some solubility problems led us to use xylene or DMSO as solvent [63,138]. The choice of the solvent depends on the solubility of the monomer precursor (Table 3.6) and has no significant influence on the yields.



Scheme 3.5. Preparation of μ -Nitrido diiron phthalocyanines.

Table 3.6. The choice of solvent to prepare N bridged diiron phthalocyanines.

| N bridged diiron phthalocyanines | Yield (%) | Solvent |
|--------------------------------------------------|-----------|-------------------|
| $[\text{FePc}]_2\text{N}$ (non substituted) [10] | 90 | chloronaphthalene |
| 25 | 57 | xylene |
| 26 | 58 | xylene |
| 27 | 59 | chloronaphthalene |
| 28 | 64 | chloronaphthalene |
| 29 | 50 | xylene |
| 30 | 48 | dimethylsulfoxide |

3.1.3.2. Characterizations

The successful preparation of μ -nitrido phthalocyanines (**25-30**) were characterized by ESI-MS analyses, FT-IR, UV-vis and EPR methods.

In addition, hexylsulfonyl **25** and t-butylsulfonyl **26** μ -nitrido phthalocyanines were more deeply studied by Mössbauer techniques as well as by X-ray photoelectron spectroscopy (XPS) and Fe K-edge X-ray absorption spectroscopy (XANES, EXAFS, high resolution K β emission spectroscopy).

Infrared Spectroscopy

The IR spectrum of unsubstituted μ -nitrido diiron phthalocyanine (PcFe)₂N exhibit characteristic absorptions due to the anti-symmetric Fe-N=Fe stretching vibration at 915 cm⁻¹ [58b]. This Fe-N=Fe vibration is red-shifted to around 930 cm⁻¹ for electron withdrawing alkyl sulfonyl substituted derivatives [138]. Fe-N=Fe vibration shifted to 938 cm⁻¹ for electron donating ^tBu N-bridged diiron complex [63]. These values clearly show that the substituent nature affects the anti-symmetric Fe-N=Fe stretching vibration shifts (Figure 3.7).

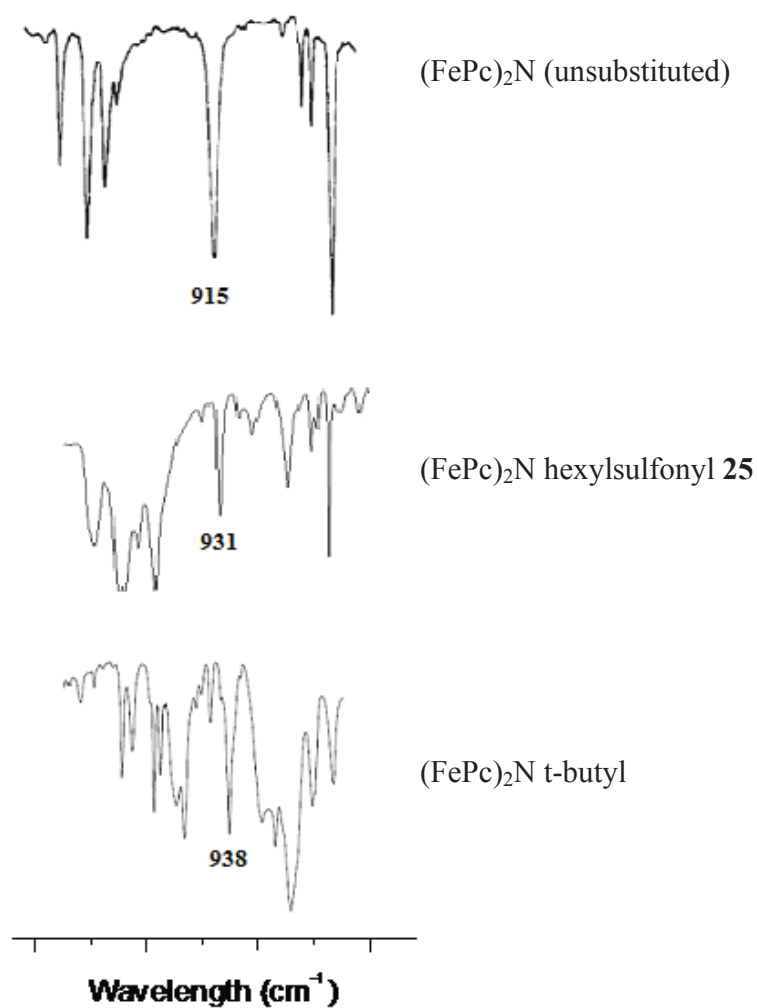


Figure 3.7. Substituent effect on the anti-symmetric Fe-N=Fe stretching vibration shifting.

Accordingly, the Fe-N-Fe anti-symmetric stretching vibrations in the IR spectra of **25**, **26**, **27**, **28**, **29** and **30** are given in Table 3.7. For each of these complexes, the Fe-N=Fe stretching vibration are the same 930 cm⁻¹.

Table 3.7. The Fe-N=Fe anti-symmetric stretching vibrations of μ -nitrido diiron phthalocyanines **25**, **26**, **27**, **28**, **29** and **30**.

| N-bridged diiron phthalocyanines | ν (Fe-N=Fe) (cm^{-1}) |
|------------------------------------------|--------------------------------------|
| [FePc] ₂ N (non substituted)* | 915 |
| 25 | 931 |
| 26 | 929 |
| 27 | 928 |
| 28 | 930 |
| 29 | 930 |
| 30 | 931 |

The μ -nitrido complexes **25**, **26**, **27**, **28**, **29** and **30** can be divided in two groups depending on the size of their substituents: **25**, **27** and **28** bear small substituents (methyl, ethyl and hexyl), while **26**, **29** and **30** have bulky substituents, respectively t-butyl, adamantyl and cyclohexyl groups. The IR spectra of **25**, **27** and **28** having small substituents (Hexyl, Methyl and Ethyl) showed a strong signal at respectively 2010, 2030 and 2034 cm^{-1} assigned to N_3^- vibration (Figure 3.8) while the signal in this range was absent in the spectra of **26**, **29** and **30** with bulky substituents. These data suggest the presence of an azide anion, needed probably for compensation of a positive charge in **25**, **27** and **28**. Thus, **25**, **27** and **28** can be tentatively assigned as $(\text{PcFe}^{\text{IV}}\text{NFe}^{\text{IV}}\text{Pc})^+\text{N}_3^-$ complexes. The absence of N_3^- signal in IR spectra of **26**, **29** and **30** suggests that **26**, **29** and **30** are neutral: that is consistent with $\text{PcFe}^{\text{III}}\text{NFe}^{\text{IV}}\text{Pc}$ structure. These suggestions were confirmed by further analyses (EPR, see below).

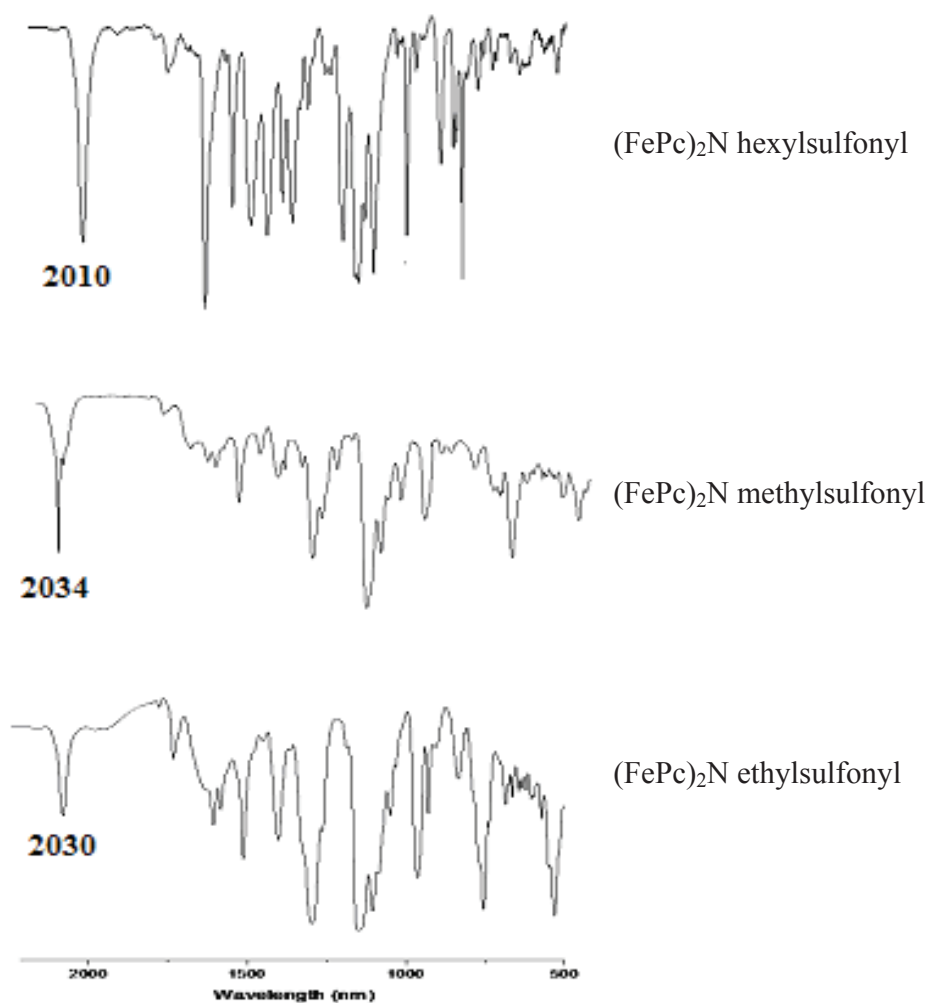


Figure 3.8. The IR spectra of **25**, **27** and **28** showing N_3^- vibration.

The two dimers with small substituents (**27** and **28**) have nearly identical IR spectra (Figure 3.9.A and B), demonstrating that both their oxidation state and their geometry are similar. By contrary, despite their same oxidation state, the IR spectra of the two dimers bearing bulky substituents (**29** and **30**) are different (Figure 3.9 C and D). This is probably due to a different geometric arrangement modifying the recorded vibrations, the steric hindrance of an adamantyl group being more important than the one of a cyclohexyl group, thus imposing maybe more rigid structures, even if adamantyl and cyclohexyl substituents can both be considered as being bulky.

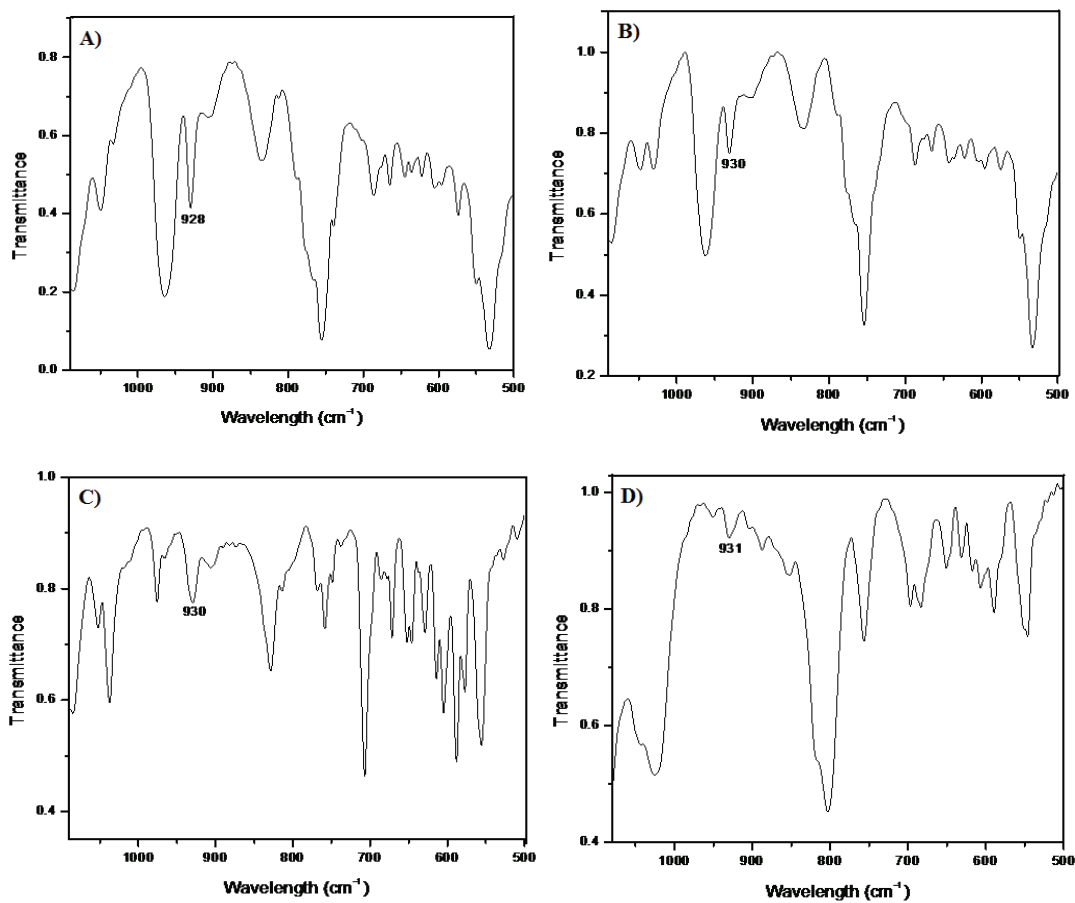


Figure 3.9. IR spectra (1100-500 cm^{-1}) of small substituted (**27**) (A), (**28**) (B) and bulky substituted (**29**) (C) and (**30**) (D) N-bridged complexes.

Mass Spectroscopy

The ESI-MS spectra of the all sulfonyl μ -nitrido complexes exhibit unique molecular peaks corresponding to the expected values of the molecular ion (Table 3.8). The isotopic patterns fit the theoretical ones (see the spectrum of the adamantyl derivative (**29**) on Figure 3.10).

Table 3.8. ESI-MS values of μ -nitrido diiron phthalocyanine **25**, **26**, **27**, **28**, **29** and **30**.

| N bridged diiron phthalocyanines | ESI-MS (m/z) |
|----------------------------------|-----------------------------|
| 25 | 2335.9 [M] ⁺ |
| 26 | 2134.6 [M+Na] ⁺ |
| 27 | 1797.04 [M+Na] ⁺ |
| 28 | 1906.36 [M+Na] ⁺ |
| 29 | 2760.02 [M+Na] ⁺ |
| 30 | 2341.43 [M+Na] ⁺ |

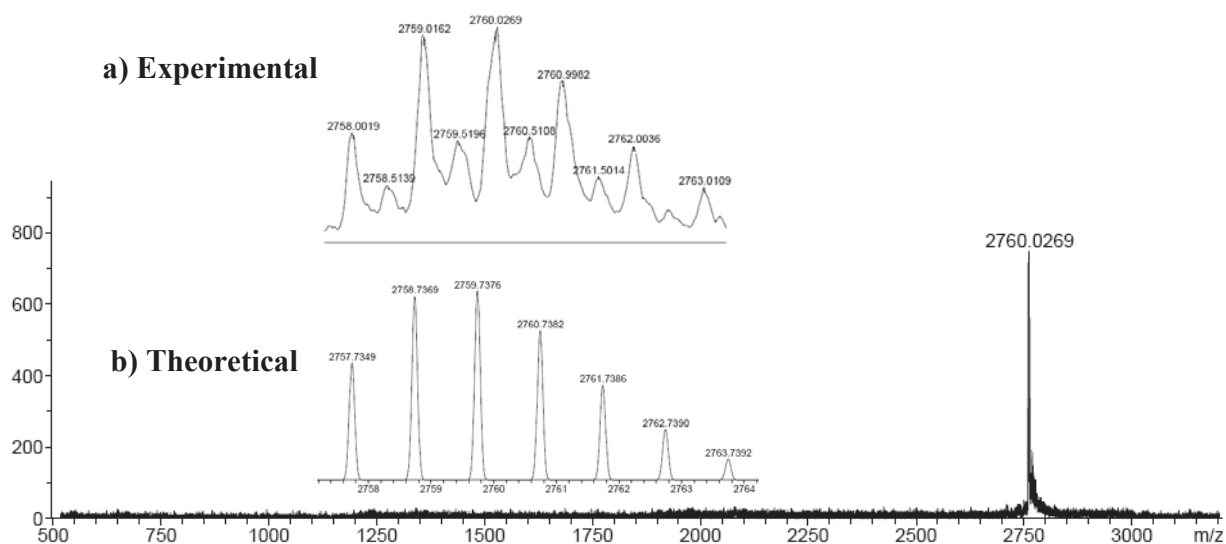


Figure 3.10. Molecular peak cluster of **29** in ESI-MS spectrum (a) and simulated molecular peak cluster for **29**, C₁₄₄H₁₄₄Fe₂N₁₇O₁₆S₈Na (b).

Electron Paramagnetic Resonance Spectroscopy

EPR spectroscopy is an important technique used to evidence the presence of an unpaired electron(s) in the compound that helps to determine the spin and oxidation state of the metal. While cationic dimers are EPR silent, neutral dimers exhibit a feature belonging to $S=1/2$ species with axial symmetry of iron environment.

Dimers bearing small groups: $[\text{FePc}(\text{SO}_2\text{hexyl})_4]_2\text{N}$ (**25**), $[\text{FePc}(\text{SO}_2\text{methyl})_4]_2\text{N}$ (**27**) and $[\text{FePc}(\text{SO}_2\text{ethyl})_4]_2\text{N}$ (**28**) show no EPR signals confirming Fe(IV)Fe(IV) formulation. $[\text{FePc}(\text{SO}_2^t\text{Bu})_4]_2\text{N}$ (**26**) $[\text{FePc}(\text{SO}_2\text{adamantyl})_4]_2\text{N}$ (**29**) and $[\text{FePc}(\text{SO}_2\text{cyclohexyl})_4]_2\text{N}$ (**30**) dimers show a typically axially symmetry spectrum, consistent with a low-spin complex having an A_1 ground state (Figure 3.11).

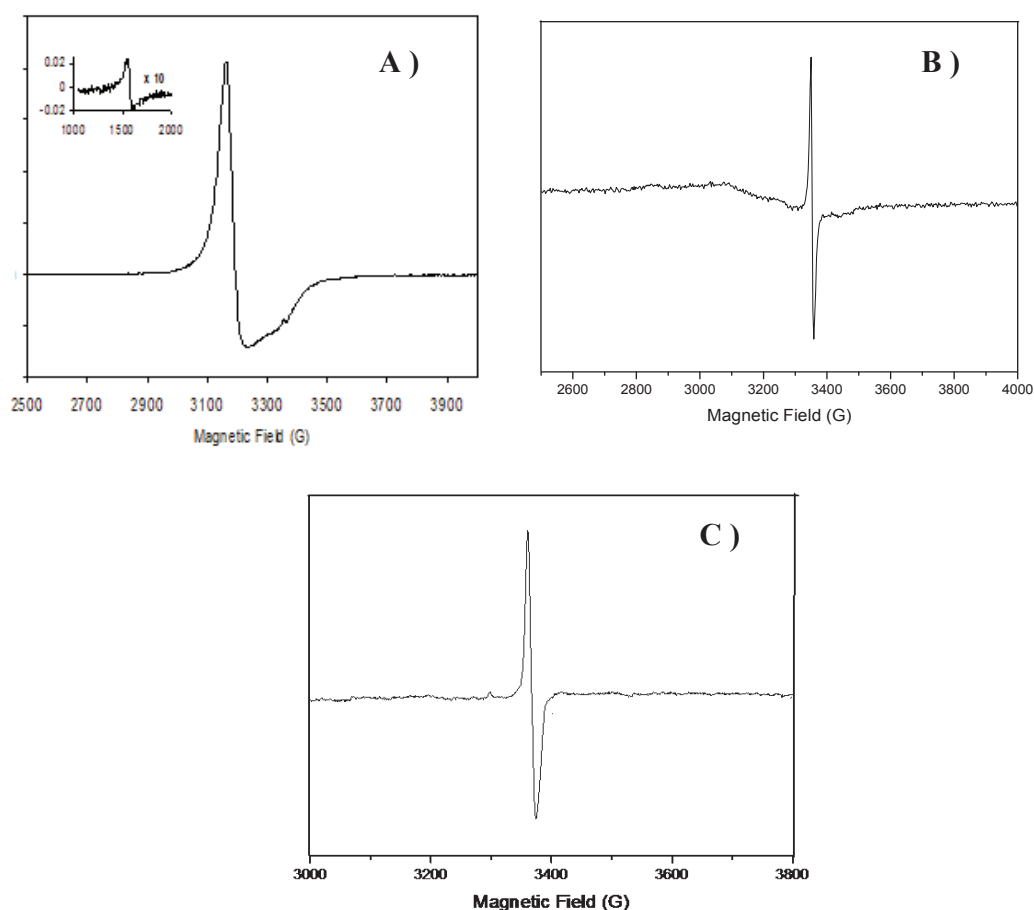


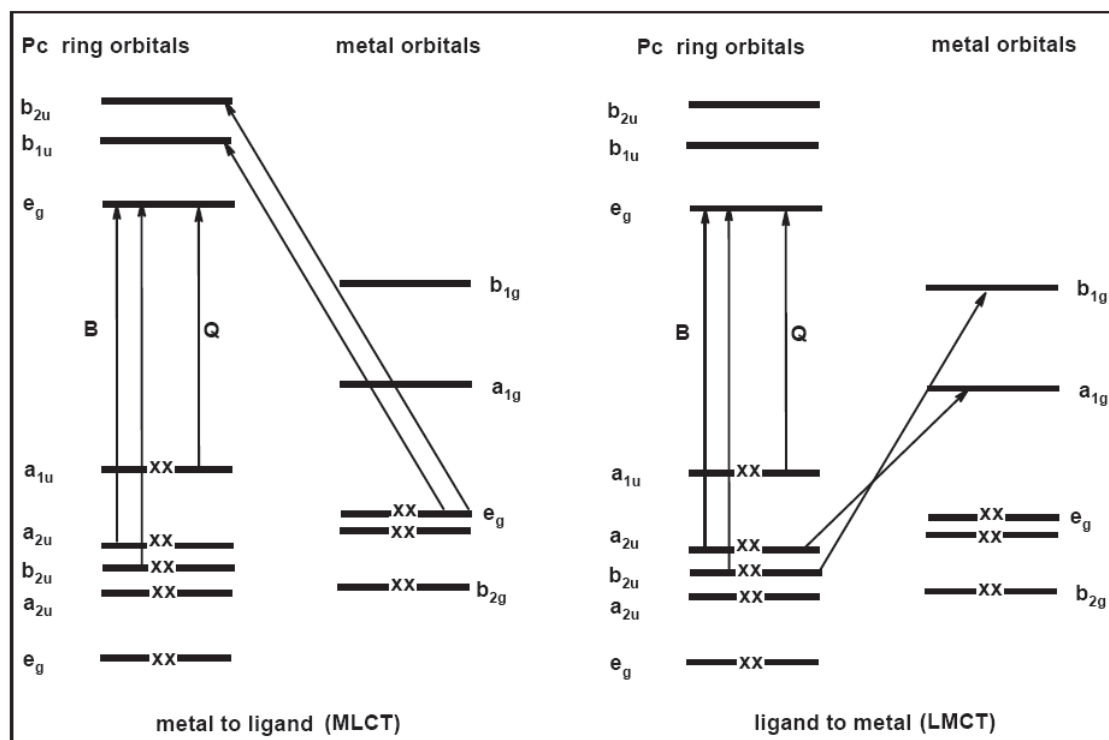
Figure 3.11. X-band 77 K EPR spectrum of **26** (A), **29** (B) and **30** (C).

The solid state EPR spectra of the four N-bridged dimers were recorded at 77 K. These parameters are similar to those observed for non-substituted nitrido-dimers of Fe(III) octaphenyltetraazaporphine and appear to be indicative of extensive delocalization over the two iron centers. Solid non-substituted (PcFe)₂N was studied by Bottomley et. al. [58b] who also found an axial signal with $g_1=2.13$ and $g_2=2.03$. It should be noted that considering exchange between Fe^{III} (S=5/2) and Fe^{IV} (S=2) centres with antiferromagnetic coupling leads to the ground state S=1/2 and X-band EPR spectra similar to one-center Fe^{III} with g values close to 2, as observed in the Fe^{III}Fe^{IV} species of a ribonucleotide reductase [139]. The absence of nitrogen hyperfine structure in EPR spectrum is in accordance with Fe^{+3.5}-N⁻³-Fe^{+3.5} formalism [140]. μ -Nitrido bridged species exhibit an exceptional inertness and stability because of the delocalisation of an unpaired electron. Data obtained by other spectroscopic methods are also in agreement with formulation of **26** with t-butylsulfonyl, **29** with adamantylsulfonyl and **30** with cyclohexylsulfonyl substituents as neutral Fe^{III}Fe^{IV} N-bridged dimer and **25** with hexylsulfonyl, **27** with methylsulfonyl and **28** with ethylsulfonyl as cationic Fe^{IV}Fe^{IV} complex containing N₃⁻ for compensation of charge. The presence of N₃⁻ in **25**, **27** and **28** were evidenced by the presence of 2010, 2034 and 2030 cm⁻¹ strong signal in IR spectrum.

UV/Visible Spectroscopy

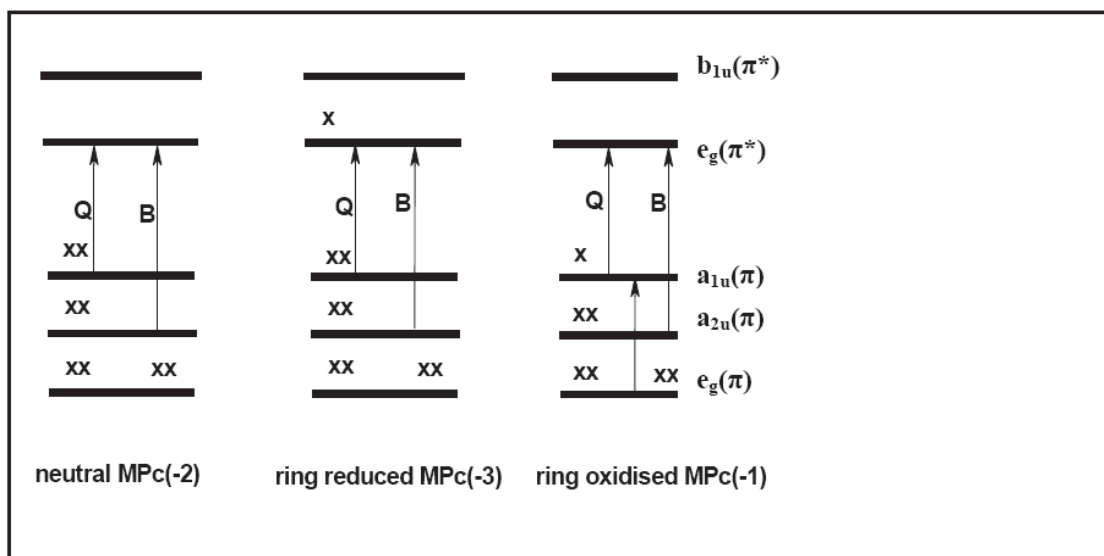
Phthalocyanine systems exhibit two strong absorption bands in electronic absorption spectra. The positions of Soret band (near 340 nm) and of intense Q band (between 600 and 700 nm due to π - π^* ligand transition) of phthalocyanine complexes are affected by electronic interaction between ligands as well as by the state of central atom, axial ligation and peripheral substitution [141-143]. The origin of the UV-Visible spectrum is well explained by Gouterman's 4-orbital linear combination of atomic orbital model, (Scheme 3.6). According to the theory, the highest occupied molecular orbitals (HOMOs) of the MPc ring are the $a_{1u}(\pi)$ and $a_{2u}(\pi)$, the lowest unoccupied orbital

(LUMO) of the MPc ring is the $e_g(\pi)$. The Q and B bands arise from transitions from the $a_{1u}(\pi)$ (Q band), and $a_{2u}(\pi)$ and b_{2u} (B bands), respectively to the e_g orbital.



Scheme 3.6. Gouterman's 4-orbital linear combination of atomic orbital model

Metal oxidation or reduction is characterised by a shift in Q band without much lowering in intensity while ring oxidation will result in collapse of the Q band and formation of a broad peak at around 500 nm. This results in a 'hole' in the $a_{1u}(\pi)$ level which allows transition from the low-lying, $e_g(\pi)$ level to the HOMO. Ring reduction also results in collapse of Q band followed by formation of new bands between 550 nm and 650 nm (Scheme 3.7).



Scheme 3.7. Energy level diagram for one-electron ring reduced or ring oxidised MPc complex

The UV-vis spectra of **25**, **26**, **27**, **28**, **29** and **30** have been recorded: the strong π – π^* interaction between two phthalocyanine moieties in dimers results in a blue shift as compared with monomer complexes: from 680 nm to 657 for **17/25**, from 683 nm to 638 for **20/26**, from 665 nm to 654 nm for **21/27**, from 670 nm to 652 nm for **22/28**, from 683 nm to 639 nm for **23/29** and from 681 nm to 634 nm for **24/30**, respectively (Figure 3.11) (Table 3.9).

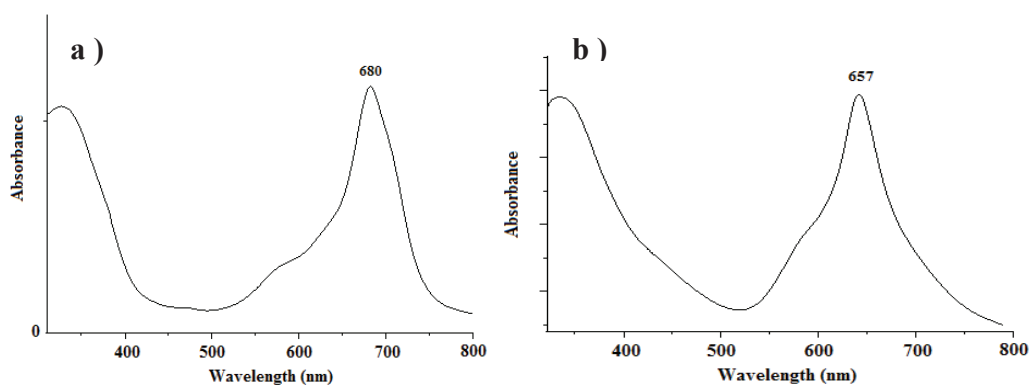


Figure 3.11. UV-vis spectra of hexylsulfonyl iron phthalocyanine **17** (a), hexylsulfonyl μ -nitrido diiron phthalocyanine **25** (b)

Table 3.9. UV-vis data of μ -nitrido diiron complexes.

| | UV-vis |
|-------------------|--------------------------------------------------|
| Compound | λ_{max} (nm)(solvent) |
| FePc-N-FePc | 625 (py) 690 (solid) |
| (TPP)Fe-N-Fe(TPP) | 531, 403, 380 (CHCl ₃) |
| 25 | 657, 344, 297 (CH ₂ Cl ₂) |
| 26 | 638, 339 (CH ₂ Cl ₂) |
| 27 | 654, 319 (CH ₂ Cl ₂) |
| 28 | 652, 319 (CH ₂ Cl ₂) |
| 29 | 639, 319 (CH ₂ Cl ₂) |
| 30 | 634, 319 (CH ₂ Cl ₂) |

Table 3.9 clearly shows that UV-vis spectra of **25**, **27** and **28** are quite different. This difference can be explained by the difference in the oxidation state of iron: it has been previously described that unsubstituted neutral (FePc)₂N can easily be oxidized to cationic (FePc)₂N⁺ complex, resulting in a red shift of Q band from 626 nm to 634 nm in pyridine [58b]. Q bands of oxidized **25**, **27** and **28** (Fe^{IV}Fe^{IV} state) are red shifted compared to those of neutral **26**, **29** and **30** (Fe^{III}Fe^{IV} state). H₅PV₂Mo₁₀O₄₀ or ferrocenium hexafluorophosphate can be used as oxidant to oxidize μ -nitrido diiron phthalocyanine to cationic forms. Thus, **26**, **29** and **30**, obtained as PcFe^{IV}NFe^{III}Pc neutral form, were oxidized by H₅PV₂Mo₁₀O₄₀ to PcFe^{IV}NFe^{IV}Pc⁺. Table 3.10 gives the UV-vis modifications for μ -nitrido diiron dimers after oxidation.

Table 3.10. UV-vis changing of μ -nitrido diiron phthalocyanines after oxidation.

| | UV-vis | |
|--------------------|-----------------------------|-------------------------------|
| Compound | λ_{max} (nm) | |
| | Neutral | Cationic (after oxidation) |
| FePc-N-FePc | 625 | 637 |
| 26 | 638 | 647 |
| 29 | 639 | 651 |
| 30 | 634 | 649 |

In turn, **25**, **27** and **28**, synthesized as $\text{PcFe}^{\text{IV}}\text{NFe}^{\text{IV}}\text{Pc}^+$ cationic oxidized form, were reduced by hydrazine. Table 3.11 gives the UV-vis changes of μ -nitrido diiron dimers after reduction.

Table 3.11. UV-vis changes of μ -nitrido diiron phthalocyanines after reduction.

| | UV-vis | |
|-----------|-----------------------------|------------------------------|
| Compound | λ_{max} (nm) | |
| | Cationic | Neutral (after reduction) |
| 25 | 657 | 638 |
| 27 | 654 | 632 |
| 28 | 652 | 633 |

Figure 3.12 shows the UV-vis spectra of the dimers in their two oxidation states. These experiments indicate interconversion between $\text{Fe}^{\text{III}}\text{Fe}^{\text{IV}}$ and $\text{Fe}^{\text{IV}}\text{Fe}^{\text{IV}}$ states.

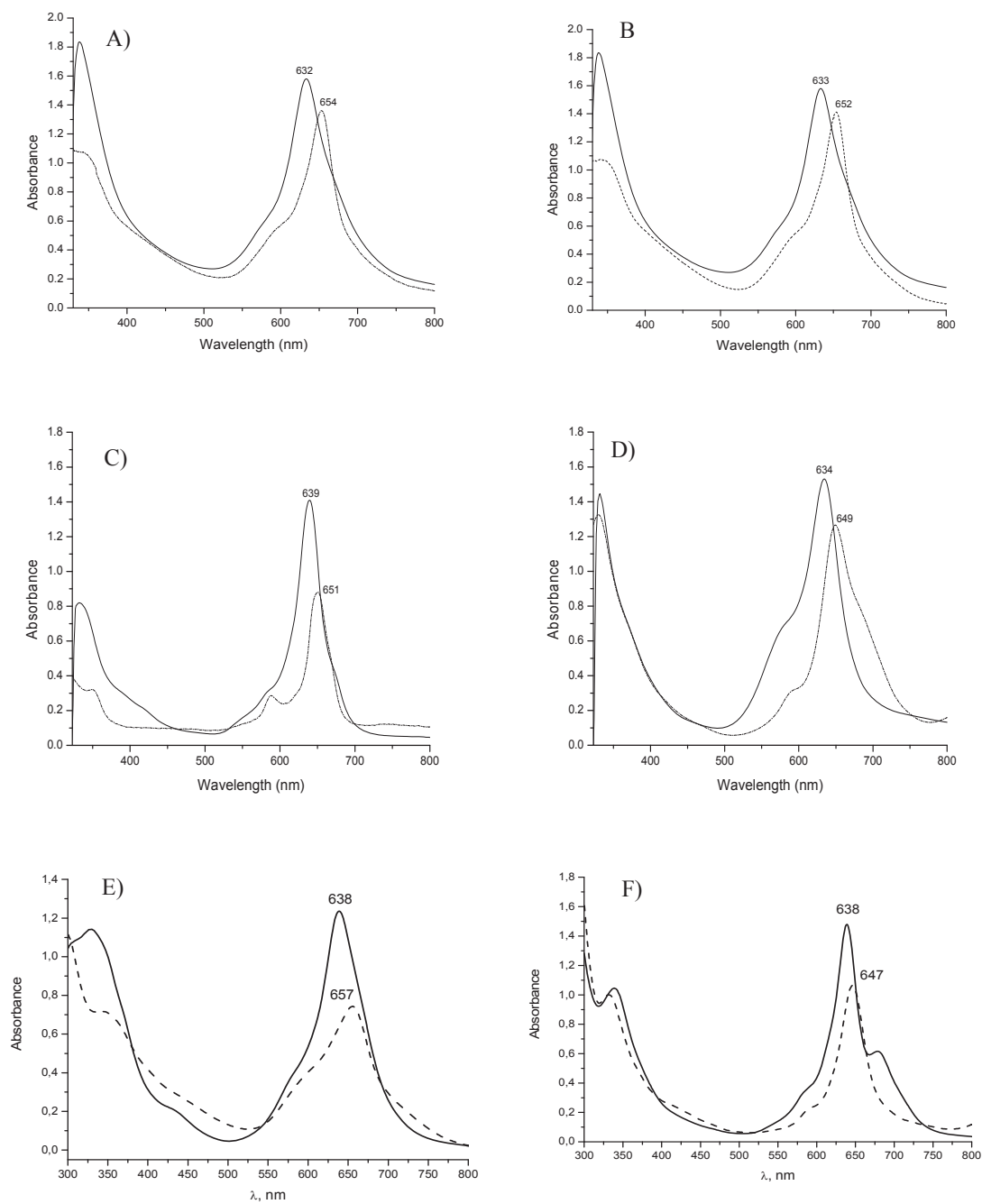


Figure 3.12. UV-vis spectra of **Me** (dash line) and reduced **Me** (solid line) (A), **Et** (dash line) and reduced **Et** (solid line) (B), **Ad** (solid line) and oxidized **Ad** (dash line) (C), **cyc** (solid line) and oxidized **cyc** (dash line) (D), **Hex** (dash line) and reduced **Hex** (solid line) (E), oxidized **^tBu** (dash line) (F), **^tBu** (solid line).

⁵⁷Fe Mössbauer spectroscopy

⁵⁷Fe Mössbauer spectroscopy was used to confirm the different oxidation states of **25** and **26**.

Figure 3.13, Figure 3.14, Figure 3.15 and Figure 3.16 give Mössbauer spectra which were obtained at 77 K for **25** and **26**. For the comparison, ⁵⁷Fe Mössbauer spectra of (FePc)₂N and ((TPP)Fe)₂N are given as well.

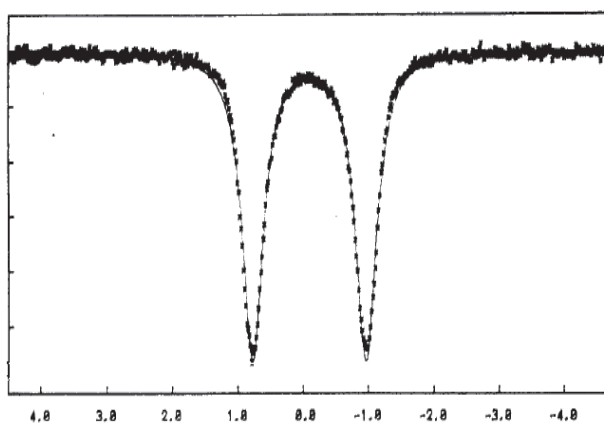


Figure 3.13. ⁵⁷Fe Mössbauer spectra of (FePc)₂N.

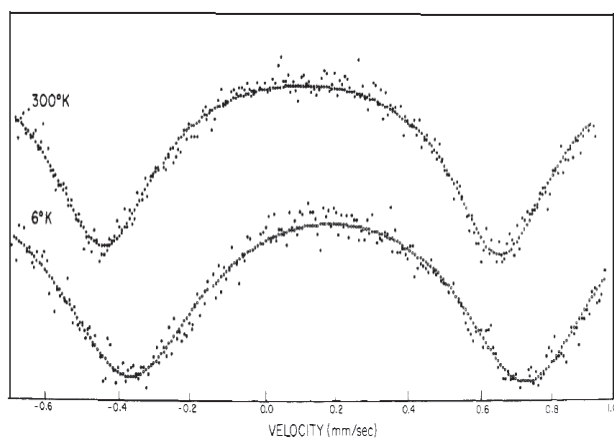


Figure 3.14. ⁵⁷Fe Mössbauer spectra of ((TPP)Fe)₂N.

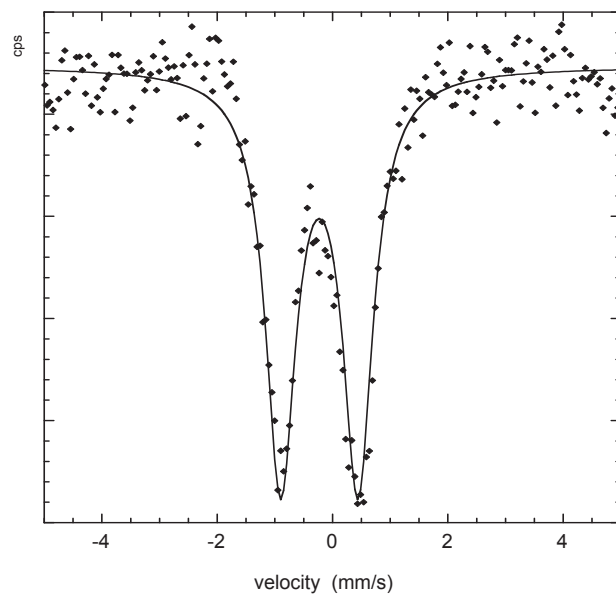


Figure 3.15. ^{57}Fe Mössbauer spectra of **25** at 77 K. Subspectra are derived from a least-squares fit.

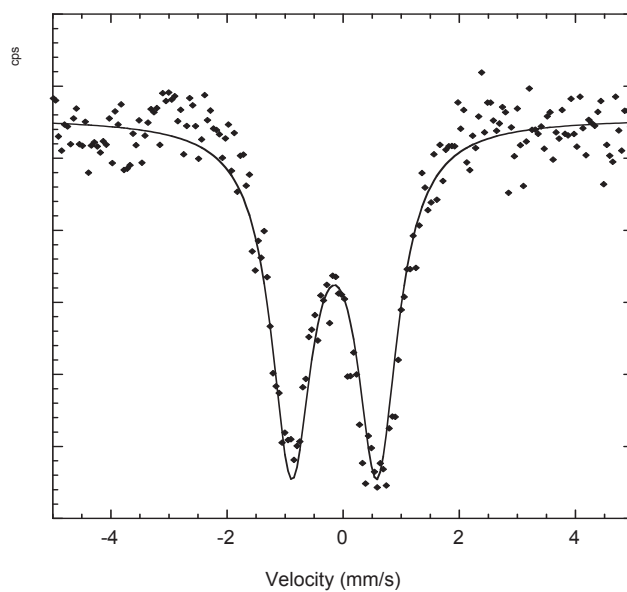


Figure 3.16. ^{57}Fe Mössbauer spectra of **26** at 77 K. Subspectra are derived from a least-squares fit.

These spectra fit to one doublet signals with hyperfine parameters listed in Table 3.12.

Table 3.12. Experimental hyperfine parameters for complexes **25** and **26** from Mössbauer spectra recorded.

| Complex | δ /mm s ⁻¹ | ΔE_Q / mm s ⁻¹ | Γ / mm s ⁻¹ | Iron state | T /K |
|--------------------------|------------------------------|-----------------------------------|-------------------------------|------------|------|
| (FePc) ₂ N | 0.06 | 1.76 | 0.19 | Fe (+3.5) | 77 |
| (Fe(TPP)) ₂ N | 0.18 | 1.08 | | Fe (+3.5) | 131 |
| 25 ^a | - 0.11 | 1.33 | 0.32 | Fe (+4) | 77 |
| 26 ^a | - 0.03 | 1.47 | 0.42 | Fe(+3.5) | 77 |

^a All experimental values are within 0.02 mm s⁻¹; δ = isomer shift, ΔE_Q = quadrupolar splitting, Γ = half width at half height.

Fe^{III}–N–Fe^{IV} unsubstituted phthalocyanine shows a single doublet with an isomer shift of 0.06 mm/s. For the μ -nitrido diiron porphyrin one doublet with δ = 0.18 mm s⁻¹ was observed [144]. Complex **25** exhibits a doublet with isomer shift δ = - 0.11 mm s⁻¹ and quadrupolar splitting ΔE_Q = 1.33. Similar hyperfine parameters were reported for Fe(IV) N-bridged phthalocyanine and porphyrin complexes [58b,59,140,145], although published ΔE_Q values for five- and six-coordinated Fe(IV) centers were higher. The negative value of the isomer shift (-0.11 mm/s) clearly corresponds to iron(IV). For the corresponding μ -nitrido diiron porphyrin complex one doublet with δ = 0.04 mm s⁻¹ was observed at 298 K. Based on these data equivalent iron sites with intermediate iron oxidation state of +3.5 were assumed. The isomer shift of -0.03 mm s⁻¹ observed for **26** is too high for Fe (IV) site. Unpaired electron in **26** having formally Fe^{III}–N–Fe^{IV} state is delocalized between two Fe sites with a time scale shorter than the hyperfine Larmor time ($\tau_L=10^{-8}$ s). The Fe sites appeared with a formal +3.5 state. The fact that **25** complex is EPR silent is in accordance with Mössbauer data which show equivalent Fe(IV) sites.

X-ray photoelectron spectroscopy (XPS)

In earlier studies of porphyrin complexes XPS has been utilized for elucidation of rapid electronic exchange [146]. The time scale of XPS is 10^8 faster as compared with Mössbauer time scale (10^{-15} vs 10^{-7} s). If two different iron sites would constitute Fe-N-Fe unit, one could expect two separate iron $2p_{3/2}$ signals. A single narrow peak (1.6 eV at half-height) was observed for $(\text{TPPFe})_2\text{N}$ (TPP = tetraphenylporphyrin) for Fe $2p_{3/2}$ by Kadish et al [146]. They concluded that only one type of Fe atom was presented in this $\text{Fe}^{3.5}\text{-N-Fe}^{3.5}$ porphyrin complex because of rapid electronic exchange. X-ray photoelectron spectra typical of the Fe 2p binding energy region (700-730 eV) are depicted in Figure 3.17. The Fe 2p XPS spectrum shows two signals. The peak of the lower binding energy (BE) is due to the Fe $2p_{3/2}$ spin component while that at higher BE is assigned to Fe $2p_{1/2}$.

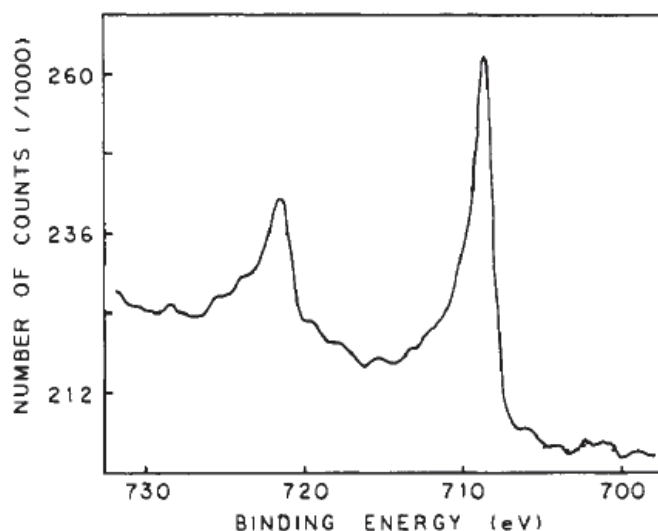


Figure 3.17. Expansion of XPS spectrum (700-730 eV, Fe 2p) for $(\text{TPPFe})_2\text{N}$. This spectrum is extracted from ref [146].

The authors concluded that only one type of Fe atom was presented in this $\text{Fe}^{3.5}\text{-N-Fe}^{3.5}$ porphyrin complex because of rapid electronic exchanges. For the μ -nitrido diiron

phthalocyanines **25** and **26**, similar expansion of XPS spectra are obtained. The Fe 2p region XPS spectra of **25** and **26** are shown in Figure 3.18.

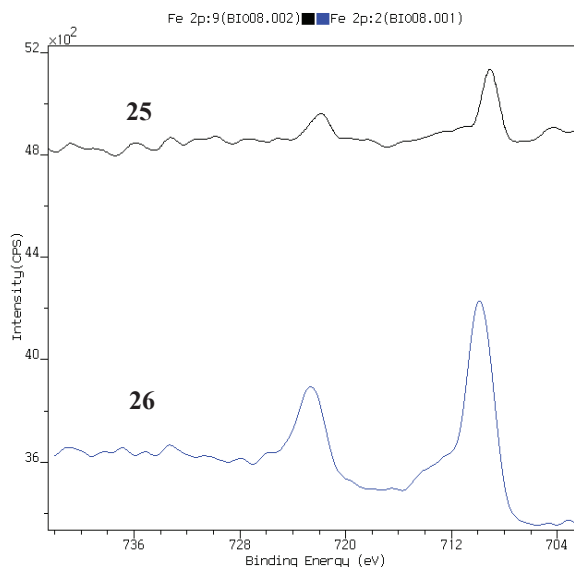


Figure 3.18. Expansion of XPS spectrum (704-742 eV, Fe 2p) for **25** and **26**.

The narrow Fe 2p_{3/2} BE peak of **25** was observed at 709.2 eV with the peak width at half-height of 1.2 eV. The Fe 2p_{3/2} signal of **26** was detected at higher BE of 709.9 eV with a greater width of 2.2 eV. Both **25** and **26** contain only one type of iron site. A lower BE of **25** with respect to that of **26** suggests charged complex in the former case.

The 1s N XPS spectra of **25** and **26** exhibit strong signals at 398.5 and 398.8 eV, respectively, due to nitrogen atoms of phthalocyanine cores with shoulders at higher BE expected for bridging nitrogen atom (Figure 3.19).

The binding energies of N 1s, Fe 2p_{3/2} were measured and are listed in Table 3.13.

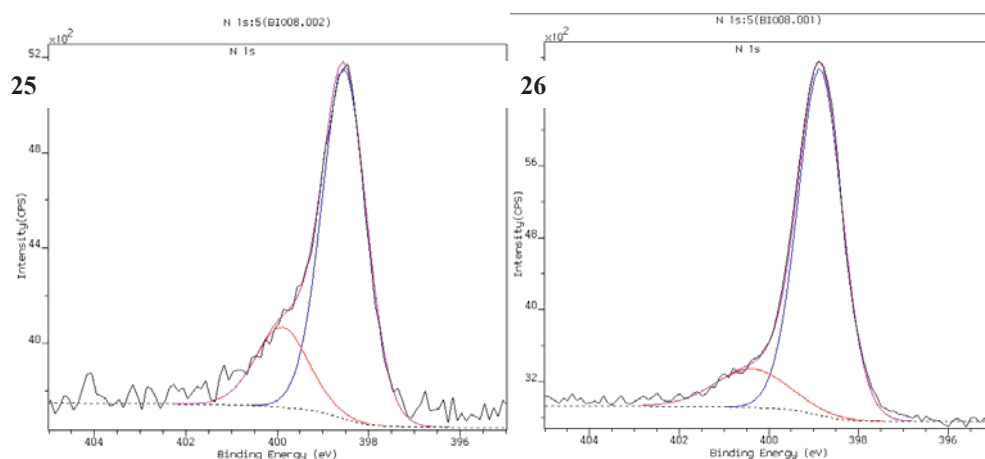


Figure 3.19. Expansion of XPS spectrum (395-405 eV, N 1s) for **25** and **26**.

Table 3.13. Binding Energies for μ -nitrido diiron complexes.

| Complex | Metal Oxidation State | Binding Energy, eV | |
|--------------------------|-----------------------|----------------------|-------|
| | | Fe 2p _{3/2} | N1s |
| (Fe(TPP)) ₂ N | +3.5 | 708.5 (1.6) | 398.3 |
| (Fe(TPP)) ₂ O | 3 | 710.5 (3.1) | 398.3 |
| 25 | +4 | 709.2 (1.2) | 398.5 |
| 26 | +3.5 | 709.9 (2.2) | 398.8 |

What is clearly suggested from the XPS data, in contrast to the Mössbauer and crystallographic data, is that the environment about the Fe center is low spin. This marks the second case of a five coordinate iron porphyrin or phthalocyanine designated as such

X-ray absorption near-edge structures (XANES)

X-Ray absorption spectroscopy can probe the relationships between stereochemistry, oxidation and spin states of iron phthalocyanine. The low-energy range is known as XANES. Both EXAFS and XANES have been applied to synthetic tetrapyrrolic macrocycles [147] and to haemoproteins [148] in particular to carbonyl myoglobin, where a polarized single-crystal study was published [149]. The Fe K-edge spectra of dimer complex **25** and **26** were recorded and compared to that of mononuclear complex to provide a basis for comparison and for simulation. The XANES spectra for mononuclear **20** and binuclear **25** and **26** are presented in Figure 3.20a.

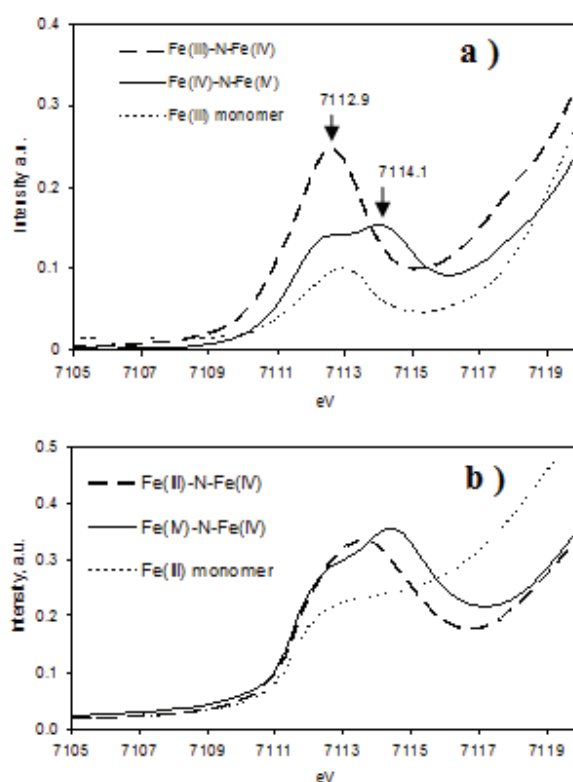


Figure 3.20. Pre-edge region of the XANES spectra for **20**, **25** and **26** : a) experimental spectra; b) FEFF simulation spectra.

The XANES spectrum of mononuclear **20** demonstrates a small but well defined pre-edge absorption peak at 7112.9 eV. Such pre-edge peak observed in the monomeric iron phthalocyanine is typical for the octahedral or square-pyramidal Fe(III) complexes (Figure 3.21) [150]. In the pre-edge weak peak attributable to the 1s - 3d transitions.

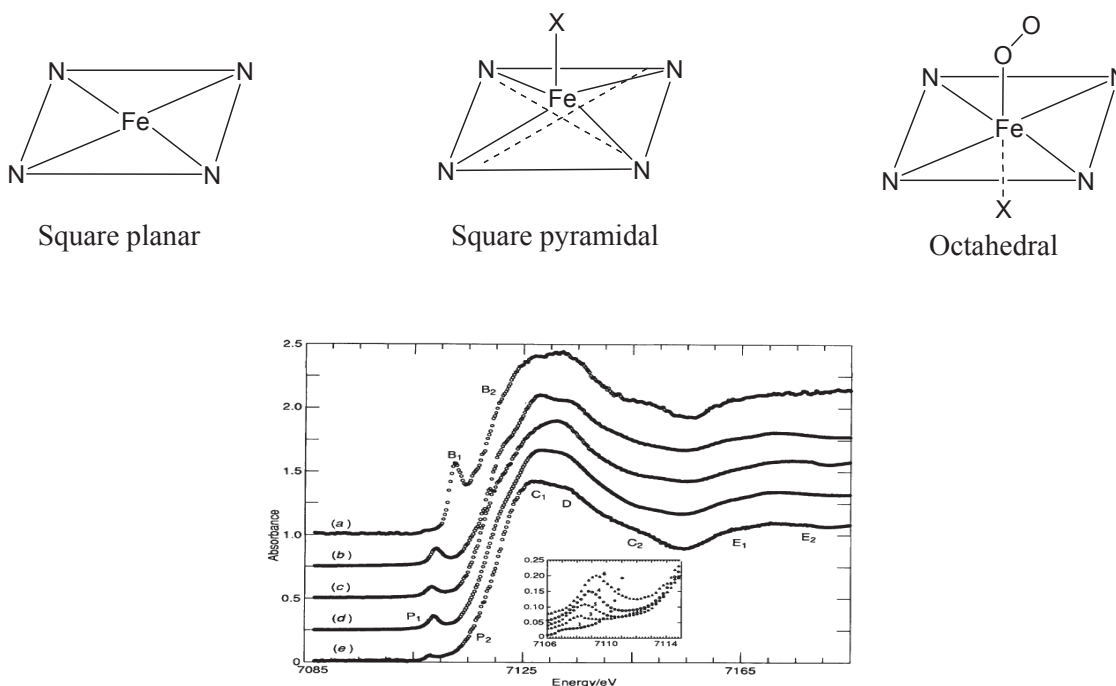


Figure 3.21. Iron K-edge spectra of (a) square-planar compound (b) square-pyramidal, (c) square-pyramidal, (d) square-pyramidal (e) octahedral.

Formation of μ -nitrido dimer led to the increase of pre-edge intensity. This can be expected because addition of short axial bond Fe-N would raise covalence character of z^2 -type iron orbitals and therefore their mixing with the p orbitals [150]. The appearance of the second lobe at 7114.1 eV was observed for the Fe(IV)-N-Fe(IV) complex **3a**. The increase of the pre-edge intensity is consistent with higher oxidation state of iron since (other parameters being equal) it increases the number of free d-orbitals and therefore the probability of 1s-3d electron transfer increases as well. An increase of the pre-edge energy is also in agreement with the hypothesis of iron oxidation state as it means an increase of the efficient positive charge on the iron central ion and therefore a stronger

electron bonding. While the general reason of the pre-edge peak splitting is obviously due to removal of 3d orbitals degeneration and existence of multiple excited states. The XANES spectrum of Fe(IV)-N-Fe(IV) complex **25** exhibits the second lobe at 7114.1 eV, while Fe(III)-N-Fe(IV) complex **26** exhibits at 7112.9. The increase of the pre-edge intensity is consistent with higher oxidation state of iron. The simulated spectra reproduced quite well the qualitative difference between three compounds, though the simulated pre-edge peak of monomer is less pronounced than in the experiment (Figure 3.20b).

EXAFS spectra and fitting

Simulation of the EXAFS part of XAS Fe K spectra and fitting of the experimental curves performed using VIPER program allowed confirming the identity of dimer compound and refining its structure. Due to the large molecular size, and inner position of iron in the μ -nitrido dimer only the environment inside one molecule may have appreciate impact on the spectra. Therefore iron integer coordination numbers are obviously imposed. The model topology was fixed for both monomer and dimer trial structures, and the numbers of neighbors (CNs) were also fixed for each simulation. Only the distances (and the concomitant angles) were variables. This strongly facilitates fitting and allows better adjusting of the distances with the precision of 0.02 Å or even better. At the same time the number of coordination shells which can be fitted also increases, due to the additional independent parameters available, liberated from the fixing of CNs. The linearity of the fragments in the structure can be relatively easy checked using the EXAFS fitting. In the nearly planar phthalocyanine complexes, due to the expected linearity of the N-Fe-N fragments both for bonding and non-bonding nitrogen atoms, the corresponding multiple scattering paths may become important despite the small nitrogen mass. By contrast, if linearity is broken and the iron atom goes out from the phthalocyanine plane, the contribution of such paths rapidly decreases. This makes simulation very sensitive to the deviations of the N-Fe-N and Fe-N-Fe angles from 180°. At the same time multiple scattering paths do not need new parameters to be introduced

in the fitting procedure since they are not independent. Their amplitudes can be taken into account automatically together with the generic single scattering paths. The EXAFS fitting results are presented in Table 3.14 and the simulated and experimental spectra in Figure 3.22.

Table 3.14. EXAFS fitting results for the Fe K edge spectrum of **26**.

| Scatterer | R / Å ^a | Number | DW factor / Å ² |
|-----------|--------------------|----------------|-------------------------------|
| N | 1.669(5) | 1 ^b | 0.0032(5) |
| N | 1.945(5) | 4 ^b | 0.0071(8) |
| C | 2.97(2) | 8 | 0.0073(8) |
| Fe | 3.33(1) | 1 ^b | 0.0032(5) |
| N | 3.41(2) | 4 | 0.0072(8) |
| N | 4.06(3) | 4 | 0.0083(8) |

^a only the mean distances are available in EXAFS, thus making this technique unable to address any small orthorhombic distortions; ^b due to closeness of the Fe-N-Fe fragment geometry to linearity, additional multiple scattering paths must be taken into account for this apparent distance.

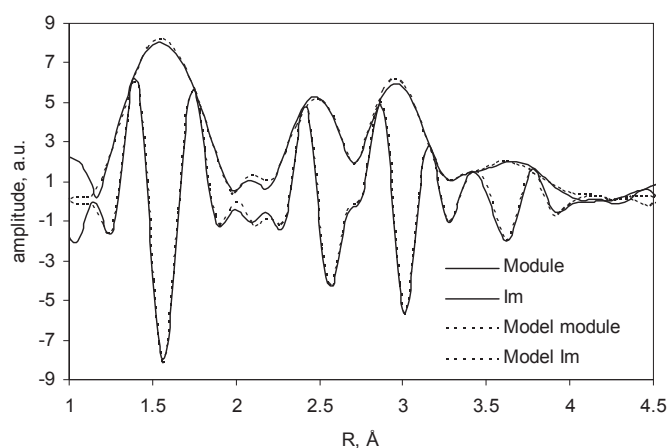


Figure 3.22. R-space fitting of real and imaginary parts of the EXAFS spectrum of μ -nitrido dimer **26**. Module – FT amplitude in the experimental and simulated (model) spectra; Im- imaginary part of FT in the experimental and simulated EXAFS spectra.

Monomeric phthalocyanine exhibits only small intensity at 3 Å distance. The axial Fe-N distance in the dimer was fitted independently on the Fe-Fe distance. The obtained ratio of Fe-Fe to Fe-N distances is very close to 2. This strongly suggests a linearity of the Fe-N-Fe fragment. From simple trigonometric considerations it follows that iron is slightly deviated out of plane towards the central nitrogen, by ca 0.24 Å. This leads to the estimation of the in-plane N-Fe-N angle of 168-170°. However, EXAFS study can not address some essential features of the complexes geometry. Thus, the symmetry of the problem prevents from determining of staggered vs. eclipsed configuration of the Pc planes of the dimer. Slight (0.01-0.02 Å) deviations of the projected iron position from the Pc ring centre can not be excluded as well.

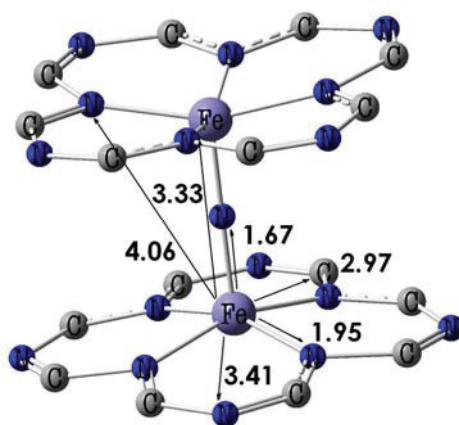


Figure 3.23. EXAFS structure of μ -nitrido dimer **26**.

Structural features of **26** determined from EXAFS data (Figure 3.23) can be compared to the X-ray structure of $(\text{Br})\text{PcFe}^{\text{IV}}\text{-N-Fe}^{\text{IV}}\text{Pc}(\text{Br})$ reported by Moubaraki et al. [60] Fe-N bond distance of linear Fe-N-Fe fragment of **26** is longer than in unsubstituted $(\text{Br})\text{PcFe}^{\text{IV}}\text{-N-Fe}^{\text{IV}}\text{Pc}(\text{Br})$: 1.669 Å vs 1.639 Å, respectively. Thus, the distance between two iron atoms is 3.33 Å suggesting π - π interaction between Pc planes. However, EXAFS data don't allow to conclude on the possible staggering in this binuclear structure. Both iron atoms are displaced out of the N_4 phthalocyanine planes by

0.24 Å indicating five-coordinated iron state. In the only published N-bridged iron phthalocyanine X-ray structure for (Br)PcFe^{IV}-N-Fe^{IV}Pc(Br) iron atoms are in the N₄ plane [60]. The similar withdrawing of iron atoms from N₄ plane of 0.32 Å with shortening of Fe–N distance was previously observed in N-bridged iron porphyrin complex [151]. The structural parameters of N-bridged diiron phthalocyanine with Fe^{III}-N-Fe^{IV} unit were determined for the first time.

High resolution Kβ emission spectra

Kβ emission can be described as a two step process. On the first stage a 1s electron is ejected from the K core and a hole is created. On the second step 3p electron is relaxed to the K core and Kβ fluorescence is emitted, while final state with a hole on 3p level is created. The strong coupling between 3p and 3d orbitals leads to the appearance of extended multiplet structure, usually containing so-called Kβ_{1,3} and Kβ' components [152]. Due to the coupling of 3p hole with 3d electrons, position and intensity of Kβ_{1,3} and Kβ' peaks strongly depend on the oxidation state and spin state of the element under study. The Kβ' structure exhibited by the iron complexes which is due to a spin flip process merges with the Kβ_{1,3} peak as the spin on the atom decreases. At the same time the Kβ_{1,3} peak moves towards lower energies. Thus, the simple qualitative distinction of high spin and low spin iron complexes is possible from the shape of emission spectra. A detailed theoretical explanation of this method can be found in the recent review [152]. μ-nitrido diiron phthalocyanine **25** shows a low-spin (S=0) iron emission spectrum which is different from monomer high spin species (Figure 3.24).

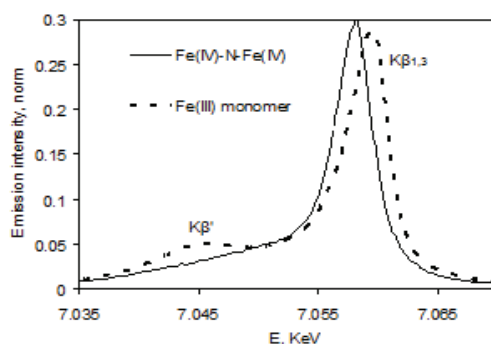


Figure 3.24. High resolution Kβ fluorescence spectra of iron of **25** and of the reference monomeric high spin Fe(III)Pc complex.

The spectra of Fe(III)-N-Fe(IV) t-butyl and non-substituted phthalocyanine complexes also showed the spectra characteristic of low spin iron.

3.1.3.3. Conclusions

Six N-bridged diiron phthalocyanines bearing electron-withdrawing alkylsulfonyl (alkyl = hexyl, t-butyl, methyl, ethyl, cyclohexyl and adamantyl) substituents have been prepared and characterized by ESI-MS analyses, FT-IR, UV-vis and EPR. Hexylsulfonyl and t-butylsulfonyl substituted complexes were characterized additional spectroscopic techniques: Mössbauer, XANES, EXAFS, high resolution K β emission and X-ray photoelectron spectroscopies. The effect of the nature of the substituents has been compared with unsubstituted and electron-donating substituted complexes. The influence of alkylsulfonyl substituents on the oxidation state of N-bridged diiron complexes is striking taking into account their very close electron-withdrawing properties. The size of alkyl substituents is clearly important. While hexylsulfonyl, methylsulfonyl and ethylsulfonyl substituted complexes are cationic $(\text{PcFe}^{\text{IV}}\text{NFe}^{\text{IV}}\text{Pc})^+\text{N}_3^-$ complexes, bulkier t-butylsulfonyl, adamantylsulfonyl and cyclohexylsulfonyl substituents are formally neutral $\text{PcFe}^{\text{III}}\text{NFe}^{\text{IV}}\text{Pc}$ complexes. Due to rapid electron exchange t-butylsulfonyl, adamantylsulfonyl and cyclohexylsulfonyl substituted complexes can be described as $\text{Fe}^{3.5}\text{--N--Fe}^{3.5}$ system with two equivalent Fe(+3.5) sites as it was proposed by Ercolani et al. in the case of the unsubstituted complex. One can suggest that geometrical conformations of dimers could not be the same in the case of small and bulky alkylsulfonyl substituents. Depending on the sterical factors the distances between two phthalocyanine planes and/or staggering angle between them could be different in two cases thus influencing on the ground oxidation state. In order to get insight further spectroscopic and theoretical studies are necessary. Especially useful would be X-ray structural determination, but in the case of tetra-substituted phthalocyanines this task is highly challenging because of the presence of four positional isomers. It is worth to note that a N-bridged diiron tetrasubstituted phthalocyanine contains ten positional isomers.

The bulky substituted complexes such as **26**, **29** and **30** should adopt more staggered conformation with respect to **25**, **27** and **28** complexes. Unfortunately, no X-ray structure of diiron $\text{Fe}^{\text{IV}}\text{--N--Fe}^{\text{III}}$ phthalocyanine complex is yet available. The only published X-ray structure was determined for $(\text{Br})\text{PcFe}^{\text{IV}}\text{--N--Fe}^{\text{IV}}\text{Pc}(\text{Br})$ species containing six-coordinated iron sites and a linear Br--Fe--N--Fe--Br fragment. The two phthalocyanine rings are staggered by an angle of 39° with in plane location of the iron atoms. Fe--N bond distance was quite short (1.639 \AA) thus suggesting the significant π -conjugation along internal bridging system.

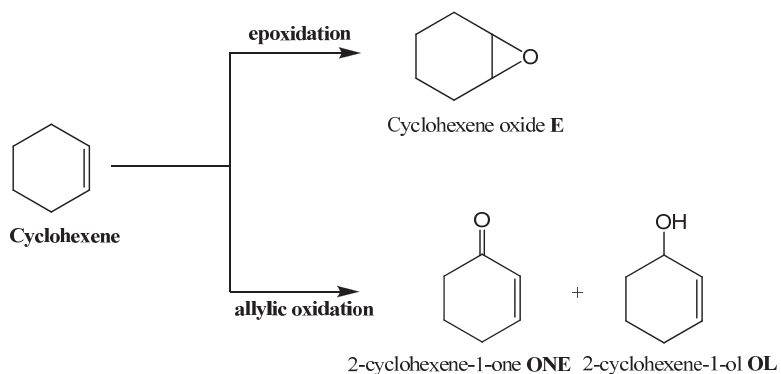
3.2 Oxidation tests

3.2.1. Oxidation of cyclohexene by monomeric sulfonyl substituted Fe(II) phthalocyanines

Hydroxylation and epoxidation reactions by iron porphyrin complexes have been studied very extensively, these complexes being bioinspired chemical models of the cytochrome P450 monooxygenase. Compared to metal porphyrins, corresponding metal phthalocyanines are much more stable against oxidative decomposition.

The oxidation of cyclohexene catalysed by Fe(II) tetra-*t*-butylphthalocyanine (FePc^{*t*}Bu) in dichloroethane was reported [99]. The main oxidation product was cyclohexene oxide (**E**), with small amounts of 2-cyclohexen-1-one (**ONE**) [99] FePcCl₁₆ was used as well for the oxidation of cyclohexene by TBHP in a 3:7 DMF-CH₂Cl₂ solvent mixture [101] Reported products for the oxidation of cyclohexene in these conditions are **E** and **ONE** and 2-cyclohexen-1-ol (**OL**) after long reaction times [101]

In this work, five monomeric iron phthalocyanine complexes: **17**, **18**, **19**, **FePcS** and **FePcF**₁₆ have been tested in oxidation of cyclohexene in the presence of TBHP at 40 °C in different solvents including acetonitrile and co-solvent systems (acetonitrile:water in different proportions). **FePcS** was used as standart catalyst to find optimal conditions for oxidation of cyclohexene. The catalytic activities of these phthalocyanines bearing electron-withdrawing sulfonyl groups or fluorine were compared. Oxidation reaction's products were identified using gas chromatography coupled with mass spectrometry method (GC-MS) and quantified by gas chromatography (GC). These products are **E**, **OL** and **ONE** (Scheme 3.1). Product yields, conversion and reaction times are shown in Table 3.1.



Scheme 3.1 : The products of oxidation of cyclohexene.

Table 3.1. Allylic oxidation of cyclohexene with TBHP in presence of mononuclear iron phthalocyanines in acetonitrile.

| Catalyst | Time (h) | Conversion (%) | ONE (%) | OL (%) | E (%) |
|---------------------------|----------|----------------|---------|--------|-------|
| 17 | 2 | 100 | 24 | 3 | 2 |
| 18 | 5.5 | 97 | 28 | 4 | 1 |
| 19 | 4 | 100 | 38 | 2 | 2 |
| FePcS | 2.5 | 100 | 22 | 1 | 5 |
| FePcF₁₆ | 2.5 | 100 | 30 | 1 | 2 |

The present work shows the formation of **ONE** as the main product (in addition to **OL** and **E**) when iron phthalocyanines **17**, **18**, **19**, **FePcS** and **FePcF₁₆** are employed as a catalyst, and in shorter times than reported before. The presence of electron withdrawing groups at catalyst molecule may affect the rate of formation and properties of active species, resulting in different product selectivities. TBHP oxidant is converted to t-butanol during the catalytic process. Among the tested iron phthalocyanine complexes, **19** emerged as the best one, providing a higher selectivity of the oxidation of cyclohexene into **ONE** (Table 3.1). Figure 3.1 shows that the yield of the **ONE** increased with time, but **OL** started to decrease after 1h. This oxidation kinetics suggests that **OL** is an

intermediate oxidation product in the course of oxidation of cyclohexene to **ONE**. Yields for **OL** and **E** were nearly similar after 4 h.

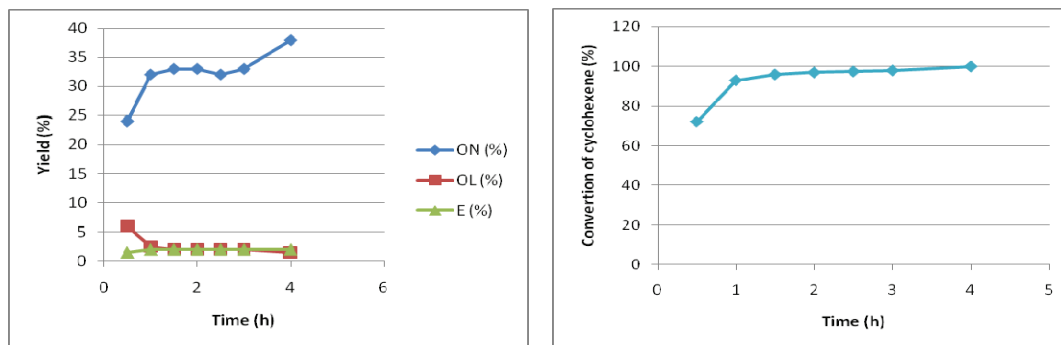


Figure 3.1. Variation of product yield with **19** catalyst and conversion of cyclohexene.

The catalytic activity of **19** was compared to other iron phthalocyanines **17**, **18**, **FePcS** and **FePcF₁₆**. Although **17** had the shortest reaction time (2 h) to complete full conversion of cyclohexene, the yield of **ONE** was low. Yields depend in small extent on the substituent nature and position: while **17** and **18** have same hexylsulfonyl substituents but in different position, they showed similar catalytic activities. Consequently, the substituent position on the phthalocyanine moiety, peripheral on **17** or non-peripheral on **18**, doesn't significantly influenced on the catalytic activity. The yield of the **ONE** increased with time, but **OL** and **E** started to decrease when **18** was the catalyst. (Figure 3.2)

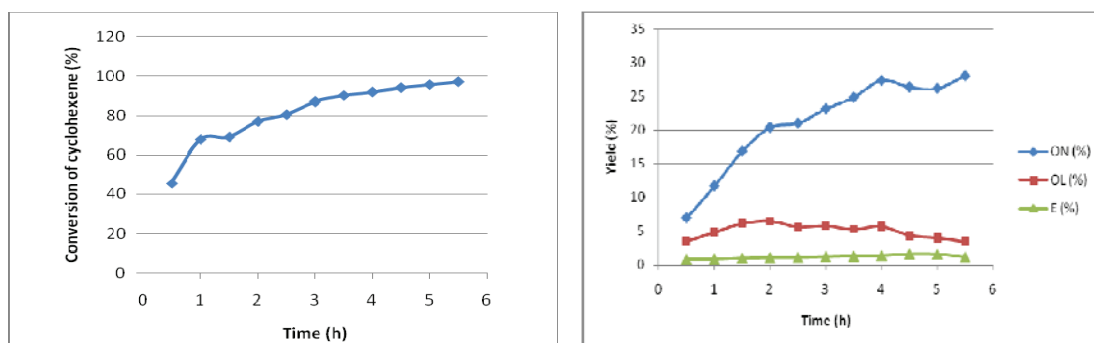
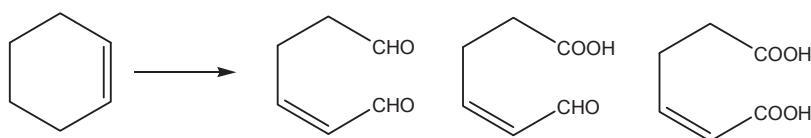


Figure 3.2. Cyclohexene conversion with catalyst **18** and evolution of product yields in time.

The yield observed for the formation of cyclohexene oxide **E** from the oxidation of cyclohexene in the presence of **FePc^tBu** and reducing agent (isobutylaldehyde) was higher (57% after 8 hours) than those reported in this work [99]. The catalytic activity of **FePcF₁₆** was compared to those of **FePcS** after 2.5 hours of reaction time. Both catalysts showed selectivity towards **ONE**, but when **FePcF₁₆** was used as catalyst, higher yield in **ONE** was obtained, probably because of ring halogenation which stabilizes the complex against oxidative degradation (Table 3.1).

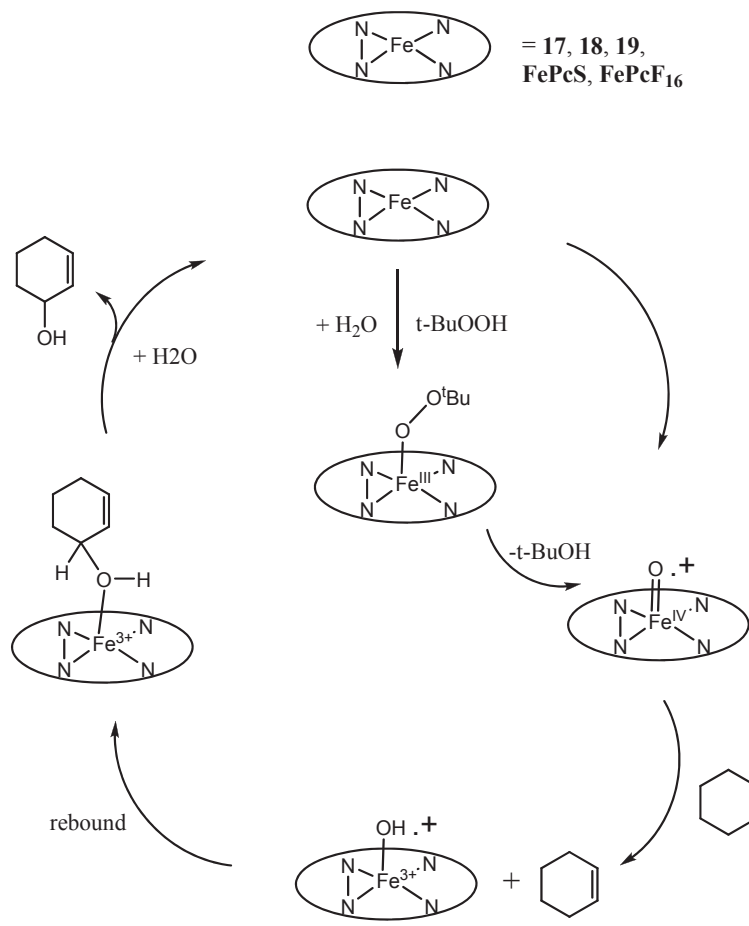
As can be seen from Table 3.1, although cyclohexene conversion was completed in several hours, the total yields of **ONE**, **E** and **OL** were only about 40%. It means that most of the oxidation products couldn't be detected by GC. These undetected products are probably cleavage products of oxidized cyclohexene (Scheme 3.2). These putative products are more difficult to analyze, this work is still in progress.



Scheme 3.2. Possible cleavage products from oxidation of cyclohexene.

Proposed mechanism of formation of **OL** is given in Scheme 3.3. At the first step iron phthalocyanine (FePc) react with TBHP with formation of $\text{PcFe}^{\text{III}}\text{-OOBu}$ peroxo complex. This peroxo complex can undergo homolytic or heterolytic cleavage of O-O bond to give the high-valent iron(IV)-oxo phthalocyanine $\text{PcFe}^{\text{IV}}=\text{O}$ and $\text{BuO}\cdot$ radical (homolytic cleavage) or high-valent iron(IV)-oxo phthalocyanine cation radical $\text{Pc}^+\text{Fe}^{\text{IV}}=\text{O}$. Both pathways can occur in this reaction. Iron(IV)-oxo species induces hydrogen abstraction from the allylic position of cyclohexene resulting in the formation of $\text{Fe}^{3+}(\text{OH})$ complex and allylic radical. In a rebound process and subsequent cleavage, the allylic alcohol is produced and the precursor catalyst is regenerated by replacement of

the axial ligand with water or solvent. In the case of homolytic O-O cleavage, BuO· radical can also react with cyclohexene via allylic hydrogen abstraction leading to the same products. Based on the product distribution, a contribution of a free radical mechanism can not be excluded.



Scheme 3.3. Proposed mechanism for the hydroxylation of cyclohexene.

The choice of the solvent was previously shown to strongly influence the oxidation results. Traylor's group used mixed solvents, such as CH_2Cl_2 – MeOH – H_2O and CH_2Cl_2 – MeOH , for the successful hydroxylation of alkanes by hydroperoxides [153]. Similar effects for other mixed solvent systems, such as CH_3CN – H_2O , CH_2Cl_2 – CH_3CN and CH_3CN – CH_2Cl_2 – H_2O , have also been observed in hydroxylating various C–H bonds [154].

We therefore decided to test the catalytic activity of **FePcS** for oxidation of cyclohexene in different solvent system (acetonitrile, dichloroethane, acetone, dichloromethane, acetic acid, methanol, dimethylformamide). Mixed solvents were tested as well (10-20 % of water in acetonitrile). Results are summarized in Table 3.2.

Table 3.2. Solvent effect on oxidation of cyclohexene with TBHP catalysed by **FePcS**

| Entry | Solvent | Time (h) | Conversion (%) | ONE (%) | OL (%) | E (%) |
|-------|-----------------------------------------------|-------------|-------------------|------------|-----------|----------|
| 1 | CH ₃ CN | 2.5 | 100 | 22 | 1 | 5 |
| 2 | C ₂ H ₄ Cl ₂ | 4 | 79 | 24 | 6 | 1 |
| 3 | CH ₃ COCH ₃ | 2.5 | 98 | 26 | 1 | 6 |
| 4 | CH ₂ Cl ₂ | 3.5 | 79 | 23 | 7 | 1 |
| 5 | CH ₃ COOH | 2.5 | 95 | 28 | 5 | 4 |
| 6 | CH ₃ OH | 3.5 | 81 | 22 | 11 | 3 |
| 7 | DMF | 3 | 42 | 7 | 2 | 3 |
| 8 | CH ₃ CN + %10H ₂ O | 3 | 98 | 35 | 2 | 8 |
| 9 | CH ₃ CN + %20H ₂ O | 3 | 96 | 34 | 2 | 7 |

CH₃CN containing 10% of H₂O (entry 8) is the best solvent system for oxidation of cyclohexene by TBHP in the presence of **FePcS**. When CH₃OH was used as solvent, the yield of **OL** increased (Entry 6). In chlorinated solvents such as dichloroethane (C₂H₄Cl₂) (entry 2) and dichloromethane (CH₂Cl₂) (entry 4), the yield of **OL** increased, while the lowest yields in **E** are observed. However, the yield of **E** increased in acetone (CH₃COCH₃), CH₃CN+%10H₂O and CH₃CN+%20H₂O, and decreased in the other solvents. As expected, the formation of the oxidation products in the tested conditions depends on the nature of the solvents. The stability of solvents in the presence of oxidant is quite important to complete conversion into oxidation products in good yield. CH₃CN is more stable solvent than the others. Using H₂O in combination with CH₃CN results in the increase of **ONE** yield because H₂O can participate in the formation of some reaction intermediates.

In conclusion, the catalytic activity of the novel electron-withdrawing phthalocyanines prepared during these works (monomeric iron phthalocyanine complexes **17**, **18**, **19**) for the oxidation of cyclohexene, using TBHP as the oxidant, has been extensively studied and compared with the catalytic activity of the known phthalocyanines **FePcS** and **FePcF₁₆**, and with literature data reporting the activity of **FePc^tBu** and **FePcCl₁₆**.

The main product of the allylic oxidation of cyclohexene in the presence of electron-withdrawing substituted phthalocyanines catalysts was cyclohexenone. The allylic alcohol **OL** and the epoxide **E** were also detected in minor amounts. Octahexylsulfonyl substituted complex **19** gave the highest yield and selectivity for **ONE**.

We investigated the effect of solvent on the oxidation of cyclohexene. The product selectivity varied with the solvent. The highest yield of **ONE** was obtained in a CH₃CN + 10 % H₂O mixture.

3.2.2. Oxidation of toluene and p-xylene by t-butylsulfonyl and hexylsulfonyl substituted μ -nitrido diiron dimers

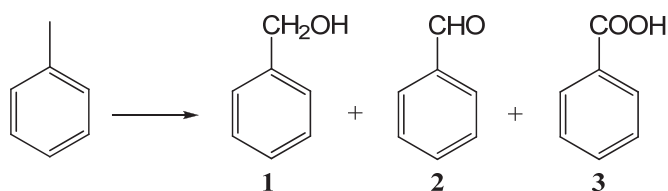
Oxidation of alkylaromatics is an important transformation in chemistry and industry. These reactions are often performed with corrosive, toxic or carcinogenic materials and with low selectivity. The composition of products obtained is dependent on the reaction conditions (catalyst, oxidizing agent and solvent). The reactivity of N-bridged diiron phthalocyanines **25**, **26**, **27**, **28**, **29** and **30** in homogeneous conditions was investigated in the oxidation of aliphatic C-H bonds vs aromatic oxidation. We studied the oxidation of toluene and p-xylene by TBHP, catalyzed by these six phthalocyanines complexes. The oxidations were carried out without solvent using neat substrate. Avoiding the use of solvent is important advantage from environmental and industrial points of view.

In addition, the catalytic activities of **25** and **26** immobilized on silica were investigated.

3.2.2.1 Oxidation of toluene and p-xylene in homogenous system

Catalytic oxidation of toluene

We played on two parameters: the catalyst concentration in the reaction mixture and the reaction temperature. First, **25** and **26** were tested in the relatively concentrated conditions (1 mM) in 1 mL of neat substrate at three different temperatures (20, 40 and 60 °C). The oxidant concentration was 206 mM. Benzylic alcohol (**1**), benzaldehyde (**2**) and benzylic acid (**3**) were the main products of oxidation of toluene (Scheme 3.4).



Scheme 3.4. Oxidation of toluene

Table 3.3 shows the results of toluene oxidation catalyzed by **25** and **26**. The oxidation was more efficient with **25** at 40 °C (total TON = 197) while **26** provided a higher total TON = 115 at 60°C. Significantly, only traces of products of aromatic oxidation, p-cresol and 2-methyl-1,4-benzoquinone were detected by GC-MS. Thus, the catalytic system demonstrates a strong preference for the oxidation of aliphatic C-H bond compared with aromatic oxidation. Among the products of benzylic oxidation, benzylic acid was the principal product, accounting for 73-83 % depending on experimental conditions. The ratio of products was very similar for these two catalysts. While **25** and **26** were quite selective to benzoic acid, up to 83 %, (**FePc^tBu₄**)₂N afforded benzaldehyde as principal product with selectivity up to 51 %. Although the reason of this selectivity change is not yet clear, the results obtained provide a possibility of tuning of selectivity of the oxidation by the appropriate modification of the structure of phthalocyanine ligand.

Table 3.3 Oxidation of toluene by TBHP catalyzed by **25** and **26**.

| Catalyst | T (°C) | TON | 1 (%) | 2 (%) | 3 (%) |
|-----------|--------|-----|-------|-------|-------|
| 25 | 20 | 92 | 6 | 21 | 73 |
| | 40 | 197 | 5 | 12 | 83 |
| | 60 | 167 | 6 | 13 | 81 |
| 26 | 20 | 59 | 7 | 20 | 73 |
| | 40 | 86 | 7 | 16 | 77 |
| | 60 | 115 | 7 | 16 | 77 |

Effect of catalyst concentration

Then, we decided to study the influence of the catalyst concentration in hope to achieve more efficient oxidation in terms of TON in the diluted conditions. **26** was chosen as the standart catalyst to test oxidation of toluene in the presence of different catalyst concentrations, from 10^{-3} M to 10^{-5} M. After determination of optimal oxidation conditions, the other complexes (**25**, **27**, **28**, **29** and **30**) have also been tested in the same conditions for oxidation of toluene and p-xylene.

The catalytic activities of **26** at different concentrations are presented in Table 3.4 and Figure 3.3.

Table 3.4. Oxidation of toluene in different concentration using TBHP by **26**.

| Concentration (M) | TON ₁ | TON ₂ | TON ₃ | Total TON |
|--------------------|------------------|------------------|------------------|-----------|
| 10^{-3} | 6 | 14 | 66 | 86 |
| 5×10^{-4} | 23 | 51 | 61 | 135 |
| 10^{-4} | 56 | 139 | 167 | 362 |
| 5×10^{-5} | 180 | 580 | 480 | 1240 |
| 10^{-5} | 930 | 2820 | 480 | 4230 |

The oxidations were carried out without solvent, in various catalyst's concentrations at 40 °C.

When the concentration of catalyst progressively decreased from 10^{-3} M to 10^{-5} M, we observed significant increase of TON from 86 to 4230. As can be seen in Table 3.4, while benzoic acid was the main product when concentration of the catalyst was between 10^{-3} M and 10^{-4} M, benzaldehyde became the principal product at lower catalyst concentrations (5×10^{-5} and 10^{-5}). The effect of catalyst concentration on TON and product distribution is shown in Figure 3.3.

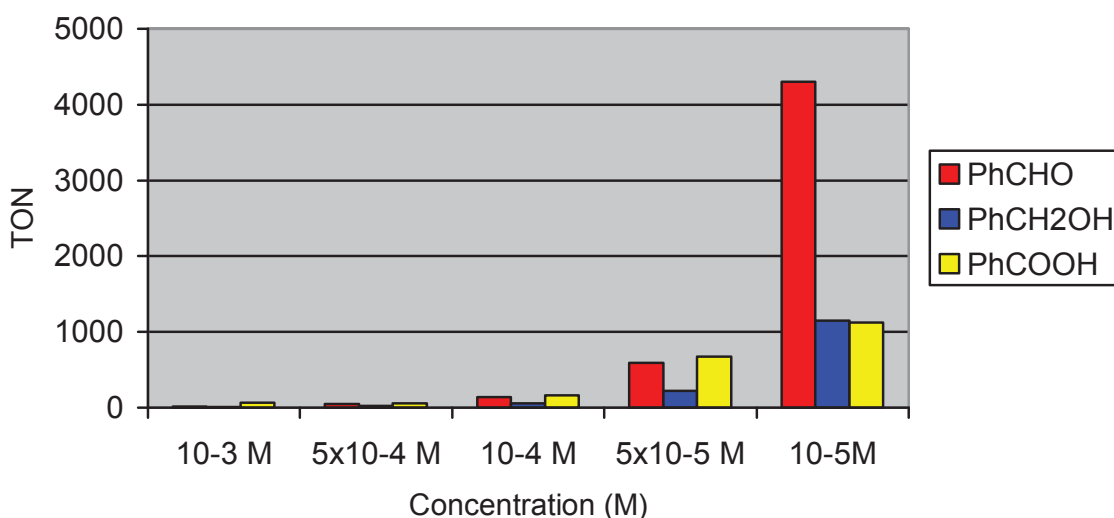


Figure 3.3. Catalyst's concentration effect on the oxidation of toluene.

It appears that the best conditions for **26** in terms of TON are reached for a catalyst concentration of 10^{-5} M. Thus, the reactivity of **25**, **26**, **27**, **28**, **29** and **30** was evaluated at this catalyst concentration in the same reaction conditions (without solvent, 40°C, 24 h). The results are summarized in Table 3.5. From the results obtained for **25** and **26** in concentrated conditions, we expected that catalysts with bulky substituents **26**, **29** and **30** would be more efficient than **25** and **28** having small substituents. Interestingly, when using **27**, the oxidation was more efficient (total TON = 9040). However, catalysts with bulkier substituents **26**, **29** and **30** were more efficient than **25** and **28**. Among the products of benzylic oxidation, benzaldehyde was always the principal product, even if

the ratio of products was slightly different for all catalysts. The catalysts **26**, **29** and **30** provided more benzyl alcohol than **25**, **27** and **28**.

Table 3.5. Oxidation of toluene in 10^{-5} M concentration by **25**, **26**, **27**, **28**, **29** and **30**.

| Catalyst | TON | 1 / % | 2 / % | 3 / % |
|-----------|------|--------------|--------------|--------------|
| 25 | 3800 | 6 | 89 | 5 |
| 26 | 6572 | 17 | 65 | 18 |
| 27 | 9040 | 14 | 80 | 6 |
| 28 | 4550 | 14 | 82 | 4 |
| 29 | 6010 | 13 | 85 | 2 |
| 30 | 7460 | 19 | 73 | 8 |

Temperature effect

The temperature effect was also studied using 10^{-5} M concentration of **26**. The results at 40 and 60 °C are compared in Table 3.6. When temperature increased, we observed an almost two-fold increase of total TON. While the total TON was 6572 at 40 °C, TON was 12280 at 60 °C. The product selectivity was changed with increasing of temperature. The selectivity for benzaldehyde was higher at 60°C as compared to that at 40°C.

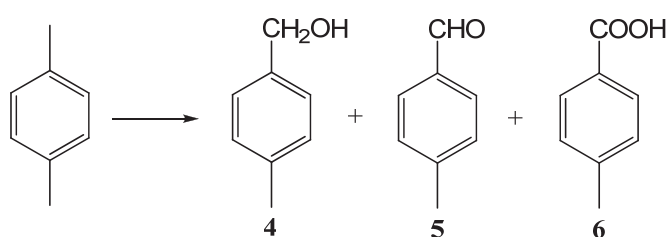
Table 3.6. Oxidation of toluene catalyzed by **26** (10^{-5} M) at 40 and 60 °C.

| T / °C | TON | 1 / % | 2 / % | 3 / % |
|--------|-------|--------------|--------------|--------------|
| 40 | 6572 | 17 | 65 | 18 |
| 60 | 12280 | 18 | 75 | 7 |

Catalytic oxidation of p-xylene

Catalytic oxidation of p-xylene in the presence of 10^{-3} M catalyst

The oxidation of *p*-xylene yields also products of benzylic oxidation: 4-methylbenzyl alcohol (**4**), *p*-tolualdehyde (**5**) and *p*-toluic acid (**6**) (Scheme 3.5).



Scheme 3.5. Oxidation of *p*-xylene

p-Toluic acid (**6**) was the main product in each case (Table 3.7). While in oxidation of toluene **25** was superior to **26** in terms of turnover numbers and selectivity to benzoic acid, **26** showed higher turnover numbers and selectivity than **25** in oxidation of *p*-xylene. A high performance was obtained at 60 °C with **26**: TON attained almost 600 catalytic cycles. Interestingly, both catalysts perform the selective oxidation of only one methyl group. We didn't observe the products of oxidation of both methyl groups. Products of aromatic oxidation were also absent. In contrast to μ -oxo iron phthalocyanines [70,71], μ -nitrido iron phthalocyanines in combination with TBHP show different selectivity in oxidation of alkylaromatics, oxidizing only methyl groups rather than aromatic ring. While Fe-O-Fe catalyst performed oxidation of aromatic rings to form quinones, Fe-N=Fe complex was quite selective in oxidation of alkyl substituents.

Table 3.7. Oxidation of *p*-xylene by TBHP catalyzed by **25** and **26** (10^{-3} M).

| Catalyst | T / °C | TON | 4 / % | 5 / % | 6 / % |
|-----------|--------|-----|--------------|--------------|--------------|
| 25 | 20 | 164 | 14 | 34 | 52 |
| | 40 | 291 | 15 | 25 | 60 |
| | 60 | 312 | 17 | 28 | 55 |
| 26 | 20 | 185 | 14 | 34 | 52 |
| | 40 | 339 | 13 | 22 | 65 |
| | 60 | 587 | 15 | 19 | 66 |

Catalytic oxidation of *p*-xylene using diluted catalyst concentrations.

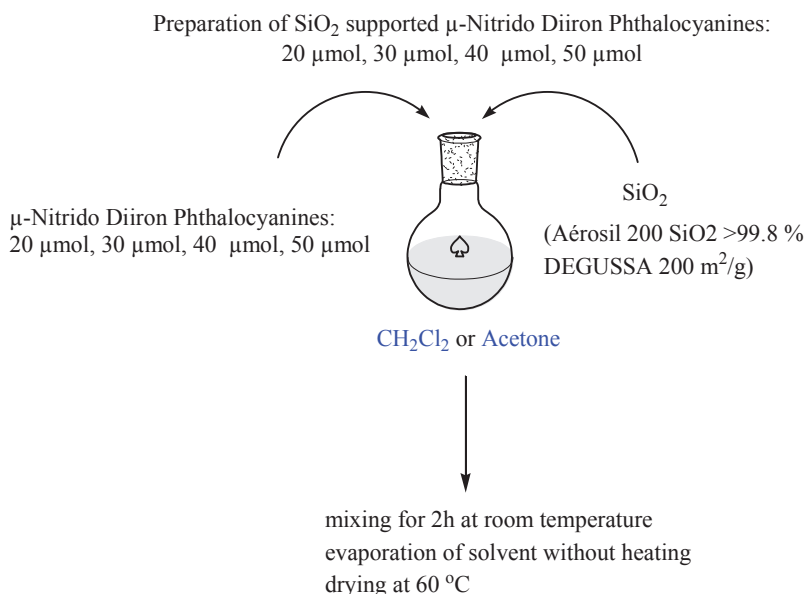
Under diluted conditions **29** was the best catalyst in the oxidation of *p*-xylene showing higher turnover numbers: TON attained almost 22000 catalytic cycles (Table 3.8). All catalysts perform the selective oxidation of only one methyl group. We didn't observe the products of oxidation of both methyl groups. Products of aromatic oxidation were also absent. While **30** showed lower turnover numbers, the selectivity of *p*-tolualdehyde higher than the others. In contrast to the experiments with 10^{-3} M catalyst concentration, the experiments with 10^{-5} M catalyst showed much higher TONs. While TON attained almost 600 catalytic cycles in oxidation of *p*-xylene in the presence of 10^{-3} M **26**, TON was 13300 when the concentration of the catalyst was 10^{-5} M. Catalysts having small substituents (**25**, **27** and **28**) were more selective to *p*-tolualdehyde.

Table 3.8. Oxidation of *p*-xylene catalyzed by **25**, **26**, **27**, **28**, **29** and **30** (10^{-5} M).

| Catalyst | TON | 3 / % | 4 / % | 5 / % |
|-----------|-------|--------------|--------------|--------------|
| 25 | 10950 | 17 | 80 | 3 |
| 26 | 13300 | 17 | 78 | 5 |
| 27 | 12420 | 16 | 80 | 4 |
| 28 | 10630 | 9 | 85 | 6 |
| 29 | 21890 | 22 | 73 | 5 |
| 30 | 7960 | 8 | 90 | 2 |

3.2.2.2. Oxidation of toluene and p-xylene by silica supported phthalocyanines

Preparation of SiO₂ supported N-bridged diiron phthalocyanines **25** and **26**.



Scheme 3.6. Preparation of supported SiO₂-N-bridged diiron phthalocyanines

We prepared 4 samples of supported SiO₂-**25** using different relative amounts of silica/**25**: 20, 30, 40 and 50 μ mol of **25** per 1 gram of silica, to modulate silica covering ratio and then to test selectivities in oxidation reaction. Resulting supported catalysts are hereafter designated as SiO₂-**25**(20), SiO₂-**25**(30), SiO₂-**25**(40), SiO₂-**25**(50). Even if it is commonly admitted that a covering ratio of 70% is optimal (corresponding in our case to SiO₂-**25**(40)), we tested the catalytic activities of SiO₂-**25** for different covering ratio.

Diffuse reflectance UV–Vis spectroscopy is a convenient method for characterization of supported catalysts. The DR UV–Vis spectrum of SiO₂-**25**(40) in solid state is shown in Figure 3.4. The spectrum of silica-supported **25** (Q band at 663 nm) is similar to the one of the unsupported phthalocyanine **25** (Q band at 657 nm) indicating that dimeric structure of **25** was retained upon supporting onto silica.

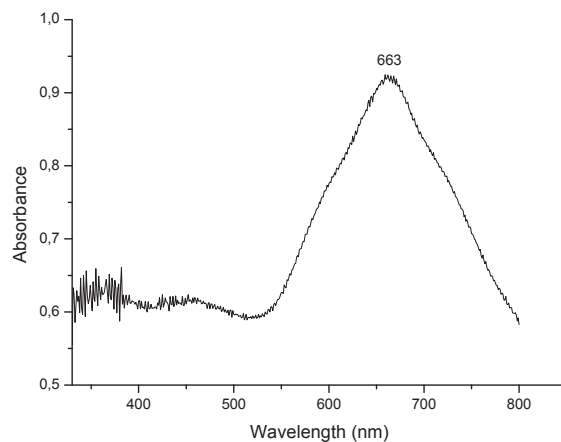


Figure 3.4. Solid state UV-vis spectrum of SiO₂-**25**(40).

Two complexes, **25** and **26**, were tested for toluene oxidation after their immobilization onto SiO₂. The results were compared to those previously obtained in homogeneous systems. The process of the immobilization is illustrated on Scheme 3.6. All immobilization procedures were performed using 1 g of silica with a specific surface of 200 m²/g. The size of iron phthalocyanine molecule can be estimated as 25Å x 25Å. Hence, one can estimated a surface occupied by iron phthalocyanine molecules according to the formulism indicated in Equation 3.1, for different amounts of phthalocyanine and different covering ratio.

| | | | | | | |
|-------------------------------------------------------------------------------------------------------------------------------------------|-------|---------------------------------------------------------------------------------------|-----------------------|--------------------------------|----------------------------------|--|
| <div style="border: 1px solid black; width: 100px; height: 50px; display: flex; align-items: center; justify-content: center;">FePc</div> | 25 Å° | $A = 25 \times 25 = 625 \text{ (Å}^\circ\text{)}^2 = 625 \times 10^{-20} \text{ m}^2$ | | | | |
| 25 Å° | | $625 \times 10^{-20} \text{ m}^2$ | 1 | 1 mol | $3762.5 \times 10^3 \text{ m}^2$ | |
| | × | | 6.02×10^{23} | $2 \times 10^{-5} \text{ mol}$ | × | |
| | | $x = 3762.5 \times 10^3 \text{ m}^2/\text{mol}$ | | $x = 7525 \times 10^{-2}$ | | |
| $\frac{7525 \times 10^{-2}}{200} \times 100 = 37.62 \%$ | | | | | | |

Equation 3.1. Calculation of covering of silica by iron phthalocyanine molecules

Catalytic oxidation of toluene with SiO₂-**25**

The results of catalytic oxidation of toluene in the presence of SiO₂-**25** are listed in Table 3.9. It is generally hoped that supported catalysts are more efficient than unsupported ones. It should be noted that TONs obtained in the presence of supported catalysts were comparable with TON obtained in homogeneous oxidation of toluene in the presence of **25**. Noteworthy, supported catalysts prepared with different amount of **25** were all more selective to benzaldehyde than unsupported iron phthalocyanine **25**. A very high selectivity of oxidation of toluene to benzaldehyde, up to 98 %, was achieved. SiO₂-**25**(40) was even more active than homogeneous catalyst (TON=4070 vs 3800). It was seen that at higher loading (case of SiO₂-**25**(50)), the catalytic activity decreases, probably because of aggregation phenomena when not all iron phthalocyanine molecules are accessible for substrate leading to decrease of the catalytic activity. These results confirm that a 70% covering ration is optimal, as generally described.

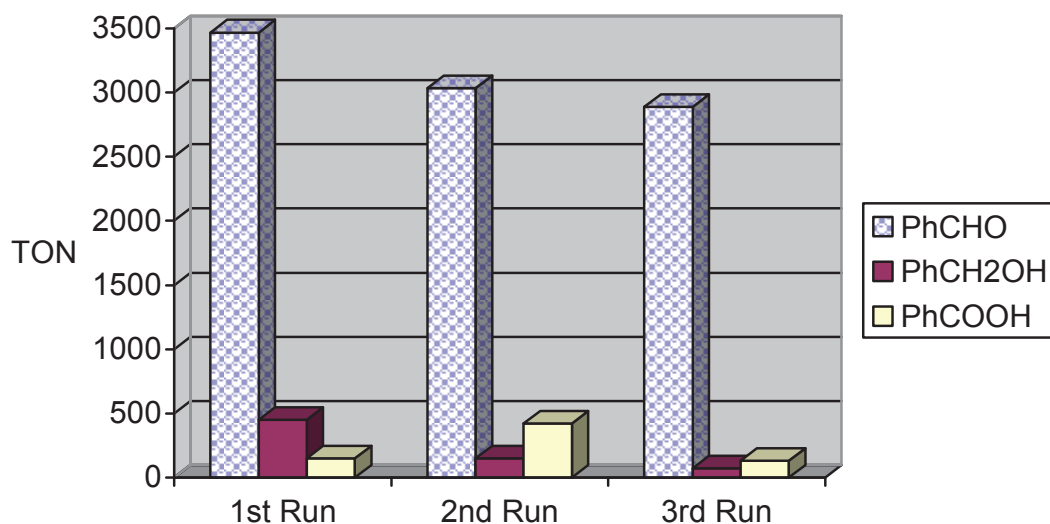
Table 3.9. Oxidation of toluene catalyzed by SiO₂-**25**

| Pc μmol^a | TON | 1 / % | 2 / % | 3 / % |
|----------------------|------|-------|-------|-------|
| 20 | 2513 | 0.1 | 98 | 1.9 |
| 30 | 3290 | 5 | 93 | 2 |
| 40 | 4070 | 4 | 94 | 2 |
| 50 | 3640 | 1 | 97 | 2 |

^a Phthalocyanine concentration used for the preparation of the supported catalyst.

The recycling experiments of SiO₂-**25**(40) in these conditions (TBHP at 40 °C for 24h) showed that the catalyst was quite stable. SiO₂-**25**(40) was still active after the 3rd run. The TON for benzaldehyde was 3470 for 1st run, 3034 for 2nd run and finally 2889 for 3rd run. It should be noted that quantitative recovering of very small amounts of the supported catalysts after reaction is a difficult task. Some part of the material could be

lost during recycling work-up. Consequently, one can conclude that the supported catalyst can be recycled and re-used with practically no loss of catalytic activity.



Scheme 3.7. The recycle testing of SiO₂-**25**(40) for oxidation of toluene

Catalytic oxidation of toluene with SiO₂-**26**

The optimal conditions determined for the preparation of SiO₂-**25** were used for supporting **26** onto silica. We prepared therefore SiO₂-**26**(40).

The results of the catalytic oxidation of toluene in the presence of SiO₂-**26**(40) are listed in Table 3.10. The high TON and selectivity to benzaldehyde were observed.

Table 3.10. Oxidation of toluene by SiO₂-**26**(40)

| T / °C | TON | 1 / % | 2 / % | 3 / % |
|--------|------|-------|-------|-------|
| 40 | 4220 | 6 | 91 | 3 |

Catalytic oxidation of p-xylene with SiO₂-**25**

SiO₂-**25**(40) was used as the catalyst for the heterogeneous oxidation of p-xylene. Significantly, we didn't observe *p*-toluic acid and *p*-tolualdehyde was obtained with 95 % selectivity (Table 3.11).

Table 3.11. Oxidation of p-xylene by SiO₂-**25**(40)

| T / °C | TON | 4 / % | 5 / % | 6 / % |
|--------|------|--------------|--------------|--------------|
| 40 | 7370 | 5 | 95 | - |

In conclusion, catalytic properties of N-bridged complexes were evaluated in the industrially important oxidation of alkylaromatic compounds (toluene and p-xylene), using TBHP as the oxidant. Heterogenous systems based on **25** and **26** silica supported were tested. Surprisingly, **6** formation wasn't observed during oxidation of p-xylene by SiO₂-**25**. Novel complexes **25**, **26**, **27**, **28**, **29** and **30** in combination with TBHP exhibit a high selectivity in oxidation of toluene and *p*-xylene with high turnover numbers.

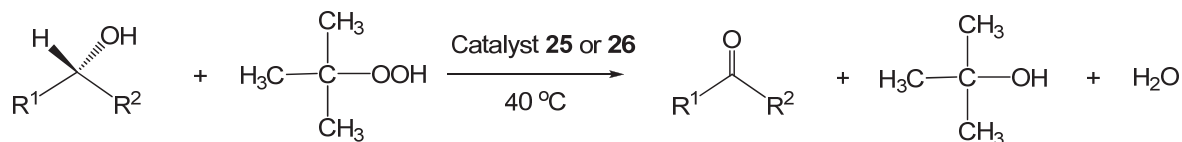
3.2.3. Oxidation of alcohols by methyl, ethyl, cyclohexyl and adamantyl sulfonyl substituted μ -nitrido diiron dimers

Oxidation of alcohols to aldehydes and ketones is one of the most important transformations in organic synthesis (Scheme 3.8) [119a]. In particular, the oxidation of primary alcohols to aldehydes is important since they find wide applications as intermediates in fine chemistry, particularly in perfume and pharmaceutical industries [120,121]. Most of the catalysts reported so far, the use of a solvent in the reaction is required, while it is highly desirable to develop a process without a solvent from the viewpoint of green chemistry. Avoiding the use of solvent is important advantage from

environmental and industrial points of view. The world-wide annual production of carbonyl compounds is over 10^7 tonnes and many of these compounds are produced from the oxidation of alcohols. [9-17] [91a,122,155-157] The oxidation of alcohols is often carried out using stoichiometric inorganic oxidants such as permanganate [158], bromate [159], or Cr(VI) based reagents which generates large amount of heavy metal waste [160]. Several transition metal-based homogeneous systems such as palladium [161], ruthenium [162], manganese [163], tungsten [164], rhenium [165], and copper [166,167], have also been reported. However, these methods have some drawbacks as the industrial processes from the environmental point of view, because they require a stoichiometric amount of toxic metal ions, harmful organic solvents, or a large amount of energy consumption with high pressures and/or high temperature. Oxidation reactions are sometimes carried out in halogenated organic solvents, typically chlorinated hydrocarbons, which are environmentally undesirable. Therefore, development of the catalytic process of alcohol oxidation under mild conditions is essential for green chemistry. In order to avoid the use of organic solvent, a use of supercritical carbon dioxide as an effective reaction medium to perform the oxidation of primary and secondary aliphatic alcohols to corresponding carbonyl compounds with chromium trioxide supported silica has been reported [168]. A clean procedure for oxidation of alcohols by O_2 was also published [169]. Transition metal complexes of phthalocyanines and porphyrins are widely investigated owing to the presence of similar structural units in biological systems such as proteins and enzymes. By contrast to porphyrins, a cheap and facile preparation of phthalocyanines, their availability at a large scale as well as their chemical and thermal stability make them industrially viable candidates for oxidation catalysis. Metallophthalocyanines have been used as efficient biomimetic catalysts for oxidation, reduction and other reactions of organic compounds [71c,170-178]. It has been also shown that cytochromes P450 and their model compounds are able to catalyze the oxidation of alcohols [179,180]. The solvent-free selective oxidation of several alcohols to aldehydes and ketones with TBHP by **25** and **26** was tested.

Benzyl alcohol was first examined as a standart substrate with TBHP as oxidant. Considering the solubility of the catalyst **25** and **26** in alcohols, the oxidation reaction was initially carried out without additional solvent in the presence of a catalytic amount

of **25** and **26**. The progress of the reaction was monitored by GC. The reaction products were identified by GC-MS.



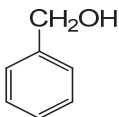
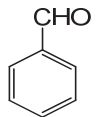
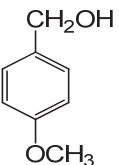
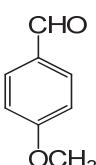
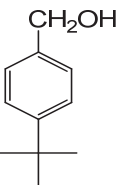
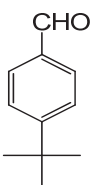
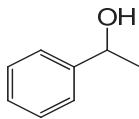
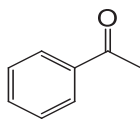
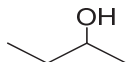
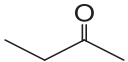
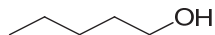
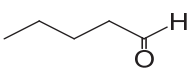
R^1 = Aryl, alkyl

R^2 = H, alkyl

Scheme 3.8. Oxidation of alcohols to aldehydes or ketones with high turnovers by **25** and **26**.

As shown in Table 3.12, secondary and primary alcohols are converted into the corresponding ketones and aldehydes respectively, with very high turnover numbers (Entries 1, 4, 5 and 6) (TON = moles of aldehyde or ketone formed per mole of the catalyst). We know that, the preparation of aromatic aldehydes from the corresponding primary alcohols is not easily achieved because they are readily converted into carboxylic acids when using strong oxidants such as permanganate. Among the various alcohols studied, n-pentanol, 2-butanol and benzylalcohol were found to be the most reactive; shorter reaction times were required for their oxidations (Entries 1, 5 and 6, Table 3.12). Table 3.12 shows the catalytic performances of the catalyst **25** and the catalyst **26** for the solvent-free oxidation of alcohols by TBHP. Both catalysts could catalyze the solvent-free selective oxidation of alcohols to aldehydes and ketones with selectivities higher than 99%. The oxidation of secondary benzylic alcohol remains general to afford the ketone in high TON (entry 4). Furthermore, aliphatic alcohols were found to be more reactive than aromatic alcohols (Table 3.12, entries 5 and 6). Very high TONs of 62750 and 41020 were obtained for propanal with **25** and **26**.

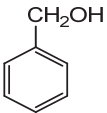
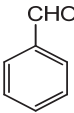
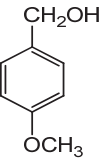
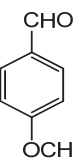
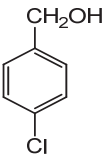
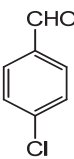
Table 3.12. Oxidation of alcohols with TBHP catalyzed by **25** and **26**

| Entry | Substrate | Product | Time (h) | TON ^b | | Selectivity (%) |
|-------|-------------------------------------------------------------------------------------|-------------------------------------------------------------------------------------|----------|------------------|-----------|-----------------|
| | | | | 25 | 26 | |
| 1 |  |  | 1 | 12370 | 14940 | > 99 |
| 2 |  |  | 24 | 6360 | 3230 | > 99 |
| 3 |  |  | 24 | 5300 | 1450 | > 99 |
| 4 |  |  | 24 | 14970 | 15430 | 100 |
| 5 |  |  | 1 | 13340 | 27380 | 100 |
| 6 |  |  | 1 | 62750 | 41020 | 100 |

^a The reactions were carried out under the following conditions: alcohol- 10 mL ; catalyst **25** or **26** - 0.01 mM ; 70 % TBHP - 206 mM; temperature, 40 °C ^b TON for aldehyde = moles of aldehyde formed per mole of catalyst.

Benzyl alcohol was converted to benzaldehyde with high TON at 80 °C (Table 3.13, entry 1). Primary benzylic alcohol with electron donating substituent such as *p*-methoxybenzyl alcohol was also converted to the *p*-methoxyaldehyde (entry 2). On the other hand, the TON of *p*-chlorobenzylalcohol oxidation significantly increased (entry 3). In the case of primary alcohol oxidation, the overoxidation of aldehyde into carboxylic acid was not observed and the corresponding aldehydes were obtained selectively.

Table 3.13. Oxidation of different aromatic alcohols with TBHP by **25** and **26** at 80 °C

| Entry | Substrate | Product | Time (h) | TON | | Selectivity (%) |
|-------|-------------------------------------------------------------------------------------|-------------------------------------------------------------------------------------|----------|-----------|-----------|-----------------|
| | | | | 25 | 26 | |
| 1 |  |  | 1 | 17680 | 18380 | > 99 |
| 2 |  |  | 24 | 14050 | 9970 | > 99 |
| 3 |  |  | 24 | 40990 | 42280 | > 99 |

The reactions were carried out under the following conditions: alcohol= 10 mL ; catalyst **25** or **26**= 0.01 mM ; 70 % TBHP = 206 mM; temperature, 80 °C

The influence of temperature on benzyl alcohol oxidation and product selectivity was examined (Table 3.14). When reaction temperature was increased gradually from 20 to 80 °C, the rate of the reaction was also increased. Both catalysts could catalyze the solvent-free selective oxidation of benzyl alcohol to benzaldehyde. Selectivity was higher than 99% for each temperature. At 80 °C highest TON (17680 for **25** and 18380 for **26**) was obtained after 1 h.

Table 3.14. Effect of temperature on benzyl alcohol oxidation to benzylaldehyde^a

| Entry | Temperature (°C) | TON | | Selectivity (%) |
|-------|------------------|-----------|-----------|-----------------|
| | | 25 | 26 | |
| 1 | 20 | 8140 | 7560 | > 99 |
| 2 | 40 | 12370 | 14940 | > 99 |
| 3 | 60 | 14310 | 15330 | > 99 |
| 4 | 80 | 17680 | 18380 | > 99 |

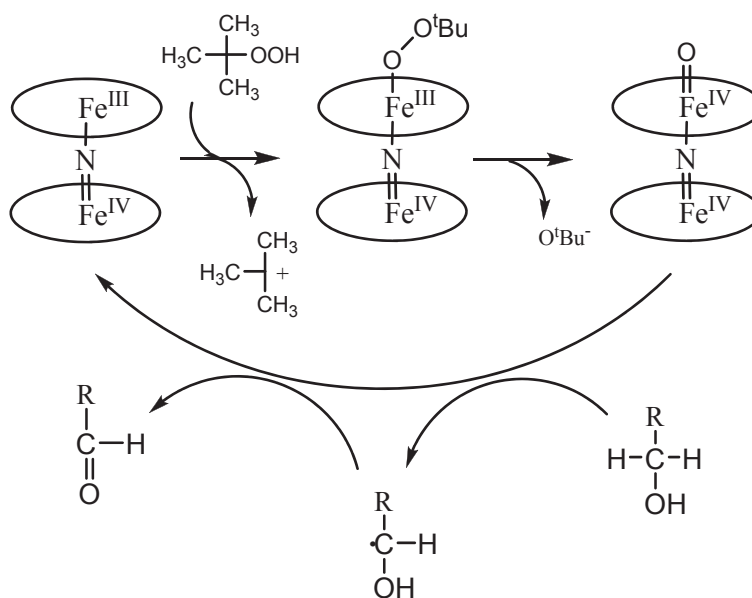
^a *The reactions were carried out under the following conditions: benzyl alcohol = 10 mL; catalyst **25** or **26** = 0.01 mM ; 70 % TBHP = 206 mM; time = 1h*

The influence of TBHP concentration increase from 1030 mM to 4120 mM on benzyl alcohol oxidation and product selectivity was examined (Table 3.15). When TBHP amount was increased gradually from 1030 to 4120, the rate of the reaction and TON increased. After adding 4120 mM TBHP, highest TON (31190 for **25** and 43270 for **26**) was obtained.

Table 3.15. Effect of TBHP concentration on benzyl alcohol oxidation to benzylaldehyde^a

| Entry | TBHP Concentration (mM) | TON | | Selectivity (%) |
|-------|-------------------------|-------|-------|-----------------|
| | | 25 | 26 | |
| 1 | 1030 | 16970 | 17390 | > 99 |
| 2 | 2060 | 23460 | 23800 | > 99 |
| 3 | 3090 | 25820 | 25510 | > 99 |
| 4 | 4120 | 31190 | 43270 | > 99 |

^a The reactions were carried out under the following conditions: benzyl alcohol= 10 mL ; catalyst **25** or **26**= 0.01 mM ; time = 1h; temperature, 40 °C.



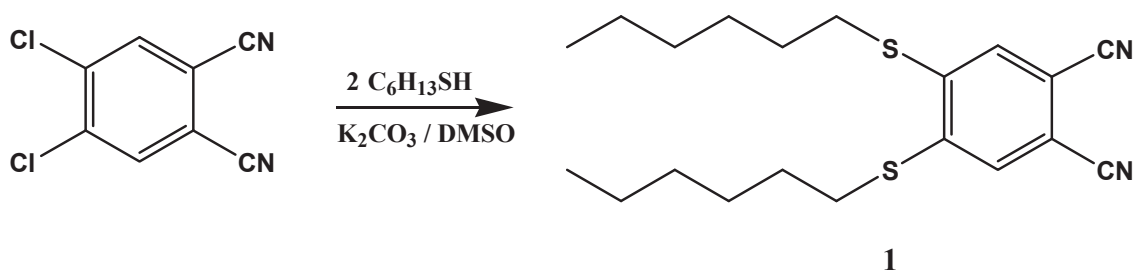
Scheme 3.9. Proposed mechanism for the oxidation of alcohol

In conclusion, electron-withdrawing substituted μ -nitrido bridged diiron phthalocyanine catalysts exhibit a very high activity and an unusual selectivity in the oxidation of aromatic and aliphatic alcohols. The proposed catalytic method is a green alternative since avoiding the use of solvent is important advantage from environmental and industrial points of view.

4. Experimental Part

4.1. Synthesis of phthalonitriles

4.1.1. 1,2-dicyano-4,5-Bis(hexylthio)benzene (**1**)



4,5-Dichloro-1,2-dicyanobenzene (10 g, 50.8 mmol) and 1-hexanethiol (14.76 g, 101.6 mmol) were dissolved in anhydrous dimethyl sulfoxide (DMSO) (64 mL) under argon atmosphere. After stirring for 15 min at room temperature, dry and finely powdered potassium carbonate (25 g, 181 mmol) was added portionwise over 15 min with efficient stirring. The reaction mixture was stirred under argon at 90°C for 24 h. Then the mixture was poured into 200 mL of ice-water. The resulting solid was collected by filtration and washed with water. After drying in vacuo at 50 °C, the crude product was recrystallised from ethanol to give pure 4,5-Bis(hexylthio)-1,2-dicyanobenzene (**1**).

15 g, Yield (82 %)

C₂₀H₂₈N₂S₂ MW: 360.17 g/mol

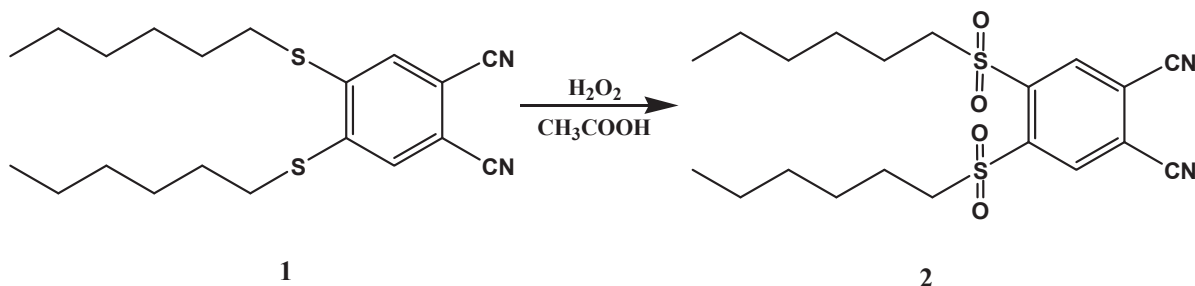
Melting Point: 70 °C

IR (KBr) ν (cm⁻¹): 2970, 2950, 2860, 2240, 1560, 1450, 1420, 1350, 1280, 1260, 1230, 1205, 1120, 935, 905, 715

EA: Calculated : C 66.62, H 7.83, N 7.77, S 17.79

Found : C 67.20, H 7.70, N 7.93, S 17.57

4.1.2. 1,2-dicyano-4,5-Bis(hexylsulfonyl)benzene (2)



4,5-Bis(hexylthio)-1,2-dicyanobenzene (1.5 g, 4.16 mmol) was dissolved in 50 mL of acetic acid at 90 °C. To the stirred solution was added a total of 23 mL of 33 % H₂O₂ in 1 mL portions in the course of 4 h. The resulting mixture was allowed to cool to room temperature and stirred overnight, and the white precipitate was collected by filtration, subsequently washed several times with water, and crystallized from ethanol (50 mL) to give pure 4,5-Bis(hexylsulfonyl)-1,2-dicyanobenzene (**2**).

1.34 g, Yield (76 %)

C₂₀H₂₈N₂O₄S₂ MW: 424.15 g/mol

Melting Point: 114 °C

IR (KBr) ν (cm⁻¹): 3097, 2959, 2928, 2861, 2244, 1545, 1464, 1336, 1314, 1149, 1125, 919, 795, 728, 648, 570, 525, 512, 474

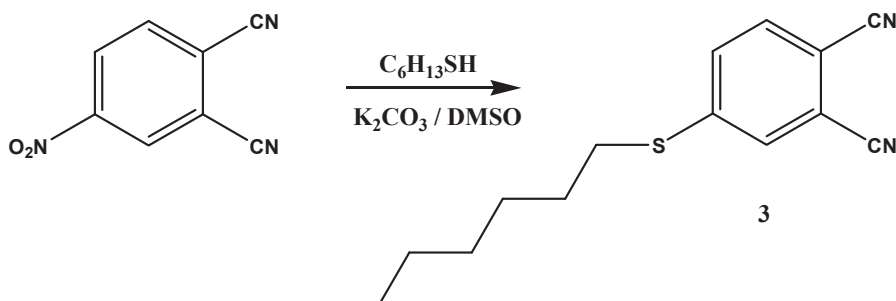
EA: Calculated: C 66.62, H 7.83, N 7.77, S 17.79

Found : C 67.20, H 7.70, N 7.93, S 17.57

Mass Spectrum (ESI-MS) m/z: 447.23 [M+Na]

¹H NMR (CDCl₃): δ = 0.8 (t, 3 H, CH₃), 1.3- 1.7 (m, 8 H, CH₂), 3.7 (t, 2 H, CH₂), 8.6 (s, 1 H, ArH).

4.1.3. 1,2-dicyano-4-(hexylthio)benzene (3)



A mixture of 4-nitrophthalonitrile (2.5 g, 14.45 mmol) and 1-hexanethiol (2.1 g, 14.45 mmol) in DMSO (10 mL) was stirred at room temperature for 10 min. Then, dry potassium carbonate (2 g, 14.5 mmol) was added in small portions during 2 h. The mixture was vigorously stirred under argon atmosphere at room temperature for 16 h. Water (50 mL) was added, and the product was extracted with CH_2Cl_2 (3 x 50 mL). The organic phase was washed with water (3 x 50 mL) and dried over sodium sulfate. The solvent was removed under reduced pressure, and the residue was recrystallized from ethanol to give 4-hexylthio-1,2-dicyanobenzene (3).

2.8 g, Yield (80 %)

$\text{C}_{14}\text{H}_{16}\text{N}_2\text{S}$ MW: 244.10 g/mol

Melting Point: 67 °C

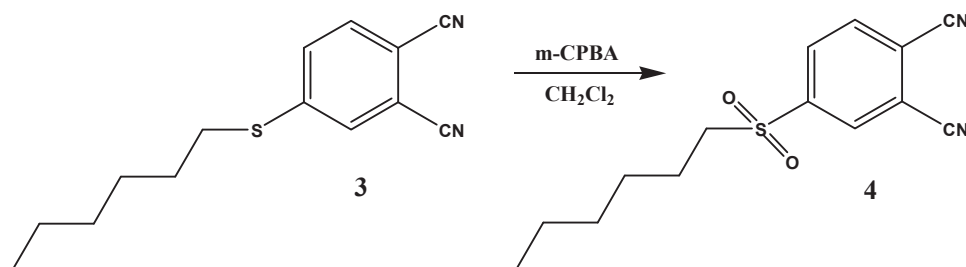
IR (KBr) $\nu(\text{cm}^{-1})$: 3068, 2917, 2855, 2232, 1568, 1474, 1453, 1422, 1297, 1198, 1155, 857, 833, 796, 728, 555

EA: Calculated: C 68.81, H 6.60, N 11.46, S 13.12

Found : C 67.36, H 6.21, N 11.76, S 13.60

Mass Spectrum (ESI-MS) m/z: 267.10 [M+Na]

4.1.4. 1,2-dicyano-4-(hexylsulfonyl)benzene (4)



To a solution of 1,2-dicyano-4-hexylthiobenzene (2 g, 15.06 mmol) in dry CH_2Cl_2 (8.5 mL) cooled at 0 °C was slowly added *m*-chloroperbenzoic acid (6.35 g, 36.75 mmol) in CH_2Cl_2 (150 mL). The mixture was warmed to room temperature and vigorously stirred at this temperature overnight (12 h). A saturated sodium sulfite solution was then added, and the organic phase was extracted with CH_2Cl_2 (3 x 50 mL) and dried over Na_2SO_4 . The solvent was removed under reduced pressure, and the solid was recrystallized from ethanol to give 1,2-dicyano-4-hexylsulfonylbenzene (4) as a white solid.

3.03 g, Yield (73 %)

$\text{C}_{14}\text{H}_{16}\text{N}_2\text{SO}_2$ MW: 276.09 g/mol

Melting Point: 104 °C

IR (KBr) $\nu(\text{cm}^{-1})$: 3097, 3037, 2950, 2867, 2241, 1540, 1476, 1398, 1317, 1286, 1147, 1111, 1075, 920, 882, 848, 774, 622, 526

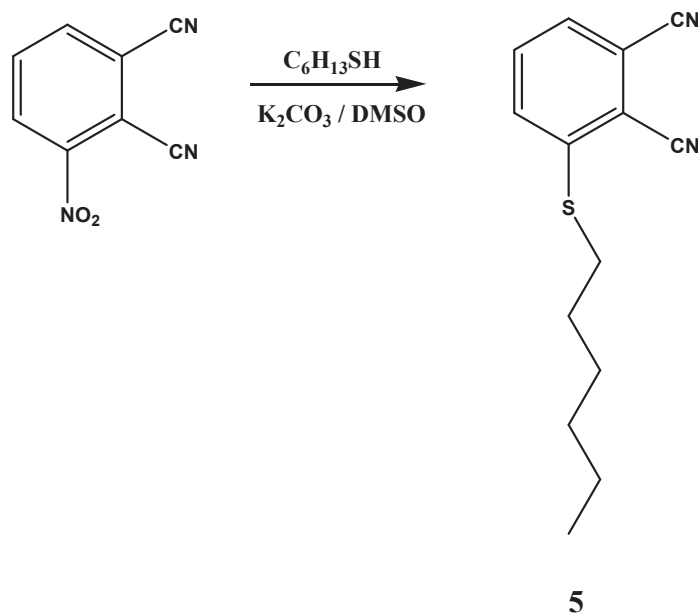
EA: Calculated: C 60.85, H 5.84, N 10.14, S 11.60

Found : C 60.16, H 5.94, N 10.29, S 11.70

Mass Spectrum (ESI-MS) m/z : 299.14 $[\text{M}+\text{Na}]$

^1H NMR (CDCl_3): δ = 1.1 (t, 3 H, CH_3), 1.4- 2 (m, 8 H, CH_2), 3.4 (t, 2 H, CH_2), 8.0 (d, 1 H, ArH), 8.1 (d, H, ArH), 8.4 (s, 1 H, ArH).

4.1.5. 1,2-dicyano-3-(hexylthio)benzene (**5**)



A mixture of 3-nitrophthalonitrile (2.5 g, 14.45 mmol) and 1-hexanethiol (2.1 g, 14.45 mmol) in DMSO (10 mL) was stirred at room temperature for 10 min. Then, dry potassium carbonate (2 g, 14.5 mmol) was added in small portions during 2 h. The mixture was vigorously stirred under argon atmosphere at room temperature for 16 h. Water (50 mL) was added, and the product was extracted with CH₂Cl₂ (3 x 50 mL). The organic phase was washed with water (3 x 50 mL) and dried over sodium sulfate. The solvent was removed under reduced pressure, and the residue was recrystallized from ethanol to give 3-hexylthio-1,2-dicyanobenzene (**5**).

3 g, Yield (85 %)

C₁₄H₁₆N₂S MW: 244.10 g/mol

Melting Point: 68 °C

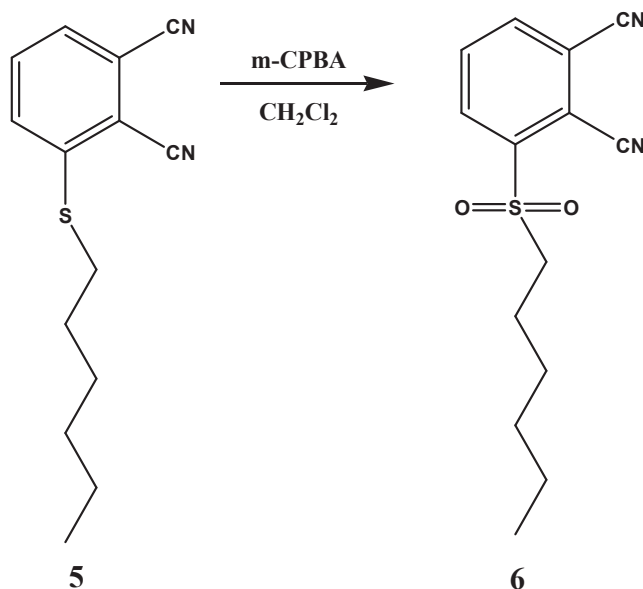
IR (KBr) ν (cm⁻¹): 3068, 2917, 2855, 2232, 1568, 1474, 1453, 1422, 1297, 1198, 1155, 857, 833, 796, 728, 555

EA: Calculated: C 68.81, H 6.60, N 11.46, S 13.12

Found : C 68.22, H 6.40, N 11.53, S 13.08

Mass Spectrum (ESI-MS) m/z: 267.10 [M+Na]

4.1.6. 1,2-dicyano-3-(hexylsulfonyl)benzene (6)



To a solution of 1,2-dicyano-4-hexylthiobenzene (2 g, 15.06 mmol) in dry CH_2Cl_2 (8.5 mL) cooled at 0 °C was slowly added *m*-chloroperbenzoic acid (6.35 g, 36.75 mmol) in CH_2Cl_2 (150 mL). The mixture was warmed to room temperature and vigorously stirred at this temperature overnight (12 h). A saturated sodium sulfite solution was then added, and the organic phase was extracted with CH_2Cl_2 (3 x 50 mL) and dried over Na_2SO_4 . The solvent was removed under reduced pressure, and the solid was recrystallized from ethanol to give 1,2-dicyano-3-hexylsulfonylbenzene (**6**) as a white solid.

3.1 g, Yield (75 %)

$\text{C}_{14}\text{H}_{16}\text{N}_2\text{SO}_2$ MW: 276.09 g/mol

Melting Point: 100 °C

IR (KBr) $\nu(\text{cm}^{-1})$: 3084, 2953, 2870, 2236, 1544, 1433, 1329, 1287, 1161, 1130, 851, 822, 764, 639, 518

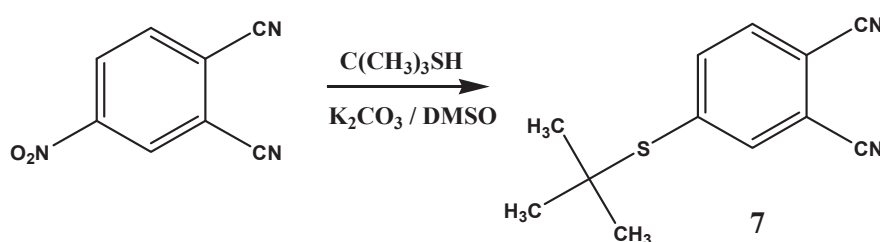
EA: Calculated: C 60.85, H 5.84, N 10.14, S 11.60

Found : C 60.33, H 5.90, N 10.19, S 11.73

Mass Spectrum (ESI-MS) m/z : 299.14 $[\text{M}+\text{Na}]$

$^1\text{H NMR}$ (CDCl_3): δ = 0.8 (t, 3 H, CH_3), 1.0- 1.8 (m, 8 H, CH_2), 3.5 (t, 2 H, CH_2), 8.0 (d, 1 H, ArH), 8.1 (t, H, ArH), 8.4 (s, 1 H, ArH).

4.1.7. 1,2-Dicyano-4-(tert-butylthio)benzene (7)



A mixture of 4-nitrophthalonitrile (2.5 g, 14.45 mmol) and tert-butylthiol (1.3 g, 14.45 mmol) in DMSO (10 mL) was stirred at room temperature for 10 min. Then, dry potassium carbonate (2 g, 14.5 mmol) was added in small portions during 2 h. The mixture was vigorously stirred under argon atmosphere for 16 h. Water (50 mL) was added, and the product was extracted with CH_2Cl_2 (2 x 50 mL). The organic phase was washed with water (3 x 50 mL) and dried over sodium sulfate. The solvent was removed under reduced pressure, and the residue was recrystallized from ethanol to give 1,2-Dicyano-4-(tert-butylthio)benzene (7).

2.4 g, Yield (75 %)

$\text{C}_{14}\text{H}_{16}\text{N}_2\text{S}$ MW: 216.07 g/mol

Melting Point: 76 °C

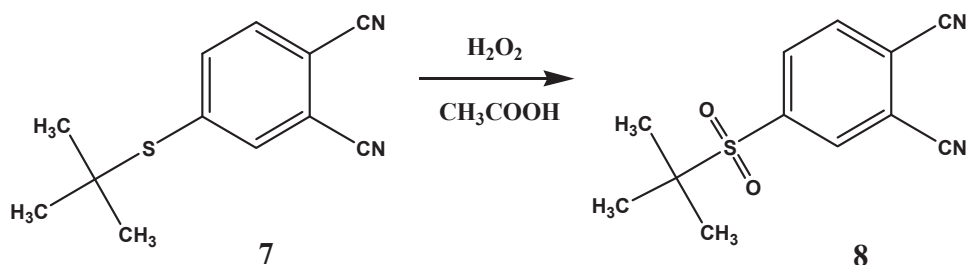
IR (KBr) $\nu(\text{cm}^{-1})$: 3092, 2972, 2234, 1582, 1537, 1478, 1356, 1162, 1076, 923, 845, 748, 618, 527

EA: Calculated: C 66.63, H 5.59, N 12.95, S 14.82

Found : C 66.32, H 6.06, N 12.73, S 14.48

Mass Spectrum (ESI-MS) m/z : 239.06 $[\text{M}+\text{Na}]$

4.1.8. 1,2-Dicyano-4-(tert-butylsulfonyl)benzene (8)



1,2-Dicyano-4-(tert-butyl thio)benzene (2.3 g, 0.011 mmol) was dissolved in 50 mL of acetic acid at 90 °C. To the stirred solution was added a total of 60 mL of 33% H_2O_2 in 1 mL portions in the course of 4 h. The resulting mixture was allowed to cool to room temperature and stirred overnight, and the white precipitate was collected by filtration, subsequently washed several times with water, and crystallized from ethanol (50 mL) to give pure 1,2-Dicyano-4-(tert-butylsulfonyl)benzene (**8**) as a white powder.

1.8 g, Yield (73 %)

$\text{C}_{14}\text{H}_{16}\text{N}_2\text{SO}_2$ MW: 248.06 g/mol

Melting Point: 180 °C

IR (KBr) $\nu(\text{cm}^{-1})$: 3106, 3087, 2982, 2233, 1590, 1472, 1302, 1286, 1128, 1107, 839, 685, 557

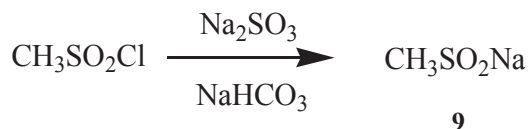
EA: Calculated: C 58.05, H 4.87, N 11.28, S 12.91

Found : C 57.47, H 5.11, N 11.16, S 12.67

Mass Spectrum (ESI-MS) m/z : 248.3 $[\text{M}]^+$

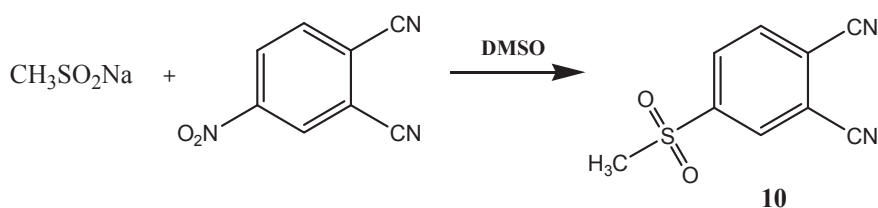
^1H NMR (CDCl_3): δ = 1.3 (s, 9H), 8.1 (d, 1H), 8.2 (d, 1H), 8.3 (dd, 1H)

4.1.9. Sodium methanesulfinate (9)



A solution of sodium sulfite (5.0 g, 39.6 mmol) in H₂O (19.0 mL) was vigorously stirred for 10 min at 20 °C NaHCO₃ (6.8 g, 81.4 mmol) was added, and the mixture was stirred for 1 h at 50 °C. Methanesulfonyl chloride (3.0 mL, 39.2 mmol) was carefully added, and after the addition, the mixture was vigorously stirred at 50 °C for 4 h. After cooling to 20 °C, the H₂O was evaporated. MeOH (5.0 mL) was added to the white residue to separate the sodium methanesulfinate from MeOH insoluble salts, and the mixture was stirred overnight. Filtration and evaporation gave 3.7 g (94%) of the title product.

4.1.10. 1,2-Dicyano-4-methylsulfonylbenzene (10)



A mixture of 4-nitrophthalonitrile (1.73 g, 10 mmol) and sodium metansulfinate (1.02 g, 10 mmol) was stirred in DMSO (50 mL) at 80 °C under argon for 24 h. Then the mixture was poured into water (500 cm³). The resulting solid was collected by filtration and washed with water. After drying in vacuo at 50 °C, the crude product was recrystallised from ethanol.

1.2 g, Yield (60 %)

C₉H₆N₂SO₂ MW: 206.01 g/mol

Melting Point: 166 °C

IR (KBr) ν (cm⁻¹): 3100, 3026, 2938, 2236, 1591, 1388, 1325, 1152, 965, 764, 645, 534

EA: Calculated: C 52.42, H 2.93, N 13.58, S 15.55

Found : C 52.20, H 2.84, N 13.29, S 15.70

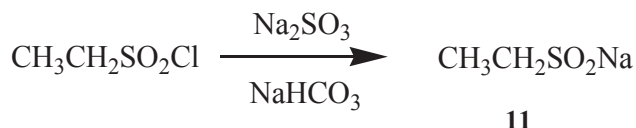
Mass Spectrum (ESI-MS) m/z: 207.03 [M+H]

¹H NMR (CDCl₃): δ = 3.1 (s, 3 H, CH₃), 8.1 (d, 1 H, ArH), 8.3 (d, H, ArH),

8.4 (s, 1 H, ArH).

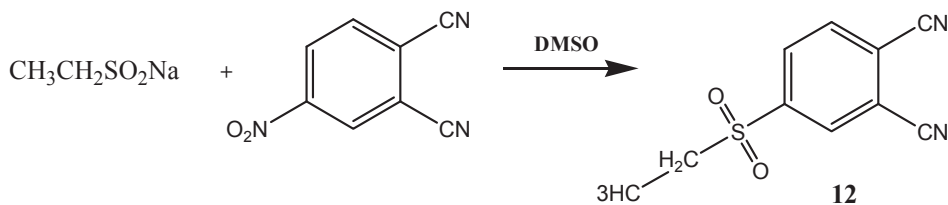
¹³C NMR (CDCl₃): δ = 145.6, 134.9, 132.6, 132.1, 120.8, 117.8, 114.2, 114.0, 44.5.

4.1.11. Sodium ethanesulfinate (11)



A solution of sodium sulfite (5.0g, 39.6 mmol) in H₂O (19.0 mL) was vigorously stirred for 10 min at 20 °C. NaHCO₃ (6.8 g, 81.4 mmol) was added, and the mixture was stirred for 1 h at 50 °C. Ethanesulfonyl chloride (3.0mL, 39.2 mmol) was carefully added, and after the addition, the mixture was vigorously stirred at 50 °C for 4 h. After cooling to 20 °C, the H₂O was evaporated. EtOH (5.0mL) was added to the white residue to separate the sodium ethanesulfinate from EtOH insoluble salts, and the mixture was stirred overnight. Filtration and evaporation gave 3.7 g (95 %) of the title product.

4.1.12. 1,2-Dicyano-4-ethylsulfonylbenzene (12)



A mixture of 4-nitrophthalonitrile (1.73 g, 10 mmol) and sodium ethanesulfonate (1.28 g, 10 mmol) was stirred in DMSO (50 mL) at 80 °C under argon for 24 h. Then the mixture was poured into water (500 cm³). The resulting solid was collected by filtration and washed with water. After drying in vacuo at 50 °C, the crude product was recrystallised from ethanol.

1.36 g, Yield (62 %)

$\text{C}_{10}\text{H}_8\text{N}_2\text{SO}_2$ MW: 220.03 g/mol

Melting Point: 130 °C

IR (KBr) $\nu(\text{cm}^{-1})$: 3103, 3077, 2943, 2239, 1591, 1387, 1314, 1133, 1051, 849, 738, 654

EA: Calculated: C 54.53, H 3.66, N 12.72, S 14.56

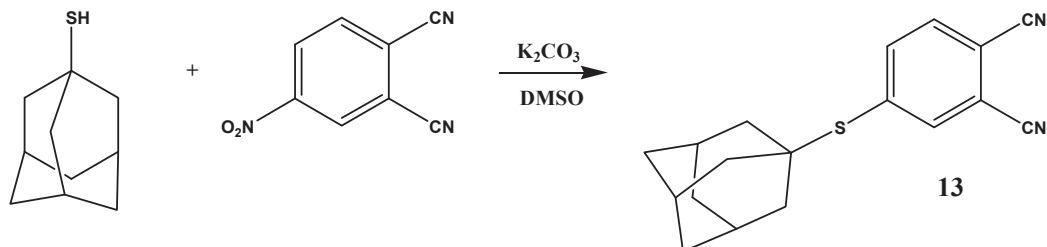
Found : C 54.12, H 3.72, N 12.90, S 14.12

Mass Spectrum (ESI-MS) m/z : 221.08 [M+H]

^1H NMR (CDCl_3): δ = 1.3 (t, 3H), 3.2 (q, 3H), 8.0 (d, 1H), 8.2 (d, 1H), 8.3 (s, 1H)

^{13}C NMR (CDCl_3): δ = 144.2, 134.7, 132.8, 132.6, 120.6, 117.8, 114.3, 114.1, 50.6, 7.2

4.1.13. 1,2-Dicyano-4-adamantylthiobenzene (13)



4-Nitrophthalonitrile (2.5 g, 14.5 mmol) and adamantanethiol (2.5 g, 14.6 mmol) were dissolved in anhydrous dimethyl sulfoxide (DMSO) (10 mL) under argon atmosphere. After stirring for 15 min at room temperature, dry and finely powdered potassium carbonate (6 g, 43.5 mmol) was added portionwise over 15 min with efficient stirring. The reaction mixture was stirred under argon at room temperature for 24 h. Then the mixture was poured into 200 cm³ of ice-water. The resulting solid was collected by filtration and washed with water. After drying in vacuo at 50 °C, the crude product was recrystallised from ethanol.

3.3 g, Yield (81 %)

C₁₈H₁₈N₂S MW: 294.1 g/mol

Melting Point: 144 °C

IR (KBr) ν (cm⁻¹): 2914, 2881, 2848, 2232, 1580, 1474, 1339, 1103, 1036, 843, 684, 526.

EA: Calculated: C 73.43, H 6.16, N 9.51, S 10.89

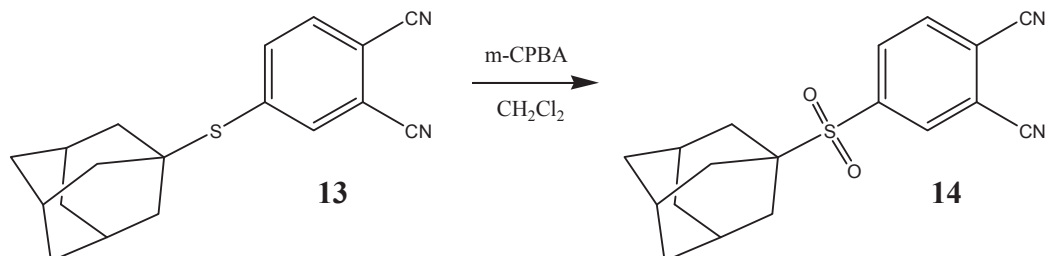
Found : C 73.10, H 6.30, N 9.45, S 10.70.

Mass Spectrum (ESI-MS) m/z: 317.2 [M+Na]

¹H NMR (CDCl₃): δ = 1.6-2.2 (m, 15H), 7.7(d, 1H), 7.8 (d, 1H), 7.9 (s, 1H)

¹³C NMR (CDCl₃): δ = 141.2, 141.0, 140.1, 133.2, 115.9, 115.4, 115.3, 115.2, 50.1, 44.1, 36.2, 30.1.

4.1.14. 1,2-Dicyano-4-adamantylsulfonylbenzene (**14**)



To a solution of 1,2-dicyano-4-adamantylthiobenzene (3 g, 10 mmol) in dry CH_2Cl_2 (50 mL) cooled at 0 °C was slowly added *m*-chloroperbenzoic acid (17.2 g, 100 mmol) in CH_2Cl_2 (500 mL). The mixture was warmed to room temperature and vigorously stirred at this temperature overnight (12 h). A saturated sodium sulfite solution was then added, and the organic phase was extracted with CH_2Cl_2 (3 x 50 mL) and dried over Na_2SO_4 . The solvent was removed under reduced pressure, and the solid was recrystallized from ethanol to give 1,2-dicyano-4-adamantylsulfonylbenzene (**14**) as a white solid.

2.4 g, Yield (73 %)

$\text{C}_{18}\text{H}_{18}\text{N}_2\text{SO}_2$ MW: 326.1 g/mol

Melting Point: 266 °C

IR (KBr) $\nu(\text{cm}^{-1})$: 3100, 3033, 2910, 2860, 2232, 1591, 1455, 1390, 1301, 1284, 1185, 1141, 1040, 856, 628, 560

EA: Calculated: C 66.23, H 5.56, N 8.58, S 9.82

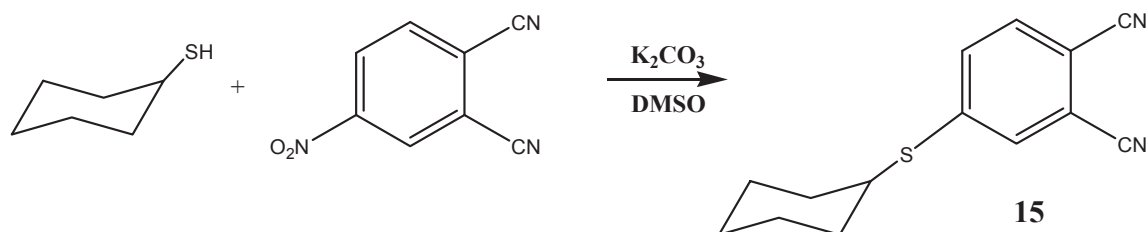
Found : C 66.11, H 5.14, N 8.09, S 9.64

Mass Spectrum (ESI-MS) m/z : 325.2 [M-H]

^1H NMR (CDCl_3): δ = 1.4-2.2 (m, 15H), 8.0(d, 1H), 8.1 (d, 1H), 8.2 (s, 1H)

^{13}C NMR (CDCl_3): $\delta = 140.8, 135.3, 134.9, 134.0, 120.4, 117.0, 114.4, 114.3, 62.5, 35.6, 35.1, 28.2$

4.1.15. 1,2-Dicyano-4-cyclohexylthiobenzene (15)



4-Nitrophthalonitrile (2.5 g, 14.5 mmol) and cyclohexanethiol (1.7 g, 14.6 mmol) were dissolved in anhydrous dimethyl sulfoxide (DMSO) (10 ml) under argon atmosphere. After stirring for 15 min at room temperature, dry and finely powdered potassium carbonate (6 g, 43.5 mmol) was added portionwise over 15 min with efficient stirring. The reaction mixture was stirred under argon at room temperature for 24 h. Then the mixture was poured into 200 cm³ of ice-water. The resulting solid was collected by filtration and washed with water. After drying in vacuo at 50 °C, the crude product was recrystallised from ethanol.

2.6 g, Yield (75 %)

$\text{C}_{14}\text{H}_{14}\text{N}_2\text{S}$ MW: 242,09 g/mol

Melting Point: 93 °C

IR (KBr) $\nu(\text{cm}^{-1})$: 2860, 2236, 1578, 1470, 1343, 1102, 1090, 837, 760, 524

EA: Calculated: C 69.39, H 5.82, N 11.56, S 13.23

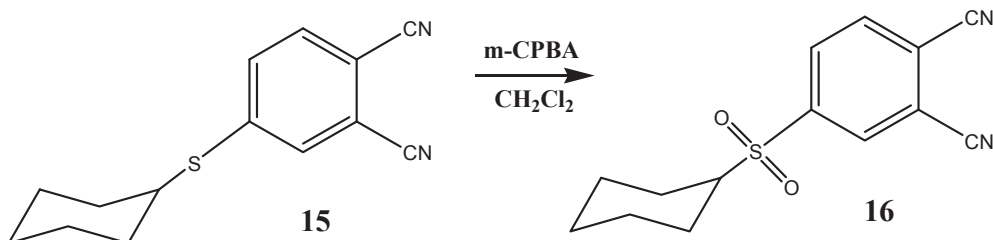
Found : C 68.90, H 5.76, N 11.89, S 13.33

Mass Spectrum (ESI-MS) m/z : 265.18 [M+Na]

^1H NMR (CDCl_3): δ = 1.2-2.2 (m, 10H), 3.3 (m, 1H), 7.5(d, 1H), 7.6 (s, 1H), 7.7 (d, 1H)

^{13}C NMR (CDCl_3): δ = 140.7, 130.3, 130.1, 130.0, 117.8, 115.8, 115.6, 111.1, 45.6, 32.8, 25.8, 25.6

4.1.16. 1,2-Dicyano-4-cyclohexylsulfonylbenzene (16)



To a solution of 1,2-dicyano-4-cyclohexylthiobenzene (3 g, 12 mmol) in dry CH_2Cl_2 (50 mL) cooled at 0 °C was slowly added *m*-chloroperbenzoic acid (20.6 g, 120 mmol) in CH_2Cl_2 (500 mL). The mixture was warmed to room temperature and vigorously stirred at this temperature overnight (12 h). A saturated sodium sulfite solution was then added, and the organic phase was extracted with CH_2Cl_2 (3 x 50 mL) and dried over Na_2SO_4 . The solvent was removed under reduced pressure, and the solid

was recrystallized from ethanol to give 1,2-Dicyano-4-cyclohexylsulfonylbenzene (**16**) as a white solid.

2.4 g, Yield (73 %)

C₁₄H₁₄N₂SO₂ MW: 274,08 g/mol

Melting Point: 161 °C

IR (KBr) ν (cm⁻¹): 3073, 3036, 2856, 2237, 1590, 1456, 1313, 1112, 1109, 847, 766, 542

EA: Calculated: C 61.29, H 5.14, N 10.21, S 11.69

Found : C 61.08, H 5.70, N 10.88, S 11.20

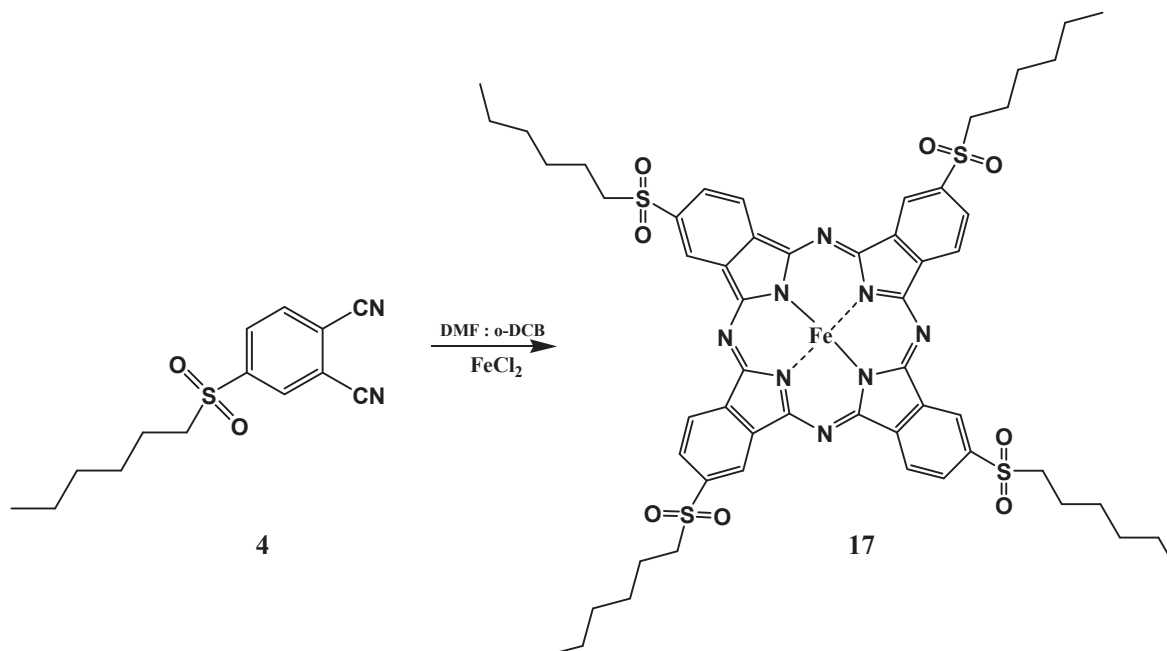
Mass Spectrum (ESI-MS) m/z: 313.18 [M+K]

¹H NMR (CDCl₃): δ = 1.0-2.1 (m, 10H), 2.9 (m, 1H), 8.0 (d, 1H), 8.2 (d, 1H), 8.3 (s, 1H)

¹³C NMR (CDCl₃): δ = 142.8, 134.2, 133.7, 133.3, 120.3, 117.2, 114.0, 113.9, 63.7, 25.3, 24.8, 24.7

4.2. Synthesis of monomeric iron phthalocyanines

4.2.1. Tetra-(hexylsulfonyl)phthalocyaninatoiron (17)



4 (300 mg, 1.08 mmol) was heated at 130°C in a mixture of *o*-dichlorobenzene-DMF (3:1) under argon for 8 h in the presence of FeCl₂ (0.27 mmol). The solvent was removed under reduced pressure. The green-blue solid was extracted with CH₂Cl₂ and washed with water. **2a** was isolated by chromatography on silica gel using a mixture of CH₂Cl₂-EtOH (100:1).

58 mg, Yield (18 %)

C₅₆H₆₄FeN₈O₈S₄ MW: 1160.3 g/mol

IR (KBr) ν (cm⁻¹): 1326, 1257, 1143, 1076, 818, 745

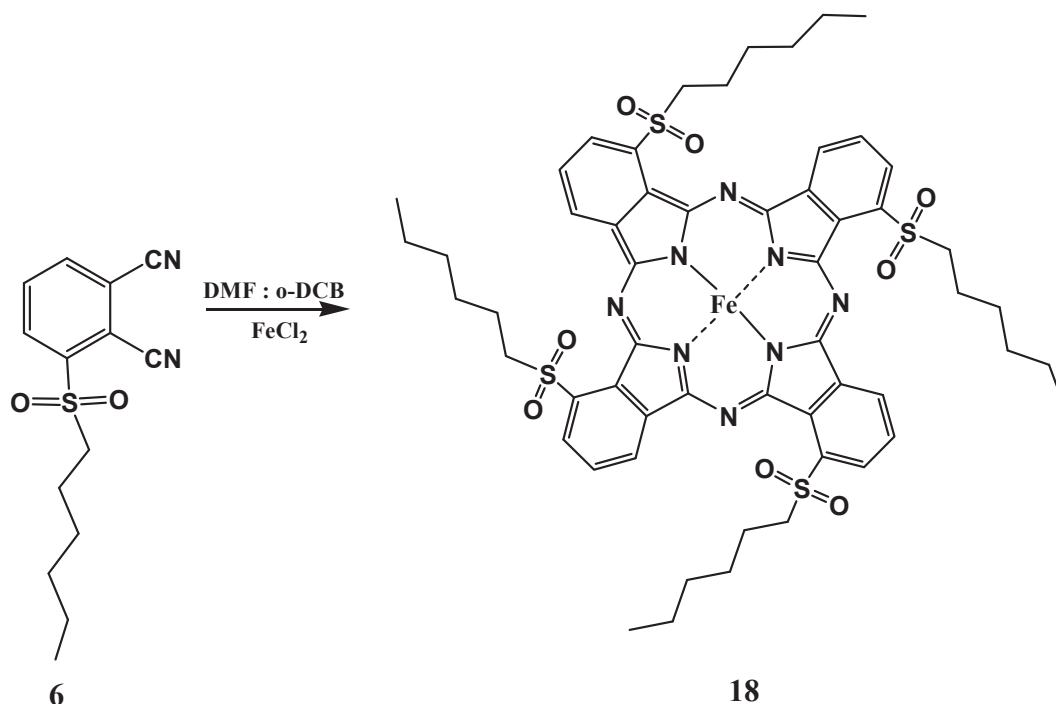
EA: Calculated: C 66.62, H 7.83, N 7.77, S 17.79

Found : C 67.20, H 7.70, N 7.93, S 17.57

Mass Spectrum (ESI-MS) m/z: 1161.3 [M+H]

UV/Vis (CHCl₃): λ_{max} = 680, 600, 306 nm

4.2.2. Tetra-np-(hexylsulfonyl)phthalocyaninatoiron (18)



A mixture of 1,2-Dicyano-3-hexylsulfonylbenzene (300 mg; 1.08 mmol) was heated at 130 °C in a mixture of *o*-dichlorobenzene-DMF (3:1) under argon for 8 h in the presence of the corresponding metallic salt, iron(II) chloride [FeCl_2] (0.27 mmol). After the solvent was concentrated under reduced pressure, the green solid was extracted with CH_2Cl_2 and washed with water. Compound **18** was isolated from the tetra-np-hexylsulfonylphthalocyaninato iron (II) by chromatography on silica gel using a mixture of CH_2Cl_2 -ethanol (100:1) was employed.

55 mg, Yield (17 %)

$\text{C}_{56}\text{H}_{64}\text{FeN}_8\text{O}_8\text{S}_4$ MW: 1160.3 g/mol

IR (KBr) $\nu(\text{cm}^{-1})$: 1326, 1257, 1143, 1076, 818, 745

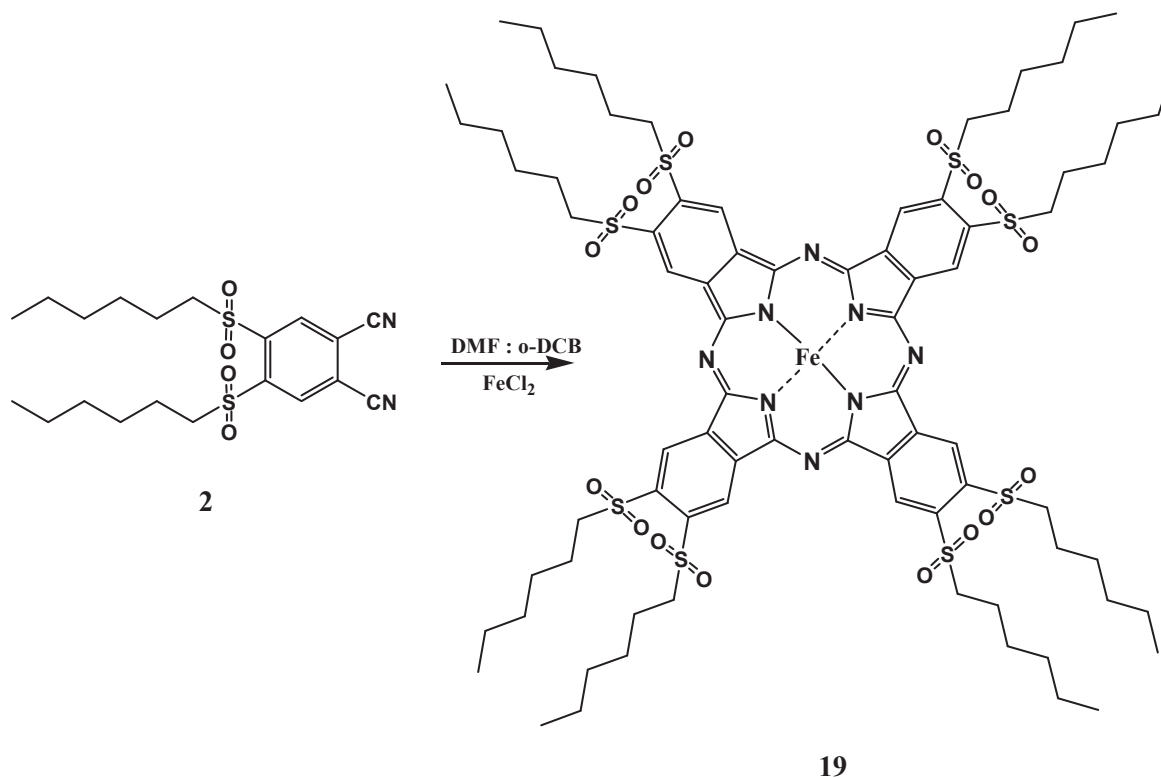
EA: Calculated: C 66.62, H 7.83, N 7.77, S 17.79

Found : C 67.20, H 7.70, N 7.93, S 17.57

Mass Spectrum (ESI-MS) m/z : 1161.2 [$\text{M}+\text{H}$]

UV/Vis (CHCl_3): λ_{max} = 670, 603, 347 nm

4.2.3. Octa-(hexylsulfonyl)phthalocyaninatoiron (19)



A mixture of 1,2-dicyano-4,5-bis(hexylsulfonyl)benzene **2** (250 mg; 0.6 mmol) was heated at 130 °C in a mixture of *o*-dichlorobenzene-DMF (3:1) under argon for 8 h in the presence of iron(II) chloride [FeCl₂] (0.15 mmol). After the solvent was concentrated under reduced pressure, the green solid was extracted with dichloromethane and washed with water. Compound **19** was isolated by chromatography on silica gel using a mixture of dichloromethane-ethanol (100:1) as eluent.

61 mg, Yield (23 %)

C₈₀H₁₁₂FeN₈O₁₆S₈ MW: 1172.5 g/mol

IR (KBr) $\nu(\text{cm}^{-1})$: 1310, 1100, 1070, 808, 740

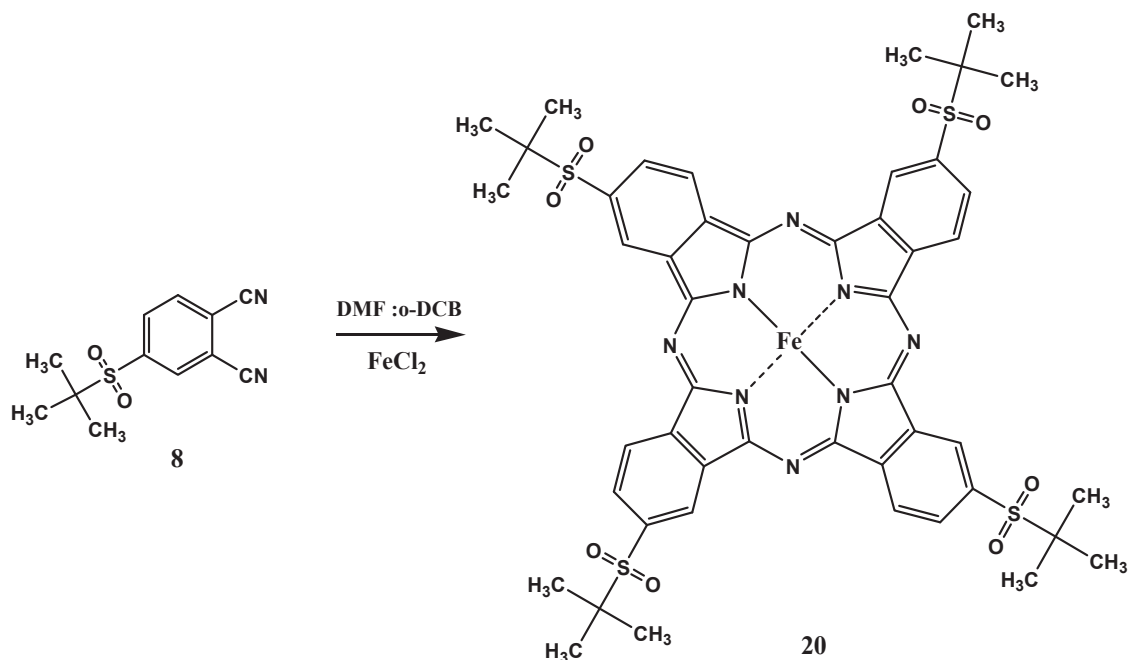
EA: Calculated: C 66.62, H 7.83, N 7.77, S 17.79

Found : C 67.20, H 7.70, N 7.93, S 17.57

Mass Spectrum (ESI-MS) m/z : 1753 [M+H]⁺

UV/Vis (CHCl₃): λ_{max} = 670, 354 nm

4.2.4. Tetra-(tert-butylsulfonyl)phthalocyaninatoiron (20)



A mixture of 1,2-Dicyano-4-(2-Methyl-2-propanesulfonyl) benzene (1 g, 4 mmol) was heated at 130°C in a mixture of *o*-dichlorobenzene-DMF (3:1) under argon for 8 h in the presence of FeCl_2 (1 mmol). The solvent was removed under reduced pressure. The blue solid was extracted with CH_2Cl_2 . **20** was isolated by chromatography on silica gel using a mixture of CH_2Cl_2 -EtOH (100:1).

250 mg, Yield (25 %)

$\text{C}_{48}\text{H}_{48}\text{FeN}_8\text{O}_8\text{S}_4$ MW: 1049.05 g/mol

IR (KBr) $\nu(\text{cm}^{-1})$: 1296, 1143, 1140, 1123, 697, 564

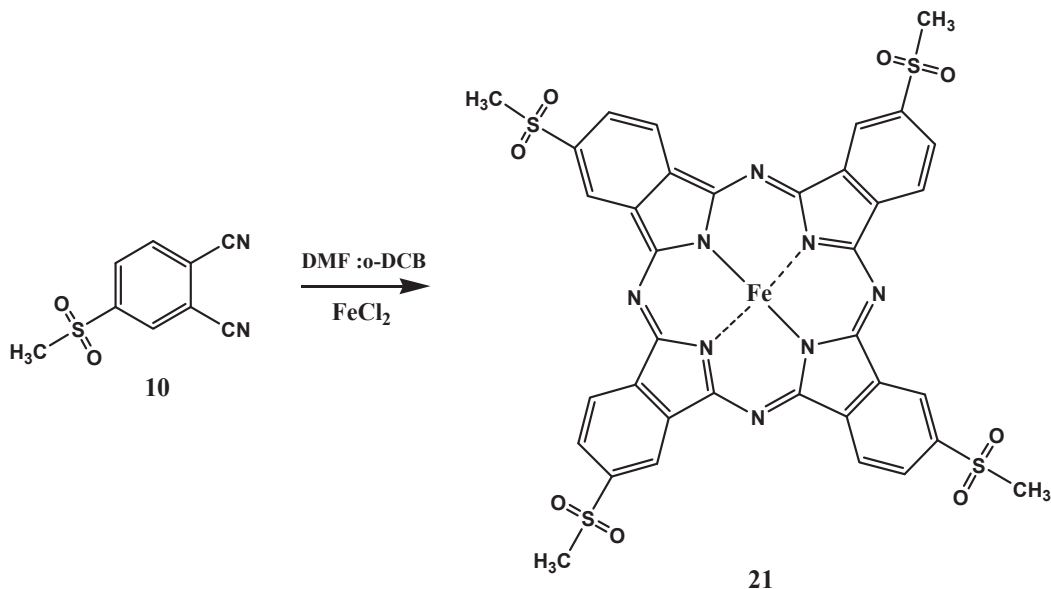
EA: Calculated: C 66.62, H 7.83, N 7.77, S 17.79

Found : C 67.20, H 7.70, N 7.93, S 17.57

Mass Spectrum (ESI-MS) m/z : 1049.1 $[\text{M}]^+$

UV/Vis (CHCl_3): λ_{max} = 683, 629, 287 nm

4.2.5. Tetra-(methylsulfonyl)phthalocyaninatoiron (21)



A mixture of 1,2-Dicyano-4-(methylsulfonyl)benzene (1g; 4.8 mmol) was heated at 130 °C in a mixture of *o*-dichlorobenzene-DMF (3:1) under argon for 8 h in the presence of the corresponding metallic salt, iron(II) chloride [FeCl_2] (1.5 mmol). After the solvent was concentrated under reduced pressure, the blue solid was extracted with CH_2Cl_2 . Compound **21** was isolated from the tetra methylsulfonyl phthalocyaninato iron by chromatography on silica gel using a mixture of CH_2Cl_2 -ethanol (1:1) was employed.

250 mg, Yield (24 %)

$\text{C}_{36}\text{H}_{24}\text{FeN}_8\text{O}_8\text{S}_4$ MW: 880.12 g/mol

IR (KBr) $\nu(\text{cm}^{-1})$: 2926, 1599, 1404, 1300, 1146, 1047, 834, 720, 578, 530

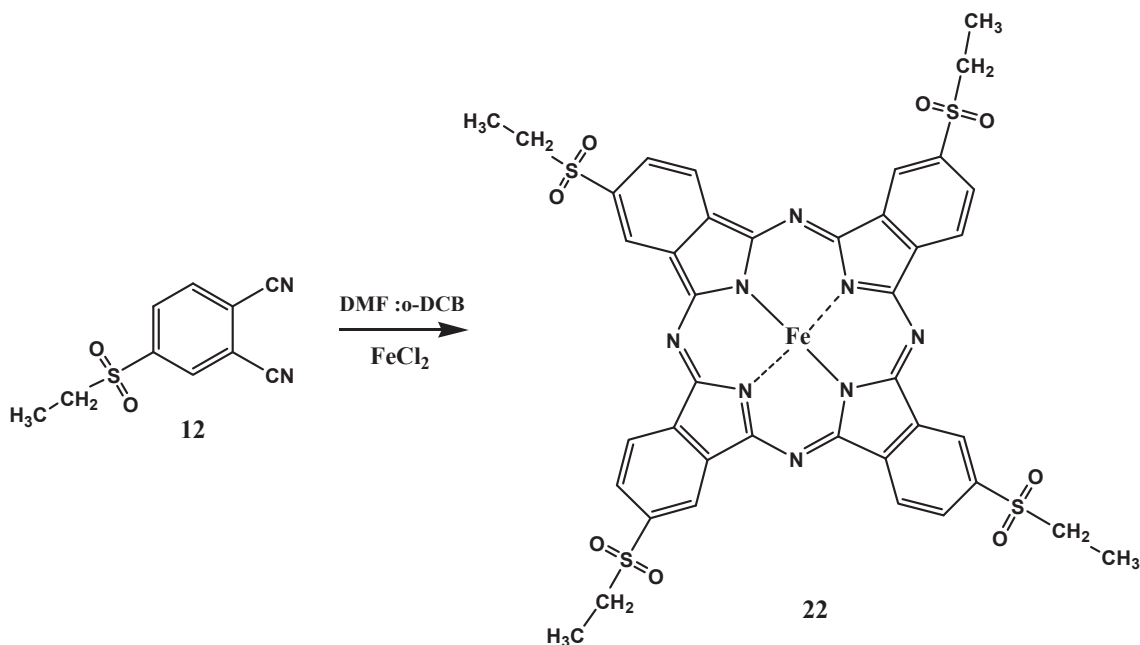
EA: Calculated: C, 49.09; H, 2.75; N, 12.72; S, 14.56

Found : C, 49.28; H, 2.70; N, 12.98; S, 14.20

Mass Spectrum (ESI-MS) m/z : 880.14 $[\text{M}]^+$

UV/Vis (CHCl_3): λ_{max} = 665, 327 nm

4.2.6. Tetra-(ethylsulfonyl)phthalocyaninatoiron (22)



A mixture of 1,2-Dicyano-4-(ethylsulfonyl)benzene (1.5 g; 7 mmol) was heated at 130 °C in a mixture of *o*-dichlorobenzene-DMF (3:1) under argon for 8 h in the presence of the corresponding metallic salt, iron(II) chloride [FeCl₂] (1.75 mmol). After the solvent was concentrated under reduced pressure, the blue solid was extracted with CH₂Cl₂. Compound **22** was isolated from the tetra ethylsulfonyl phthalocyaninato iron by chromatography on silica gel using a mixture of CH₂Cl₂-ethanol (1:1) was employed.

995 mg, Yield (62 %)

C₄₀H₃₂FeN₈O₈S₄ MW: 936.06 g/mol

IR (KBr) ν (cm⁻¹): 2938, 1605, 1455, 1402, 1306, 1143, 1046, 838, 724, 582, 533

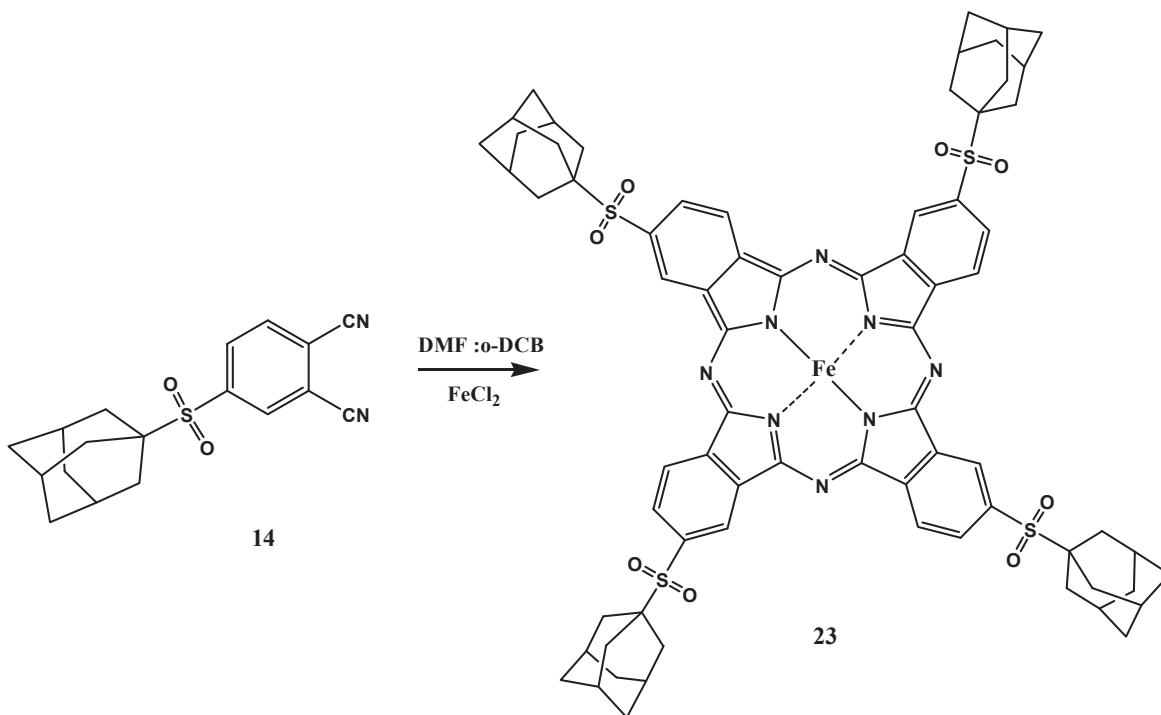
EA: Calculated: C, 51.28; H, 3.44; N, 11.96; S, 13.69

Found : C, 51.08; H, 3.37; N, 11.18; S, 12.94

Mass Spectrum (ESI-MS) m/z: 936.21 [M]⁺

UV/Vis (CHCl₃): λ_{max} = 670, 606, 336 nm

4.2.7. Tetra-(adamantylsulfonyl)phthalocyaninatoiron (23)



A mixture of 1,2-Dicyano-4-(adamantylsulfonyl)benzene (1 g; 3 mmol) was heated at 130 °C in a mixture of *o*-dichlorobenzene-DMF (3:1) under argon for 8 h in the presence of the corresponding metallic salt, iron(II) chloride [FeCl₂] (0.7 mmol). After the solvent was concentrated under reduced pressure, the blue solid was extracted with CH₂Cl₂. Compound **23** was isolated from the tetra adamantylsulfonyl phthalocyaninato iron by chromatography on silica gel using a mixture of CH₂Cl₂-ethanol (100:1) was employed.

495 mg, Yield (47 %)

C₃₆H₂₄FeN₈O₈S₄ MW: 1360.37 g/mol

IR (KBr) ν (cm⁻¹): 2925, 2848, 1602, 1513, 1404, 1300, 1140, 1090, 1037, 970, 826, 750, 704, 580

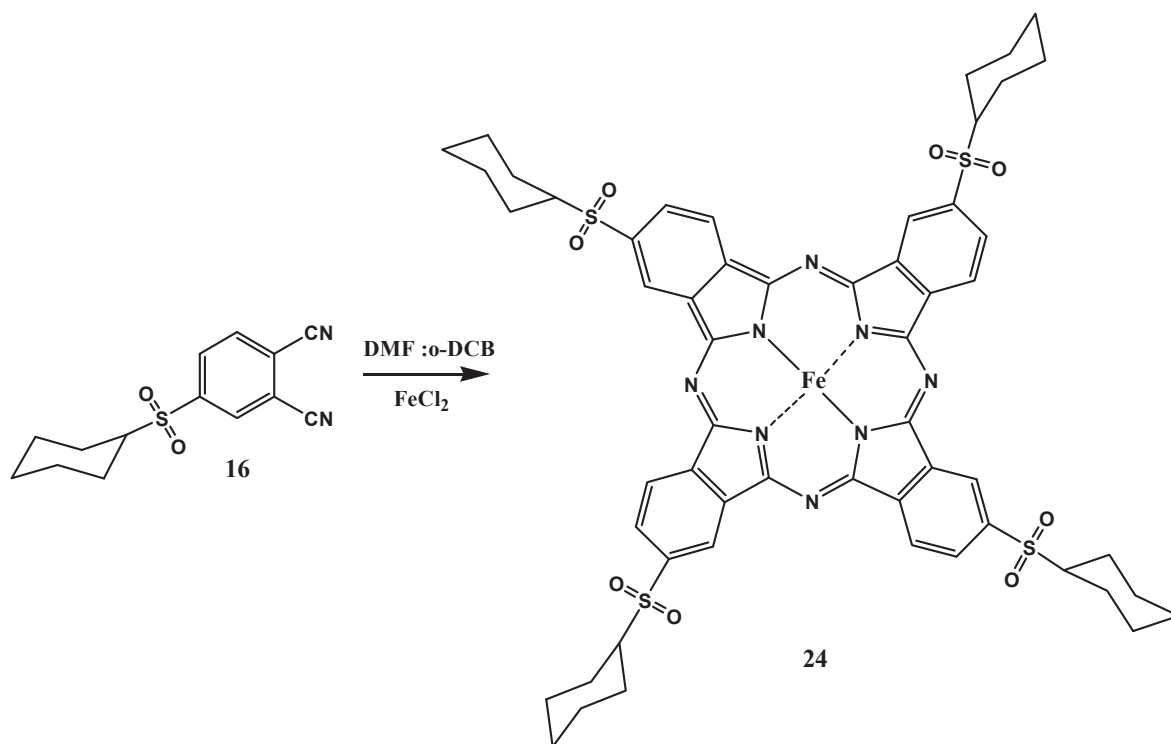
EA: Calculated: C, 63.52; H, 5.33; N, 8.23; S, 9.42

Found : C, 63.21; H, 5.67; N, 8.16; S, 9.88

Mass Spectrum (MALDI-MS) m/z : 1361.54 [M+H]⁺

UV/Vis (CHCl₃): λ_{max} = 683, 336 nm

4.2.8. Tetra-(cyclohexylsulfonyl)phthalocyaninatoiron (24)



A mixture of 1,2-Dicyano-4-(cyclohexylsulfonyl)benzene (1 g; 3.65 mmol) was heated at 130 °C in a mixture of *o*-dichlorobenzene-DMF (3:1) under argon for 8 h in the presence of the corresponding metallic salt, iron(II) chloride [FeCl_2] (1 mmol). After the solvent was concentrated under reduced pressure, the blue solid was extracted with CH_2Cl_2 . Compound **24** was isolated from the tetra cyclohexylsulfonyl phthalocyaninato iron by chromatography on silica gel using a mixture of CH_2Cl_2 -ethanol (100:1) was employed.

420 mg, Yield (40 %)

$\text{C}_{56}\text{H}_{56}\text{FeN}_8\text{O}_8\text{S}_4$ MW: 1152.25 g/mol

IR (KBr) $\nu(\text{cm}^{-1})$: 2938, 2856, 1605, 1449, 1402, 1306, 1145, 1102, 1050, 1002, 889, 824, 758, 683, 591, 548

EA: Calculated: C, 58.32; H, 4.89; N, 9.72; S, 11.12

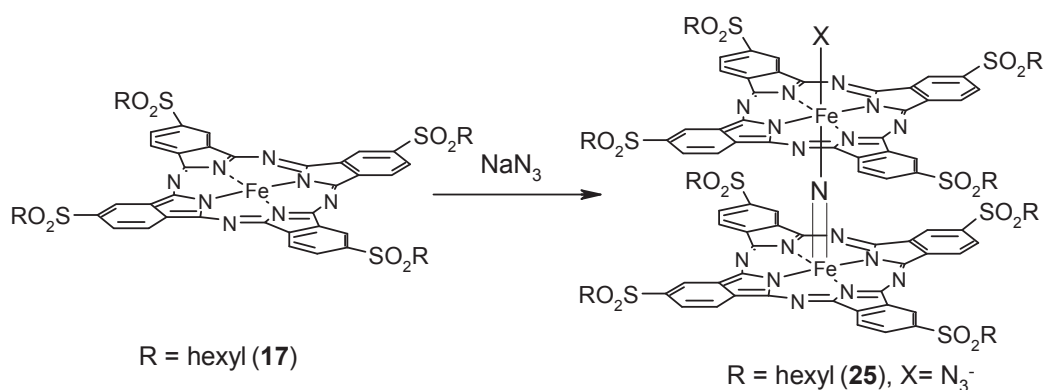
Found : C, 58.06; H, 4.37; N, 9.95; S, 10.88

Mass Spectrum (MALDI-MS) m/z : 1152.77 $[\text{M}]^+$

UV/Vis (CHCl_3): λ_{max} = 681, 326 nm

4.3. Synthesis of μ -nitrido diiron phthalocyanines

4.3.1. μ -Nitrido-bis [tetra-(hexylsulfonyl)phthalocyaninatoiron] (**25**)



17 (200 mg, 0.17 mmol) and sodium azide (2g) were suspended in 70 ml of oxygen-free xylene (mixture of isomers) under argon. The mixture was heated for 24 h at 150°C under intensive stirring. The reaction mixture was cooled and resulting blue green solution was separated from insoluble material by filtration. The solution was chromatographed on Al_2O_3 (neutral) with CH_2Cl_2 to remove impurities. Then **25** was collected using CH_2Cl_2 :EtOH (100:1) mixture as eluent.

115 mg, Yield (57 %)

$\text{C}_{112}\text{H}_{128}\text{Fe}_2\text{N}_{17}\text{O}_{16}\text{S}_8$ MW: 2335.6 g/mol

IR (KBr) $\nu(\text{cm}^{-1})$: 931 ($\text{Fe}=\text{N}-\text{Fe}$)

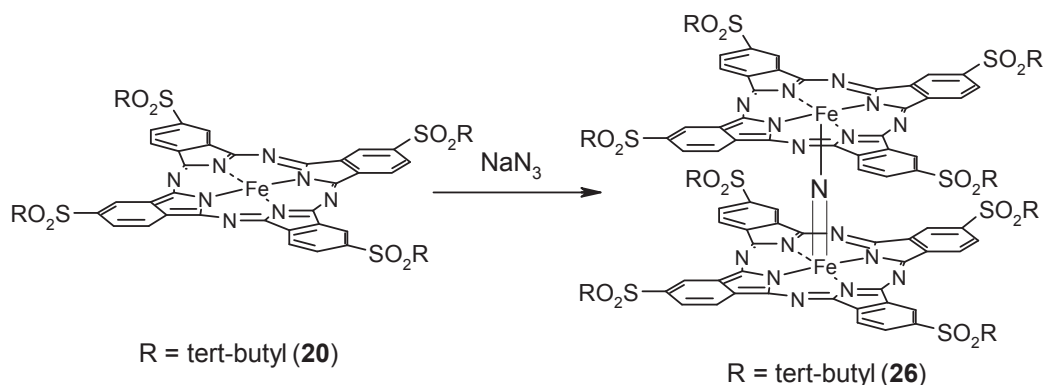
EA: Calculated: C, 57.16; H, 5.52; N, 10.12; S, 10.90

Found : C, 57.42; H, 5.62; N, 8.53; S, 9.61

Mass Spectrum (ESI-MS) m/z: 2335.9 $[\text{M}-\text{N}_3]^+$

UV/Vis (CHCl_3): λ_{max} = 657, 344 nm

4.3.2. μ -Nitrido-bis [tetra-(tert-butylsulfonyl)phthalocyaninatoiron] (**26**)



20 (170 mg, 0.16 mmol) and sodium azide (1.5 g) were suspended in 70 ml of oxygen-free xylene (mixture of isomers) under argon. The mixture was heated for 24 h at 150°C under intensive stirring. The reaction mixture was cooled and resulting dark blue solution was separated from insoluble material by filtration. The solution was chromatographed on Al_2O_3 (neutral) with CH_2Cl_2 to remove impurities. Then **26** was collected using CH_2Cl_2 :EtOH (100:1) mixture as eluent. Evaporation of solvent afforded pure **26** as a dark blue powder.

100 mg, Yield (58 %)

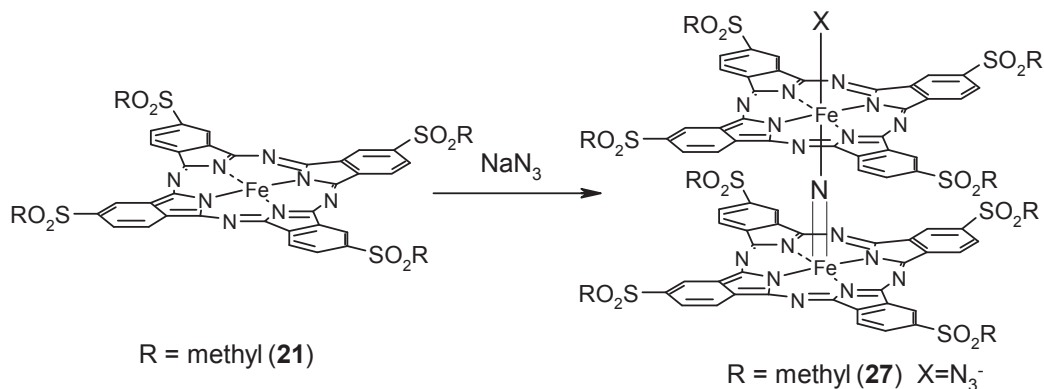
$\text{C}_{96}\text{H}_{96}\text{Fe}_2\text{N}_{17}\text{O}_{16}\text{S}_8$ MW: 2134.4 g/mol

IR (KBr) $\nu(\text{cm}^{-1})$: 929 (Fe=N-Fe)

Mass Spectrum (ESI-MS) m/z : 2134.6 $[\text{M}+\text{Na}]^+$

UV/Vis (CHCl_3): λ_{max} = 657, 344 nm

4.3.3. μ -Nitrido-bis [tetra-(methylsulfonyl)phthalocyaninatoiron] (**27**)



21 (170 mg, 0.16 mmol) and sodium azide (1.1 g) were suspended in 70 ml of α -chloronaphthalene under argon. The mixture was heated for 24 h at 190 °C under intensive stirring. The reaction mixture was cooled and resulting dark blue solution was filtered. The dark blue solid was washed with water and ethanol. The solution was chromatographed on Al₂O₃ (neutral) with CH₂Cl₂ to remove impurities. Then **27** was collected using CH₂Cl₂:EtOH (1:1) as eluent. Evaporation of solvent afforded pure **27** as a dark blue powder.

100 mg, Yield (59 %)

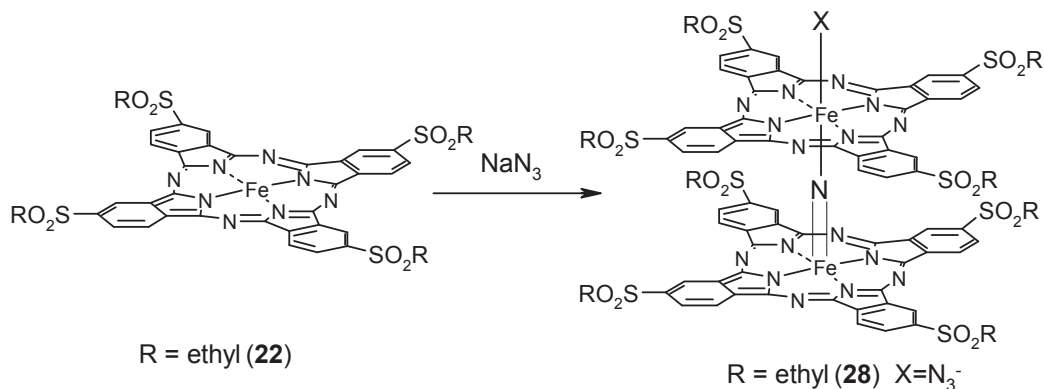
C₇₂H₄₈Fe₂N₁₇O₁₆S₈ MW: 1796.98 g/mol

IR (KBr) ν (cm⁻¹): 928 (Fe=N-Fe)

Mass Spectrum (ESI-MS) m/z: 1797.04 [M+Na]⁺

UV/Vis (CHCl₃): λ_{max} = 645, 319 nm

4.3.4. μ -Nitrido-bis [tetra-(ethylsulfonyl)phthalocyaninatoiron] (**28**)



22 (170 mg, 0.18 mmol) and sodium azide (1.1 g) were suspended in 70 ml of α -chloronaphthalene under argon. The mixture was heated for 24 h at 190 °C under intensive stirring. The reaction mixture was cooled and resulting dark blue solution was filtered. The dark blue solid was washed with water and ethanol. The solution was chromatographed on Al₂O₃ (neutral) with CH₂Cl₂ to remove impurities. Then **28** was collected using CH₂Cl₂:EtOH (1:1) as eluent. Evaporation of solvent afforded pure **28** as a dark blue powder

110 mg, Yield (64 %)

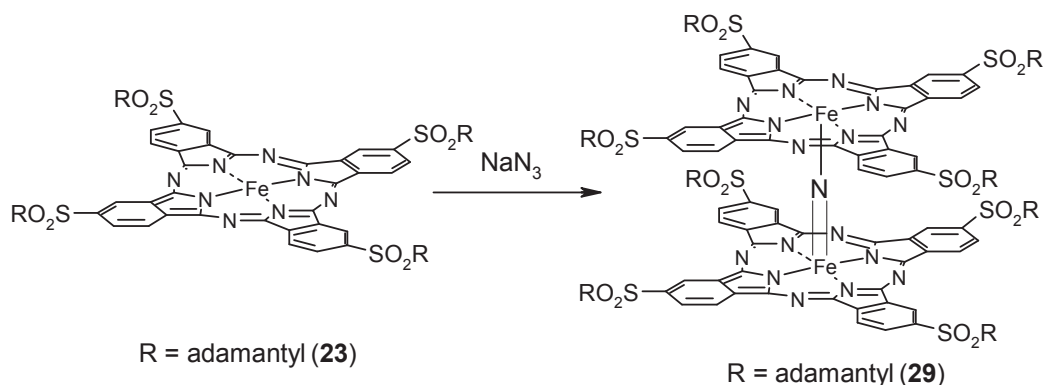
C₈₀H₆₄Fe₂N₁₇O₁₆S₈ MW: 1886.11 g/mol

IR (KBr) ν (cm⁻¹): 930 (Fe=N-Fe)

Mass Spectrum (ESI-MS) m/z: 1906.36 [M+Na]⁺

UV/Vis (CHCl₃): λ_{max} = 652, 319 nm

4.3.5. μ -Nitrido-bis [tetra-(adamantylsulfonyl)phthalocyaninatoiron] (**29**)



23 (200 mg, 0.16 mmol) and sodium azide (1.5 g) were suspended in 70 ml of oxygen-free xylene (mixture of isomers) under argon. The mixture was heated for 24 h at 150 °C under intensive stirring. The reaction mixture was cooled and resulting dark blue solution was separated from insoluble material by filtration. The solution was chromatographed on Al₂O₃ (neutral) with CH₂Cl₂ to remove impurities. Then **29** was collected using CH₂Cl₂:EtOH (100:1) mixture as eluent. Evaporation of solvent afforded pure **29** as a dark blue powder.

100 mg, Yield (50 %)

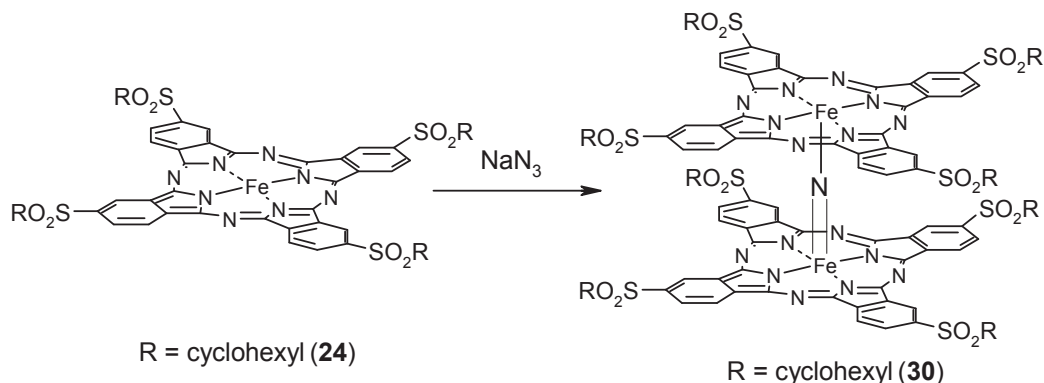
C₁₄₄H₁₄₄Fe₂N₁₇O₁₆S₈ MW: 2734.74 g/mol

IR (KBr) ν (cm⁻¹): 930 (Fe=N-Fe)

Mass Spectrum (ESI-MS) m/z: 2774.91 [M+K]⁺

UV/Vis (CHCl₃): λ_{max} = 639, 319 nm

4.3.6. μ -Nitrido-bis [tetra-(cyclohexylsulfonyl)phthalocyaninatoiron] (**30**)



24 (100 mg, 0.16 mmol) and sodium azide (1.5 g) were suspended in 70 ml of dry dimethylsulfoxide (DMSO) under argon. The mixture was heated for 24 h at 170 °C under intensive stirring. The reaction mixture was cooled and resulting dark blue solution was separated from insoluble material by filtration. The solution was chromatographed on Al₂O₃ (neutral) with CH₂Cl₂ to remove impurities. Then **30** was collected using CH₂Cl₂:EtOH (100:1) mixture as eluent. Evaporation of solvent afforded pure **30** as a dark blue powder.

48 mg, Yield (48 %)

C₁₄₄H₁₄₄Fe₂N₁₇O₁₆S₈ MW: 2318.48 g/mol

IR (KBr) ν (cm⁻¹): 931 (Fe=N-Fe)

Mass Spectrum (ESI-MS) m/z: 2341.43 [M+Na]⁺

UV/Vis (CHCl₃): λ_{max} = 634, 319 nm

Reduction of μ -Nitrido dimers 25 and 27, 28.

25, 27 or 28 (25 mg) was dissolved in CH_2Cl_2 and hydrazine (1 mL) was added. This mixture was kept at constant stirring for 2h under argon. After evaporation of all the components, the crude product was dissolved in CH_2Cl_2 and the solution was chromatographed on Al_2O_3 (neutral) with CH_2Cl_2 :EtOH (100:1) mixture. The product was recovered by evaporation of the solvent.

Oxidation of μ -Nitrido dimers 26, 29 and 16.

26, 29 or 30 (25 mg) was dissolved in CH_2Cl_2 and 1.0 g of oxidant ($\text{H}_5\text{PV}_2\text{Mo}_{10}\text{O}_{40}$) was added. This mixture was kept at constant stirring for 2h under argon. The reaction mixture was then filtered and the solution was chromatographed on Al_2O_3 (neutral) with CH_2Cl_2 :EtOH (100:1) mixture. The product was recovered by evaporation of the solvent.

GENERAL CONCLUSION

From the available data on bioinspired heme-like oxidation catalysts, we decided to prepare several monomeric and N-bridged iron phthalocyanines, substituted by electron-withdrawing hexylsulfonyl substituents of various number, size and position, and to test them as oxidation catalysts.

The catalytic activity of monomeric iron phthalocyanines tetra peripheral and nonperipheral, as well as octa peripheral, has been tested for the oxidation of cyclohexene and compared with the catalytic activity of the known phthalocyanines **FePcS** and **FePcF₁₆**. The main product of the oxidation of cyclohexene in the presence of electron-withdrawing substituted phthalocyanines catalysts was cyclohexenone, in very satisfying yields.

Six N-bridged diiron phthalocyanines bearing electron-withdrawing alkylsulfonyl (alkyl = hexyl, t-butyl, methyl, ethyl, cyclohexyl and adamantyl) substituents were prepared and deeply characterized by ESI-MS, UV-visible, FTIR, EPR. Moreover, Mössbauer, XANES, EXAFS, high resolution K β emission and X-ray photoelectron spectroscopies were used to characterize hexyl and t-butyl substituted dimers. An interesting effect related to the size of the substituents on the electronic state of iron atoms was evidenced: while small substituted complexes (hexylsulfonyl, methylsulfonyl and ethylsulfonyl) are cationic $(\text{PcFe}^{\text{IV}}\text{NFe}^{\text{IV}}\text{Pc})^+\text{N}_3^-$, bulky substituted complexes (t-butylsulfonyl, adamantylsulfonyl and cyclohexylsulfonyl) are neutral $\text{PcFe}^{\text{III}}\text{NFe}^{\text{IV}}\text{Pc}$. The catalytic activity of the six electron-withdrawing dimeric phthalocyanines was tested in the industrially important oxidation of alkylaromatic compounds (toluene and *p*-xylene). These N-bridged diiron phthalocyanines show high selectivity in oxidation of toluene and *p*-xylene.

In addition, hexyl and t-butyl substituted dimers were used in the oxidation of aromatic and aliphatic alcohols and exhibit high selectivity.

This thesis proved the efficiency of N-bridged diiron phthalocyanines substituted by electron-withdrawing alkylsulfonyl groups as oxidation catalysts, in conditions required by environmental and industrial preoccupations.

The results obtained during this PhD gave rise to two publications (one published and included at the end of this manuscript, one accepted), and at two other are being written.

1. Isci U, Afanasiev P, Millet JMM, Kudrik EV, Ahsen V and Sorokin AB. *Dalton Trans.* 2009, 7410-7420.
2. Isci U, Dumoulin F, Ahsen V and Sorokin AB. *J. Porphyrins Phthalocyanines* 2009, accepted.

BIBLIOGRAPHIC REFERENCES

- [1] Braun A and Tcherniac J, *Ber. Dtsch. Chem. Ges.* 1907, **40**, 2709.
- [2] de Diesbach H and von der Weid E, *Helv. Chim. Acta*, 1927, **10**, 886.
- [3] Gregory P, *J. Porphyrins Phthalocyanines* 1999, **3**, 468.
- [4] Gregory P, *J. Porphyrins Phthalocyanines* 2000, **4**, 432.
- [5] Fox MR, *A History of British Dye-Makers* 1987, 1856.
- [6] Byrne GT, Linstead RP and Lowe AR, *J. Chem. Soc.*, 1934, 1017.
- [7] Dent CE and Linstead RP, *J. Chem. Soc.*, 1934, 1027.
- [8] Dent CE and Linstead RP, *J. Chem. Soc.*, 1934, 1033.
- [9] Linstead RP and Lowe AR, *J. Chem. Soc.*, 1934, 1022.
- [10] Linstead RP and Lowe AR, *J. Chem. Soc.*, 1934, 1031.
- [11] Linstead RP, *J. Chem. Soc.*, 1934, 1016.
- [12] Robertson JM, *J. Chem. Soc.*, 1935, 615.
- [13] Robertson JM, *J. Chem. Soc.*, 1936, 1195.
- [14] Robertson JM, Woodward I, *J. Chem. Soc.*, 1937, 219.
- [15] Robertson JM, *Organic Crystals and Molecules*, Cornell University Press: Ithaca, NY, (1953).
- [16] McKeown NB, *The Porphyrin Handbook*, Eds.: Kadish KM, Smith KM and Guillard R., Elsevier Science, San Diego, 2003, Vol. 15, p 61.
- [17] Barret PA, Dent CE and Linstead RP, *J. Chem. Soc.*, 1936, 1719.
- [18] Linstead RP and Lowe AR, *J. Chem. Soc.*, 1934, 1022.
- [19] Snow AW, Griffith JR and Marulla NP, *Macromolecules*, 1984, **17**, 1614.
- [20] U.S. Patent Appl. 768004 (1986); *Chem. Abstr.*, 1986, **105**, 145325f.
- [21] Moser FH, U.S. Patent (1949) 2, 469, 663.
- [22] Decreau R, Chanon M and Julliard M, *Inorg.Chim.Acta* 1999, **293**, 80.
- [23] Palmer FS and Gross PF, U.S. Patent (1946) 2, 413, 191.
- [24] Weber JH and Busch DH, *Inorg. Chem.* 1965, **4**, 469.
- [25] Bonderman D, Cater ED and Bennett WE. *J. Chem. Eng. Data.* 1970, **15**, 396.
- [26] Jones JG and Twigg MV. *Inorg. Chem.* 1969, **8**, 2018.
- [27] Moser FH and Thomas AL. *Phthalocyanine Compounds*, Reinhold: New York, (1963).

- [28] Moser FH and Thomas AL. The Phthalocyanines, CRC: Boca Raton, FL, (1983); Vol. 1.
- [29] Moser FH and Thomas AL. The Phthalocyanines, CRC Press: Boca Raton, Florida, (1983) Volume 2.
- [30] Kim S, Matsumoto M and Shigehara K. *Synthetic Metals* 1999, **107**, 27.
- [31] Shirai H, Maruyama A, Kobayashi K, Hojo N and Urushido K., *Makromol. Chem.* 1980, **181**, 575.
- [32] Boston DR and Bailar JC Jr, *Inorg. Chem.* 1972, **11**, 1578.
- [33] Ohya T, Takeda J, Kobayashi N and Sato M. *Inorg. Chem.* 1990, **29**, 3734.
- [34] Ohya T, Kobayashi N and Sato M. *Inorg. Chem.* 1987, **26**, 2506.
- [35] Hanack M, Gül A, Hirsch A, Mandal BK, Subramanian LR and Witke E, *Mol. Cryst. Liq. Cryst.* 1990, **187**, 365.
- [36] Gal'pern MG, Donyagina VF, Shalaev VK, Skvarchenko VR, Bundina NI, Mekhryakova NG, Kaliya OL and Luk'yanets EA. *Zh. Obshch. Khim.* 1982, **52**, 715.
- [37] Mikhaleenko SA and Luk'yanets EA. *Zh. Obshch. Khim.* 1969, **39**, 2129.
- [38] Gojkovic SL, Gupta S and Savinell RF J. *Electroanal. Chem.* 1999, **462**, 63.
- [39] Wöhrle D and Huendorf U. *Makromol. Chem.* 1985, **186**, 2177.
- [40] Shirai H, Maruyama A, Kobayashi K, Hojo N and Urushido K. *Makromol. Chem.* 1980, **181**, 575.
- [41] Nevin WA, Liu W, Melnik M and Lever ABP. *J. Electroanal. Chem.* 1986, **213**, 217.
- [42] Kobayashi N, Nishiyama Y, Ohya T and Sato M. *J. Chem. Soc. Chem. Commun.* 1987, 390.
- [43] Vonderschmitt D, Bernauer K and Fallab S. *Helv. Chim. Acta* 1965, **48**, 951.
- [44] Dale BW, *Trans. Faraday Soc* 1969, **65**, 331.
- [45] Jones JG and Twigg MV., *Inorg. Chem.* 1969, **8**, 2120.
- [46] Collamati I., Ercolani C and Rossi G. *Inorg. Nucl. Chem. Lett.*, 1976, **12**, 799.
- [47] Ercolani C, Rossi G and Monacelli F. *Inorg. Chim. Acta*, 1980, **44**, 215.
- [48] Dieinig R, Schmid D, Witke E, Feucht C, Dreben M, Pohmer J and Hanack M. *Chem. Ber.* 1995, **128**, 589.

- [49] Ercolani C, Gardini M, Monacelli F, Pennesi G and Rossi G. *Inorg. Chem.* 1983, **22**, 2584.
- [50] Ercolani C, Monacelli F, Dzugan S, Goedken VL, Pennesi G and Rossi G. *J. Chem. Soc. Dalton Trans.* 1991, 1309.
- [51] Ercolani C, Gardini M, Murray KS, Pennesi G and Rossi G. *Inorg. Chem.* 1986, **25**, 3972.
- [52] Bottomley LA, Ercolani C, Gorce JN, Pennesi G and Rossi G. *Inorg. Chem.* 1986, **25**, 2338.
- [53] Mansuy D, Lecomte JP, Chottard JC and Bartoli JF. *Inorg. Chem.* 1981, **20**, 3119.
- [54] Goedken VL, Deakin MR and Bottomley LA, *J. Chem. Soc., Chem. Comm.* 1982, 607.
- [55] Rossi G, Goedken L and Ercolani C. *J. Chem. Soc. Chem. Commun.* 1988, 46.
- [56] Ercolani C, Gardini M, Goedken VL, Pennesi G, Rossi G, Russo U and Zanonato P. *Inorg. Chem.* 1989, **28**, 3097.
- [57] Summerville DA and Cohen IA. *J. Am. Chem. Soc.* 1976, **98**, 1747.
- [58] (a) Goedken VL and Ercolani, C. *J. Chem. Soc. Chem. Commun.* 1984, 378. (b) Bottomley LA, Gorce J, Goedken VL and Ercolani C. *Inorg. Chem.* 1985, **24**, 3733.
- [59] Ercolani C, Gardini M, Pennesi G, Rossi G and Russo U. *Inorg. Chem.* 1988, **27**, 422.
- [60] Moubaraki BP, Benlian D, Baldy A and Pierrot A. *Acta Cryst.* 1989, **C45**, 393.
- [61] Ercolani C, Jubb J, Pennesi G, Russo U and Trigante G. *Inorg. Chem.* 1995, **34**, 2535.
- [62] Donzello MP, Ercolani C, Kadish KM, Ou Z and Russo U. *Inorg. Chem.*, 1998, **37** (15), 3682.
- [63] a) Sorokin AB, Kudrik EV and Bouchu D. *Chem Commun.* 2008, 2562. b) Kudrik EV and Sorokin AB. *Chem. Eur. J.* 2008, **14**, 7123. c) Kudrik EV, Afanasiev P, Bouchu D, Millet JMM and Sorokin AB. *J. Porphyrins Phthalocyanines* 2008, **12**, 1078.
- [64] Balkus KJ Jr, Eissa M and Levado R. *J. Am. Chem. Soc.* 1995, **117**, 10753.
- [65] Parton RF, Vankelecom IFJ, Casselman MJA, Bezoukhanova CP, Uytterhoeven JB and Jacobs PA. *Nature* 1994, **370**, 541.

- [66] Parton RF, Venkelecom IFJ, Tas D, Janssen KBM, Knops-Gerrits PP and Jacobs PA. *J. Mol. Catal. A: Chem.* 1996, **113**, 283.
- [67] Parton RF, Neys PE, Jacobs PA, Sosa RC and Rouxhet PG. *J. Catal.* 1996, **164**, 341.
- [68] Ernst S, Gläser R and Selle M. *Stud. Surf. Sci. Catal.* 1997, **105**, 1021.
- [69] Schubert U, Lorenz A, Kundo N, Stuchinskaya T, Gogina L, Salanov A, Zaikovskii V, Maizlish V and Shaposhnikov GP. *Chem. Ber.* 1997, **130**, 1585.
- [70] a) Sorokin AB and Tuel A. *New J. Chem.*, 1999, **23**, 473. b) Sorokin AB and Tuel A. *Catal. Today*, 2000, **57**, 45.
- [71] a) Sorokin AB, Mangematin S and Pergrale C. *J. Mol. Catal. A: Chem.* 2002, **182–183**, 267. b) Pergrale C and Sorokin AB. *C. R. Acad. Sci. Paris, Série IIc, Chimie : Chemistry* 2000, **3**, 803. c) Perollier C and Sorokin AB. *Chem. Commun.*, 2002, 1548.
- [72] Beyrhouty M, Sorokin AB, Daniele S and Hubert-Pfalzgraf LG. *New J. Chem.* 2005, **29**, 1245.
- [73] Holm RH. *Chem. Rev.* 1987, **87**, 1401.
- [74] Mijs WJ and de Jonge CRHI. *Organic Syntheses by Oxidation with Metal Complexes*; Plenum Press: New York, 1986.
- [75] a) *Cytochrome P-450 Structure, Mechanism and Biochemistry*; Ortiz de Montellano P. Ed.; Plenum Press: New York, 1985. b) Ullrich V. *Top. Curr. Chem.* 1979, **83**, 67. c) Porter TD and Coon MJ. *J. Biol. Chem.* 1991, **266**, 13469. d) Groves JT and McClusky GA. *J. Am. Chem. Soc.* 1976, **98**, 859.
- [76] a) *Peroxidases in Chemistry and Biology*; Everse J, Everse KE and Grisham MB Eds.; CRC Press: Boca Raton, 1991; Vols. I and II. b) Dunford HP. *Adv. Inorg. Biochem.* 1982, **4**, 41.
- [77] a) Frew JE, Jones P. *Adv. Inorg. Bioinorg. Mech.* 1984, **3**, 175. b) Fita I and Rossmann MG. *J. Mol. Biol.* 1985, **185**, 21.
- [78] Dawson, J. H. *Science* 1988, **240**, 433.
- [79] Griffin, B. W.; Peterson, J. A. *Biochemistry* 1972, **11**, 4740.
- [80] Lever ABP, Milaeva ER and Speier G. in: Leznoff CC and Lever ABP (Eds.), *Phthalocyanines: Properties and Applications*, Vol. 3, VCH, New York, 1993, pp. 1–69.
- [81] Meunier B. *Chem. Rev.* 1992, **92**, 1411.
- [82] Sono M, Roach MP, Coulter ED and Dawson JH. *Chem. Rev.*, 1996, **96**, 2841.

- [83] Groves JT, Nemo TE and Myers RS. *J. Am. Chem. Soc.*, 1979, **101**, 1032.
- [84] Nappa MJ and Tolman CA. *Inorg. Chem.* 1985, **24**, 4711.
- [85] Nam W, Goh YM, Lee YJ, Lim MH and Kim C. *Inorg. Chem.* 1999, **38**, 3238.
- [86] Zhang XB, Guo CC, Xu JB and Yu RQ. *J. Mol. Catal. A: Chem.* 2000, **154**, 31.
- [87] Moore KT, Horváth IT and Therien MJ. *Inorg. Chem.* 2000, **39**, 3125.
- [88] Milos M. *Appl. Catal. A: General*. 2001, **216**, 157.
- [89] Chan YW and Wilson RB Jr. *ACS Natl. Meeting*. 1988, **33**, 453.
- [90] Murahashi SI. *Angew. Chem., Int. Ed. Engl.* 1995, **34**, 2443.
- [91] a) Sheldon RA and Kochi JK. *In Metal-Catalyzed Oxidations of Organic Compounds*; Academic Press: New York, 1981. (b) Barton DHR, Doller D. *Acc. Chem. Res.* 1992, **25**, 504. (c) Shilov AE and Shul'pin G. *Chem Rev.* 1997, **97**, 2879.
- [92] (a) Nam W, *Acc. Chem. Res.* 2007, **40**, 522; (b) Shaik S, Hirao H and Kumar D, *Acc. Chem. Res.* 2007, **40**, 532; (c) Shaik S, Cohen S, de Visser SP, Sharma PK, Kumar D, Kozuch S, Ogliaro F and Danovich D, *Eur. J. Inorg. Chem.* 2004, 207.
- [93] Appleton AJ, Evans S and Lindsay Smith JR, *J. Chem. Soc., Perkin Trans. 2* 1996, 281.
- [94] Groves JT and Nemo TE. *J. Am. Chem. Soc.* 1983, **105**, 578.
- [95] Song WJ, Ryu YO, Song R and Nam W. *J. Biol. Inorg. Chem.* 2005, **10**, 294.
- [96] Agarwala A and Bandyopadhyay D. *Catal. Lett.* 2008, **124**, 256.
- [97] Birnbaum ER, Le Lacheur RM, Horton AC and Tumas W. *J. Mol. Catal. A: Chem.* 1999, **139**, 11.
- [98] Murahashi SI, Zhou XG and Komiya N. *Synlett* 2003, **3**, 321.
- [99] Kasuga K, Tsuboi K, Handa M, Sugimori T and Sogabe K. *Inorg. Chem. Comm.* 1999, **2**, 507.
- [100] Weber, M. Grosche, H. Hennig, G. Haufe, *J. Mol. Catal.* 1993, **78**, 9.
- [101] Sehlotho N and Nyokong T. *J. Mol. Catal. A: Chem.* 2004, **209**, 51.
- [102] Gonzalez LM, Villa AL, Montes C and Sorokin AB. *Tetrahedron Letters* 2006, **47**, 6465.
- [103] a) *Modern Oxidation Methods*, (Ed.: J.-E. Bäckvall), Wiley-VCH, Weinheim, 2004; b) Punniyamurthy T, Velusamy S and Iqbal J, *Chem. Rev.* 2005, **105**, 2329; c)

Active Oxygen in Chemistry, (Eds.: Foote CS, Valentine JS, Greenberg A and Liemann JF), Chapman and Hall, New York, 1995.

[104] Brégeault JM, *Dalton Trans.* 2003, 3289.

[105] a) Khenkin AM and Neumann R, *Inorg. Chem.* 2000, **39**, 3455; b) Chavan SA, Srinivas D and Ratnasamy P, *Chem. Commun.* 2001, 1124; c) Evans S and Smith JRL, *J. Chem. Soc., Perkin Trans. 2* 2000, 1541; d) Hirai N, Sawatari N, Nakamura N, Sakaguchi S and Ishii Y, *J. Org. Chem.* 2003, **68**, 6587; e) Zhu J, Robertson A and Tsang SC, *Chem. Commun.* 2002, 2044.

[106] a) Muzart J, *Chem. Rev.* 1992, **92**, 113; b) Das T, Chaudari K, Nandanan E, Chandwadkar AJ, Sudalai A, Ravindranathan T and Sivasanker S, *Tetrahedron Lett.* 1997, **38**, 3631.

[107] a) Modica E, Bombieri G, Colombo D, Manchini N, Ronchetti F, Scala A and Toma L, *Eur J. Org. Chem.* 2003, 2964; (b) Jurado-Gonzalez M, Sullivan AC and Wilson JRH, *Tetrahedron Lett.* 2003, **44**, 4283.

[108] Pan JF and Chen KM, *J. Mol. Catal. A: Chem.* 2001, **176**, 19.

[109] Nakanishi M and Bolm C, *Adv. Synth. Catal.* 2007, **349**, 861.

[110] Catino AJ, Nichols JM, Choi H, Gottipamula S and Doyle MP, *Org Lett.* 2005, **7**, 5167.

[111] Khenkin AM and Neumann R, *J. Am. Chem. Soc.* 2004, **126**, 6356.

[112] Balland V, Mathieu D, Pons Moll N, Bartoli JF, Banse F, Battioni P, Girerd JJ and Mansuy D, *J. Mol. Catal. A: Chem.* 2004, **215**, 81.

[113] a) Mathieu D, Bartoli JF, Battioni P and Mansuy D, *Tetrahedron* 2004, **60**, 3855; (b) Rebelo SLH, Simoes MMQ, Neves MGP and Cavaleiro JAS, *J. Mol. Catal. A: Chem.* 2004, **201**, 9.

[114] Huang G, Luo J, Cai CC, Guo YA and Luo GW. *Catal. Commun.* 2008, **9**, 1882.

[115] Guo CC, Song JX, Chen XB and Jiang GF, *J. Mol. Catal. A: Chem.* 2000, **157**, 31.

[116] Hu HQ, Liu Q and Lin WY. *J. Porphyrins Phthalocyanines* 2006, **10**, 948.

[117] O'Shea SK, Wang W, Wade RS and Castro CE. *J. Org. Chem.* 1996, **61**, 6388.

[118] Zhao X, Kong A, Shan C, Wang P, Zhang X and Shan Y. *Catal Lett.* 2009, **131**, 526.

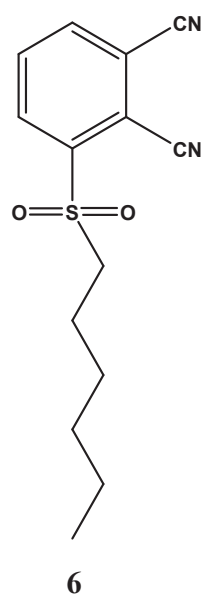
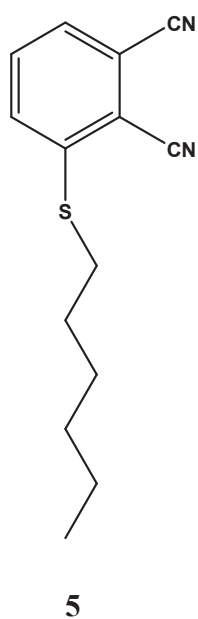
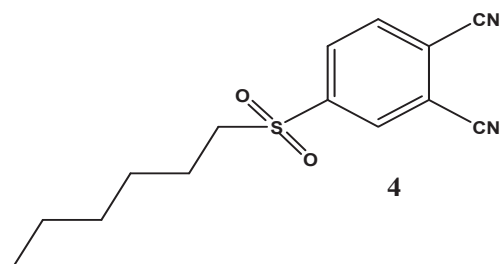
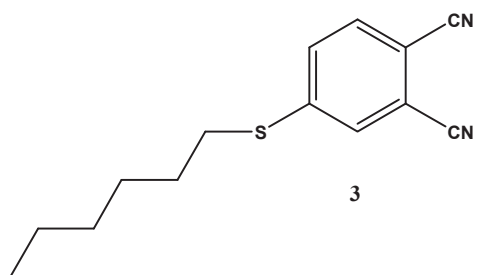
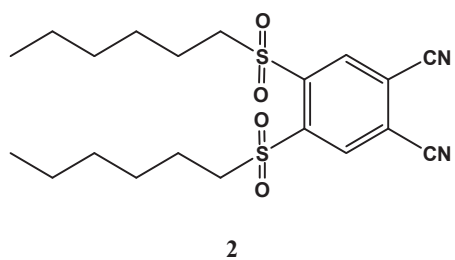
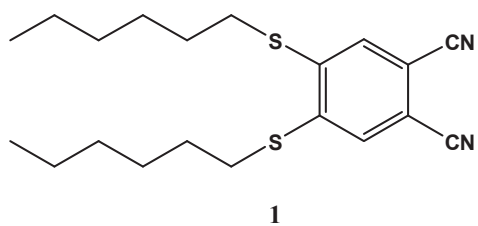
- [119] a) March J. *Advanced Organic Chemistry: Reactions, Mechanisms, and Structure*; Wiley: New York, 1992. b) Brink GT, Arends IWCE and Sheldon RA. *Science*, 2000, **47**, 1636.
- [120] Enache DI, Edwards JK, Landon P, Solsona-Espriu B, Carley AF, Herzing AA, Watanabe M, Kiely CJ, Knight DW and Hutchings GJ. *Science* 2006, **311**, 362.
- [121] a) Pillai UR and Sahle-Demessie E. *Appl. Catal. Gen*, 2003, **245**, 103. b) Hudlicky M. *Oxidations in Organic Chemistry*; American Chemical Society: Washington, DC, 1990.
- [122] a) Weissermel K and Arpe HJ. *In Industrial organic chemistry*, 3rd ed; Lindley, C. R., Ed.; VCH: New York, 1997; b) Satterfield CN, Backvall JE (Ed.), *Modern Oxidation Methods*, Wiley-VCH, Germany, 2004. c) Larock RC. *Comprehensive Organic Transformations*, Wiley-VCH, New York, 1999, pp. 1234–1250. d) Ishii Y, Sakaguchi S and Iwahama T. *Adv. Synth. Catal.*, 2001, **343**, 393. e) Schultz MJ and Sigman MS. *Tetrahedron*, 2006, **62**, 8227.
- [123] Oh NY, Suh Y, Park MJ, Seo MS, Kim J and Nam W. *Angew. Chem. Int. Ed.* 2005, **44**, 4235.
- [124] Huang JY, Li SJ and Wang YG *Tetrahedron Lett.* 2006, **47**, 5637.
- [125] Labat G and Meunier B. *J. Org. Chem.* 1989, **54**, 5008.
- [126] Geraskin IM, Luedtke MW, Neu HM, Nemykin VN, Zhdankin VV. *Tetrahedron Lett.* 2008, **49**, 7410.
- [127] Hampton KW and Ford WT. *J. Mol. Catal. A: Chem.* 1996, **113**, 167.
- [128] Young JG and Onyebuagu W, *J. Org. Chem.*, 1990, **55**, 2155.
- [129] Lacour J, Monchauda D, Mareda J, Favarger F and Bernardinelli G. *Helv. Chim. Acta* 2003, **86**, 65.
- [130] Wöhrle D, Eskes M, Shigehara K and Yamada A. *Synthesis*, 1993, 194.
- [131] del Rey B, Keller U, Torres T, Rojo G, Agullo-Lopez F, Nonell S, Martí C, Brasselet S, Ledoux I and Zyss J. *J. Am. Chem. Soc.* 1998, **120**, 12808.
- [132] Sastre A, del Rey B and Torres T *J. Org. Chem.* 1996, **61**, 8591.
- [133] Maya EM, Vaazquez P and Torres T *Chem. Eur. J.* 1999, **5**, 2004.
- [134] Maya EM, Garcia C, Garcia-Frutos EM, Vaazquez P and Torres T. *J. Org. Chem.* 2000, **65**, 2733.

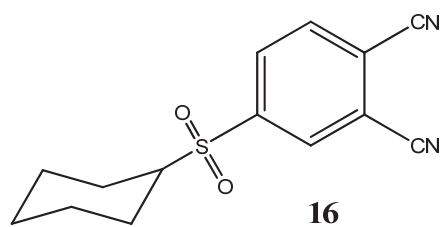
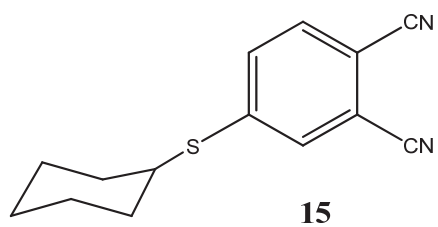
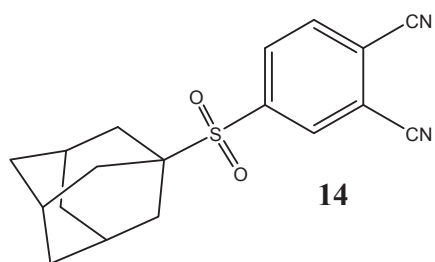
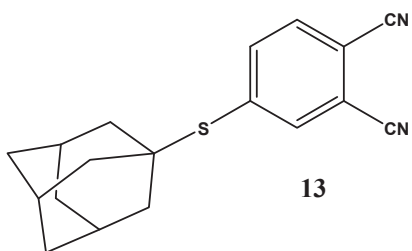
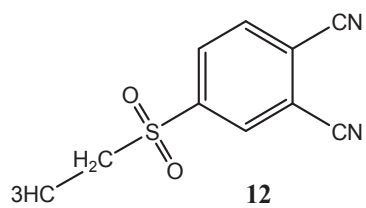
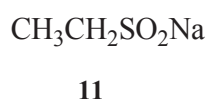
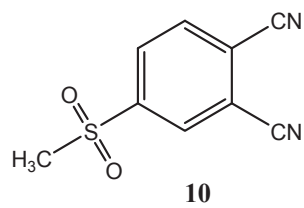
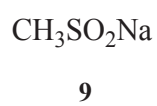
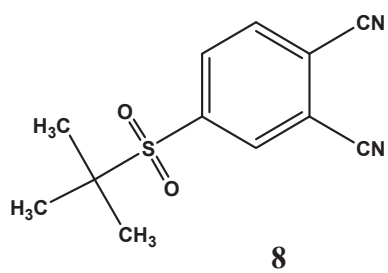
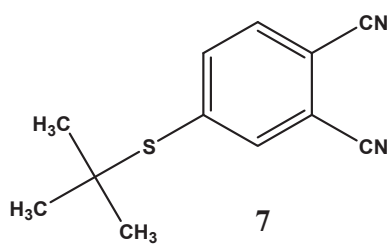
- [135] Gonzalez-Rodrigues D and Torres T. *Tetrahedron Lett.* 2009, **50**, 860.
- [136] Kroenke WJ. and Kenney ME, *Inorg. Chem.* 1964, **3**, 696.
- [137] a) Ercolani C, Hewage S, Heucher R and Rossi G. *Inorg. Chem.* 1993, **32**, 2975. b) Donzello MP, Ercolani C, Russo U, Chiesi-Villa A and Rizzoli C. *Inorg. Chem.* 2001, **40**, 2963. e) Stuzhin PA, Hamdush M and Homborg H. *Mendeleev Commun.* 1997, **7**, 196.
- [138] Isci U, Afanasiev P, Millet JMM, Kudrik EV, Ahsen V and Sorokin AB. *Dalton Trans.* 2009, 7410.
- [139] Voevodskaya N, Galander M, Högbom M, Stenmark P, McClarty G, Gräslund A and Lendzian F, *Biochim. Biophys. Acta*, 2007, **1774**, 1254.
- [140] Floris B, Donzello MP and Ercolani C. in *Porphyrin Handbook, Vol. 18* (Eds.: K. M. Kadish, K. M. Smith and R. Guillard), Elsevier Science, San Diego, 2003, pp.1-62.
- [141] Stillman MJ and Nyokong T. in *Phthalocyanines: Properties and Applications*, vol. 1, Leznoff CC and Lever ABP. (Eds.), VCH: New York, 1989, 133.
- [142] a) Ferraudi G. in *Phthalocyanines: Properties and Applications*, vol. 1, Leznoff CC and Lever ABP. (Eds.), VCH: New York, 1989, 291. b) Nyokong T and Isago H. *J. Porphyrins Phthalocyanines* 2004, **8**, 1083. c) Rio Y, Rodriguez-Morgade MS and Torres T. *Org. Biomol. Chem.* 2008, **6**, 1877.
- [143] Satake A and Kobuke Y. *Org. Biomol. Chem.* 2007, **5**, 1679.
- [144] Li M, Shang M, Ehlinger N, Schulz CE and Scheidt WR, *Inorg. Chem.* 2000, **39**, 580.
- [145] Kennedy BJ, Murray KS, Homborg H and Kalz W, *Inorg. Chim. Acta* 1987, **134**, 19.
- [146] Kadish KM, Bottomley LA, Brace JG and Winograd N, *J. Am. Chem. Soc.* 1980, **102**, 4341.
- [147] a) Goulon J, Friant P, Goulon Ginet C, Coutsolelos A and Guillard R. *Chem. Phys.* 4, **83**, 367. b) Weiss R, Goulon J, Friant P, Fischer J, Ricard L and Momenteau M. *Nouv. J. Chim.*, 1985, **9**, 33. c) Poncet JL, Guillard R, Friant P, Goulon Ginet C and Goulon J. *Nouv. J. Chim.*, 1984, **8**, 583. d) Bortolini O, Ricci M, Meunier B, Friant P, Ascone I and Goulon J, *Nouv. J. Chim.* 1986, **10**, 9. e) *Iron porphyrins*, eds. Gray HB and Lever ABP. VCH, Weinheim, 1989.

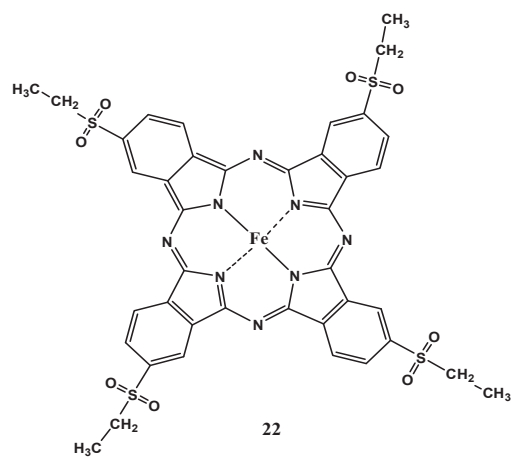
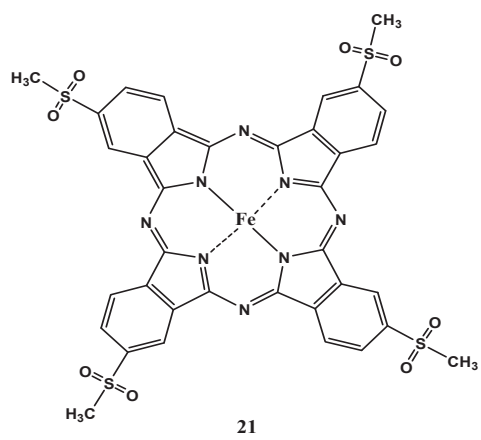
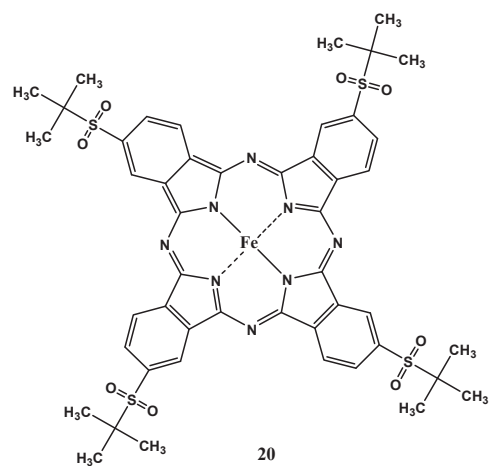
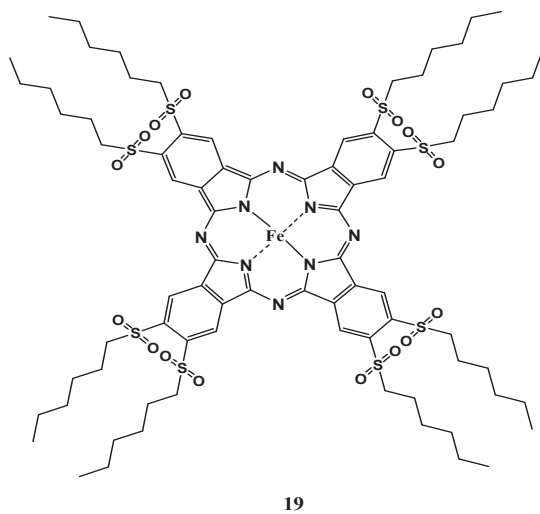
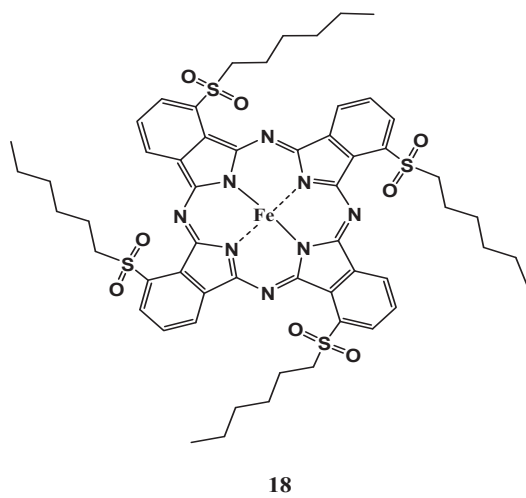
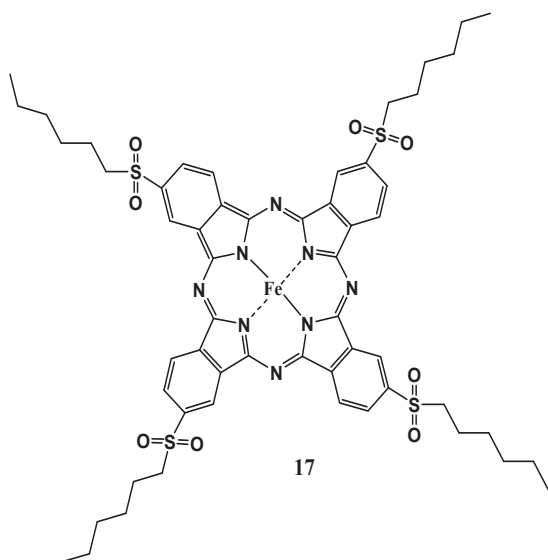
- [148] a) Eisenberger P, Schulman RG, Brown GS and Ogawa S. *Proc. Natl. Acad. Sci. USA*, 1976, **73**, 491. b) Pin S, Alpert A and Michalowicz A. *FEBS Lett.*, 1982, **147**, 106. c) Penner Hahn JE, McMurry T, Renner M, Latos Graszynski L, Eble KS, Davis IM, Balch A, Groves JT, Dawson JH and Hodgson KO, *J. Biol. Chem.*, 1983, **258**, 12761. d) Durham PJ, Bianconi A, Congiu Castellano A, Giovanelli A, Hasnain SS, Incoccia L, Morante S and Pendry JB, *Eur. Mol. Biol. Organization J.*, 1983, 1441.
- [149] Bianconi A, Congiu Castellano A, Durham PJ, Hasnain SS and Phillips S, *Nature*, 1985, **318**, 685.
- [150] a) Cartier C, Momenteau M, Dartyge E, Fontaine A, Tourillon G, Michalowicz A and Verdaguer M, *J. Chem. Soc. Dalton Trans.* 1992, 609. b) Westre TE, Kennepohl P, de Witt J, Hedman B, Hodgson KO and Solomon EI, *J. Am. Chem. Soc.* 1997, **119**, 6297.
- [151] Scheidt WR, Summerville DA and Cohen IA, *J. Am. Chem. Soc.* 1976, **98**, 6623.
- [152] Tsutsumi K, *J. Phys. Soc. Japan* 1959, **14**, 1696.
- [153] Traylor TG, Hill KW, Fann WP, Tsuchiya S and Dunlap BE, *J. Am. Chem. Soc.* 1992, **114**, 1308.
- [154] Bartoli JF, Barch KL, Palacio M, Battioni P and Mansuy D, *Chem. Commun.* 2001, 1718.
- [155] Trost BM, Fleming I and Ley SV. *Comprehensive Organic Synthesis*, vol. 7, Pergamon, Oxford, 1991.
- [156] Zhan BZ and Thompson A. *Tetrahedron* 2004, **60**, 2917.
- [157] Beller M and Bolm C. *Transition Metals for Organic Synthesis*, 2nd ed.; Verlag GmbH & Co. KGaA: Weinheim, Germany, 2004.
- [158] Menger FM and Lee C. *Tetrahedron Lett.* 1981, **22**, 1655.
- [159] Lee CK, Koo BS, Lee YS, Cho H and Lee KK. *J. Bull. Korean Chem. Soc.* 2002, **23**, 1667.
- [160] Cainelli G and Cardillo G. *Chromium Oxidants in Organic Chemistry*; Springer: Berlin, 1984;
- [161] a) Seddon KR and Stark A. *Green Chem.* 2002, **4**, 119. b) Ganchegui B, Bouquillon S, Henin F and Muzart J. *Tetrahedron Lett.* 2002, **43**, 6641. c) Muzart J. *Tetrahedron* 2003, **59**, 5789.

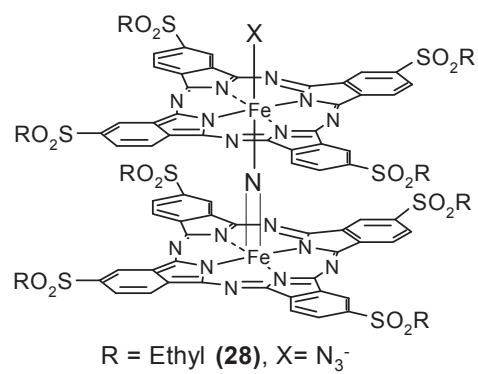
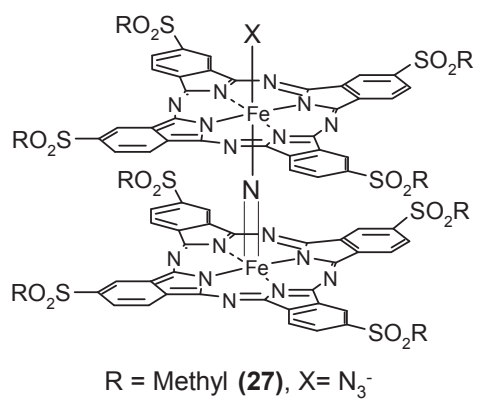
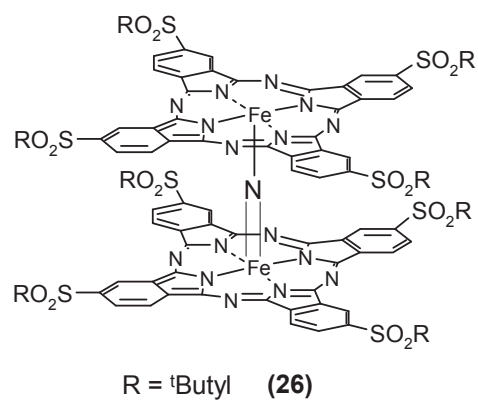
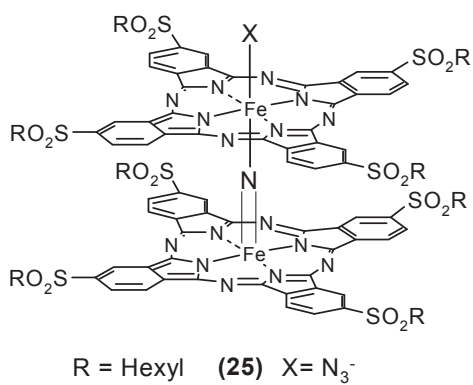
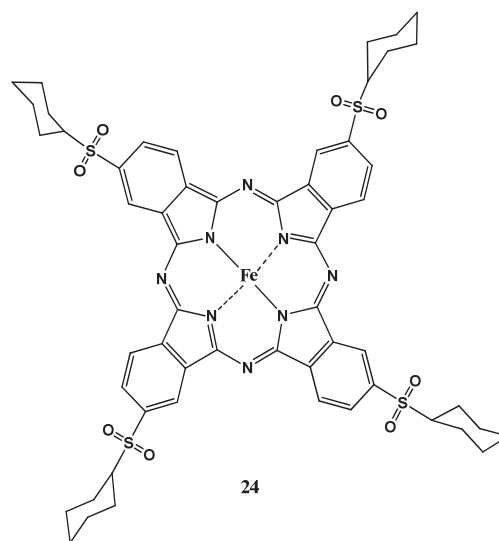
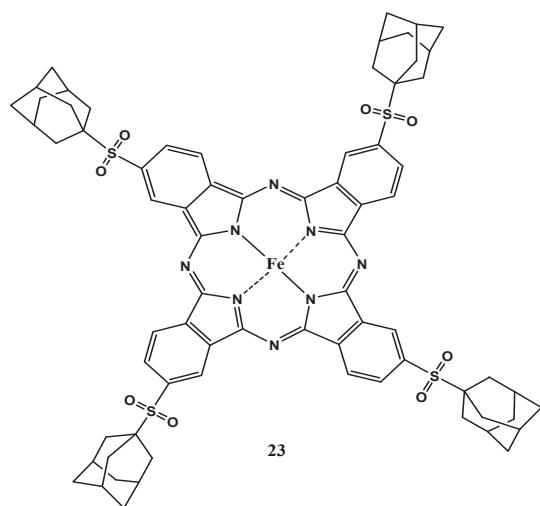
- [162] a) Wolfson A, Wuyts S, De VD, Vankelecom IFJ and Jacobs PA. *Tetrahedron Lett.* 2002, **43**, 8107. b) Tang WM and Li CJ. *Acta Chim. Sini.* 2004, **62**, 742. c) Roberto FDS, Jairton D, Jeane E and Braz DJ. *Chem. Soc.* 2006, **17**, 48. d) Shi F, Tse M and Beller M. *Chem. Asian J.* 2007, **2**, 411.
- [163] Chhikara BS, Chandra R and Tandon V. *J. Catal.* 2005, **230**, 436.
- [164] Bianchini G, Crucianelli M, de Angelis F, Neri V and Saladino R. *Tetrahedron Lett.* 2005, **46**, 2427.
- [165] Kumar A, Jain N and Chauhan SMS. *Synlett* 2007, 411.
- [166] Gamez P, Arends IWCE, Sheldon RA and Reedijk J. *Adv. Synth. Catal.* 2004, **346**, 805.
- [167] Jiang N and Ragauskas AJ. *J. Org. Chem.* 2006, **71**, 7087.
- [168] Gonzalez-Nunez ME, Mello R, Olmos A, Acerete R and Asensio G. *J. Org. Chem.* 2006, **71**, 1039.
- [169] Shaabani A, Farhangi E and Rahmati A. *Applied Catalysis A: General* 338 (2008) 14.
- [170] Choudhary VR, Dumbre DK, Narkhede VS and Jana SK. *Catal. Lett.* 2003, **86**, 229.
- [171] Choudhary VR, Dumbre DK, Uphade BS and Narkhede VS. *J. Mol. Catal. A: Chem.* 2004, **215**, 129.
- [172] Sharma VB, Jain SL and Sain B. *Tetrahedron Lett.* 2003, **44**, 383.
- [173] Naik R, Joshi P and Deshpande RK. *J. Mol. Catal. A Chem.* 2005, **238**, 46.
- [174] Sorokin AB and Meunier B. *Acc. Chem. Res.* 1997, **30**, 470.
- [175] d'Alessandro N, Tonucci L, Bonetti M, Deo MD, Bressan M and Morvillo A. *New J. Chem.* 2003, **27**, 989.
- [176] Alvaro M, Carbonell E, Espla M and Carcia H. *Appl. Catal. B. Environ.* 2005, **57**, 37.
- [177] Jain SL and Sain B. *J. Mol. Catal. A Chem.* 2001, **176**, 101.
- [178] Grootboom N and Nyokong T. *J. Mol. Catal. A Chem.* 2002, **179**, 113.
- [179] Vaz ADN and Coon MJ. *Biochemistry* 1994, **33**, 6442.
- [180] Han JH, Yoo SK, Seo JS, Hong SJ, Kim SK and Kim C. *Dalton Trans.* 2005, 402.

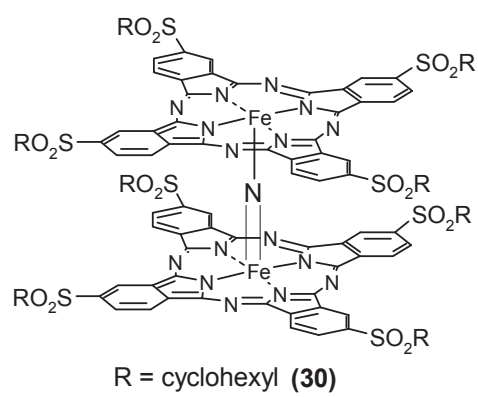
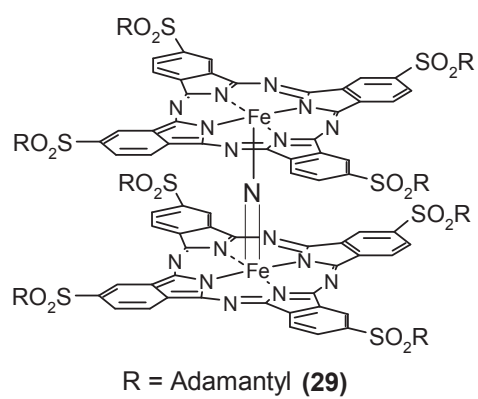
List and number of the molecules described in the manuscript











PUBLICATIONS RELATED TO THESE WORKS

Preparation and characterization of μ -nitrido diiron phthalocyanines with electron-withdrawing substituents: application for catalytic aromatic oxidation†

Ümit İşci,^{a,b} Pavel Afanasiev,^a Jean-Marc M. Millet,^a Evgeny V. Kudrik,^a Vefa Ahsen^{b,c} and Alexander B. Sorokin^{*a}

Received 9th February 2009, Accepted 10th June 2009

First published as an Advance Article on the web 21st July 2009

DOI: 10.1039/b902592h

μ -Nitrido-bis [tetra-(hexyl-sulfonyl)phthalocyaninatoiron] (**3a**) and μ -nitrido-bis [tetra-(*tert*-butylsulfonyl) phthalocyaninatoiron] (**3b**) complexes have been prepared and fully characterized by electrospray ionization mass spectrometry, UV-Vis, FTIR, EPR, Mössbauer techniques as well as by X-ray photoelectron and Fe K-edge X-ray absorption spectroscopies. Small changes at the periphery of the phthalocyanine ligand introduce a difference in the iron oxidation state. While **3b** with *tert*-butyl substituents is a neutral complex with a mixed-valence $\text{Fe}^{3.5}\text{--N--Fe}^{3.5}$ structural unit, **3a** having *n*-hexyl substituents is an oxidized cationic $\text{Fe}^{\text{IV}}\text{--N--Fe}^{\text{IV}}$ complex. The structural parameters of N-bridged diiron phthalocyanine with a $\text{Fe}^{3.5}\text{--N--Fe}^{3.5}$ unit were determined for the first time. Iron atoms in **3b** are displaced out of plane by 0.24 Å and the Fe–N bond distance of the linear Fe–N–Fe fragment is equal to 1.67 Å. Both complexes selectively catalyze benzylic oxidation of alkyl aromatic compounds by *t*-BuOOH. Toluene was oxidized to benzoic acid with 80% selectivity, and the total turnover number was as high as 197. *p*-Toluic acid was the principal product of *p*-xylene oxidation. In this case the turnover number achieved 587 substrate molecules per molecule of catalyst. The described catalytic system is complementary to the recently reported system based on μ -nitrido diiron tetrabutylphthalocyanine– H_2O_2 which effectively oxidizes the benzene ring.

Introduction

Binuclear iron complexes constitute active sites of many metallo-proteins, *e.g.* soluble methane monooxygenase (MMO), toluene monooxygenases, phenol hydroxylase, alkene monooxygenase, butane monooxygenase and others.¹ These enzymes mediate demanding oxidations of alkanes, including methane, olefins and aromatic compounds. Numerous biomimetic studies have been directed to model active sites of these enzymes with the objective of reproducing their catalytic activity.² A number of structural and spectroscopic models of MMO using diiron non-heme complexes have been published although no systems capable of oxidizing methane are yet available.

Phthalocyanine complexes are widely used in numerous technological and catalytic applications due to their outstanding electronic and optical properties.³ Recently, we proposed the use of a stable binuclear N-bridged diiron tetrabutylphthalocyanine complex as a catalyst for oxidation.⁴ This unusual complex with

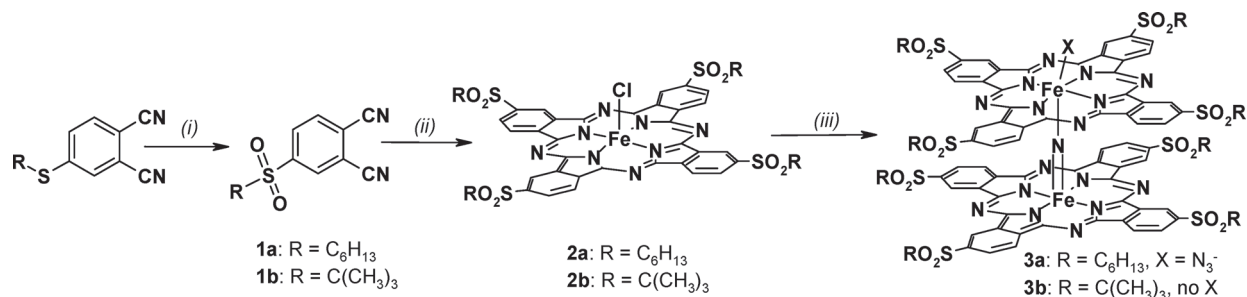
formally a $\text{Fe}^{\text{III}}\text{--N--Fe}^{\text{IV}}$ structural unit is a $\text{Fe}^{3.5}\text{--N--Fe}^{3.5}$ mixed-valence compound with equivalent iron atoms. This complex bearing electron-donating *tert*-butyl substituents on the macrocycle activates H_2O_2 to give a very strong oxidizing species. We have shown an efficient oxidation of CH_4 at extremely mild conditions: in pure water at 25–60 °C. This is the first example of a bio-inspired oxidation of methane.^{4a} The same catalyst performs the oxidation of benzene, another difficult-to-oxidize substrate, to phenol *via* benzene oxide accompanied by a NIH shift that is usually associated with oxidation mediated by cytochrome P-450 and toluene monooxygenase.^{4b} Thus, this binuclear macrocyclic complex with a $\text{Fe}^{3.5}\text{--N--Fe}^{3.5}$ motif exhibits very interesting catalytic properties and represents a novel scaffold in the oxidation catalysis. A limited number of N-bridged binuclear phthalocyanine complexes containing an unsubstituted phthalocyanine ligand has been described in the literature.⁵ N-bridged complexes involving porphyrin⁶ and mixed ligands systems⁷ have been prepared and characterized. Binuclear μ -nitrido complexes of non-heme ligands have also been reported.⁸ Before our work, μ -nitrido bridged binuclear complexes have never been evoked as oxidation catalysts. In order to enlarge the choice of N-bridged complexes and to gain a deeper insight into this new catalytic chemistry we decided to prepare μ -nitrido diiron phthalocyanine with electron-withdrawing substituents to check how the changes to the structure of this complex influences its catalytic properties. Two novel N-bridged diiron complexes have been prepared and fully characterized by electrospray ionization mass spectrometry (ESI-MS), UV-Vis, FTIR, EPR, Mössbauer techniques as well

^aInstitut de Recherches sur la Catalyse et l'Environnement de Lyon IRCELYON, UMR 5256, CNRS Université Lyon 1 2, av. A. Einstein, 69626 Villeurbanne Cedex, France. E-mail: alexander.sorokin@ircelyon.univ-lyon1.fr; Fax: +33 472445399; Tel: +33 472445337

^bDepartment of Chemistry, Gebze Institute of Technology, P.O. Box 141, Gebze 41400, Turkey

^cMaterials Institute, TUBITAK Marmara Research Center, P.O. Box 21, Gebze 41470, Turkey

† Electronic supplementary information (ESI) available: ESI-MS and IR spectra of **3a** and **3b**. See DOI: 10.1039/b902592h



Scheme 1 Synthetic pathway for the preparation of μ -nitrido dimers **3a** and **3b**.

as X-ray photoelectron spectroscopy (XPS) and Fe K-edge X-ray absorption spectroscopy (XANES, EXAFS, high resolution K β emission spectroscopy). The catalytic properties of these novel complexes were studied in the oxidation of alkylaromatic compounds exemplified by toluene and *p*-xylene.

Results

Synthesis

μ -Nitrido diiron phthalocyanines are usually prepared by the treatment of monomeric iron complexes with NaN₃ at high temperatures in chloronaphthalene.⁵ Our attempts to use iron tetrasulphophthalocyanine as the starting material were unsuccessful, probably due to the electrostatic repulsion of the negatively charged sulfonate groups in the formed dimeric structure. To overcome this problem we employed a phthalocyanine bearing neutral alkylsulfonyl groups (Scheme 1). Alkylsulfonyl-1,2-dicyanobenzenes (**1a**, alkyl = C₆H₁₃; **1b**, alkyl = C(CH₃)₃) were prepared from 4-alkylthio derivatives by oxidation with H₂O₂ or *m*-chloroperbenzoic acid. Iron tetra-(alkylsulfonyl)phthalocyanines **2a** and **2b** were obtained by heating 4-alkylsulfonyl-1,2-dicyanobenzenes in an *o*-dichlorobenzene–DMF (3 : 1) mixture in the presence of FeCl₂. μ -Nitrido dimeric complexes **3a** and **3b** were obtained by the treatment of **2a** and **2b** with NaN₃ in xylene at 140 °C with good yields. The successful preparation of **3a** and **3b** was evidenced by ESI-MS. The ESI-MS spectrum of **3a** exhibits a strong molecular peak at m/z = 2335.9 with an isotopic pattern identical to a simulated pattern for C₁₁₂H₁₂₈N₁₇O₁₆S₈Fe₂ with a maximum at m/z = 2335.6 (see ESI†). The small peak of (M + Na)⁺ at m/z = 2358.9 with an expected isotopic cluster pattern was also detected. In the case of **3b** the parent peak was (M + Na)⁺ at m/z = 2134.6. Again, an isotopic pattern of this peak was identical to those for a simulated pattern of C₉₆H₉₆N₁₇O₁₆S₈Fe₂Na with m/z = 2134.4. IR spectra of **3a** and **3b** exhibits strong absorptions at 931 and 929 cm⁻¹, respectively, due to the Fe–N–Fe anti-symmetric stretching mode (see ESI†).^{5b,7c} These values are close to those observed for unsubstituted (PcFe)₂N^{5b} at 915 cm⁻¹ and for (PcFe^tBu₄)₂N^{4a} at 938 cm⁻¹. The IR spectrum of **3a** shows a strong signal at 2010 cm⁻¹ assigned to N₃⁻ vibration. As expected, upon reduction with sodium dithionite this signal disappeared (see ESI†).

Electron paramagnetic resonance

The EPR spectrum of monomeric precursor **2b** shows an anisotropic feature with three *g* values, 2.177, 2.062 and 1.950, due

to orthorhombic distortion, common for low spin Fe(III) species ($S = 1/2$). Since low spin Fe(III) phthalocyanines complexes are usually hexa-coordinated, one can suggest the coordination of a water molecule along with Cl⁻. Formation of the μ -nitrido dimer leads to the increase of symmetry from rhombic to axial. In the 77 K EPR spectrum of **3b** in the solid state, the major feature belongs to a $S = 1/2$ species with axial symmetry of an iron environment and the corresponding values of *g*-tensor of 2.115 and 2.005, respectively, with a line width of 50 G for both components.

High spin impurity ($S = 5/2$) was also detected in the weak field region (*g* values near 4.3), which represents less than 0.5% of the signal intensity (Fig. 1). The signal has no observable hyperfine splitting. The small deviation of the *g* values from 2.0 suggests that the unpaired electron is in the d_{xy} orbital with a d_{xz}²d_{yz}²d_{xy}¹ ground state configuration.⁹ The d_{x²-y²} orbital in the low spin d⁵ complexes is therefore unoccupied, allowing iron to drop closer to the phthalocyanine plane. Therefore small displacement of iron from the planar structure can be expected. The parameters of the EPR spectrum are similar to those of the earlier reported non-substituted nitrido-dimers of Fe(III) octaphenyltetraazaporphine,¹⁰ but no hyperfine structure caused by nitrogen could be seen in our case. Solid non-substituted (PcFe)₂N was studied by Bottomley *et al.*,^{5a} who also found an axial signal with *g*₁ = 2.13 and *g*₂ = 2.03. It should be noted that considering exchange between Fe^{III} ($S = 5/2$) and Fe^{IV} ($S = 2$) centres with antiferromagnetic coupling leads to the ground state $S = 1/2$ and X-band EPR spectra similar to

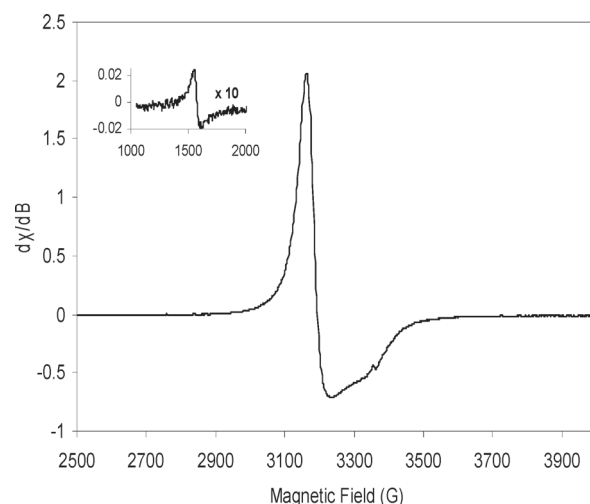


Fig. 1 X-Band 77 K EPR spectrum of μ -nitrido dimer **3b**. Insert: signal of high spin Fe(III) species impurity.

one-center Fe^{III} with g values close to 2, as observed in the $\text{Fe}^{\text{III}}\text{Fe}^{\text{IV}}$ species of a ribonucleotide reductase.¹¹ However, Mössbauer spectroscopy showed that the two iron sites in complexes **3a** and **3b** are electronically identical, suggesting the valence-delocalized description for both $\text{Fe}^{\text{IV}}\text{Fe}^{\text{IV}}$ and $\text{Fe}^{\text{III}}\text{Fe}^{\text{IV}}$ species. Therefore, a common molecular orbital system should be considered for these complexes. In a DFT study by Ghosh *et al.*,¹² a $S = 0$ ground state was predicted for μ -nitrido bridged $\text{Fe}^{\text{IV}}\text{Fe}^{\text{IV}}$ heme, with filled xz – xz , yz – yz and xy – xy orbitals, while LUMOs are z^2 -like orbitals. Addition of one electron would create a $S = 1/2$ $\text{Fe}^{\text{III}}\text{Fe}^{\text{IV}}$ system, in agreement with our findings. The **3a** compound shows no EPR signals at 77 K.

UV-Vis spectra

The positions of the Soret band (near 340 nm) and of the intense Q band (between 600 and 700 nm due to π – π^* ligand transition) of phthalocyanine complexes are affected by electronic interactions between the ligands as well as by the state of the central atom, axial ligation and peripheral substitution.^{13,14} The strong π – π interaction between two phthalocyanine moieties in dimers results in a blue-shift as compared with monomer complexes: from 690 nm to 657 nm for **2a/3a** and from 683 nm to 638 nm for **2b/3b**, respectively. It should be noted that despite the apparently small differences in the structures of the phthalocyanine ligands (*n*-hexylsulfonyl vs. *tert*-butylsulfonyl substituents), the UV-Vis spectra of **3a** and **3b** are quite different (Fig. 2). This difference can be explained by the difference in the state of the iron. Taking into account the absence of EPR signals for **3a** one can propose the $\text{Fe}^{\text{IV}}\text{Fe}^{\text{IV}}$ oxidation state for this complex. Indeed, unsubstituted $(\text{FePc})_2\text{N}$ can easily be oxidized to the cationic $(\text{FePc})_2\text{N}^+$ complex resulting in the red shift of Q band from 626 nm to 634 nm in pyridine.^{5a} Thus, **3b** was oxidized by $\text{H}_3\text{PV}_2\text{Mo}_{10}\text{O}_{40}$ under argon or by ferrocenium hexafluorophosphate.^{5a} The UV-Vis spectrum of oxidized **3b** showed a maxima at 334 and 647 nm as compared to 339 and 638 nm for **3b** (Fig. 2(b)). In turn, **3a** was reduced by hydrazine or $\text{Na}_2\text{S}_2\text{O}_4$ in CH_2Cl_2 solution resulting in the species with the Q band blue-shifted to 638 nm compared to 657 nm for **3a** in $\text{Fe}^{\text{IV}}\text{Fe}^{\text{IV}}$ oxidation state (Fig. 2(a)). The initial **3a** and the oxidized **3b** as well as the initial **3b** and the reduced **3a** exhibit similar UV-Vis features. These UV-Vis data are in agreement with the proposed assignment of iron oxidation states in **3a** and **3b** indicating the conversion of the $\text{Fe}(\text{IV})$ – N – $\text{Fe}(\text{IV})$ core to $\text{Fe}(\text{III})$ – N – $\text{Fe}(\text{IV})$ for **3a** and $\text{Fe}(\text{III})$ – N – $\text{Fe}(\text{IV})$ core to $\text{Fe}(\text{IV})$ – N – $\text{Fe}(\text{IV})$ for **3b**.

⁵⁷Fe Mössbauer spectroscopy

⁵⁷Fe Mössbauer spectroscopy is a useful technique for the determination of iron oxidation and spin states in phthalocyanine complexes.¹⁵ The existence of two forms of μ -oxo diiron phthalocyanines, bent μ -oxo(1) and linear μ -oxo(2), was proven using this method.^{5b,15} Zero-field Mössbauer spectra of **3a** and **3b** were recorded at 77 K (Fig. 3,4). These spectra fit to one doublet signals with hyperfine parameters listed in Table 1. Complex **3a** exhibits a doublet with isomer shift $\delta = -0.11$ mm s^{–1} and quadrupolar splitting $\Delta E_Q = 1.33$. Similar hyperfine parameters were reported for $\text{Fe}(\text{IV})$ N-bridged phthalocyanine and porphyrin complexes,^{5,15} although published ΔE_Q values for five- and six-coordinated $\text{Fe}(\text{IV})$

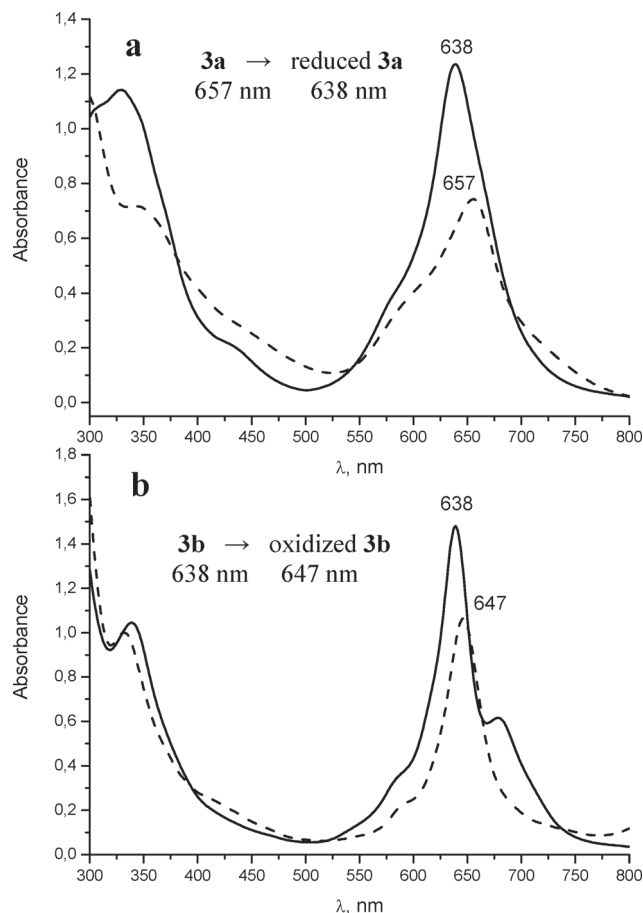


Fig. 2 (a) UV-Vis spectra of **3a** (8.56×10^{-6} M in CH_2Cl_2 , ---) and reduced **3a** (—) after reduction by hydrazine in CH_2Cl_2 . (b) UV-Vis spectra of **3b** (1.0×10^{-5} M in CH_2Cl_2 , —) and oxidized **3b** (---) after oxidation by $\text{H}_3\text{PV}_2\text{Mo}_{10}\text{O}_{40}$ in CH_2Cl_2 under argon.

Table 1 Experimental hyperfine parameters for complexes **3a** and **3b** from Mössbauer spectra recorded at 77 K^a

| Complex | $\delta/\text{mm s}^{-1}$ | $\Delta E_Q/\text{mm s}^{-1}$ | $\Gamma/\text{mm s}^{-1}$ | Iron state |
|-----------|---------------------------|-------------------------------|---------------------------|------------|
| 3a | –0.11 | 1.33 | 0.32 | Fe (+4) |
| 3b | –0.03 | 1.47 | 0.42 | Fe (+3.5) |

^a All experimental values are within 0.02 mm s^{–1}; δ : isomer shift, ΔE_Q : quadrupolar splitting, Γ : half width at half height.

centers were higher. One doublet signal with such a negative isomer shift value indicates $\text{Fe}^{\text{IV}}\text{N–Fe}^{\text{IV}}$ state for **3a**.

For $\text{Fe}^{\text{III}}\text{N–Fe}^{\text{IV}}$ unsubstituted phthalocyanine complexes one doublet with $\delta = 0.06$ mm s^{–1} has previously been observed at 77 K.^{5b–5d} For the corresponding μ -nitrido diiron porphyrin complex one doublet with $\delta = 0.04$ mm s^{–1} was observed at 298 K.^{6g} Based on these data equivalent iron sites, intermediate iron oxidation states of +3.5 were assumed.^{5b,15} The isomer shift of –0.03 mm s^{–1} observed for **3b** is too high for an $\text{Fe}(\text{IV})$ site. An unpaired electron in **3b** having a formally $\text{Fe}^{\text{III}}\text{N–Fe}^{\text{IV}}$ state is delocalized between two Fe sites with a time scale shorter than the hyperfine Larmor time ($\tau_L = 10^{-8}$ s). The Fe sites appeared with a formal +3.5 state. The fact that complex **3a** is EPR silent is in accordance with Mössbauer data which show equivalent $\text{Fe}(\text{IV})$ sites.

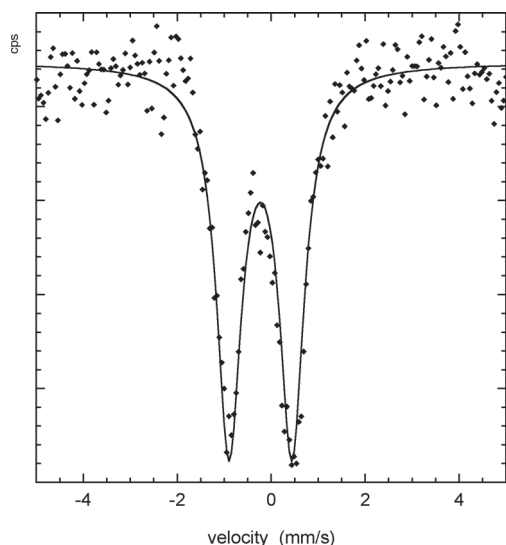


Fig. 3 ^{57}Fe Mössbauer spectra of **3a** at 77 K. Subspectra are derived from a least-squares fit.

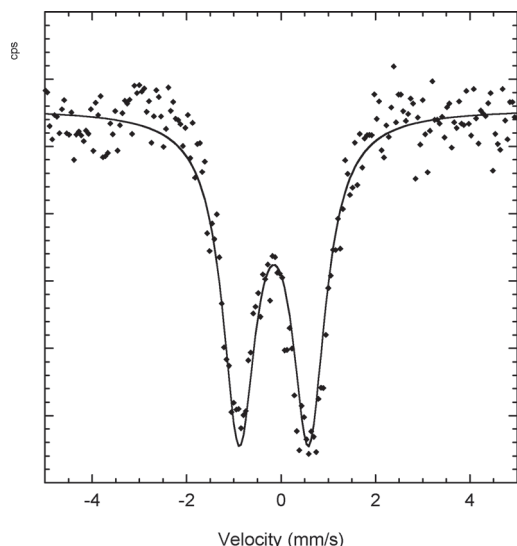


Fig. 4 ^{57}Fe Mössbauer spectra of **3b** at 77 K. Subspectra are derived from a least-squares fit.

X-Ray photoelectron spectroscopy

X-Ray photoelectron spectroscopy (XPS) is not often used for characterization of porphyrin-like complexes, although it can provide useful information.¹⁶ In earlier studies of porphyrin complexes XPS has been utilized for elucidation of rapid electronic exchange.^{6c} The time scale of XPS is 10^8 faster as compared with Mössbauer time scale (10^{-15} vs. 10^{-7} s). If two different iron sites would constitute an Fe–N–Fe unit, one could expect two separate iron $2p_{3/2}$ signals. A single narrow peak (1.6 eV at half-height) was observed for $(\text{TPPFe})_2\text{N}$ (TPP = tetraphenylporphyrin) for Fe $2p_{3/2}$ by Kadish *et al.*^{6c} They concluded that only one type of Fe atom was presented in this $\text{Fe}^{3.5}\text{--N--Fe}^{3.5}$ porphyrin complex because of rapid electronic exchange. The Fe 2p region XPS spectra of **3a** and **3b** are shown in Fig. 5.

The peaks of the lower binding energy (BE) are due to the Fe $2p_{3/2}$ spin component while those at higher BE are assigned to Fe

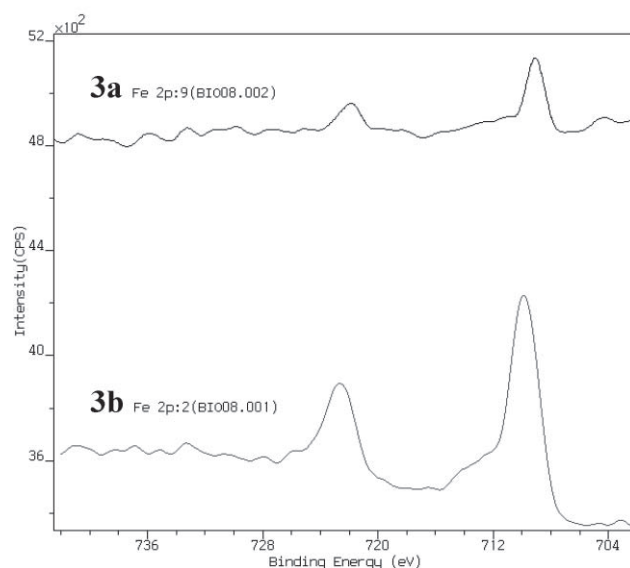


Fig. 5 Expansion of XPS spectrum (704–742 eV, Fe 2p) for **3a** and **3b**.

$2p_{1/2}$. The narrow Fe $2p_{3/2}$ BE peak of **3a** was observed at 709.2 eV with the peak width at half-height of 1.2 eV. The Fe $2p_{3/2}$ signal of **3b** was detected at higher BE of 709.9 eV with a greater width of 2.2 eV. The broadening of the Fe $2p_{3/2}$ signal was associated with the involvement of the paramagnetic metal ions.^{6c} Both **3a** and **3b** contain only one type of iron site. A lower BE of **3a** with respect to that of **3b** suggests a charged complex in the former case.

The 1s N XPS spectra of **3a** and **3b** exhibit strong signals at 398.5 and 398.8 eV, respectively, due to the nitrogen atoms of the phthalocyanine cores with shoulders at a higher BE expected for a bridging nitrogen atom (Fig. 6).

These peaks are situated at 399.9 and 400.4 eV for **3a** and **3b**, respectively. In this case the resolution of signals from the N atoms of the phthalocyanine cycles and the N-bridging atom is not so clear as that observed for N-bridged diiron tetra-*tert*-butylphthalocyanine.^{16b} The 1s N XPS spectrum of the latter complex along with a strong signal at 398.7 eV showed a small well-resolved signal at quite high BE of 402.4 eV which can be assigned to the strongly bonded bridging nitrogen. One can propose that the Fe–N–Fe unit is stronger bonded in the electron-donating $(\text{FePc}'\text{Bu}_4)_2\text{N}$ with respect to **3a** and **3b** containing electron-withdrawing phthalocyanine moieties. Indeed, ESI-MS data support this proposal. While the ESI-MS spectrum of $(\text{FePc}'\text{Bu}_4)_2\text{N}$ exhibits only a strong molecular peak with no signals due to fragmentation to monomer units, the signals of monomer fragments of **3a** and **3b** were observed in their ESI-MS spectra.

X-Ray absorption near-edge structures (XANES)

Depending on the iron oxidation state, the XANES varies in the position and shape of the pre-edge peaks and of the main jump. The pre-edge is more characteristic and sensitive to the oxidation state variations and to the ligand environment of the absorbing center. XANES technique was shown to be very useful for the structural characterization of a variety of mononuclear Fe complexes and Fe containing enzymes.¹⁷ However, very limited XANES and EXAFS data are available for diiron structures.¹⁸ The Fe K-edge spectra of dimer complexes **3a** and **3b** were recorded

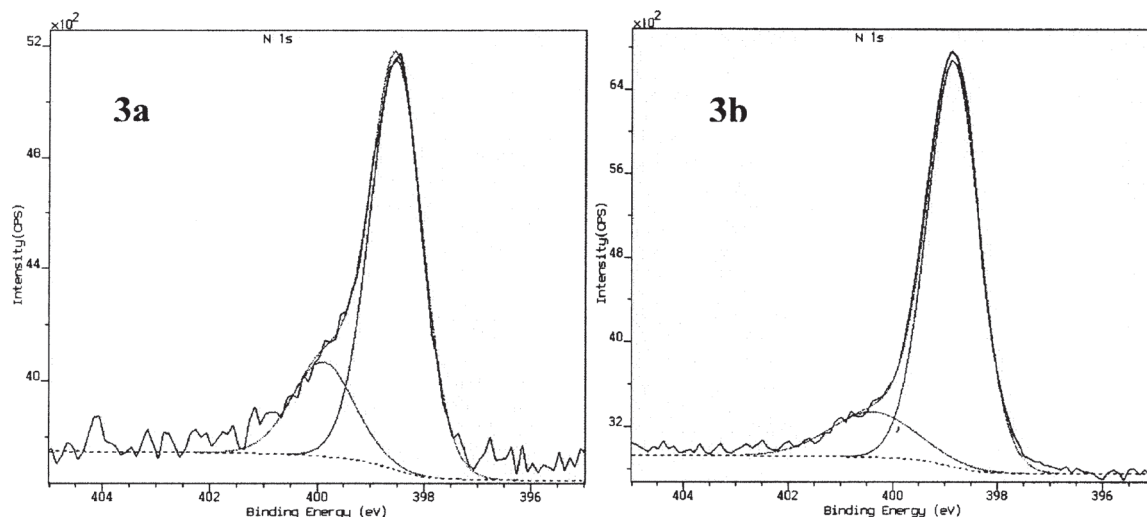


Fig. 6 Expansion of XPS spectrum (395–405 eV, N 1s) for **3a** and **3b**.

and compared to that of a mononuclear complex to provide a basis for comparison and for simulation. The XANES spectra for mononuclear **2b** and binuclear **3a** and **3b** are presented in Fig. 7(a).

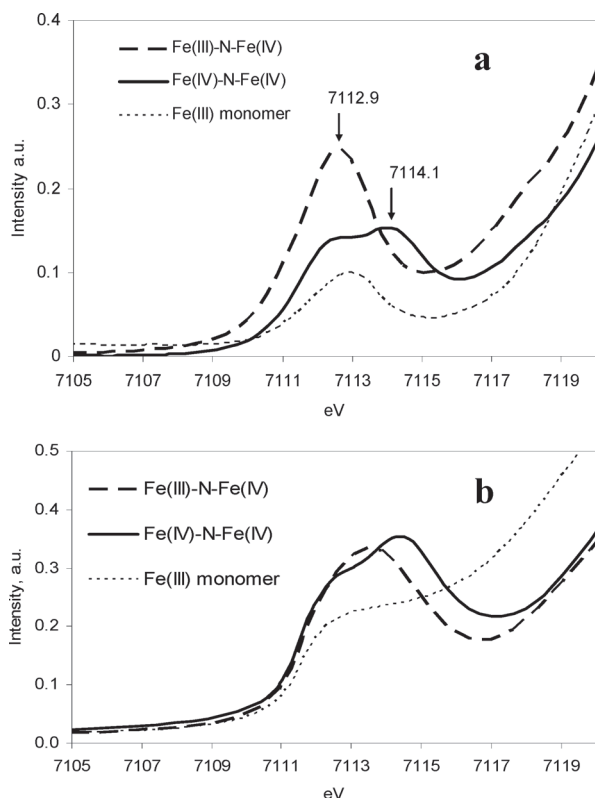


Fig. 7 Pre-edge region of the XANES spectra for **2b**, **3b** and **3a**: (a) experimental spectra; (b) FEFF simulation spectra.

The XANES spectrum of mononuclear **2b** demonstrates a small but well defined pre-edge absorption peak at 7112.9 eV. Such a pre-edge peak observed in the monomeric iron phthalocyanine is typical for the octahedral or square-pyramidal Fe(III) complexes.¹⁹ The pre-edge transition is assigned to a dipole-forbidden but quadrupole-allowed $1s \rightarrow 3d$ transition. In the absence of the

inversion symmetry (C_{4v}), the only mechanism of the pre-edge intensity increase is that of the $3d$ – $4p$ orbital mixing. The rising part of the curve at a higher energy corresponds to a $1s \rightarrow 4p$ Fe orbital transition.²⁰ In **2b** the geometry around Fe(III) is presumably square-pyramidal due to an anion located at the axial position.

The formation of a μ -nitrido dimer led to an increase of pre-edge intensity. This can be expected because the addition of a short axial bond Fe–N would raise the covalence character of z^2 -type iron orbitals and therefore their mixing with the p orbitals.^{19b} The appearance of the second lobe at 7114.1 eV was observed for the Fe(IV)–N–Fe(IV) complex **3a**. The increase of the pre-edge intensity is consistent with a higher oxidation state of iron since (other parameters being equal) it increases the number of free d-orbitals and therefore the probability of $1s \rightarrow 3d$ electron transfer increases as well. An increase of the pre-edge energy is also in agreement with the hypothesis of high iron oxidation state as it means an increase of the efficient positive charge on the iron central ion and therefore a stronger electron bonding. The magnitude of the effect observed is consistent with earlier work on Fe K pre-edge position vs. oxidation state.²¹ While the general reason of the pre-edge peak splitting is obviously due to removal of 3d orbitals degeneration and existence of multiple excited states,^{19b} the exact attribution of lobes remains beyond of the scope of this work. If the electronic structure of μ -nitrido dimers resembles in general features that of the dimers described in ref. 12 then the possible $1s \rightarrow 3d$ transitions should occur to promote an electron to the empty lowest lying z^2 orbitals as well as degenerate ($xz + xz$, $yz + yz$) and highest energy ($x^2 - y^2$)-like manifolds. According to the DFT calculations,¹² these orbitals in the low spin heme dimers are separated by ca. 1 eV energy value, that is in agreement with the observed splitting of pre-edge lobes.

Multiple scattering *ab initio* calculations performed using FEFF 8 software provided a coherent description of the changes in the pre-edge peak between the monomer and two dimers. The simulated spectra reproduced quite well the qualitative difference between these three compounds, though the simulated pre-edge peak of the monomer is less pronounced than in the experiment (Fig. 7(b)). The typical absolute errors in the estimation of density

of state for first row metals compounds pre-edge peak and Fermi level absorption edge by FEFF are 1 eV.²² However in the case of similar compounds the FEFF8 simulations provide much better precision achieving 0.2 eV.

EXAFS spectra and fitting

Simulation of the EXAFS part of the XAS Fe K spectra, and fitting of the experimental curves performed using the VIPER program confirmed the identity of the dimer compound and the refinement of its structure. Due to the large molecular size, and inner position of iron in the μ -nitrido dimer only the environment inside one molecule may have an appreciable impact on the spectra. Therefore iron integer coordination numbers are obviously imposed. The model topology was fixed for both monomer and dimer trial structures, and the number of neighbors (CNs) were also fixed for each simulation. Only the distances (and the concomitant angles) were variables. This strongly facilitates fitting and allows better adjusting of the distances with the precision of 0.02 Å or even better. At the same time the number of coordination shells which can be fitted also increases due to the additional independent parameters available, liberated from the fixing of CNs. The linearity of the fragments in the structure can be relatively easily checked using the EXAFS fitting. In the nearly planar phthalocyanine complexes, due to the expected linearity of the N–Fe–N fragments both for bonding and non-bonding nitrogen atoms, the corresponding multiple scattering paths may become important despite the small nitrogen mass. By contrast, if linearity is broken and the iron atom goes out from the phthalocyanine plane, the contribution of such paths rapidly decreases. This makes simulation very sensitive to the deviations of the N–Fe–N and Fe–N–Fe angles from 180°. At the same time multiple scattering paths do not need new parameters to be introduced in the fitting procedure since they are not independent. Their amplitudes can be taken into account automatically together with the generic single scattering paths. Table 2 resumes the results of fitting, whereas the simulated and experimental spectra are presented in Fig. 8.

The principal structural features of the complexes can be deduced from the EXAFS data. First, the intense peak at about 3 Å indicates a binuclear diiron structure because this peak comes from the relatively heavy iron neighbor. The monomeric phthalocyanine exhibits only a small intensity at 3 Å distance (data not shown). The axial Fe–distance in the dimer was fitted independently on the Fe–Fe distance. The obtained ratio of Fe–Fe to Fe–N distances is

Table 2 EXAFS fitting results for the Fe K edge spectrum of **3b**

| Scatterer | $R/\text{Å}^a$ | Number | DW factor/ Å^2 |
|-----------|----------------|----------------|-------------------------|
| N | 1.669(5) | 1 ^b | 0.0032(5) |
| N | 1.945(5) | 4 ^b | 0.0071(8) |
| C | 2.97(2) | 8 | 0.0073(8) |
| Fe | 3.33(1) | 1 ^b | 0.0032(5) |
| N | 3.41(2) | 4 | 0.0072(8) |
| N | 4.06(3) | 4 | 0.0083(8) |

^a Only the mean distances are available in EXAFS, thus making this technique unable to address any small orthorhombic distortions. ^b Due to the closeness of the Fe–N–Fe fragment geometry to linearity, additional multiple scattering paths must be taken into account for this apparent distance.

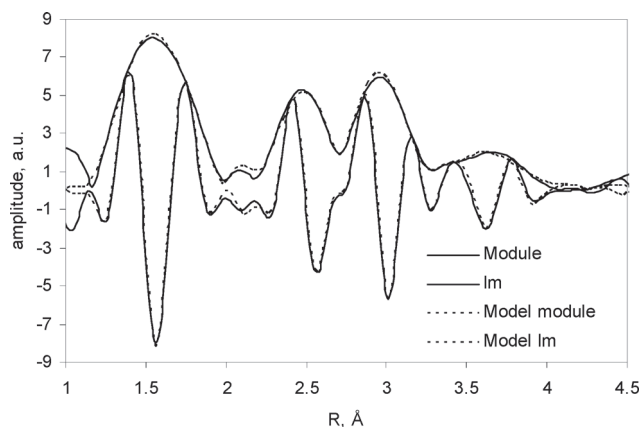


Fig. 8 R -space fitting of real and imaginary parts of the EXAFS spectrum of μ -nitrido dimer **3b**. Module-FT amplitude in the experimental and simulated (model) spectra; Im: imaginary part of FT in the experimental and simulated EXAFS spectra.

very close to 2. This strongly suggests a linearity of the Fe–N–Fe fragment. Moreover, the FT amplitude of this peak placed at *ca.* 3 Å (presented in Fig. 8 without phase correction) cannot be explained without taking into account multiple scattering paths with the contribution of nitrogen situated at half-distance. Therefore, both Fe–N distances should be nearly equal.

From simple trigonometric considerations it follows that iron is slightly deviated out of plane towards the central nitrogen, by *ca.* 0.24 Å. This leads to the estimation of the in-plane N–Fe–N angle of 168–170°. However, the EXAFS study cannot address some essential features of the complexes geometry. Thus, the symmetry of the problem prevents the determination of staggered *vs.* eclipsed configuration of the Pc planes of the dimer. Slight (0.01–0.02 Å) deviations of the projected iron position from the Pc ring centre cannot be excluded as well. Higher DW factors for the in-plane nitrogen and carbon, as compared to the axial Fe–N–Fe fragment suggest higher rigidity of the last with smaller amplitude of bending vibrations. However, this can be also explained by some small static orthorhombic distortion of the ring, increasing the apparent DW factors. It should be noted that the EXAFS optimized geometry of our complexes bears a striking similarity to the DFT-optimized geometry of the μ -nitrido bridged heme dimers, described in ref. 12 They are also close to the relevant crystallographic data for the bromide adduct to the N-bridged diiron non-substituted phthalocyanine dimer²³ and the crystal structure of the $[(\text{TPP})\text{Fe}]_2\text{N}$ (TPP = *meso*-tetrakis(*p*-tolyl)porphyrin).²⁴

High resolution K β emission spectra

In order to gain an insight into the spin state of iron in the μ -nitrido dimers, high resolution K β emission spectra were measured. K β emission can be described as a two step process. In the first stage a 1s electron is ejected from the K core and a hole is created. In the second step a 3p electron is relaxed to the K core and K β fluorescence is emitted, while the final state with a hole at the 3p level is created. The strong coupling between 3p and 3d orbitals leads to the appearance of an extended multiplet structure, usually containing so-called K $\beta_{1,3}$ and K β' components.²⁵ Due to the coupling of the 3p hole with 3d electrons, the position and

intensity of $K\beta_{1,3}$ and $K\beta'$ peaks strongly depend on the oxidation state and spin state of the element under study. The $K\beta'$ structure exhibited by the iron complexes which is due to a spin flip process merges with the $K\beta_{1,3}$ peak as the spin on the atom decreases. At the same time the $K\beta_{1,3}$ peak moves towards lower energies. Thus, the simple qualitative distinction of high spin and low spin iron complexes is possible from the shape of emission spectra. A detailed theoretical explanation of this method can be found in the recent review.²⁶ In this study we have measured the spectra of complex **3a**. Complex **3a** exhibits a typical emission spectrum of low spin ($S = 0$) iron, very different from that of reference monomer high spin species (Fig. 9).

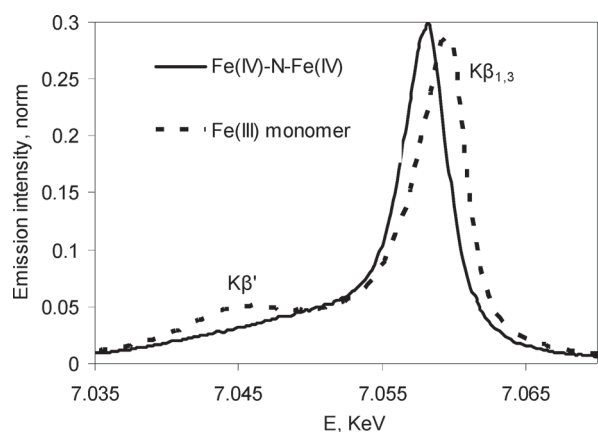


Fig. 9 High resolution $K\beta$ fluorescence spectra of iron of the **3a** complex and of the reference monomeric high spin Fe(III)Pc complex.

This is again in agreement with the results of the DFT calculations on the μ -nitrido heme dimer,¹² predicting low spin state for these type of compounds. Obviously, for the Fe(III)-N-Fe(IV) complex, $S = 1/2$ state should be formed by adding one electron to the z^2 type orbital, detectable by EPR. The spectra of Fe(III)-N-Fe(IV) *tert*-butyl and non-substituted phthalocyanine complexes also showed the spectra characteristic of low spin iron.

Discussion on the structure of two μ -nitrido dimers

Despite the same synthetic protocol for the preparation of complexes **3a** and **3b**, several lines of evidence indicate their different structures. Mössbauer spectra of **3a** and **3b** show one doublet signal in each case with parameters corresponding to Fe^{+4} and $\text{Fe}^{+3.5}$ states for **3a** and **3b**, respectively. EPR experiments strongly support this assignment. While **3a** was EPR-silent, **3b** exhibited a feature belonging to $S = 1/2$ species with axial symmetry of an iron environment with g -tensor values of 2.115 and 2.005. The absence of a nitrogen hyperfine structure in the EPR spectrum is in accordance with a $\text{Fe}^{+3.5}\text{-N}^{3-}\text{-Fe}^{+3.5}$ formalism.^{6c} μ -Nitrido bridged species exhibit an exceptional inertness and stability because of delocalisation of an unpaired electron. In accordance with the cationic nature of **3a** ($\text{Fe}^{\text{IV}}\text{Fe}^{\text{IV}}$) and neutral state of **3b** ($\text{Fe}^{\text{III}}\text{Fe}^{\text{IV}}$) the parent peaks in the ESI-MS were $[\text{M}]^+$ and $[\text{M} + \text{Na}]^+$, respectively. Data obtained by other spectroscopic methods are also in agreement with the formulation of **3b** with *tert*-butylsulfonyl substituents as a neutral $\text{Fe}^{\text{III}}\text{Fe}^{\text{IV}}$ N-bridged dimer and **3a** with *n*-hexylsulfonyl as a cationic $\text{Fe}^{\text{IV}}\text{Fe}^{\text{IV}}$ complex containing N_3^- for compensation of charge. The presence of

N_3^- in **3a** was evidenced by the presence of a 2010 cm^{-1} strong signal in the IR spectrum. Upon reduction of **3a** with sodium dithionite this signal disappeared.

The synthesis of **3a** and **3b** was reproducible. The **3a** and **3b** materials with the same spectroscopic properties have been obtained in three preparations of each complex. The reason for the difference in the iron oxidation state is not yet clear. Electron-withdrawing properties of *n*-hexylsulfonyl and *tert*-butylsulfonyl substituents should be practically the same and should not induce such a difference. One can speculate that the divergence in the oxidation state of the Fe-N-Fe structural unit can be attributed to the different steric properties of these substituents. The **3b** complex with bulkier *tert*-butylsulfonyl groups should adopt a more staggered conformation with respect to complex **3a**. Unfortunately, no X-ray structure of diiron $\text{Fe}^{\text{IV}}\text{-N-Fe}^{\text{III}}$ phthalocyanine complex is yet available. The only published X-ray structure was determined for $(\text{Br})\text{PcFe}^{\text{IV}}\text{-N-Fe}^{\text{IV}}\text{Pc}(\text{Br})$ species²³ containing six-coordinated iron sites and a linear Br-Fe-N-Fe-Br fragment. The two phthalocyanine rings are staggered by an angle of 39° with an in plane location of the iron atoms. The Fe-N bond distance was quite short (1.639 \AA) thus suggesting the significant π -conjugation along internal bridging system.^{5b} The structural features of **3b** determined from EXAFS data (Fig. 10) can be compared to the X-ray structure of $(\text{Br})\text{PcFe}^{\text{IV}}\text{-N-Fe}^{\text{IV}}\text{Pc}(\text{Br})$ reported by Moubaraki *et al.*²³ The Fe-N bond distance of the linear Fe-N-Fe fragment of **3b** is longer than in unsubstituted $(\text{Br})\text{PcFe}^{\text{IV}}\text{-N-Fe}^{\text{IV}}\text{Pc}(\text{Br})$: 1.669 \AA vs. 1.639 \AA , respectively. Thus, the distance between two iron atoms is 3.33 \AA suggesting π - π interaction between Pc planes. However, EXAFS data does not allow the conclusion on the possible staggering in this binuclear structure. Both iron atoms are displaced out of the N_4 phthalocyanine planes by 0.24 \AA indicating five-coordinated iron state. In the only published N-bridged iron phthalocyanine X-ray structure for $(\text{Br})\text{PcFe}^{\text{IV}}\text{-N-Fe}^{\text{IV}}\text{Pc}(\text{Br})$ iron atoms are in the N_4 plane.²³

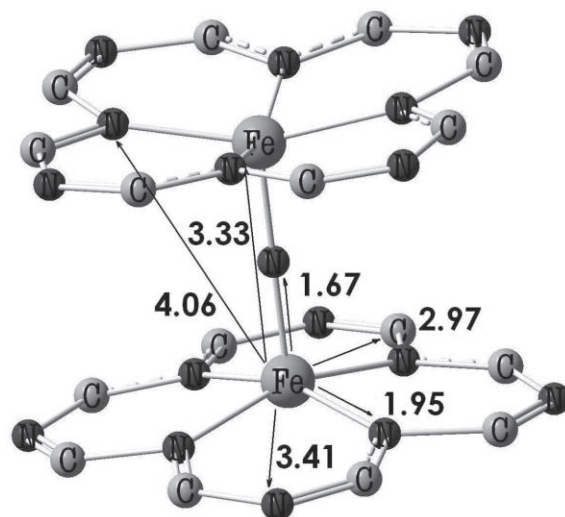


Fig. 10 EXAFS structure of μ -nitrido dimer **3b**.

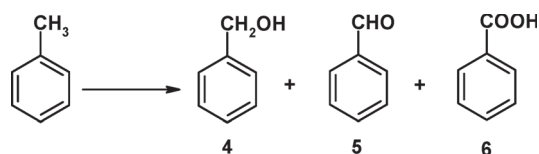
The similar withdrawing of iron atoms from the N_4 plane of 0.32 \AA with shortening of the Fe-N distance was previously observed in a N-bridged iron porphyrin complex.^{6b} The structural

parameters of N-bridged diiron phthalocyanine with a Fe^{III}–N–Fe^{IV} unit were determined for the first time.

Catalytic oxidation of toluene

The catalytic potential of these novel complexes **3a** and **3b** was evaluated in aromatic oxidation. Oxidation of alkyl aromatics is a very important process in industrial chemistry.²⁷ The production of terephthalic acid by oxidation of *p*-xylene is probably the most sound example of industrial benzylic oxidation: its worldwide annual production is about 44 million t/y. The industrial process is based on the radical oxidation in the presence of Co and Mn ions in acetic acid at harsh conditions (about 200 °C, 1.5 MPa).²⁸ Stoichiometric oxidation by permanganate or Cr^{VI} oxidants are also used to perform benzylic oxidations. Several catalytic approaches have been described in quest of cleaner and more general processes. Along with dioxygen,²⁹ *t*-BuOOH is widely used as the oxidant in combination with Cr,³⁰ Co,³¹ Mn³², Fe³³ and Rh³⁴ based catalysts. Vanadium-based polyoxometalates have been shown to be useful catalysts for benzylic oxidation.³⁵ Alkyl aromatic compounds can be oxidized either at benzylic positions or in the aromatic nuclear. Consequently, the selectivity issue is very important. Catalytic systems capable of selectively oxidizing either only benzylic or only aromatic sites are highly desirable. However, this task is difficult to achieve. For example, toluene was oxidized by iron(II) complexes bearing hexa-, penta- or tetra-azadentate ligands–H₂O₂ system to a mixture of isomeric cresols, benzyl alcohol and benzaldehyde.³⁶ Benzylic and ring oxidation products were obtained with comparable yields. The addition of reducing agents shifted oxidation in favour of aromatic ring oxidation to give a total TON ~ 7.³⁶ Oxidation of toluene performed by metalloporphyrin systems has often resulted in the mixture of products of benzylic and aromatic oxidation.³⁷

In order to estimate the reactivity of **3a** and **3b** towards oxidation of aliphatic C–H vs. aromatic oxidation we have studied the oxidation of toluene and *p*-xylene by *t*-BuOOH. The oxidations were carried out without solvent, in 1 mL of neat substrate at 20, 40 and 60 °C. Avoiding the use of solvent is an important advantage from environmental and industrial points of view. The concentrations of catalyst and oxidant were 1 mM and 206 mM, respectively. Benzylic alcohol (**4**), benzaldehyde (**5**) and benzoic acid (**6**) were the main products of oxidation of toluene (Scheme 2).



Scheme 2 Oxidation of toluene.

Table 3 shows the results of toluene oxidation catalyzed by **3a** and **3b**. Using **3a** the oxidation was more efficient at 40 °C (total TON = 197) while **3b** provided a higher total TON = 115 at 60 °C.

Significantly, only traces of products of aromatic oxidation, *p*-cresol and 2-methyl-1,4-benzoquinone, were detected by GC-MS. Thus, the catalytic system demonstrates a strong preference for the oxidation of aliphatic C–H bonds compared with aromatic oxidation. Among the products of benzylic oxidation, benzylic acid was the principal product, accounting for 73–83% depending

Table 3 Oxidation of toluene by *t*-BuOOH catalyzed by **3a** and **3b**^a

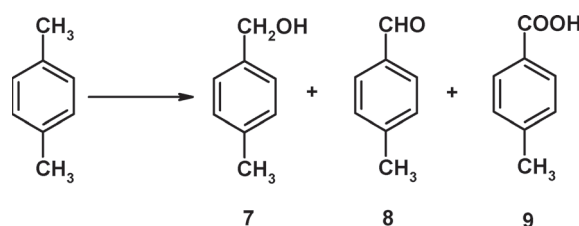
| Catalyst | <i>T</i> /°C | TON | PhCH ₂ OH (%) | PhCHO (%) | PhCOOH (%) |
|---------------------------------------|--------------|-----|--------------------------|-----------|------------|
| 3a | 20 | 92 | 6 | 21 | 73 |
| | 40 | 197 | 5 | 12 | 83 |
| | 60 | 167 | 6 | 13 | 81 |
| 3b | 20 | 59 | 7 | 20 | 73 |
| | 40 | 86 | 7 | 16 | 77 |
| | 60 | 115 | 7 | 16 | 77 |
| (FePcBu ₄) ₂ N | 20 | 73 | 12 | 51 | 37 |
| | 40 | 99 | 12 | 49 | 39 |
| | 60 | 137 | 16 | 47 | 37 |

^a Reaction conditions: [catalyst] = 1 mM, [*t*-BuOOH] = 206 mM in 1 mL of toluene, reaction time 24 h.

on experimental conditions. The ratio of products was very similar for two catalysts. We have previously used the complex (FePc^{*i*}Bu₄)₂N with electron-donating *tert*-butyl substituents for oxidation of methane and benzene.⁴ The comparative experiments with (FePc^{*i*}Bu₄)₂N as catalyst for the oxidation of toluene showed the influence of the structure of the diiron N-bridged phthalocyanine on the catalytic properties (Table 3). While **3a** and **3b** were quite selective to benzoic acid, up to 83%, (FePc^{*i*}Bu₄)₂N afforded benzaldehyde as the principal product with selectivity up to 51%. Although the reason of this selectivity change is not yet clear, the results obtained provide a possibility of tuning of selectivity of the oxidation by the appropriate modification of the structure of phthalocyanine ligand. The catalytic activity of (FePc^{*i*}Bu₄)₂N in terms of turnover numbers is comparable to that of **3a** and **3b**.

Catalytic oxidation of *p*-xylene

The oxidation of *p*-xylene has also resulted in the products of benzylic oxidation: 4-methylbenzyl alcohol (**7**), *p*-tolualdehyde (**8**) and *p*-toluic acid (**9**) (Scheme 3). Interestingly, this benzylic oxidation occurred only at one methyl group. *p*-Toluic acid was the main product (Table 4). While in the oxidation of toluene **3a** was superior than **3b** in terms of turnover numbers and selectivity to benzoic acid, **3b** showed higher turnover numbers and selectivity in oxidation of *p*-xylene. A high performance was obtained at 60 °C with **3b**: TON attained almost 600 catalytic cycles. Both catalysts performed the selective oxidation of only one methyl group. We did not observe any products of the oxidation of both methyl groups. Products of aromatic oxidation were also absent. In contrast to μ -oxo iron phthalocyanines, μ -nitrido iron phthalocyanines in combination with *t*-BuOOH show different selectivity in oxidation of alkylaromatics. While the Fe–O–Fe catalyst performed oxidation of aromatic rings to form quinones,³⁸ the Fe–N=Fe complex was quite selective in oxidation of alkyl substituents.



Scheme 3 Oxidation of *p*-xylene.

Table 4 Oxidation of *p*-xylene by *t*-BuOOH catalyzed by **3a** and **3b**^a

| Catalyst | <i>T</i> /°C | TON | 7 (%) | 8 (%) | 9 (%) |
|-----------|--------------|-----|--------------|--------------|--------------|
| 3a | 20 | 164 | 14 | 34 | 52 |
| | 40 | 291 | 15 | 25 | 60 |
| | 60 | 312 | 17 | 28 | 55 |
| 3b | 20 | 185 | 14 | 34 | 52 |
| | 40 | 339 | 13 | 22 | 65 |
| | 60 | 587 | 15 | 19 | 66 |

^a Reaction conditions were the same as those in footnote of Table 3.

Conclusions

We have prepared two novel N-bridged diiron phthalocyanine complexes bearing electron-withdrawing alkylsulfonyl substituents which were characterized by ESI-MS, UV-Vis, FTIR, EPR, Mössbauer, XANES, EXAFS, high resolution K β emission and X-ray photoelectron spectroscopies. Both complexes contain one type of iron, but iron states are not the same. The complex **3a** having *n*-hexylsulfonyl substituents contains a Fe^{IV}–N–Fe^{IV} fragment while complex **3b** with *tert*-butylsulfonyl substituents is formally a Fe^{IV}–N–Fe^{III} complex. Due to rapid electron exchange, **3b** can be described as Fe^{3.5}–N–Fe^{3.5} with two equivalent +3.5 Fe sites as was proposed by Ercolani *et al.* in the case of the unsubstituted complex.^{5a,5b} EXAFS fitting results for the Fe K edge spectrum of **3b** revealed a short Fe–N bond of 1.67 Å.

The catalytic properties of both complexes were evaluated in the industrially important oxidation of alkylaromatic compounds by *t*-BuOOH. Novel complexes **3a** and **3b** in combination with *t*-BuOOH exhibit a high selectivity in oxidation of toluene and *p*-xylene. This catalytic system is complementary to the recently reported μ -nitrido diiron tetrabutylphthalocyanine–H₂O₂ system which oxidizes benzene to phenol *via* benzene oxide with NIH shift.^{4b} The results obtained in this work indicates the versatility of diiron N-bridged phthalocyanines as oxidation catalysts.

Experimental

General methods

X-Band (9.5 GHz) EPR spectra were recorded at 77 K on a Bruker ESP 300E spectrometer using a standard rectangular (TE102) EPR cavity (Bruker ER4102ST). Microwave power of 1.6 mW and modulation amplitude 1 G was used. For quantitative analysis the EPR spectra were simulated and the experimental spectra were fitted using the simulation program EasySpin.³⁹ Two stage fitting was implemented, beginning with Nelder/Mead downhill simplex with coarse termination criteria and followed by refinement using Levenberg/Marquardt iterative algorithm. XAS experiments were carried out at the BM01 beam line of the ESRF synchrotron facility. The Fe *K*-edge spectra were monitored in the transmission mode, using a Si(111) crystal monochromator. The data were treated with FEFF²¹ and VIPER⁴⁰ programs. Then the edge background was extracted using Bayesian smoothing with variable number of knots. The curve fitting was done alternatively in the *R* and *k* spaces, and the fit was accepted only in the case of simultaneous convergence in *k*- and *R*-spaces (absolute and imaginary parts for the latter). Coordination numbers (CN), interatomic distances (*R*), Debye–Waller parameter (σ^2), and

energy shifts (ΔE_0) were used as fitting variables. True Debye–Waller (DW) factors and amplitude factor were decorrelated from the coordination numbers using fitting of spectra multiplied by different powers of *k*, similarly to the spectra treating in the previous work.⁴¹ Constraints were introduced on the variables such as DW factors or energy shifts to get values lying in physically reasonable intervals. Constraints imposed by the molecular structure were also introduced. The quality of the fit was evaluated using the values of variance and goodness. To simulate XANES spectra real space full multiple scattering *ab initio* FEFF8.10 code was applied to simulate XANES spectra and pre-edge peaks with the FMS and SCF radii between 4 and 5 Å, *i.e.* including the whole molecule plane of the scatterer and the closest nitrogen and carbon atoms of the second plane of the dimer. In order to address the spin states and oxidation states of iron in the complexes under study, we performed high resolution X-ray fluorescence measurements on selected samples. The X-ray K β emission spectra were measured on the undulator beamline ID26 of the European Synchrotron Radiation Facility (ESRF). The energy of the beam was selected using Si(220) crystals. The emission spectroscopy was performed using a spherically bent analyzer crystal (Si(531)). In order to minimize radiation damage, the samples were cooled in a cryostat to 30–50 K. The UV-Vis spectra were recorded on a Perkin-Elmer Lambda 35 spectrophotometer. Infrared spectra were recorded on a Bruker Vector 22 FTIR spectrometer using KBr pellets. X-Ray photoelectron spectroscopy (XPS) spectra were collected with a Kratos Axis Ultra DLD instrument using a hemispherical analyzer and working at a vacuum better than 10^{−9} mbar. All the data were acquired using monochromated Al K α X-rays (1486.6 eV, 150 W), a pass energy 160 eV and 1 eV step size for wide scan and 40 eV pass energy with 0.1 eV step size for elemental scan, and a hybrid lens mode. The area analysed is 700 μm \times 300 μm . Charge neutralisation was required for all samples. The peaks were referenced to the C–(C,H) components of the C1s band at 284.6 eV. The Mössbauer spectra of the powder samples were recorded at 77 and 293 K using a 2 GBq ⁵⁷Co/Rh source and a conventional constant acceleration spectrometer, operated in triangular mode. The isomer shifts are given with respect to α -Fe and were calculated, as the quadrupole splittings, with a precision of about 0.02 mm s^{−1}.

The reaction oxidation products were identified and quantified by GC-MS (Hewlett Packard 5973/6890 system; electron impact ionization at 70 eV, He carrier gas, 30 m \times 0.25 mm cross-linked 5% PHME siloxane [0.25 mm coating] capillary column, HP-5MS), GC (Agilent 4890D system, N₂ carrier gas, 15 m \times 0.25 mm cross-linked 5% PHME siloxane [0.25 mm coating] capillary column, HP-5MS).

Materials

Solvents and chemicals were obtained from Sigma-Aldrich and used without purification unless indicated. 1,2-Dicyano-4-hexylthiobenzene⁴² and 1,2-dicyano-4-*tert*-butylthiobenzene⁴³ were prepared according to literature protocols.

1,2-Dicyano-4-hexylsulfonylbenzene (1a)

To a solution of 1,2-dicyano-4-hexylthiobenzene (2 g, 15.06 mmol) in dry CH₂Cl₂ (8.5 mL) cooled at 0 °C was slowly added

m-chloroperbenzoic acid (6.35 g, 36.75 mmol) in CH₂Cl₂ (150 mL). The mixture was warmed to room temperature and vigorously stirred at this temperature overnight (12 h). A saturated sodium sulfite solution was then added, and the organic phase was extracted with CH₂Cl₂ (3 × 50 mL) and dried over Na₂SO₄. The solvent was removed under reduced pressure, and the solid was recrystallized from ethanol to give 3.1 g (73%) of **1a** as a white solid. Anal. Calcd for C₁₄H₁₆N₂O₂S: C, 60.85; H, 5.84; N, 10.14; S, 11.60. Found: C, 60.16; H, 5.94; N, 10.29; S, 11.70. ¹H NMR (250 MHz, CDCl₃): δ = 0.8 (t, 3H), 1.2–1.5 (m, 8H), 3.4 (t, 2H), 8.0 (d, 1H), 8.1 (d, 1H), 8.4 (dd, 1H) ppm; EI-MS: *m/z* 276 [M]⁺; IR (KBr): ν = 1111, 1147, 2241 cm⁻¹.

1,2-Dicyano-4-*tert*-butylsulfonylbenzene (1b)

1,2-Dicyano-4-*tert*-butylthiobenzene (2.3 g, 0.011 mmol) was dissolved in 50 mL of acetic acid at 90 °C. To the stirred solution was added a total of 60 mL of 33% H₂O₂ in 1 mL portions over the course of 4 h. The resulting mixture was allowed to cool to room temperature and stirred overnight. The white precipitate was collected by filtration, washed with water, and crystallized from ethanol (50 mL) to give 1.8 g (73%) of pure **1b** as a white powder. ¹H NMR (250 MHz, CDCl₃): δ = 1.3 (s, 9H), 8.1 (d, 1H), 8.2 (d, 1H), 8.3 (dd, 1H) ppm; EI-MS: *m/z* 248.3 [M]⁺. IR (KBr): ν = 1125, 1130, 2235 cm⁻¹.

Tetra-(hexylsulfonyl)phthalocyaninatoiron (2a)

Compound **1a** (300 mg, 1.08 mmol) was heated at 130 °C in a mixture of *o*-dichlorobenzene–DMF (3 : 1) under argon for 8 h in the presence of FeCl₂ (0.27 mmol). The solvent was removed under reduced pressure. The green solid was extracted with CH₂Cl₂ and washed with water. **2a** was isolated by chromatography on silica gel using a mixture of CH₂Cl₂–EtOH (100 : 1). Yield: (58 mg, 18%). ESI-MS: *m/z* 1161.3 [M]⁺; calculated for C₅₆H₆₄FeN₈O₈S₄: 1161.2; UV-Vis (CHCl₃): λ_{max} (log ε) = 680 (4.7), 600 (4.2), 306 (4.6) nm; IR (KBr): ν = 1326, 1257, 1143, 1076, 818, 745 cm⁻¹.

Tetra-(*tert*-butylsulfonyl)phthalocyaninatoiron (2b)

Compound **2b** (1 g, 4 mmol) was heated at 130 °C in a mixture of *o*-dichlorobenzene–DMF (3 : 1) under argon for 8 h in the presence of FeCl₂ (1 mmol). The solvent was removed under reduced pressure. The blue solid was extracted with CH₂Cl₂. **2b** was isolated by chromatography on silica gel using a mixture of CH₂Cl₂–EtOH (100 : 1). Yield: (250 mg, 25%). ESI-MS: *m/z* 1049.1 [M]⁺ (100); calculated for C₄₈H₄₈FeN₈O₈S₄: 1049.05; IR (KBr): ν = 1296, 1143, 1140, 1123, 697, 564 cm⁻¹; UV-Vis (CHCl₃): λ_{max} (log ε) = 683(4.8), 629(4.6), 287 (4.7) nm.

μ-Nitrido-bis [tetra-(hexylsulfonyl)phthalocyaninatoiron] [FePc(SO₂C₆H₁₃)₄]₂N⁺ N₃⁻ (3a)

Compound **2a** (200 mg, 0.17 mmol) and sodium azide (2 g) were suspended in 70 ml of oxygen-free xylene (mixture of isomers) under argon. The mixture was heated for 24 h at 150 °C under intensive stirring. The reaction mixture was cooled and a resulting blue green solution was separated from insoluble material by filtration. The solution was chromatographed on Al₂O₃ (neutral) with CH₂Cl₂ to remove impurities. Then **3a** was collected using

CH₂Cl₂:EtOH (100 : 1) mixture as eluent. The IR spectrum showed the presence of azide anion compensating a positive charge of complex. Yield: (115 mg, 57%). ESI-MS: *m/z* 2335.9 [M – N₃]⁺ (100); calculated for C₁₁₂H₁₂₈Fe₂N₁₇O₁₆S₈: 2335.6; IR (KBr): ν = 931 cm⁻¹ (Fe=N–Fe); UV-Vis (CH₂Cl₂) λ_{max}, nm (log ε) = 657 (4.94), 344 (4.92), 297 (4.6) nm. Anal. Calcd for C₁₁₂H₁₂₈Fe₂N₁₇O₁₇S₈: C, 57.16; H, 5.52; N, 10.12; S, 10.90. Found: C, 57.42; H, 5.62; N, 8.53; S, 9.61.

μ-Nitrido-bis [tetra-(*tert*-butylsulfonyl)phthalocyaninatoiron] [FePc(SO₂Bu)₄]₂N (3b)

Compound **2b** (170 mg, 0.16 mmol) and sodium azide (1.5 g) were suspended in 70 ml of oxygen-free xylene (mixture of isomers) under argon. The mixture was heated for 24 h at 150 °C under intensive stirring. The reaction mixture was cooled and a resulting dark blue solution was separated from insoluble material by filtration. The solution was chromatographed on Al₂O₃ (neutral) with CH₂Cl₂ to remove impurities. Then **3b** was collected using CH₂Cl₂:EtOH (100 : 1) mixture as eluent. Evaporation of solvent afforded pure **3b** as a dark blue powder. Yield: (100 mg, 58%). ESI-MS: 2134.6 [M + Na]⁺ (100); calculated for C₁₁₂H₁₂₈Fe₂N₁₇O₁₆S₈Na: 2134.4; IR (KBr): ν = 929 cm⁻¹ (Fe=N–Fe); UV-Vis (CH₂Cl₂) λ_{max}, nm (log ε) = 638 (5.09), 339 (4.91).

Typical procedure for the oxidation of toluene and *p*-xylene

A 25 mL flask was charged with 1 mL of toluene or *p*-xylene containing 1 mM catalyst. The reaction was started by the addition of 70% ^tBuOOH aqueous solution to obtain 206 mM oxidant concentration in the reaction mixture. The reaction was run under stirring at the desired reaction temperature under air for 24 h. The course of the reaction was monitored by GC and the product yields were determined using chlorobenzene as the external standard.

Acknowledgements

We acknowledge the European Synchrotron Radiation Facility for provision of synchrotron radiation facilities and we would like to thank Dr O. Safonova, J. Grattage and M. Sikora for their assistance in using beam lines BM01 and ID26. Mr. U. Isci thanks the French Embassy in Ankara for a PhD fellowship. Mr Prakash is greatly acknowledged for the XPS measurements.

Notes and references

- (a) E. G. Kovaleva, M. B. Neibergall, S. Chakrabarty and J. D. Lipscomb, *Acc. Chem. Res.*, 2007, **40**, 475–483; (b) S. J. Lippard, *Philos. Trans. R. Soc. London, Ser. A*, 2005, **363**, 861–877.
- (a) E. Y. Tshuva and S. J. Lippard, *Chem. Rev.*, 2004, **104**, 987–1012; (b) A. A. Shteinman, *Russ. Chem. Rev.*, 2008, **77**, 945–966.
- (a) *The Porphyrin Handbook*, ed. K. M. Kadish, K. M. Smith and R. Guilard, Elsevier Science, San Diego, 2003, vol. 15–20; (b) G. de la Torre, C. G. Claessens and T. Torres, *Chem. Commun.*, 2007, 2000–2015.
- (a) A. B. Sorokin, E. V. Kudrik and D. Bouchu, *Chem. Commun.*, 2008, 2562–2564; (b) E. V. Kudrik and A. B. Sorokin, *Chem.–Eur. J.*, 2008, **14**, 7123–7126; (c) E. V. Kudrik, P. Afanasiev, D. Bouchu, J.-M. M. Millet and A. B. Sorokin, *J. Porphyrins Phthalocyanines*, 2008, **12**, 1078–1089.
- (a) L. A. Bottomley, J.-N. Gorce, V. L. Goedken and C. Ercolani, *Inorg. Chem.*, 1985, **24**, 3733–3737; (b) B. Floris, M. P. Donzello and C. Ercolani, in *Porphyrin Handbook*, ed. K. M. Kadish, K. M. Smith and

- R. Guillard, Elsevier Science, San Diego, 2003, vol. 18, pp. 1–62; (c) C. Ercolani, M. Gardini, G. Pennesi, G. Rossi and U. Russo, *Inorg. Chem.*, 1988, **27**, 422–424; (d) B. J. Kennedy, K. S. Murray, H. Homborg and W. Kalz, *Inorg. Chim. Acta*, 1987, **134**, 19–21.
- 6 (a) D. A. Summerville and I. A. Cohen, *J. Am. Chem. Soc.*, 1976, **98**, 1747–1752; (b) W. R. Scheidt, D. A. Summerville and I. A. Cohen, *J. Am. Chem. Soc.*, 1976, **98**, 6623–6628; (c) K. M. Kadish, L. A. Bottomley, J. G. Brace and N. Winograd, *J. Am. Chem. Soc.*, 1980, **102**, 4341–4344; (d) G. A. Schick and D. F. Bocian, *J. Am. Chem. Soc.*, 1983, **105**, 1830–1838; (e) D. F. Bocian, E. W. Findsen, J. A. Hofmann, Jr., G. A. Schick, D. R. English, D. N. Hendrickson and K. S. Suslick, *Inorg. Chem.*, 1984, **23**, 800–807; (f) D. R. English, D. N. Hendrickson and K. S. Suslick, *Inorg. Chem.*, 1985, **24**, 121–122; (g) M. Li, M. Shang, N. Ehlinger, C. E. Schulz and W. R. Scheidt, *Inorg. Chem.*, 2000, **39**, 580–583.
- 7 (a) C. Ercolani, S. Hewage, R. Heucher and G. Rossi, *Inorg. Chem.*, 1993, **32**, 2975–2977; (b) C. Ercolani, J. Jubb, G. Pennesi, U. Russo and G. Trigiante, *Inorg. Chem.*, 1995, **34**, 2535–2541; (c) M. P. Donzello, C. Ercolani, K. M. Kadish, Z. Ou and U. Russo, *Inorg. Chem.*, 1998, **37**, 3682–3688; (d) M. P. Donzello, C. Ercolani, U. Russo, A. Chiesi-Villa and C. Rizzoli, *Inorg. Chem.*, 2001, **40**, 2963–2976; (e) P. A. Stuzhin, M. Hamdush and H. Homborg, *Mendeleev Commun.*, 1997, 196–198.
- 8 (a) K. Meyer, E. Bill, B. Mienert, T. Weyhermüller and K. Wieghardt, *J. Am. Chem. Soc.*, 1999, **121**, 4859–4876; (b) T. Jüstel, M. Müller, T. Weyhermüller, K. Kressl, E. Bill, P. Hildebrandt, M. Lenglen, M. Grodzicki, A. X. Trautwein, B. Nuber and K. Wieghardt, *Chem.–Eur. J.*, 1999, **5**, 793–810; (c) T. Jüstel, T. Weyhermüller, K. Wieghardt, E. Bill, M. Lenglen, A. X. Trautwein and P. Hildebrandt, *Angew. Chem., Int. Ed. Engl.*, 1995, **34**, 669–672.
- 9 A. Srekanth and M. R. P. Kurup, *Polyhedron*, 2004, **23**, 969–978.
- 10 P. A. Stuzhin, L. Latos-Grażyński and A. Jezierski, *Transition Met. Chem.*, 1989, **14**, 341–346.
- 11 N. Voevodskaya, M. Galander, M. Högbom, P. Stenmark, G. McClarty, A. Gräslund and F. Lendzian, *Biochim. Biophys. Acta*, 2007, **1774**, 1254–1263.
- 12 A. Ghosh, E. Tangen, E. Gonzalez and L. Que, Jr., *Angew. Chem., Int. Ed.*, 2004, **43**, 834–838.
- 13 (a) M. J. Stillman and T. Nyokong, in *Phthalocyanines: Properties and Applications*, ed. C. C. Leznoff and A. B. P. Lever, VCH, New York, 1989, vol. 1, pp. 133–290; (b) G. Ferraudi, in *Phthalocyanines: Properties and Applications*, ed. C. C. Leznoff and A. B. P. Lever, VCH, New York, 1989, vol. 1, pp. 291–339; (c) T. Nyokong and H. Isago, *J. Porphyrins Phthalocyanines*, 2004, **8**, 1083–1090; (d) Y. Rio, M. S. Rodriguez-Morgade and T. Torres, *Org. Biomol. Chem.*, 2008, **6**, 1877–1894.
- 14 A. Satake and Y. Kobuke, *Org. Biomol. Chem.*, 2007, **5**, 1679–1691.
- 15 (a) M. Hanack, U. Keppeler, A. Lange, A. Hirsch and R. Dieing, in *Phthalocyanines: Properties and Applications*, ed. C. C. Leznoff and A. B. P. Lever, VCH, New York, 1993, vol. 2, pp. 46–96; (b) V. N. Nemykin, A. E. Polshina, V. Y. Chernyi, E. V. Polshin and N. Kobayashi, *J. Chem. Soc., Dalton Trans.*, 2000, 1019–1025.
- 16 (a) V. N. Nemykin, P. Galloni, B. Floris, C. R. Barrett, R. G. Hadt, R. I. Subbotin, A. G. Marrani, R. Zanon and N. M. Loim, *Dalton Trans.*, 2008, 4233–4246; (b) See ESI in ref. 3a.
- 17 (a) J.-U. Rohde, S. Torelli, X. Shan, M. H. Lim, E. J. Klinker, J. Kaizer, K. Chen, W. Nam and L. Que, Jr., *J. Am. Chem. Soc.*, 2004, **126**, 16750–16761; (b) G. D. Pirngruber, J.-D. Grunwaldt, P. K. Roy, J. A. van Bokhoven, O. Safonova and P. Glatzel, *Catal. Today*, 2007, **126**, 127–134; (c) X. Shan, J.-U. Rohde, K. D. Koehntop, Y. Zhou, M. R. Bukowski, M. Costas, K. Fujisawa and L. Que, Jr., *Inorg. Chem.*, 2007, **46**, 8410–8417; (d) M. Newcomb, J. A. Halgrimson, J. H. Horner, E. C. Wasinger, L. X. Chen and S. G. Sligar, *Proc. Natl. Acad. Sci. U. S. A.*, 2008, **105**, 8179–8184; (e) F. T. de Oliveira, A. Chanda, D. Banerjee, X. Shan, S. Mondal, L. Que, Jr., E. L. Bominaar, E. Münck and T. J. Collins, *Science*, 2007, **315**, 835–838.
- 18 (a) G. Xue, D. Wang, R. De Hont, A. T. Fiedler, X. Shan, E. Münck and L. Que, Jr., *Proc. Natl. Acad. Sci. U. S. A.*, 2007, **104**, 20713–20718; (b) Y. Dong, Y. Zang, L. Shu, E. C. Wilkinson, L. Que, Jr., K. Kauffmann and E. Münck, *J. Am. Chem. Soc.*, 1997, **119**, 12683–12684.
- 19 (a) C. Cartier, M. Momenteau, E. Dartyge, A. Fontaine, G. Tourillon, A. Michalowicz and M. Verdager, *J. Chem. Soc., Dalton Trans.*, 1992, 609–618; (b) T. E. Westre, P. Kennepohl, J. de Witt, B. Hedman, K. O. Hodgson and E. I. Solomon, *J. Am. Chem. Soc.*, 1997, **119**, 6297–6314.
- 20 S. Y. Ha, J. Park, T. Ohta, G. Kwag and S. Kim, *Electrochem. Solid-State Lett.*, 1999, **2**, 461–464.
- 21 G. A. Waychunas, M. J. Apter and G. E. Brown, Jr., *Phys. Chem. Miner.*, 1983, **10**, 1–9.
- 22 A. L. Ankudinov, C. E. Bouldin, J. J. Rehr, J. Sims and H. Hung, *Phys. Rev. B: Condens. Matter Mater. Phys.*, 2002, **65**, 104107.
- 23 P. Moubaraki, D. Benlian, A. Baldy and A. Pierrot, *Acta Crystallogr., Sect. C: Cryst. Struct. Commun.*, 1989, **45**, 393–394.
- 24 M. Li, M. Shang, N. Ehlinger, C. E. Shultz and W. R. Scheidt, *Inorg. Chem.*, 2000, **39**, 580–583.
- 25 K. Tsutsumi, *J. Phys. Soc. Jpn.*, 1959, **14**, 1696–1706.
- 26 P. Glatzel and U. Bergman, *Coord. Chem. Rev.*, 2005, **249**, 65–95.
- 27 (a) R. A. Sheldon and J. K. Kochi, *Metal-Catalyzed Oxidations of Organic Compounds*, Academic Press, New York, 1981; (b) *Modern Oxidation Methods*, ed. J.-E. Bäckvall, Wiley-VCH, Weinheim, 2004; (c) T. Punniyamurthy, S. Velusamy and J. Iqbal, *Chem. Rev.*, 2005, **105**, 2329–2363; (d) *Active Oxygen in Chemistry*, ed. C. S. Foote, J. S. Valentine, A. Greenberg and J. F. Liemann, Chapman and Hall, New York, 1995.
- 28 J.-M. Brégeault, *Dalton Trans.*, 2003, 3289–3302.
- 29 Selected examples: (a) A. M. Khenkin and R. Neumann, *Inorg. Chem.*, 2000, **39**, 3455–3462; (b) S. A. Chavan, D. Srinivas and P. Ratnasamy, *Chem. Commun.*, 2001, 1124–1125; (c) S. Evans and J. R. L. Smith, *J. Chem. Soc., Perkin Trans. 2*, 2000, 1541–1552; (d) N. Hirai, N. Sawatari, N. Nakamura, S. Sakaguchi and Y. Ishii, *J. Org. Chem.*, 2003, **68**, 6587–6590; (e) J. Zhu, A. Robertson and S. C. Tsang, *Chem. Commun.*, 2002, 2044–2045.
- 30 (a) J. Muzart, *Chem. Rev.*, 1992, **92**, 113–140; (b) T. Das, K. Chaudari, E. Nandan, A. J. Chandwadkar, A. Sudalai, T. Ravindranathan and S. Sivasanker, *Tetrahedron Lett.*, 1997, **38**, 3631–3634; (c) B. M. Choudary, A. D. Prasad, V. Bhuma and V. Swapna, *J. Org. Chem.*, 1992, **57**, 5841–5844.
- 31 (a) E. Modica, G. Bombieri, D. Colombo, N. Manchini, F. Ronchetti, A. Scala and L. Toma, *Eur. J. Org. Chem.*, 2003, 2964–2971; (b) M. Jurado-Gonzalez, A. C. Sullivan and J. R. H. Wilson, *Tetrahedron Lett.*, 2003, **44**, 4283–4286.
- 32 (a) J. F. Pan and K. M. Chen, *J. Mol. Catal. A: Chem.*, 2001, **176**, 19–22; (b) G. Blay, I. Fernandez, T. Gimenez, J. R. Ruiz, E. Pardo, F. Lloret and M. C. Muñoz, *Chem. Commun.*, 2001, 2102–2103.
- 33 M. Nakanishi and C. Bolm, *Adv. Synth. Catal.*, 2007, **349**, 861–864.
- 34 A. J. Catino, J. M. Nichols, H. Choi, S. Gottipamula and M. P. Doyle, *Org. Lett.*, 2005, **7**, 5167–5170.
- 35 A. M. Khenkin and R. Neumann, *J. Am. Chem. Soc.*, 2004, **126**, 6356–6362.
- 36 V. Baland, D. Mathieu, N. Pons-Y-Moll, J. F. Bartoli, F. Banse, P. Battioni, J.-J. Girerd and D. Mansuy, *J. Mol. Catal. A: Chem.*, 2004, **215**, 81–87.
- 37 (a) D. Mathieu, J. F. Bartoli, P. Battioni and D. Mansuy, *Tetrahedron*, 2004, **60**, 3855–3862; (b) S. L. H. Rebelo, M. M. Q. Simoes, M. G. P. M. S. Neves and J. A. S. Cavaleiro, *J. Mol. Catal. A: Chem.*, 2004, **201**, 9–22.
- 38 (a) A. B. Sorokin and A. Tuel, *New J. Chem.*, 1999, **23**, 473–476; (b) A. B. Sorokin and A. Tuel, *Catal. Today*, 2000, **57**, 45–59; (c) Sorokin, S. Mangematin and C. Pergrale, *J. Mol. Catal. A: Chem.*, 2002, **182**, 267–281; (d) C. Pérollicr, C. Pergrale-Mejean and A. B. Sorokin, *New J. Chem.*, 2005, **29**, 1400–1403; (e) O. V. Zalomaeva and A. B. Sorokin, *New J. Chem.*, 2006, **30**, 1768–1773.
- 39 S. Stoll and A. Schweiger, *J. Magn. Reson.*, 2006, **178**, 42–55.
- 40 K. V. Klementiev, *J. Synchrotron Radiat.*, 2001, **8**, 270–272.
- 41 D. Genuit, P. Afanasiev and M. Vrinat, *J. Catal.*, 2005, **235**, 302–317.
- 42 İ. Gürol, V. Ahsen and Ö. Bekaroğlu, *J. Chem. Soc., Dalton Trans.*, 1994, 497–500.
- 43 O. V. Dolotova, N. I. Bundina, V. M. Derkacheva, V. M. Negrimovsky, V. V. Minin, G. M. Larin, O. L. Kaliya and E. A. Lukyanets, *Zh. Obshch. Khim.*, 1992, **62**, 2064–2075.